

Differential expression of nicotinic acetylcholine receptor subunits is critical for the embryonic development of zebrafish muscle and neuromuscular junction

by

Kazi Tanveer Ahmed

A thesis submitted in partial fulfillment of the requirements for the degree of

Doctor of Philosophy

In Physiology, Cell and Developmental Biology

Department of Biological Sciences
University of Alberta

© Kazi Tanveer Ahmed, 2020

Abstract

Nicotinic acetylcholine receptors (nAChRs) are ligand gated ion channels primarily expressed on muscle fibers and neurons. They are comprised of five subunits arranged in different stoichiometries. nAChRs expressed at the neurons are comprised of different combinations of α_{1-10} and β_{1-4} subunits, whereas muscle acetylcholine receptors are comprised of α_1 , β_1 , δ and γ/ϵ subunits. At neuromuscular junctions (NMJs), nAChRs are activated by binding to the neurotransmitter- Acetylcholine (ACh), which is released from motor axon terminals. Activation of the receptors allows the passage of Na^+ , K^+ and Ca^{2+} which leads to muscle depolarization. Thus, nAChRs play a critical role in muscle contraction and movement. Mammalian twitch muscle fibers express γ subunit containing receptors during embryonic stages, but this subunit is eventually replaced by ϵ subunit-containing receptors. Here, I studied zebrafish tonic red and twitch white muscle fibers to determine if the NMJs of zebrafish red and white fibers show a development pattern similar to mammalian muscle. Additionally, the scientific literature describing the development of zebrafish NMJs was inconsistent and controversial, and I sought to add clarity to the literature. My results show that the NMJs of zebrafish red and white muscle fibers show different synaptic properties during embryonic development. To determine the properties of nAChRs in developing fish I recorded mEPCs obtained from muscle fibers of animals aged between 1 dpf (day post fertilization) and 5 dpf and examined the characteristics of the mEPCs. I found that miniature end plate currents (mEPCs) recorded from white fibers exhibit single exponential decay at 1.5 dpf. However, by 2 dpf, mEPCs exhibit double exponential decays, and then revert to single exponential decays between 4 and 5 dpf. Therefore, by 5 dpf all mEPCs decay with fast, single exponential decays. In contrast, red fiber mEPCs exhibit double exponential decays throughout development between

1.5 and 5 dpf. Single channel recordings reveal the presence of long and short open channels with two conductance classes at 2 dpf in both fiber types. Red muscle fibers retain both the long and short open channels at 5 dpf whereas only short open channels are present in white muscle fibers at 5 dpf. RT-PCR of whole embryos shows that zebrafish express both the γ and ϵ subunits even in adult animals. But RT-qPCR from isolated red and white fibers indicate that ϵ subunits are predominantly expressed in white fibers by 5 dpf, whereas both γ and ϵ subunits are continuously expressed in red fibers. Next, to determine a role for the ϵ or γ subunits, I used morpholino oligonucleotides (MOs) to knockdown the expression of these subunits during early development. To achieve my goals, I used two sets of MOs. The first was a set of translation blocking MOs (MO-E_M and MO-G_M targeting ϵ and γ subunits respectively) previously used by Mongeon et al. (2011). I found that the development of motor neurons and muscle fibers, and locomotor activity of 2 dpf and 5 dpf animals were unaffected in the morphants. However, similar to published results, the decay kinetics of mEPCs obtained from 2 dpf white, 5 dpf red and 5 dpf white fibers were prolonged with MO-E_M. These results suggested that the ϵ and γ subunits have little roles in zebrafish embryonic development. I observed that the concentration of the MOs injected by Mongeon et al. (2011) was nearly 1000 fold less than generally used concentrations. Therefore, I designed and injected a set of splice blocking MOs (MO-E and MO-G targeting ϵ and γ subunits respectively). RT-PCR confirmed that both splice-blocking MOs resulted in altered splicing. Zebrafish injected with MO-E exhibited slight tail curvature at both 2 dpf and 5 dpf, and reduced expression of nAChRs at 5 dpf. But similar to translation blocking MO, MO-E did not affect the development of motor neurons. In contrast, injection of MO-G resulted in severe morphological defects, and significantly affected the development of motor neuron branches. Expression of nAChRs was not greatly reduced but showed a disorganized

pattern. Whole cell recordings of mEPCs showed properties that were mostly similar to those obtained from the translation blocking MOs, where MO-E resulted in increased decay times of mEPCs from white muscle fibers. Red muscle fibers remained unaffected. Synaptic properties of both red and white fibers remained unaffected following MO-G injections. The single channel properties of nAChRs were unaffected in MO-G morphants. Injection of MO-E resulted in a greater number of long open channel activity in red fibers, whereas single channel recordings from white fibers were rarely observed and were largely non-existent. The locomotor activity of 2 dpf embryos and 5 dpf larvae was also severely affected by MO-G, but not by MO-E. Therefore, the ϵ subunit appears to affect the synaptic properties of only white fibers and not red fibers. In contrast, the γ subunit appears to have minimal effects on synaptic properties but a much greater effect on motor neuron development and locomotion. Thus, my results show that the ϵ and γ subunits of nAChRs play different roles in embryonic development of zebrafish red and white muscle fibers.

Preface

This thesis is an original work of Kazi Tanveer Ahmed. All the experiments were conducted according to the research ethics approval from University of Alberta Research Ethics Board, Project name “Synaptic maturation in the fish embryos”, AUP00000816.

Results presented in chapter 3, and parts of the discussion has been published as Ahmed, KT. and Ali, Declan; 2016; ‘Nicotinic acetylcholine receptors (nAChRs) at zebrafish red and white muscle show different properties during development’, *Developmental Neurobiology*, vol 6, issue 8, page 916-36. I was responsible for data collection, analysis and manuscript writing. Dr. Declan W Ali was the supervisory author. He was involved with concept formation and assisted with data collection, analysis and manuscript composition.

Acknowledgement

Writing an acknowledgement seems to be harder than writing a thesis itself, since so many people to be thanked in so little space I have. First and foremost, my gratitude goes to the Almighty who kept me going to reach this point of life. Big thanks goes to Edmonton weather and particularly the occasional heat waves termed ‘Summer’, without which it would be difficult to survive with sanity in this part of the world. Along the same line, some credit goes to Tim Hortons too.

But the person who owes the greatest level of gratitude would undoubtedly be Dr. Declan W. Ali, my supervisor and mentor. He helped me cope up to the new condition as I arrived as a foreign student, then allowed me to jump into the agonizing journey, while constantly holding a rope of hope to be grabbed whenever I needed. He has always been there when I had difficulties- sometimes to create them, but mostly to solve them. The scientific aspects I learned from him were humongous, but he overshadowed them with his conscientiousness, humanity, perseverance and mostly his intention for not wanting to be a “jerk” (Ali, D. 2012). It has been an honor to be a member of Ali lab.

That brings me to the other members of Ali lab, to whom I was grateful. First, I must mention one name, Dr. Birbickram Roy aka Bipu. He has been my mentor ever since I came in the lab till present days. Sometimes he is like a big brother, sometimes like a father figure, always giving me the best suggestions and helping me whenever I needed him, disregarding his own needs/problems. I won’t say much about him, since it will be difficult to stop.

I am grateful to former Ali lab members- Dan, Marcus and Lindsey from whom I have learnt a lot. Current Ali lab members- Sufian, Hae-Won and Lakkhan were there to encourage me too, thanks for all your help and support. A separate sentence would be required for Ruhul, who has been a great companion, offering me helps throughout my last few years in the lab, and helped me carrying on. All the undergrads, I may not spell all your names correctly, so I will skip your names. Out of the lab, it was great to be around with Dr. Joshua Pemberton (Dr. Chang lab), a significant grad student figure-physically and scientifically. Then there were Rigan, Sonia, Tushar, Moushumi, Russel, Popy, Azad, Farhana, Samrat, Rikta, Shihab, Sraboni, Rakib, Fabila, Mizan, Akhi, Touhid, Shammi and so on- whose love directly touched my life. It will be selfish

not to include the names of Gerry from Cross Cancer Institute, Troy from MBSU and Aleah, Miranda and Auriana from aquatic facility.

I skipped the name of Jannatul from Ali lab members. It was because her contributions extended beyond Ali lab. She is my companion, my wife. She has been accompanying me with my life and I can't find the exact words to describe her impacts (rarely any husband does!!!). We have produced a couple of papers together and a couple of offspring too. 'Mrinmoyee' and 'Oronyo', our significant work together, have given me a different meaning and purpose to life.

My parents, Kazi Tazuddin Ahmed and Mrs. Farida Ahmed, how can I miss you? Yet I missed you entirely during this journey, knowing that you are always there with big hopes and all the love of the world. My Nana, Nanu and Dadu- I have lost all of you, but you are always in my heart, and I can feel your love and blessings all the time. My siblings- Eva and Progga, my mother in law- Mrs. Rehana Delower, my brother in laws- Topu, Shohag and Babu, my lovely niece- Tazkia, my cousins, friends and families... so many names to whom I owe much gratitude. But they will be kept waiting due to page limit.

I would like to mention one more name, without whom, I could not have reached this point in my life, and I don't know where I would be standing now if he was not there. He sacrificed a lot for me and my family and became an inseparable part of the family. He is none other than our "Sir", our "Mannan Sir". I am and will always be grateful for what you have done for me Sir.

Finally, back to academia, I have to express my gratitude to my committee members too (can I dare to ignore them and expect to be successful?). Dr. John Chang and Dr. Kelvin Jones- thanks for weathering me during the meetings and discussions, and allowing me to follow the path I seek to walk through. It would have been impossible without your guidance and assistance. You were great teachers, but more importantly, I have found you to be wonderful human beings, and I am glad that I get to know great people like you.

Ahh, no more space... I am sorry to skip you, but thank you all whose names are held at my heart, but I could not put down here. And finally, thanks to you too, who just read it.

Table of Contents

Chapter 1. Introduction and Literature Review	1
1.1 Introduction	1
1.2 Skeletal Muscle	3
1.2.1 Organization of Skeletal Muscle	4
1.2.2 Muscle Contraction	6
1.3 Motor Neuron	7
1.3.1 Motor Neuron Classification	7
1.4 Nicotinic Acetylcholine Receptors (nAChRs)	8
1.4.1 Structure of nAChRs	9
1.4.2 Evolution, Expression and Development of nAChRs	10
1.5 Zebrafish as a Model Organism for Studying Development of NMJ	14
1.5.1 Zebrafish Skeletal Muscle Fiber	15
1.5.2 Zebrafish Motor Neurons	17
1.5.3 nAChRs in Zebrafish NMJ	20
1.3.4 Locomotion in Embryonic Zebrafish	22
1.4 Research Objectives and Hypothesis	25
Chapter 2. Materials and Methods	38
2.1 Animals	38
2.2 Morphological Observations and Imaging	39
2.3 Immunohistochemistry Staining	39
2.4 Reverse-Transcription Polymerase Chain Reaction (RT-PCR) of RNA from Whole Embryos and Adult Muscle	40
2.4.1 RNA Extraction	40
2.4.2 Reverse Transcription	41
2.4.3 RT-PCR	41
2.5 Dissection	42
2.6 Identification and Access to Muscle Fibers	43
2.7 Quantitative Real Time PCR (RT-qPCR) of Individual Muscle Fibers	43

2.7.1 Individual Muscle Fiber Intracellular Content Collection	43
2.7.2 Quantitative Real Time PCR	44
2.8 Morpholino Oligonucleotide Mediated Knock-down of nAChR Subunits	45
2.8.1 Morpholino Design	46
2.8.2 Microinjection	47
2.8.3 Confirmation of Altered Splicing	47
2.9 Electrophysiology	48
2.9.1 mEPC Recording	48
2.9.2 Analysis of mEPCs	49
2.9.3 Single Channel Recording	50
2.9.4 Single Channel Analysis	50
2.9.5 Ensemble Average of Single Channel Recordings	51
2.10 Fictive Swimming of 2 dpf Embryos	51
2.11 Sound Mediated Free-swimming of 5 dpf Larvae	52
2.12 Spontaneous Free-swimming Behavior at 5 dpf Larvae	52
2.13 Statistical Analysis	53
Chapter 3. Results- General Development	56
3.1 mEPC Recording from Developing Red and White Muscle Fibers	56
3.2 ACh-activated Single Channel Currents from Red and White Muscle Fibers	61
3.3 Expression of nAChR Subunits	64
Chapter 4- Results- Effect of γ and ϵ Subunits in Embryonic Development (Translation Blocking MO)	105
4.1 General Morphology	106
4.2 Expression of nAChR	106
4.3 Effect on Motor Neuron Axonal Branching	108
4.4 Effect on Muscle Fiber Morphology	109
4.5 Effect on Larval Locomotive Behavior at 5 dpf	110
4.6 Effect on mEPC Recorded from Red and White Muscle Fibers	111
Chapter 5- Results- Role of γ and ϵ Subunits in Embryonic Development (Splice Blocking MOs)	139
5.1 Efficacy of Splice-blocking MOs	139
5.2 Morphological Analysis	140

5.3 Expression of nAChR	141
5.4 Colocalization of Synaptic Vesicles	142
5.5 Motor Neuron Branching	143
5.6 mEPC Recording from Red and White Muscle Fibers	145
5.7 Single Channel Recording	147
5.8 Escape Response and Swimming Behavior	151
5.8.1 Escape Response at 2 dpf	152
5.8.2 Response to Sound Stimulus 5 dpf	153
5.8.3 Spontaneous Swimming at 5 dpf	154
Chapter 6. Discussion	213
6.1 Synaptic Development in White and Red Muscle Fibers	214
6.2 Red vs White Fibers	218
6.3 Different Effects of γ and ϵ Subunit Knockdown on Development	223
6.4 Role of γ Subunit during Development	229
6.5 nAChRs and MN Development	231
6.6 Conclusion and Future Directions	233
References	241

List of Tables

Table 2.1: List of primers used for RT-PCR	54
Table 2.2. RT-PCR primer sequences used for validation of splice blocking MOs	55
Table 3.1: Summary of mEPC decay kinetics after force-fitting all events with a single exponential decay, τ	67
Table 3.2: Decay time course of the fast and slow exponential components from red fibers	68
Table 3.3: Decay time course of the fast and slow exponential components from white fibers	69
Table 3.4: Relative mRNA expression ($2^{-\Delta\Delta C_t}$) of nAChR subunits in different fibers	70
Table 5.1: Decay time course of the fast and slow exponential components from red and white fibers following injection of control MO (MO-Cntr.) and splice blocking MOs (MO-E and MO-G)	155

List of Figures

Figure 1.1: Ultrastructural details of skeletal muscle fibers	28
Figure 1.2: Schematic of nAChR subunit	30
Figure 1.3: Organization of zebrafish skeletal musculature	32
Figure 1.4: Schematic of motor neuron branching of zebrafish	34
Figure 1.5: Proposed distribution of nAChRs in zebrafish red and white muscle fibers according to Mongeon et al. (2011) and Park et al. (2014).	36
Figure 3.1: Sample miniature end plate current (mEPC) traces from Red muscle fibers	71
Figure 3.2: Sample mEPC traces from white muscle fibers	73
Figure 3.3: Frequency of mEPC events during development	75
Figure 3.4: Amplitude of mEPC events during development	77
Figure 3.5: Single exponential decay time vs. amplitude distributions of mEPC events recorded from red and white fibers during development	79
Figure 3.6: Averaged mEPCs obtained from red muscle fit with a single exponential decay over the fast component or slow component	81
Figure 3.7: Averaged mEPCs obtained from white muscle fit with a single exponential decay over the fast component or slow component	83
Figure 3.8: Graphs showing the percentage of mEPCs better fit with a single exponential decay component in red and white fibers	85
Figure 3.9: Single channel recording of nAChRs from outside-out patch configuration	87
Figure 3.10: Sample traces of single channel events recorded from outside-out patches taken from red fibers at 1.5 and 5 dpf	89

Figure 3.11: Sample traces of single channel events recorded from outside-out patches taken from white fibers at 1.5 and 5 dpf	91
Figure 3.12: Properties of single channel events obtained from red fibers	93
Figure 3.13: Properties of single channel events obtained from white fibers	95
Figure 3.14: Ensemble average of single channel events from patches held at -100 mV for red and white fibers from 1.5 dpf, 2 dpf and 5 dpf fish	97
Figure 3.15: RT-PCR bands seen in agarose gels for $\alpha 1$, $\beta 1$, γ , δ and ϵ subunits during various stages of zebrafish life cycle	99
Figure 3.16: Validation of RT-qPCR experiment for nAChR subunit primers by semi-log regression analysis	101
Figure 3.17: Relative expression of various subunits in red vs. white fibers examined by RT-qPCR	103
Figure 4.1: Morphology of 2 dpf embryos and 5 dpf larvae following injection of translation blocking MO	115
Figure 4.2: α -bungarotoxin staining of nAChRs in 2 dpf and 5 dpf embryos of uninjected control, MO-EM and MO-GM.	117
Figure 4.3: Quantification of nAChR clusters in 2 dpf embryos and 5 dpf larvae	119
Figure 4.4: Primary motor neuron axonal branching in 2 dpf and 5 dpf fish of uninjected control, MO-EM and MO-GM	121
Figure 4.5: Secondary motor neuron axonal branching in 2 dpf embryos and 5 dpf larvae of uninjected control, MO-EM and MO-GM	123
Figure 4.6: White muscle fiber in 2 dpf embryos of uninjected control, MO-EM and MO-GM	125
Figure 4.7: Quantification of free-swimming activity in 5 dpf larvae of uninjected control, MO-EM and MO-GM	127

Figure 4.8: Raw traces of miniature endplate currents (mEPCs) recorded from red and white muscle fibers of embryonic and larval zebrafish	129
Figure 4.9: Comparison of mEPC frequency recorded from uninjected control and MO-E _M fish	131
Figure 4.10: Comparison of mEPC amplitude recorded from uninjected control and MO-E _M fish	133
Figure 4.11: Averaged mEPCs fit with a single exponential decay over the fast component or slow component	135
Figure 4.12: Comparison of mEPC decay time constant recorded from uninjected control and MO-E _M fish	137
Figure 5.1: RT-PCR exhibiting alternate splicing in 5 dpf larvae following splice blocking morpholino injections	157
Figure 5.2: Morphology of zebrafish embryos injected with MO-Cntr., MO-E and MO-G.	159
Figure 5.3: Quantification of morphological defects induced by MO-Cntr., MO-E and MO-G	161
Figure 5.4: α -bungarotoxin staining of nAChRs in 2 dpf embryos and 5 dpf larvae of MO-Cntr., MO-E and MO-G	163
Figure 5.5: Quantification of nAChR puncta in MO-Cntr., MO-E and MO-G	165
Figure 5.6: Colocalization of nAChRs and synaptic vesicles in 2 dpf embryo of MO-Cntr., MO-E and MO-G	167
Figure 5.7: Colocalization of nAChRs and synaptic vesicles in 5 dpf larvae of MO-Cntr., MO-E and MO-G	169
Figure 5.8: Primary MN branching in 2 dpf embryos and 5 dpf larvae of MO-Cntr., MO-E and MO-G	171

Figure 5.9: Secondary MN branching in 2 dpf embryos and 5 dpf larvae of MO-Cntr. MO-E and MO-G.	173
Figure 5.10: Raw traces of miniature endplate currents (mEPCs) recorded from red and white muscle fibers of embryonic and larval zebrafish of MO-Cntr., MO-E and MO-G	175
Figure 5.11: Comparison of mEPC frequency recorded from MO-Cntr., MO-E and MO-G fish	177
Figure 5.12: Comparison of mEPC amplitude recorded from MO-Cntr., MO-E and MO-G fish	179
Figure 5.13: Comparison of the average mEPC events recorded from MO-Cntr., MO-E and MO-G fish	181
Figure 5.14: Comparison of mEPC decay time constant recorded from MO-Cntr., MO-E and MO-G fish	183
Figure 5.15: Single channel events obtained from outside-out patches of red and white fibers at 2 dpf and 5 dpf time points from MO-E and MO-G fish	185
Figure 5.16: Amplitude histograms of single channel events obtained from MO-E and MO-G fish red fibers held at -100 mV.	187
Figure 5.17: Histograms of dwell time constant of single channel events obtained from MO-E and MO-G fish red fibers	189
Figure 5.18: Comparison of single channel dwell time constants recorded from red fibers of untreated control, MO-E and MO-G fish	191
Figure 5.19: Comparison of events (%) with short and long dwell times recorded from red fibers of uninjected control, MO-E and MO-G	193
Figure 5.20: Amplitude histograms of single channel events obtained from MO-E and MO-G fish white fibers held at -100 mV	195
Figure 5.21: Histograms of dwell time constant of single channel events obtained from	197

MO-E and MO-G fish white fibers

Figure 5.22: Comparison of fast dwell time constants (τ_{Fast}) recorded from white fibers of uninjected control, MO-E and MO-G fish	199
Figure 5.23: Quantification of C-bend escape response in 2 dpf embryos following tactile stimulation at the head	201
Figure 5.24: Comparison of maximum speed and acceleration attained during eliciting a C-bend escape response by MO-Cntr., MO-E and MO-G embryos at 2 dpf	203
Figure 5.25: Comparison of response rate of 5 dpf MO-Cntr., MO-E and MO-G larvae responding to sound stimulus	205
Figure 5.26: Quantification of free-swimming activity in 5 dpf larvae of MO-Cntr., MO-E and MO-G	207
Figure 5.27: Comparison of velocity and acceleration of 5 dpf MO-Cntr., MO-E and MO-G larvae during spontaneous free-swimming activity	209
Figure 5.28: Comparison of turn angle and angular velocity of 5 dpf MO-Cntr., MO-E and MO-G fish during spontaneous free-swimming activity	211
Figure 6.1: Schematic of nAChR expression pattern in zebrafish red and white muscle fibers during development.	237
Figure 6.2: Schematic of my proposed role of different nAChR subunits during development of MN.	239

List of Abbreviations

ACh- Acetylcholine

AChR- Acetylcholine receptor

AR- Adult red fiber

bFGF- Basic fibroblast growth factor

CaP- Caudal primary motor neuron

CMS- Congenital myasthenic syndrome

CNS- Central nervous system

CSQ- Calsequestrin

DHPR- Dihydropyridine receptor

dpf- Days post fertilization

dS- Dorsally projecting secondary MN

dvS- Dorsoventrally projecting secondary MN

DW- Deep white fibers

ECS- Extracellular solution

E_mR- Embryonic red muscle fiber

E_mW- Embryonic white fiber

ER- Endoplasmic reticulum

EVMPS- Escobar variant multiple pterygium syndrome

FF- Fast twitch fatigable fiber

FFR- Fast twitch fatigue resistant fiber

HM- Horizontal myoseptum

hpf- Hours post fertilization

ICS- Intracellular solution

IF- Intermediate fibers

iS- Intermyotomal secondary MN

iS-c- Inter-myotomal secondaries with collateral

iS-nc- Inter-myotomal secondaries with no collateral

M-cell- Mauthner cell

mEPC- Miniature endplate current

mEPP- Miniature endplate potential

MiP- Middle primary motor neuron

MN- Motor neuron

MO- Morpholino oligonucleotide

MP- Multiple pterygia

MyHC- Myosin heavy chain

nAChR- Nicotinic acetylcholine receptor

NGF- Nerve growth factor

NMJ- Neuromuscular junction

NRG-1- Neuregulin-1

NT- Notochord

PNS- Peripheral nervous system

RoP- Rostral primary motor neuron

RT-PCR- Reverse transcription polymerase chain reaction

RT-qPCR- Quantitative reverse transcription polymerase chain reaction

RyR- Ryanodine receptor

SC- Spinal cord

SCCMS- Slow channel congenital myasthenic syndrome

SD- Scattered dorsal fiber

SERCA - Sarco/endoplasmic reticulum ATPase

SFR- Slow twitch fatigue resistant fiber

SR- Sarcoplasmic reticulum

SV- Scattered ventral fiber

TTX- Tetrodotoxin

TM- Transmembrane domain

VaP- Variable primary MN

vS- Ventrally projecting secondary MN

Chapter 1. Introduction and Literature Review

1.1 Introduction

The power of effective communication and collaboration cannot be overstated, particularly at the verge of this historic moment, when a collaborative effort of more than 200 scientists and 8 telescopes captured the event-horizon image of a supermassive black hole, situated nearly 500 million trillion KMs away (Akiyama et al., 2019). However, the importance of communication does not only extend to such massive distances, but it is critical for the functioning of something as minute as in subcellular molecules. In vertebrates, the role of communication has particularly been ascribed to the nervous system, which perceives physical, environmental and emotional cues and transforms this information into electrical signals. Next, they integrate the signals, store them, process them and then will often elicit responses by directing the organs and limbs. The principle functional component of the nervous system is the neuron, of which there are billions in the human body. Neurons communicate with each other or with peripheral systems by establishing special connecting structures called synapses. The word 'synapse' originated from Greek word 'synaptein', meaning 'to clasp or join together'. Synapses can be electrical, in which case, the signaling ends are connected by connecting channels that allow the direct passage of ions from one cell to another. However, many synapses are chemical, in which communication occurs via chemical neurotransmitters that are released from one cell to diffuse across a small extracellular space to bind to receptors on the postsynaptic membrane. Upon binding of neurotransmitters, the post synaptic cell undergoes physiological changes, converting the chemical signal to electrical signal for further transduction or to exert an

appropriate physical response to the signal. Electrical synapses can be bidirectional, whereas chemical synapses are typically unidirectional (Nicholls et al., 2012).

The neuromuscular junction (NMJ) is a chemical synapse formed between the axon of a motor neuron and a muscle fiber. NMJs can be found in both smooth muscle and skeletal muscles, and activity at the NMJ can induce the muscles to contract when the appropriate signal occurs. NMJs at skeletal muscles are particularly important, for they allow voluntary muscle contractions, which is required for locomotion. NMJs have been extensively utilized as a model to understand formation, stabilization, maintenance, differentiation and elimination of chemical synapses due to its large size, accessibility, and simplicity. The study of the NMJ can be traced back to the mid-19th century, when Claude Bernard investigated how curare blocked muscle activity (Bernard, 1857). In 1928, Santiago Ramon y Cajal described some main structural features of NMJ synaptogenesis and regeneration. In 1936, Dale et al provided a detail description of vertebrate skeletal NMJ as a model of chemical synapse (Dale, Feldberg, & Vogt, 1936). In the 1950s and 60s, seminal work of Katz and colleagues extended the field by identifying quantal release properties of neurotransmitters (Fatt & Katz, 1952b), spontaneous activity of motor endplate (Fatt & Katz, 1952a), and biophysical and chemical properties involving signal transmission through NMJ (Del Castillo & Katz, 1956; Katz, 1979; Katz & Miledi, 1967b, 1967a). With the advent of advanced imaging, molecular biology and genetic tools, study of the NMJ revealed further insights into extracellular details and molecular mechanisms involving architecture, development and functioning of NMJ, which is often shared by other synapses at the central nervous system (CNS) (Lai & Ip, 2003).

At the presynaptic terminal of NMJs, motor axons release the neurotransmitter, acetylcholine (ACh). Acetylcholine receptors (AChRs) located postsynaptically on the muscle fibers bind to the neurotransmitter. Nicotinic Acetylcholine Receptors (nAChRs) may also be activated by exogenous application of nicotine. While various other molecules and structural features are involved for successful transduction of the signals, skeletal muscle, motor neurons and the nAChRs are the key components being focused in my study.

1.2 Skeletal Muscle

Skeletal musculature provides structural organization to the body, helps in protecting internal organs, acts as a source of energy in extreme environments, and most importantly allows the organism to move voluntarily. In humans, skeletal muscles comprise 40% of the total body weight and 50-75% of body protein (Frontera & Ochala, 2015). The organization of musculature differs between species, providing specific properties necessary for the organism to thrive in its environment and ecosystem. Even in the same organism muscle organization in different parts of the body differs, allowing specific limbs or body parts to carry out their specific functions. Myotomes possess complex architecture involving muscle fibers or myocytes, nerves, connective tissues, fibroblasts, skeletal osteocytes, adipocytes and capillary endothelial cells. Muscle fibers contract in response to nerve signaling, providing the basis of movement of the entire myotome. Coordinated contraction and relaxation of different muscle fibers manifest the various movements seen in the organism- including flexing a single finger to picking up objects of different weights, walking, running, jumping, swimming, or simply sitting down, maintaining the posture and rolling the eyeball over a manuscript.

1.2.1 Organization of Skeletal Muscle

A single muscle is comprised of bundles of muscle cells commonly known as muscle fibers or myocytes. A muscle fiber is an elongated multinucleated cell, comprising bundles of myofibrils sheathed by a cell membrane or sarcolemma. 20-80 muscle fibers are arranged in parallel and are encapsulated by a layer of connective tissue called perimysium, forming a muscle fascicle. Several fascicles are grouped together in a muscle, and a muscle in its entirety is covered by a connective tissue called epimysium. Extension of the epimysium forms tendon, which attaches the muscle to the bone. (Frontera & Ochala, 2015).

Mammalian skeletal myocytes are broadly classified into two groups based on their contraction speed and metabolic properties. Type 1 or slow twitch fibers, a.k.a. the red fibers are muscle fibers that exhibit slow contraction speed. They are rich in myoglobin and oxidative enzymes. Type 2 or the fast twitch fibers have fast contraction speeds, high glycolytic metabolism and are specialized for phasic activity. They are also called the white fibers. Type 2 muscle fibers can be subdivided into three further groups- 2A, 2X and 2B based on properties such as myosin heavy chain composition, mitochondrial concentration and resistance to fatigue. Group 2A fibers are fatigue resistant and have both oxidative and glycolytic enzymes whereas 2B fibers are fast-fatigable and have low level of oxidative enzymes. Contraction speed, fatigue resistance and concentration of oxidative enzymes are intermediate in 2X fibers. All these fibers also express different types of myosin heavy chain (MyHC) (Schiaffino & Reggiani, 2011). A single skeletal muscle is comprised of bundles of muscle fibers, mostly of multiple types. Whereas a mixture of different fiber populations gives more flexibility to the muscle in performing different types of tasks, depending on the position and principle functionality of the

muscle, some fibers are more abundant than others (Edstrom & Kugelberg, 1968; Schiaffino & Reggiani, 2011).

Muscle fibers are multinucleated and post-mitotic. They are covered by capillaries for nutrient and gas exchange. A single muscle fiber is composed of thousands of myofibrils, several nuclei and mitochondria and a network of sarcoplasmic reticulum, all encapsulated by the sarcolemma. The invagination of the sarcolemma also forms the T-tubule system, which is a tubular structure around myofibrils that helps in the conduction of action potential to the interior of the cell. The sarcoplasmic reticulum (SR) is another tubular structure of the muscle fiber which stores, releases and reuptakes Ca^{2+} ions. It therefore regulates the calcium required for muscle contraction. The end of the SR, which is apposed to the T-tubule is called the terminal cisternae. Ca^{2+} remains bound to the calsequestrin protein in the terminal cisternae. Terminal cisternae also contain ryanodine receptors (RyR) through which Ca^{2+} are released into the sarcoplasm, and sarco/endoplasmic reticulum ATPases (SERCA) which pumps Ca^{2+} back to the SR (Fig 1.1 A). Muscle mitochondria are distributed along the muscle fiber forming a three-dimensional network and are required for generation of energy in presence of oxygen (Dahl et al., 2015). The number of mitochondria varies in different types of muscles and can be increased in a muscle by endurance exercise (Yan, Lira, & Greene, 2012).

To the naked eye, the myofibril of skeletal muscles appears to have many stripes, thus leading to the term striated skeletal muscle. Under the electron microscope, myofibrils exhibit an alternating pattern of light and dark regions with distinctive bands and lines (C. E. Hall, Jakus, & Schmitt, 1946). The dark area is termed the A band, and the light area is called the I band. The I band lies in between 2 A bands, and the Z line runs through the middle of the I band. At the

middle of the A band, there is a central M line with adjacent H-bands. The Z line or telophragma, delimits the contractile functional unit of the myofibril, the sarcomere. The sarcomere comprises thick and thin filament that are composed of myosin and actin filaments. The molecular arrangement of these filaments and bands is critical for a functional sarcomere to generate muscle contraction (Fig 1.1 B).

1.2.2 Muscle Contraction

Muscle contraction starts with a signal coming from the neurons and requires a cascade of events to be completed properly to generate a precise level of contraction. Skeletal muscles receive signals from motor neurons. The terminal branches of the motor neurons innervate the muscle fibers and form neuromuscular junctions (NMJs). At the NMJ, axons release acetylcholine (ACh) molecules, which bind to the nAChRs of the muscle fibers. Na^+ , K^+ , and Ca^{2+} are the predominant ions that flow through nAChRs at NMJs. The influx of cations depolarizes the muscle membrane and if the depolarization is large enough, it activates voltage gated Na^+ channels, allowing a large and sudden influx of more Na^+ into the fiber. This large influx creates action potentials.

Action potentials propagate along the muscle through T-tubules. Induction of action potential and depolarization of muscle fibers allow dihydropyridine receptors (DHPRs), a voltage gated L-type Ca^{2+} channels, present inside the muscle membrane to open. The DHPRs are physically linked to ryanodine receptors (RyR), the calcium release channels of sarcoplasmic reticulum. Opening of RyRs allow Ca^{2+} ions to flow from sarcoplasmic reticulum to the muscle cytoplasm, inducing a transient spike in intracellular calcium. The increased calcium is needed for the ultrastructural movements of muscle fibers to induce muscle contraction through the

sliding filament mechanism. Two molecules of Ca^{2+} bind to troponin C on the actin filament and induce formation of myosin-actin cross-bridges. Actin slides over the myosin and the sarcomere shortens in length. The coordinated shortening of all the myofibers result in contraction of the entire muscle (A. F. Huxley & Niedergerke, 1954; H. Huxley & Hanson, 1954).

If enough ATP and Ca^{2+} are available, the muscle contractions can be repeated. However, the cytoplasmic Ca^{2+} is actively pumped back into the sarcoplasmic reticulum by sarco/endoplasmic reticulum calcium-ATPase (SERCA) pumps, lowering the Ca^{2+} concentration in the cytoplasm, and thus ensuring that muscle contractions do not occur unless another round of neuronal signal is perceived (Kuo & Ehrlich, 2015).

1.3 Motor Neuron

Motor neurons are the neuronal subtype that specializes in transmitting signals from the brain to peripheral terminals. A single motor neuron and all the muscle fibers it innervates is called a motor unit. All of the motor neurons that innervate a single muscle are collectively called a motor neuron pool. Both the specificity of the motor unit and the diversity of the motor neuron pool play critical roles in tuning the various levels of movements and gestures of an organism.

1.3.1 Motor Neuron Classification

Motor neurons that transmit signals from the brain to the muscles can be subdivided into two broad groups- upper motor neurons and lower motor neurons. Cell bodies of upper motor neurons are located in the cerebral cortex. These motor neurons make glutamatergic connections with lower motor neurons. Pathophysiological conditions with upper motor neuron lesions

include spasticity, hyperreflexia and uncontrolled movements. Lower motor neuron cell bodies reside in the cerebrum and the brainstem of the brain and in the ventral horn of the spinal cord. These motor neurons receive inputs from sensory neurons, interneurons and upper motor neurons. Lower motor neurons are cholinergic, and their lesions generally cause paralysis. Based on the target tissue they innervate, lower motor neurons can be subdivided into Branchial (innervate face and neck muscle), Visceral (innervate smooth muscles and glands), and Somatic (innervate skeletal muscles for posture and movement) motor neurons (Stifani, 2014).

Somatic motor neurons can be further subdivided based on the skeletal muscle structures they innervate. Skeletal muscles are composed of two types of fibers: extrafusal and intrafusal. Extrafusal fibers generate force while intrafusal fibers are involved with proprioception. Based on physiological and molecular characteristics, extrafusal fibers are divided into three types- (i) slow twitch fatigue resistant fibers (SFR), (ii) fast twitch fatigue resistant fibers (FFR), and (iii) fast twitch fatigable fibers (FF). Accordingly, somatic motor neurons are divided into- alpha motor neurons that innervate extrafusal fibers only, beta motor neurons that innervate both extrafusal and intrafusal fibers, and gamma motor neurons innervating intrafusal fibers exclusively. Alpha motor neurons are further classified into SFR, FFR and FR motor neurons, each exclusively innervating corresponding extrafusal fiber types. Such a great variety of motor neurons ensures the complex nature of vertebrate physiology and locomotion in fine detail (Stifani, 2014).

1.4 Nicotinic Acetylcholine Receptors (nAChRs)

Nicotinic acetylcholine receptors (nAChRs) are ligand gated ion channels. They are activated by binding to the acetylcholine (ACh) ligand and allow passage of ions upon

activation. Na^+ , K^+ and Ca^{2+} are the ions that can pass through the ion channels. They are called ‘nicotinic’ since exogenous application of nicotine can also activate these channels.

1.4.1 Structure of nAChRs

nAChRs are members of the “Cys-loop” receptor family, which also includes the ionotropic receptors for GABA, glycine and 5-HT. The name comes from the fact that there is a disulfide bond between two cysteine residues separated by 13 highly conserved amino acids in the extracellular N-terminal domain. All of the receptors in this family are comprised of five subunits that together form the ion-conducting pore (Thompson, Lester, & Lummis, 2010).

nAChRs were first identified and purified from the torpedo electric organ (Changeux, Kasai, & Lee, 1970). In vertebrates, 17 different subunits ($\alpha 1$ - $\alpha 10$, $\beta 1$ - $\beta 4$, γ , δ , ϵ) of nAChR have been identified so far. The subunits assemble in different stoichiometries to give rise to different subtypes of the pentameric nAChRs. nAChRs are expressed at the neuromuscular junction, in the CNS, PNS (peripheral nervous system) and some non-neuronal cell types (Sharma & Vijayaraghavan, 2002). Neuronal nAChRs are mostly comprised of various combinations of $\alpha 2$ - $\alpha 10$ and $\beta 2$ - $\beta 4$ subunits, whereas muscle nAChRs are comprised of $\alpha 1\beta 1\gamma\delta$ or $\alpha 1\beta 1\delta\epsilon$ subunit combinations only (Galzi & Changeux, 1995; Kalamida et al., 2007; Mishina et al., 1986). The diversity in receptor subunits and their stoichiometry attribute to different structural, pharmacological, physiological and functional properties.

All of the subunits share some common structural features. They have a large extracellular N-terminal domain, four transmembrane domains (TM1-TM4) and a large intracellular domain between TM3 and TM4 (Fig 1.2). The ligand binding region is located in

the extracellular N-terminus of some subunits. Two adjacent subunits containing ligand binding regions form the hydrophobic pocket of agonist binding site. One of the regions, called the primary (or plus) component is located on the α subunit, whereas the secondary (or minus) component of the agonist binding pocket is located on the non- α subunit (Colombo, Mazzo, Pistillo, & Gotti, 2013; Pedersen & Cohen, 1990). The second transmembrane domain, TM2 lines the central hydrophilic ion pore, whereas TM4 is situated away from the pore, and TM1 and TM3 are positioned opposite to each other, at 90 degrees from TM2 and TM4. The extracellular N-terminal domain is mostly comprised of β -strands, and is configured as a barrel like structure, termed the β -barrel. Upon ligand binding, considerable rearrangement of hydrogen bonding occurs in the β -barrel. This rearrangement creates enough torque to shift the extracellular surface of the receptor, which in turn causes a 15-degree clockwise rotation of TM2. This relocates the amino acid residues of TM2 lining the central pore and allows the receptor to attain open-channel conformation from closed state (Albuquerque, Pereira, Alkondon, & Rogers, 2009).

1.4.2 Evolution, Expression and Development of nAChRs

Based on phylogenetic analysis, Tsunoyama & Gojobori (1998) predicted the evolution of different nAChR subunits in vertebrates. According to their prediction, an ancestral subunit with a ligand binding site appeared first and formed homomeric receptors. This ancestral subunit then gave rise to $\alpha 7$, $\alpha 8$ and $\alpha 9$ subunits, which function as homo-oligomers in the CNS. Subsequent genome duplication gave rise to two types of subunits- an ancestral α type with ligand binding capacity, and an ancestral β type that lacked ligand binding capacity. Current $\alpha 1$ - $\alpha 6$ and $\beta 3$ subunits diverged from the ancestral α -type, whereas $\beta 1$, $\beta 2$, $\beta 4$, γ , δ and ϵ emerged from the ancestral β -type (Tsunoyama & Gojobori, 1998).

Diversity in the expression of subunits also originates from cell specific transcription of nAChR subunits. $\alpha 3$ and $\beta 4$ subunits are abundant in the autonomic nervous system, while $\alpha 4$ and $\beta 2$ subunits dominate in the CNS, and γ and ϵ subunits are only expressed in muscle (Albuquerque et al., 2009). Cell specific variations in the transcription of different subunits can be contributed by various factors including developmental stage, cellular status, linkage between genomic regions, conserved noncoding regions, trophic factors such as nerve growth factor (NGF) and transcription factors such as SCIP/Tst-1/Oct-6 (Albuquerque et al., 2009; Boyd, 1996; Melnikova & Gardner, 2001; Xu, Scott, & Deneris, 2006).

From transcription to cell surface expression, nAChRs must go through some critical and time-consuming steps. The assembly process takes more than 90 mins and only ~30% of the synthesized subunits form functional receptors (Merlie & Lindstrom, 1983). The ribosomal complex of the endoplasmic reticulum (ER) translates the nAChR subunits and inserts them into the ER membrane translocon (Alder & Johnson, 2004). Following translation, the nascent polypeptide chain undergoes critical posttranslational modifications including proteolytic cleavage, glycosylation, palmitoylation, disulfide-bond formation and prolin isomerization (Millar & Harkness, 2008). The ER also regulates subunit assembly and directs the misassembled proteins to the proteasome for degradation. Two different models have been proposed for subunit assembly, the heteromeric model and the sequential model. The heteromeric model proposes that two dimers ($\alpha 1\delta$ and $\alpha 1\gamma$) are formed first and are later assembled with the β subunit to form the pentameric receptor (Blount, Smith, & Merlie, 1990; Kreienkamp, Maeda, Sinet, & Taylor, 1995). According to the sequential model, there is an initial rapid binding of α , β and γ subunits to form a trimer. The δ subunit then joins the trimer to form a tetramer, and finally a second α subunit joins the protein to form the pentameric structure

(Green & Claudio, 1993; Wanamaker, Christianson, & Green, 2003). Molecular chaperons including calnexin, ERp75, BiP, 14-3-3- β -protein, and RIC-3 aids in the appropriate subunit folding and exportation of the receptors from the ER (Albuquerque et al., 2009; Colombo et al., 2013; Millar & Harkness, 2008). After exiting the ER, vesicles containing the nAChRs travel to the Golgi apparatus, where they are further processed and are then destined to move to the plasma membrane for surface expression.

Extensive studies on skeletal muscle NMJs have provided further insight into the molecular pathways involved in nAChR aggregation. During development, agrin, a nerve-secreted proteoglycan activates a receptor tyrosine kinase, MuSK (muscle specific kinase) via activity of Lrp4 and Dok-7 protein. Agrin can also activate Src and Fyn, two members of Src family kinases, which phosphorylate AChR β and δ subunits. Agrin also associates with MuSK separately. The MuSK-bound complex acts as a primary synaptic scaffold and recruits the nAChR complexes associated with rapsyn. Other elements such as Ca^{2+} , NO, actin filaments, activation of small GTPases like Rac and Cdc42 have also shown to be critical for the clustering of nAChRs. Besides agrin, other molecules have been shown to induce receptor clustering such as laminin, VVA-B4, basic fibroblast growth factor (bFGF), heparin-binding growth-associated molecules etc. However, agrin can also induce clustering of the protein neuregulin-1 (NRG-1), which activates ErbBs, members of EGF receptor family of RTKs. ErbB activation can trigger a signaling cascade including several kinases such as Ras, Raf, MAP kinase, PI3K, adapter protein Shc and tyrosine phosphatase SHP2, which ultimately results in enhanced transcription of nAChR genes (Fuhrer & Huh, 2002).

Stability of the synaptic nAChRs is dependent on activity, and the receptors are internalized slower at active synapses. The endocytosed receptors can be recycled back to the membrane by activity of protein tyrosine phosphatase (Fuhrer & Huh, 2002) or they may be degraded by the cellular proteasomes. Neuregulin-1 β , membrane cholesterol and subunit composition have been shown to be critically involved in receptor recycling and endocytosis, however the details of this mechanism are not fully elucidated (St John, 2009).

nAChRs at the NMJ also show developmental changes. In mammalian neonates, nAChRs contain the γ subunit, but they are gradually replaced by ϵ subunit containing receptors during postnatal development (Mishina et al., 1986; Veit Witzemann, Barg, Nishikawa, Sakmann, & Numa, 1987; Yamane, Saito, Nakagawa, Ohnuki, & Saeki, 2002). Missias, Chu, Klocke, Sanes, & Merlie (1996) found that the subunit switch occurs differentially in different muscle fiber types. In mice, fast twitch muscles start replacing γ subunit with ϵ at P1 (P, Postnatal Day) and by P17 they are completely replaced in various muscles. In contrast, slow twitch muscles retain the γ subunit up until P30 and extraocular muscles maintain its expression even in adults (Missias et al., 1996). In human, γ to ϵ switching occurs during gestational development in thigh and intercostal muscles (Hesselmans, Jennekens, Van Den Oord, Veldman, & Vincent, 1993), but thymus and extraocular muscles maintain the expression of γ subunit into adulthood (Horton, Manfredi, & Conti-Tronconi, 1993; Marx et al., 1989; Navaneetham, Penn, Howard, & Conti-Fine, 2001). However, γ subunit containing receptors do not go through postnatal reduction or reappear ectopically in the muscle fibers during injury, denervation or various pathophysiological conditions (Goldman & Staple, 1989; Martinou & Merlie, 1991; Veit Witzemann, Barg, Criado, Stein, & Sakmann, 1989). Interestingly, such re-expression of γ

subunit occurs in type I (slow twitch) fibers but not type II (fast twitch) fibers in human (Gattenlöhner et al., 2002).

1.5 Zebrafish as a Model Organism for Studying Development of NMJ

Formation of the NMJ is a dynamic process where various molecules, trophic factors and signals interplay in regulating the proper expression and development of the NMJ components. Expression of various molecules, particularly nAChR shows subunit switching during development. Why the subunit switching occurs, and what role is played by the subunits is not clear yet. Particularly if there are any differences in the subunit expression and function across different types of muscle fibers has not been extensively studied. Therefore, my research has been focused on determining the role played by the nAChR subunits during development. I particularly examined how kinetic properties associated with the nAChRs expressed in different muscle fibers NMJs change during embryonic development, and how different nAChR subunits contribute in ensuring proper development of the NMJs. I used zebrafish as a model organism to pursue this study.

While vertebrates exhibit a great repertoire of structural and physiological divergence, at the earliest stages of development, they share startling similarities. Neuronal development is well conserved in embryonic vertebrates. Zebrafish is a wonderful model for studying physiological and neuronal development, particularly during embryonic development. Following fertilization, a developing zebrafish is considered to be an embryo until it hatches out of the chorion between 2-3 dpf (Kimmel, Ballard, Kimmel, Ullmann, & Schilling, 1995). A newly hatched embryo is referred as larva until ~4 weeks. At the end of larval stage, the fish acquires most of the adult traits except sexual maturity, and labelled as a juvenile fish. Sexual maturity is attained around 3

months of age, at which point it becomes an adult (Parichy, Elizondo, Mills, Gordon, & Engeszer, 2009). The fecundity of adult zebrafish is high. A single pair of male and female can lay several hundred eggs in a single clutch. Zebrafish are oviparous, meaning fertilization and embryonic development occurs outside the mother's body. This mode of development also makes zebrafish a lucrative model to study embryonic development, because dissection of a pregnant animal is not required to observe and study the developing embryo. Moreover, zebrafish embryos are transparent, making it suitable to observe development by simple microscopy or molecular tagging and immunolabelling. Its genome has been sequenced and has been identified to have high genetic similarity with higher vertebrates. Therefore, it is highly suitable for genetic screening and understanding gene functions. Finally, zebrafish are easy to raise and maintain in a laboratory environment. Thus, zebrafish has become a great model for studying the early stages of development. Moreover, they offer advantages for the study of NMJ development. They have relatively simple, yet highly organized nervous systems compared with adults. Their musculature is well arranged and distinct, allowing easy identification, access and examination of different types of axial muscles and NMJs. Embryonic muscle contractions are required for locomotion and the locomotion of zebrafish embryos are simple and well characterized, which can be easily assessed. Thus, zebrafish stands out as a simple yet powerful model to determine physiology, function, development and pathophysiological conditions related to the NMJ.

1.5.1 Zebrafish Skeletal Muscle Fiber

Axial musculature of zebrafish is arranged in W-shaped horizontal segments. Adjacent segments are separated by myosepta and ribs. A horizontal myoseptum divides each segment

into dorsal and ventral regions (van Raamsdonk, Pool, & Te Kronnie, 1978; Waterman, 1969).

Fig 1.3 shows schematics of the organization of zebrafish musculature in embryos and in adults.

Compared to mammals that have mixed fiber populations in each skeletal muscle bundle, fish skeletal musculature is relatively simple and has distinct spatial organization. Raamsdonk, Veer, Veeken, Heyting, & Pool (1982) studied the organization of adult zebrafish musculature and have provided a detailed description. Adult zebrafish have five types of skeletal muscle fibers- adult red fibers, intermediate pink fibers, white fibers, red muscle rim fibers and scattered intermediate fibers. These muscle fibers are localized in distinct locations. Red fibers are located on the top layer of the musculature, just beneath the skin and are slow contracting and fatigue resistant. Deep white fibers, which are the predominant musculature in the trunk are arranged in several layers. They contract at a fast rate and fatigue rapidly. In between the red and the white, lies the intermediate pink fibers, which are arranged in a wedge-shaped area around the horizontal septum and are fast-contracting but fatigue-resistant. Red muscle rim fibers lie between the adult red and intermediate pink fibers and have physiological properties similar to red fibers. The scattered intermediate fibers are scattered in dorsal (scattered dorsal; SD) or ventral regions (scattered ventral; SV) within the deep white muscle and they have physiological properties similar to the intermediate fibers. Fiber composition in the tail myotomes differ from the mid body. Adult red and intermediate fibers are more stretched out in the tail region, rather than arranged in a triangular shape as they are in the mid body. The scattered intermediate fibers are also found in higher proportions whereas red muscle rim fibers are scarce in the tail region. Such alterations in the muscle composition likely gives a physiological advantage to the tail region, which is required to be active for sustained swimming, whereas denser white fibers in the

mid body ensures fast and efficient bending that is needed occasionally (van Raamsdonk et al., 1982).

In contrast, embryonic zebrafish predominantly have two types of skeletal muscle fibers- embryonic red and white fibers (Waterman, 1969). Embryonic red fibers are located as a superficial single layer, running parallel to the body axis. These are mononucleated tonic fibers that lack voltage gated sodium channels and are unable to generate action potentials (Buckingham & Ali, 2004). Embryonic white fibers make up the rest of the embryo musculature and are arranged in chevron shape beneath the red fibers. These white fibers are multinucleated, larger in diameter than the red fibers and are twitch fibers. Both red and white fibers remain extensively coupled by gap junctions at 1 day post fertilization (dpf), however coupling decreases up to 70% by 3 dpf. Embryonic red fibers are coupled in both the dorso-ventral and rostro-caudal direction whereas white fibers mostly exhibit rostro-caudal coupling (Buss & Drapeau, 2002). White fibers can conduct action potentials by the virtue of possessing voltage gated sodium channels (Buckingham & Ali, 2004). Red fibers are rich in mitochondria and their energy metabolism is aerobic, whereas the white fibers have fewer mitochondria and have predominantly anaerobic enzyme activities (van Raamsdonk et al., 1978).

1.5.2 Zebrafish Motor Neurons

Zebrafish axial muscles are segmentally arranged, and each segment is innervated by motor neurons located at the ipsilateral hemisegment of the spinal cord. Most vertebrate muscles are innervated by a single motor axon forming a single endplate. In contrast zebrafish muscles receive polyneuronal, multiterminal innervation (Westerfield, McMurray, & Eisen, 1986).

Zebrafish motor neurons can be classified into two classes- primary and secondary- based on the

origin, size, location and innervation pattern (Fig 1.4). Primary MNs originate between 9-16 hours post fertilization (hpf), whereas first secondary MN is observed 5-6 hours later than first primary MN. Secondary MNs continue to be born even after 25 hpf. Primary motor neurons are relatively large MNs ($11.3 \pm 1.4 \mu\text{m}$ in diameter). They are located towards the center of the spinal cord and have large axons ($\sim 2 \mu\text{m}$ in diameter) (Myers, Eisen, & Westerfield, 1986). Secondary MNs have smaller soma ($6.7 \pm 1.0 \mu\text{m}$ in diameter), smaller axon diameter ($> 0.5 \mu\text{m}$), and are located at the ventral third of the spinal cord. MNs within the spinal cord are spatially organized in repeated manner, so that each myotomal segment contains a similar organization of primary and secondary MNs. Along each segment, there are 3 to 4 primary motor neurons and nearly two dozen secondary motor neurons.

The primary motor neurons are classified into Caudal (CaP), Middle (MiP), Rostral (RoP) and Variable (VaP) primary MNs, based on the specific location occupied in the spinal cord (Eisen, Myers, & Westerfield, 1986). The CaP cell body is located in the middle of the spinal segment near the ventral root. The growth cone of the CaP MNs first exits the spinal cord starting around 17 hpf and grows ventrally along the medial surface of the myotome. It pauses for about an hour upon reaching the horizontal myoseptum and then extends further ventrally (Eisen et al., 1986). The axon branches extensively to innervate all of the white muscle fibers located ventral to the horizontal myoseptum (Westerfield et al., 1986). MiP MNs are located in between the RoP and CaP MN cell bodies. The MiP growth cone initially follows the pathway of CaP growth cone until it reaches the horizontal myoseptum where it pauses for nearly 30 mins and then extends caudally and dorsally to enter the dorsal myotome. As the axon grows dorsally, the ventral branches are eliminated. MiP branching is restricted to the dorsal segment, and never extends pass the horizontal myoseptum. RoP MNs are located at the rostral end of a segment.

Branching of RoP is exclusive at the dorsal segment of the ventral muscles. The RoP growth cone extends caudally within the spinal cord to exit the ventral root. They follow the path of the MiP extension to reach the horizontal myoseptum. At this point, they grow laterally forming horizontal branches, and innervate muscles flanking the horizontal myoseptum (Eisen et al., 1986). VaP MNs are present in about half of the spinal hemisegment. They are located adjacent to the CaP in the spinal cord. VaP axons only extend up to the horizontal myoseptum. Most of the VaP MNs die before further development, however a few of them can live up to the juvenile stage, where they innervate muscles dorsal to the horizontal myoseptum (Eisen, 1991). Primary MN somata show dorsal movement within spinal cord. They are first found in a ventral position and then slowly move dorsally at approximately $0.7 \mu\text{m/hr}$ between 18 and 36 hpf to finally occupy dorsolateral position of spinal cord (Myers et al., 1986).

Unlike primary MNs, secondary MNs do not have a distinct rostro-caudal relationship. Their somata do not show any movement within the spinal cord either. Menelaou & Mclean (2012) provided a categorization of secondary MNs based on their muscle innervation pattern. The dorsally projecting secondary MNs (dS) innervate muscles on the dorsal side of the body. These cells are located in a more rostral and ventral region of the spinal cord. Ventrally projecting secondary MNs (vS) are located dorsal to the dS and innervate ventral muscles only. A third class of secondary motor neurons has both dorsal and ventral axon branching and termed dorsoventrally projecting secondary MNs (dvS). These cells are located more dorsally than vS, and they are the largest secondary MNs in diameter. Axons of dS, vS and dvS have more extensive branching at deep musculature than superficial layers, suggesting they preferentially innervate white muscle fibers. Another group of secondary MNs, intermyotomal secondaries (iS) have axon collateral running superficially along the intermyotomal boundary. They preferentially

innervate red muscle fibers. Two subgroups within iS were clearly identified. One group, the inter-myotomal secondaries with collateral (iS-c) have extensive axon collaterals in both deep and superficial musculature. The other group of iS have a single axon that terminates superficially along the inter-myotomal region. They were termed as inter-myotomal secondaries with no collateral (iS-nc). iS-c MN soma are located more dorsally than iS-nc within the spinal cord (Menelaou & McLean, 2012). Axonal growth of secondary MNs is initiated around 26 hpf. Secondary MN axons exit the spinal cord as a nerve bundle, following the common path established by the primary motor axons and later arborize and innervate the muscle fibers (Pike, Melancon, & Eisen, 1992). Several axon guidance molecules including sema3A1, sema3A2, GDNF, neurexin, chondroitin sulfate have been identified that play crucial roles in the proper development of primary and secondary axogenesis (Menelaou & McLean, 2012).

1.5.3 nAChRs in Zebrafish NMJ

In zebrafish, nAChR clusters are first visible around 16-17 hpf, when CaP axons leave the spinal cord. Interestingly, the first twitching behavior is also observed along the same timeline in zebrafish embryos. At the beginning, the nAChR clusters are visible on muscle pioneer cells and close to the horizontal septum, where CaP growth cones pause before extending into the ventral myotome. As axonal branches extend along the muscle, clusters of nAChR form in a pattern that closely follows the branching of the motor neuron, initially on the medial surface of the myotome and then throughout the muscle. When muscles were devoid of MN innervation, these clusters were delayed and aberrant. However, the clustering itself does not depend on MN activity, rather it appears to depend on molecular interactions between the axonal growth cone and the postsynaptic membranes (Liu & Westerfield, 1992).

In embryonic zebrafish, nAChRs show two patterns of expression; at the myoseptum, which is located at the edge of the muscle cells, there is a condensed level of expression. The synapses in these regions are termed myoseptal synapses. Secondly, nAChR clusters are located in discrete puncta along the muscle fibers in a more distributed manner, and these synapses are called distributed synapses. Immunohistochemical studies suggest that myoseptal synapses are present on red muscle fibers whereas distributed synapses represent synapses in white muscle fibers (Park et al., 2014).

Nguyen and co-workers recorded mEPCs from dissociated muscle fibers from 1 dpf to 6 dpf and identified several changes occurring in mEPC kinetics during development. Both amplitude and frequency of mEPCs increased during the developmental period. The onset and decay kinetics of mEPCs also became faster from 1 dpf to 3 dpf and remained stable from there onwards. Single channel recordings from these fibers showed two distinct groups of events with conductance values of 45 pS and 60 pS and a mean open time of <1 ms. Additionally, there were occasional conductance levels of ~20, 35 and >100 pS, and these properties remained unaltered, suggesting that similar nAChRs are expressed during the first 3 days of development (Nguyen, Aniksztejn, Catarsi, & Drapeau, 1999).

Synaptic currents recorded from zebrafish red and white muscle fibers also show many differences. For instance, mEPCs recorded from red fibers show 5x slower decay kinetics compared to white muscle fibers (Nguyen et al., 1999). Additionally, mEPCs from red muscle fibers show inward rectification, while white fibers show no rectification (Mongeon et al., 2011). Based on single channel currents recorded from cell attached patches from the muscle fibers, and outside out patches from *Xenopus* oocyte injected with zebrafish nAChR subunits, Mongeon et

al. (2011) proposed that red muscle fibers only express $\alpha\beta\delta$ subunits whereas white muscle fibers express receptors that contain $\alpha\beta\gamma\delta$ and $\alpha\beta\delta\varepsilon$ subunits. Using morpholinos that reduced the expression of the γ subunit they observed that there were no changes in the properties of mEPCs recorded from either red or white muscle in 3 dpf animals. This result suggested that the γ subunit does not play a role in synaptic function (in 3 dpf embryos). On the other hand, knockdown of the ε subunit resulted in mEPCs from white fibers that exhibited slower decay kinetics. Thus, they argued that the NMJs of white muscle fibers express nAChRs that contain the ε subunit (Mongeon et al., 2011). Figure 1.5 shows their overall findings.

1.3.4 Locomotion in Embryonic Zebrafish

The ultimate function of the NMJ and its components is manifested through locomotion. Proper development of locomotor activity is critical for survival of an organism. Larval zebrafish exhibit two distinct types of turning behavior, a) spontaneous slow speed turn or routine turn, and b) a high velocity escape turn. Swimming in the larvae can also be categorized into slow swimming and burst swimming (Budick & O'Malley, 2000). Embryos in comparison show a changing pattern of locomotion as they develop, as described by Saint-Amant and Drapeau (1998). The first locomotor response starts at 17 hpf, when the embryos exhibit spontaneous tail coiling with alternating side to side contractions of the tail. The spontaneous behavior reaches its peak by 19 hpf and then gradually declines by 26 hpf. Around 21 hpf, embryos become sensitive to touch and exhibit vigorous coiling. Swimming is first seen at 27 hpf in response to touch (Saint-Amant & Drapeau, 1998). By the time of hatching, swimming occurs infrequently in bursts, but the frequency increases to mature levels. By 5 dpf, when the air bladder and sensory

systems are much more developed, zebrafish larvae show more frequent spontaneous bouts of beat-and glide swimming (Drapeau et al., 2002).

These different forms of locomotion require different neural and neuromuscular circuitry and are concomitant with the development of these systems. Primary motor neurons start innervating muscle fibers at 17 hpf. It is the same time when nAChRs are first detected at NMJs. Thus, the onset of spontaneous coiling at 17 hpf clearly links the development of the NMJ with this embryonic coiling activity. A subset of interneurons shows spontaneous and rhythmic activity and periodic depolarizations which are consistent with coiling contractions, suggesting a role of these interneurons in mediating the coiling activity. Interestingly, coiling contractions do not require descending inputs, and blocking chemical synaptic transmission on to the motor neurons did not affect this behavior either. However, when gap junctions were blocked, coiling contractions were significantly suppressed (Saint-Amant & Drapeau, 2001). Thus, spontaneous coiling is likely mediated by an electrically coupled spinal network.

Around 21 hpf, embryos coil their tail around their head in response to tactile stimulation. This response is the earliest manifestation of the more mature startle response, that becomes more evident around 27 hpf (Eaton, Lee, & Foreman, 2001). From 27 hpf onwards, touching the head causes a full coiling response, followed by brief swimming, that allows the embryo to reorient and escape from the stimulus. In contrast, upon receiving tactile stimulation on the tail, only partial coiling occurs followed by a brief bout of swimming, which causes the embryo to move forward, but does not reorient the fish (Saint-Amant & Drapeau, 1998). The difference in response likely occurs due to activation of a different sensory-motor system activated via head touch or tail touch. Tactile stimuli to the head activate trigeminal sensory neurons whereas

touching the tail activates Rohon-Beard sensory neurons (Drapeau et al., 2002). Both types of neurons activate Mauthner cells (M-cells), the largest interneuron pair in the hindbrain, and other reticulospinal neurons of the hindbrain (Kimmel, Sessions, & Kimmel, 1981). Activation of M-cells induces the early coiling phase of the response (Kimmel, Eaton, & Powell, 1980). The bending often causes the embryo to appear as the letter 'C', which is why it is termed C-bend response. Besides M-cells, tactile stimulation to the head activates rostral hindbrain neurons whereas more caudal neurons are activated following stimulation on the tail. Activation of these neurons likely account for the differences in locomotion observed (Drapeau et al., 2002).

Swimming, which starts around 27 hpf in response to touch, has a lower frequency of contractions in very young animals (<10Hz), but increases gradually as the embryo develops (Saint-Amant & Drapeau, 1998). At the time of hatching (2-3 dpf), the frequency approaches 80 Hz (Buss & Drapeau, 2001). Post hatched embryos generally remain idle except when they exhibit spontaneous bursts of swimming. Around 4 dpf, the larvae switch to beat-and-glide swimming, where rapid tail beats cause propulsion of the fish (beat period) and then cessation of beating allows the larvae to glide to a stop (glide period) (Buss & Drapeau, 2001). Swimming distance and frequency increases as the larva grows (Fuiman & Webb, 1988). During spontaneous swimming, the larva makes a slow and short routine turn (24-34 ms, 60°) where the greatest degree of bending occurs close to the tail. The tail beats side-to-side, with a rostral-caudal propagation of contractile waves, but the rostral half of the body only bends a little. The overall swimming episode is relatively short, and the larva only travels a small distance. During escape from a potentially harmful condition, zebrafish larvae show a fast form of swimming which is associated with a higher bend angle and they travel a greater distance. In such cases, the response starts with the generation of a rapid M-cell evoked C-bend (6-14 ms, 90-220°) followed

by a large counter-bend and then vigorous swimming. The greatest bending angle occurs around mid-body (Budick & O'Malley, 2000). Another form of swimming behavior is observed particularly during prey capturing. In such cases, the larva reorients itself to the food with several small routine-like turns. Once aligned, it moves towards the food with slow swimming, often using fins, and then uses suction to engulf the food (Budick & O'Malley, 2000). Zebrafish exclusively recruits red muscle fibers during slow swimming, whereas both red and white muscle fibers are recruited during fast swimming, and only white muscles are recruited during the fastest unsteady burst of swimming (Buss & Drapeau, 2002; Jayne & Lauder, 1994).

1.4 Research Objectives and Hypothesis

During early development, a series of key events occur which results in proper development of the NMJs and motor units' function. How development occurs in vertebrate muscle, motor neurons and nAChRs, has been extensively studied. But how development of one component affects the development of another is less well known. In particular, nAChRs undergo subunit changes which alter their kinetic properties. While this subunit switching is evident in many vertebrates, it is not clear what roles are played by these subunits during development.

In this thesis, I have tried to address these questions, using zebrafish as a model organism. Zebrafish has become a very powerful model to study vertebrate development. It is particularly advantageous to use zebrafish for studying development of NMJs in different muscle types since zebrafish muscle fibers are easily identifiable and accessible in live intact preparations. Previous studies on the development of the zebrafish NMJ examined mixed populations of red and white fibers from 3 specific time points: 24-36 hpf, 3 dpf and 6 dpf and

suggested that muscle fibers contain 2 population of nAChRs at all the ages (Drapeau et al., 2002; Nguyen et al., 1999). However, the two types of muscle fibers have very different structures, innervation patterns and functions, and thereby likely require different developmental program. Indeed, later studies examining the properties and subunit composition of nAChRs associated with zebrafish muscle fibers at 3 dpf, suggest that red fibers primarily express a receptor composed of only $\alpha_2\beta\delta_2$ subunits, whereas white fibers likely express a combination of $\alpha\beta\gamma\delta$ and $\alpha\beta\delta\varepsilon$ (Mongeon et al., 2011; Park et al., 2014). Additionally, Mongeon et al. (2011) did not find any effect of γ subunit knockdown in developing zebrafish. This was surprising since expression of the γ subunit, and the developmental switch of γ to ε subunits has been found to be conserved in various vertebrate niches. Therefore, to clarify these ambiguities in the literature as well as to determine the roles of nAChR subunits in development, I pursued my studies with two objectives-

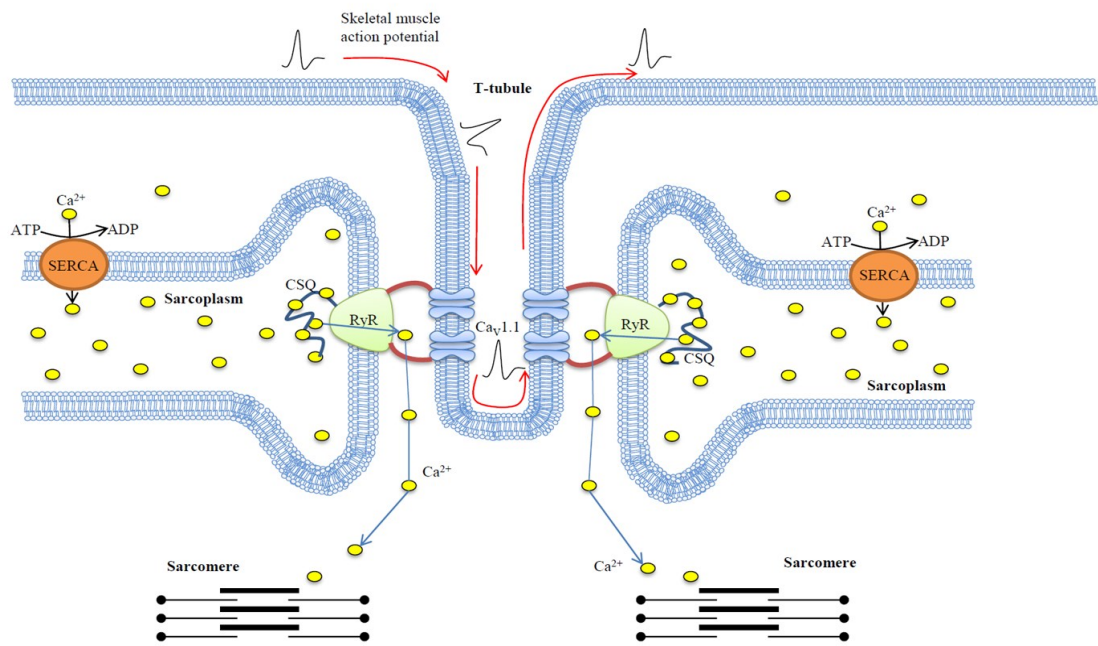
1. To determine the differential properties of nAChRs during development of zebrafish red and white muscle fibers
2. To determine the roles of the γ and ε subunits in zebrafish embryonic development.

Due to physiological and functional differences observed in red and white muscle fibers, I hypothesized that kinetic properties associated with nAChRs in red and white muscle fibers follow different developmental patterns. Also, nAChR subunits are known to play critical roles during development. Mutations in both γ and ε subunits have been linked to pathological conditions in human (Hoffmann et al., 2006; Missias et al., 1997; N. V Morgan et al., 2006; V Witzemann et al., 1996). Therefore, I hypothesize that the dynamic expression of γ and ε

subunits is pivotal for proper development of zebrafish muscle and NMJ. Particularly expression of the γ subunit at the earliest time point serves a critical role in establishing NMJ, and its persistence in red but not in white fibers in zebrafish embryos (Ahmed & Ali, 2016) is critical for locomotion of the embryos and larvae.

Figure 1.1

A)



B)

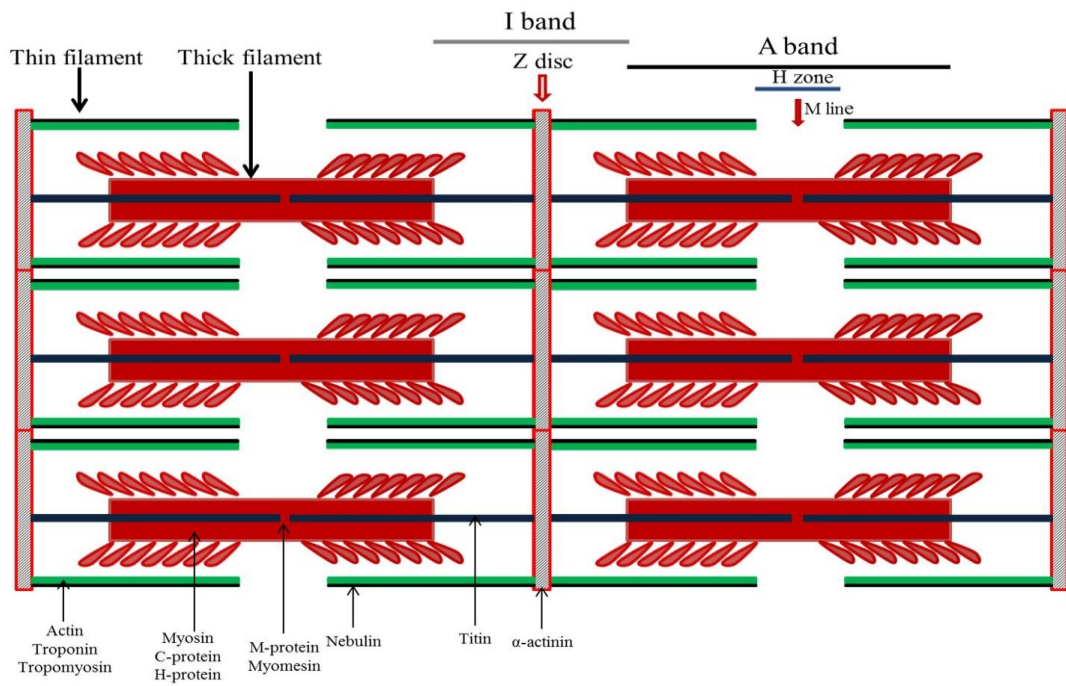


Figure 1.1

Ultrastructural details of skeletal muscle fibers. (A) Ca^{2+} transduction inside skeletal muscle. Ca^{2+} ions are stored inside sarcoplasm of sarcoplasmic reticulum. They often remain bound to network of calsequestrin (CSQ) proteins, which are associated with ryanodine receptors (RyR). RyR are physically linked to voltage sensitive calcium channel 1.1 (Ca_v 1.1) that are present on T-tubule. When action potentials traverse through the T-tubule, activation of Ca_v 1.1 physically opens RyRs. CSQ bound Ca^{2+} ions get unbound and traverse to cytosol through RyR. Ca^{2+} is necessary for activation of sarcomere complex and muscle contraction. Ca^{2+} ions are actively pumped back into sarcoplasm via sarco/endoplasmic reticulum ATPases (SERCA) pumps. **(B)** Ultrastructure of sarcomere assembly. Sarcomeres are seen as a series of dark and light bands under microscope, referred as A-band and I-band respectively. They are comprised of thick filaments and thin filaments sequentially organized and bound to Z disk. Principal proteins associated with the myofilament structures are indicated at the bottom.

Figure 1.2

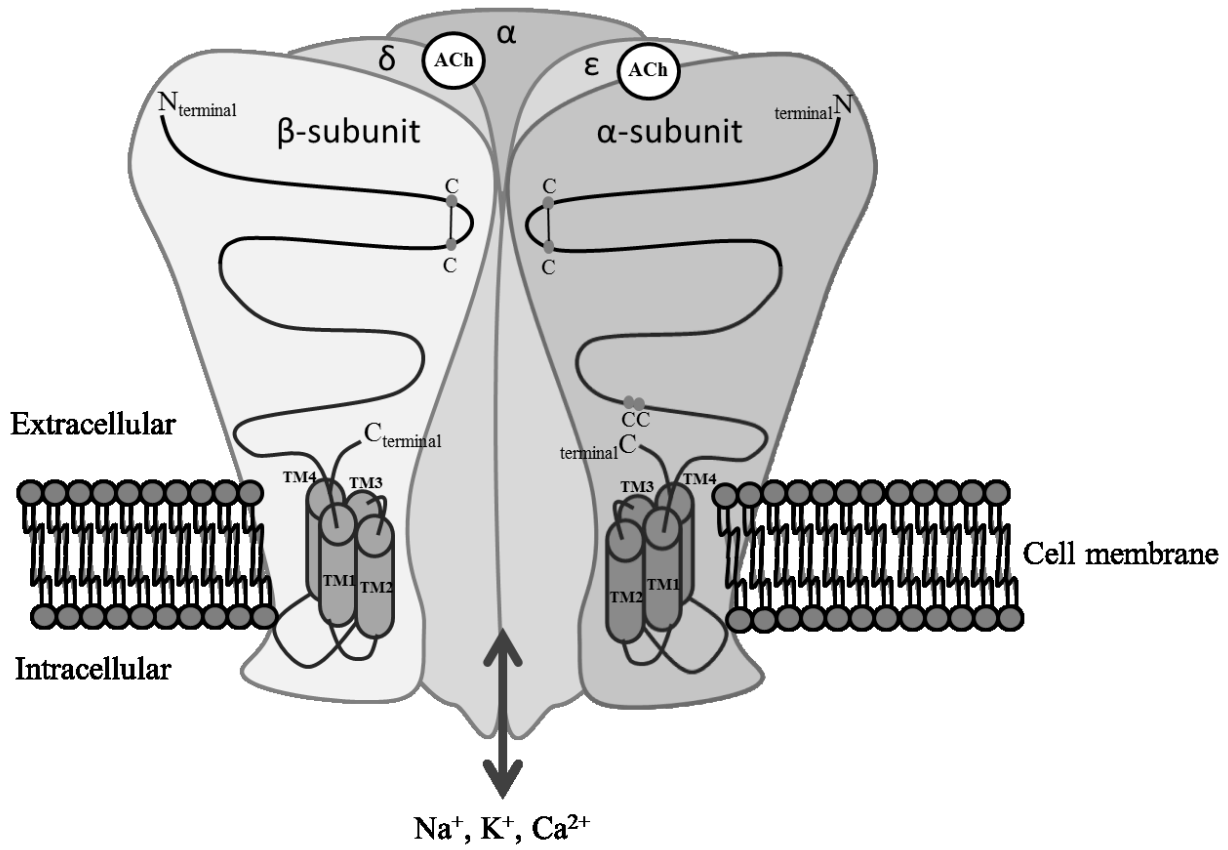


Figure 1.2

Schematic of a nAChR. nAChRs are comprised of five subunits- two α 1, one β 1, one δ and one γ/ϵ subunit. Each subunit is comprised of four transmembrane domains (TM1-4), one long extracellular N-terminal domain, and one short extracellular C-terminal domain. TM2 lines the channel pore. All subunits have characteristic cysteine disulfide bonds (C-C) at the N-terminal domain but only the α subunit contains two adjacent cysteine residues (CC) at the N-terminal side. Two acetylcholine molecules (Ach) bind to the extracellular interacting regions between α - δ and α - γ/ϵ . Upon activation, the channels allow passage of Na^+ , K^+ and Ca^{2+} ions.

Figure 1.3

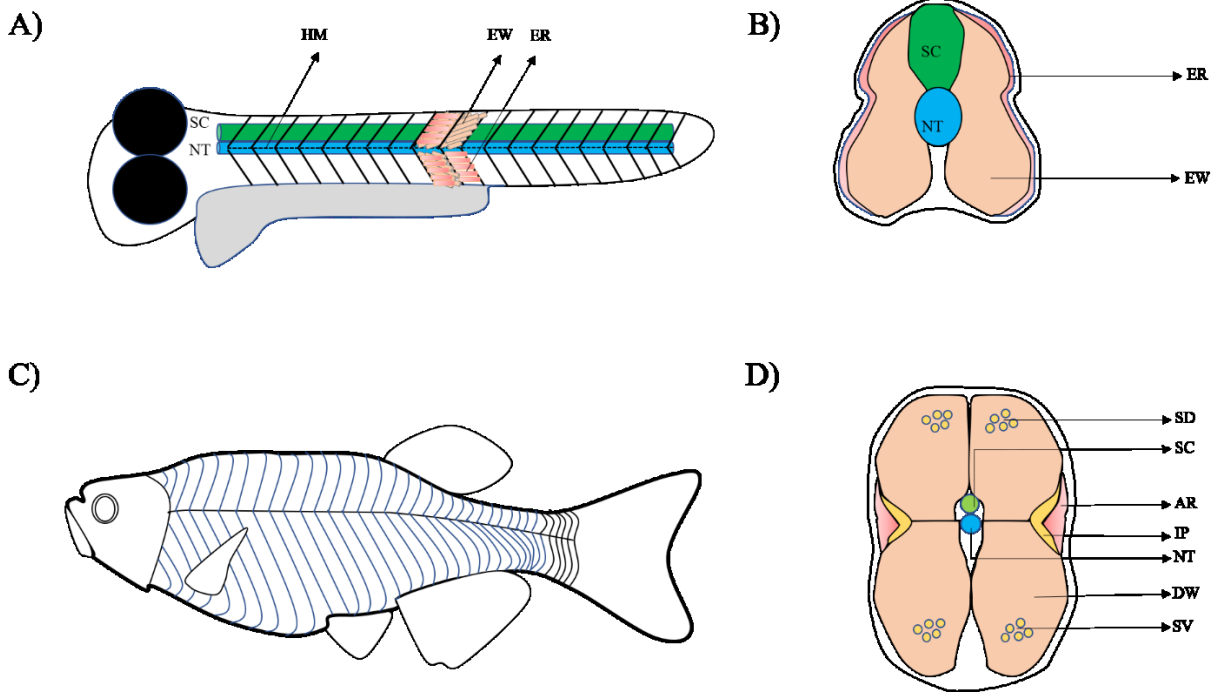


Figure 1.3

Organization of zebrafish skeletal musculature. Schematics representing zebrafish axial muscle fibers in embryos and adults. (A) Schematic of zebrafish embryo with segmented myotomes and muscle arrangement. Myotomes are separated dorso-ventrally by horizontal myoseptum (HM). Embryonic red (E_mR) muscle fibers are located on the top layer of the muscle, arranged in parallel to the body axis. Embryonic white (E_mW) muscle fibers are multilayered and located next to red fibers, forming the deeper segment of the myotome. Notochord (NT) and spinal cord (SC) are centrally located. (B) Shows a cross section of the embryo exhibiting position of the NT, SC, E_mW and E_mR . (C) Schematic of adult zebrafish. Myotomes are arranged in W-shaped segments. (D) Shows a cross section of the adult fish. Adult red fibers (AR) are the superficial layer of muscle next to the layer of intermediate fibers (IF). The deeper layers of the myotomes are comprised with deep white fibers (DW) and scattered intermediate fibers (scattered ventral, SV and scattered dorsal, SD). Notochord (NT) and spinal cord (SC) are centrally located.

Figure 1.4

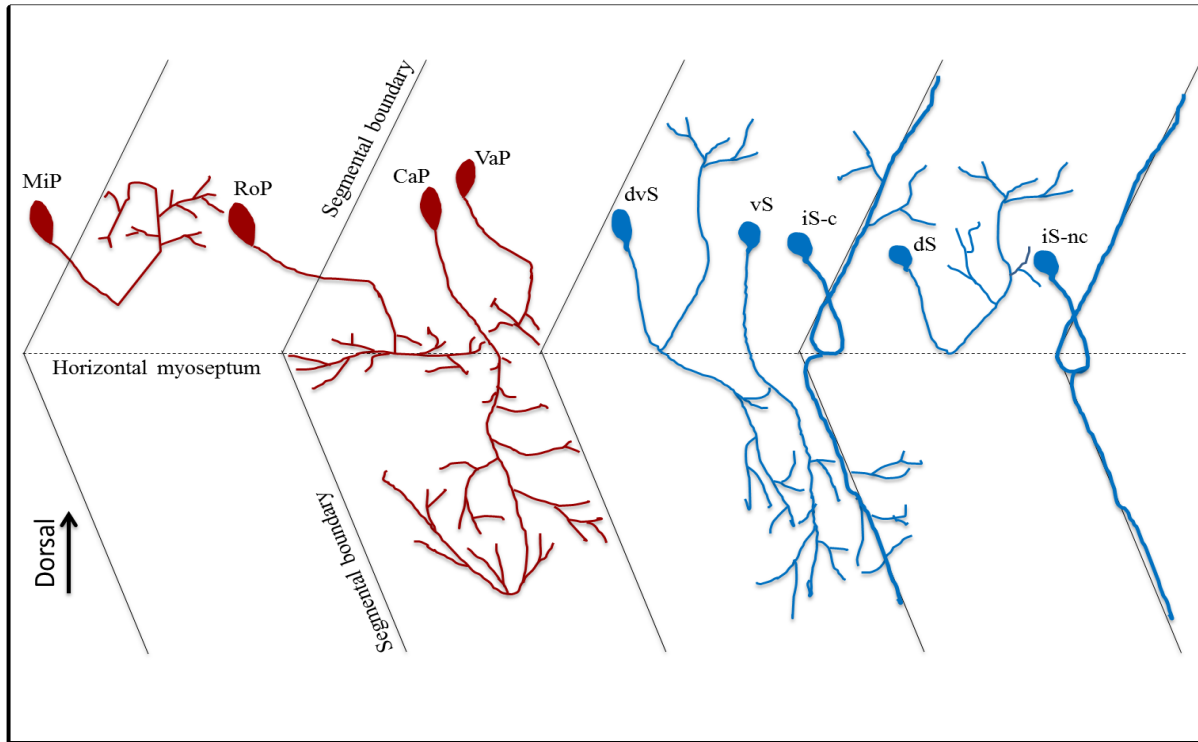


Figure 1.4

Schematic of motor neuron branching of zebrafish. Zebrafish motor neurons are classified into Primary MNs (shown in red) and Secondary MNs (shown in blue). Each motor neuron has characteristic soma location and axonal branching, based on which they are further divided. Primary MNs are subdivided into Middle Primary MN (MiP), Rostral Primary MN (RoP), Caudal Primary MN (CaP) and Variable Primary MN (VaP). Secondary MNs can be divided into dorsally projecting Secondary MNs (dS), ventrally projecting secondary MNs (vS), dorsoventrally projecting Secondary MNs (dvS), intermyotomal secondaries with collateral (iS-c), and intermyotomal secondaries with no collateral (iS-nc). Each muscle segment contains all subset of the MNs, but they are spread along the figure for easy visualization.

Figure 1.5

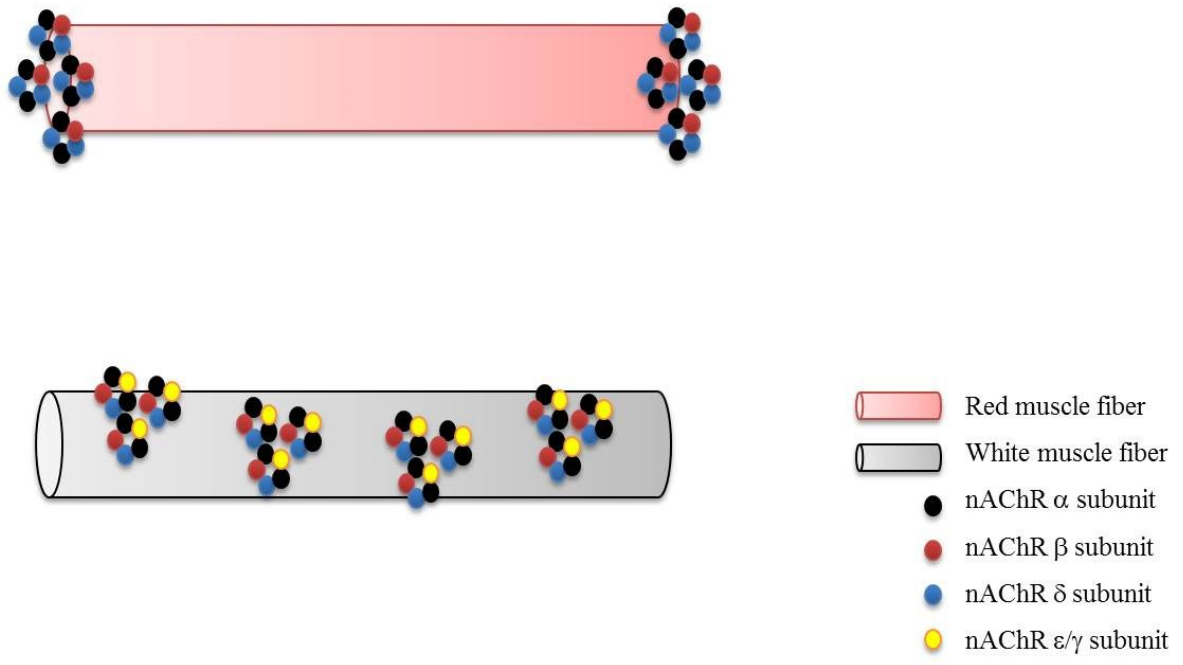


Figure 1.5

Proposed organization of nAChRs in zebrafish red and white muscle fibers according to Mongeon et al (2011) and Park et al (2014). Park et al. (2014) suggested that nAChRs are located at the myoseptal region of red fibers while they are distributed along the white fibers. Mongeon et al. (2011) suggested that nAChRs of red muscle fibers are comprised of $\alpha\beta\delta$ subunits, whereas white muscle fibers contain $\alpha\beta\delta\varepsilon/\gamma$ subunits.

Chapter 2. Materials and Methods

2.1 Animals

Wild-type zebrafish (*Danio rerio*) embryos were bred from AB colonies originally collected from the University of Oregon. Fish were raised in the aquatic facility in the Department of Biological Sciences at the University of Alberta according to established procedures (Westerfield, 2000). For breeding purposes, 2 adult female and 1 adult male was put into a breeding tank, the evening before eggs were required. The males and female were kept separated by a gate until next morning. The breeding tank had perforation at the bottom and it was placed inside a collection tank for easy separation of the eggs from the fish. The tanks were filled with facility water which is strictly maintained for ionic composition and water quality-most suitable for zebrafish maintenance. The fish were kept in the breeding tank until next morning, when eggs were required. In the morning of egg collection, gates were removed and the fish were allowed to swim and spawn together. Female fish spawn eggs while males spawn sperms and the fertilization occur in the tank almost instantaneously. Fertilized eggs were collected within 25 mins of raising the gate by replacing the breeding tank into a new collection tank filled with water. A single group of fish can thus be put into several cycle of spawning over a period of 2-3 hours. Eggs settle down at the bottom of the collection tank and can be collected by tilting the tank to discard most of the water while collecting the eggs in a petri dish. Collected eggs were immediately cleaned to remove any debris and rinsed with Egg Water (60 µg/mL “Instant Ocean”, United Pet Group, Cincinnati, OH, USA). Embryos were raised in the petri dish containing Egg Water and kept inside an incubator at 28.5° C until they were used for

experiments. If the embryo remained unhatched at the time of the experiment, a pair of forceps was used to tear open the chorion to allow it to swim freely.

2.2 Morphological Observations and Imaging

For morphological observations, whole embryos or larvae were placed in a 16-well plate with one fish per well and observed using a dissecting microscope. Curved body (axial malformation), swelling in the pericardium (pericardial edema) and curved tail regions were scored as abnormal morphology. Fish were imaged using a Lumenera Infinity2-1RC (1.4 Megapixel) microscope camera (Lumenera Corp., ON, Canada) mounted on a light microscope (Leica DM2500, Leica Microsystems Inc) with 2.5x optical lens.

2.3 Immunohistochemistry Staining

For immunohistochemistry staining, embryos were raised in embryo media containing 0.003% Phenylthiocarbamide (PTU, Sigma Aldrich) from 1 dpf onwards. Embryos (2 dpf) or Larvae (5 dpf) were fixed in 2% paraformaldehyde (PFA, Sigma Aldrich) for 2 h and washed with 0.1 M phosphate buffered saline (PBS) every 15 minutes for 2 hours. The preparations were then permeabilized for 30 min in 4% Triton-X 100 containing 2% BSA and 10% goat serum. Tissues were incubated in the primary antibodies for 48 hours at 4°C. Next, they were washed in PBS twice every 15 minutes for 2-3 hours and then incubated for 4 hours at room temperature in the secondary antibody conjugated with Alexa Fluor® 555 or Alexa Fluor® 488 (Molecular Probes, Life Technologies), at a dilution of 1:1000. To stain nAChRs, tissues were incubated overnight with 100 nM of α -Bungarotoxin, Alexa Fluor® 488 Conjugate (Molecular Probes, Life Technologies) at 4° C. They were then washed for 7 h with PBS and mounted on glass slides

with Mowiol mounting media (Mowiol 4-88, Glycerol, Tris-Cl, DABCO). All embryos were imaged on a Zeiss LSM confocal microscope and photographed under 20x or 40x objective lenses. Images were compiled using Zeiss LSM Image Browser software and are shown as maximum intensity compilation of z-stack images.

All of the primary and secondary MN images were visually inspected to determine if there were any abnormalities in branching patterns that could be readily identified when comparing to control fish. No further quantification was done on the primary MN and secondary MN images. For calculating the number of nAChR puncta stained by α -bungarotoxin, maximum intensity projections of the α -bungarotoxin stained images were created using ZEN 2.3. Puncta were quantified from the images using ImageJ. A color threshold was applied to each image in such a way that distinct puncta were acquired, whereas non-uniform or faint stains were discarded. The image was then split into grids, with each grid-square covering 30000 pixel² (1450 μm^2). Puncta were counted from a total of 3 grid-squares along the same myoseptum pair using ImageJ's particle analyzer and were sorted based on size. Puncta less than 10 pixel² (0.483 μm^2) akin to scattered dots did not conform to known NMJ structures and were excluded from further analysis.

2.4 Reverse-Transcription Polymerase Chain Reaction (RT-PCR) of RNA from Whole Embryos and Adult Muscle

2.4.1 RNA Extraction

For RNA extraction, muscle from 5 adult fish were dissected out, or set of 30-60 whole embryos or larva was used at a time. Fish or their dissected muscles were placed in a sterile 1.5

mL microtube (Axygen) and 1 mL TRIzol reagent (Ambion, Life Technologies) was added into each tube. Autoclaved pellet pestles and pellet pestle motor (Kimble Kontes) were used to homogenize the samples. The homogenized samples were incubated for 5 mins at room temperature followed by addition of 0.2 mL chloroform and centrifugation at 12000 x g. The mixture then separates into an upper aqueous phase, an interphase and a lower phenol-chloroform phase. RNA remains exclusively in the upper aqueous phase. The aqueous phase was pipetted out into a new sterile 1.5 mL microtube, 0.5 mL isopropanol was added, and the mixture was centrifuged for 10 mins at 12000 x g. The RNA formed a pellet at this point which was washed with 75% ethanol and resuspended in 20 μ L nuclease free water. The concentration and purity of this RNA was determined by NanoDrop spectrophotometry (Thermo Scientific). RNA stocks were stored at -80°C when not in use.

2.4.2 Reverse Transcription

cDNA was synthesized from 1 μ g of the RNA stocks using a Maxima First Strand cDNA Synthesis kit (Thermo Scientific). The template RNA was mixed with 4 μ L of 5x Reaction Mix, 2 μ L of Maxima Enzyme Mix and nuclease free water to make up to 20 μ L solution. The mixture was incubated for 10 min at 25° C, 15 min at 50° C and 5 min at 85° C to complete the reverse transcription reaction. The final cDNA concentration was measured using NanoDrop spectrometry. cDNA stocks were stored at -20° C when not in use.

2.4.3 RT-PCR

RT-PCR was carried out using DreamTaq Green PCR MasterMix (Thermo Scientific). Primers (Table 2.1) were designed using the NCBI's Primer-BLAST program. The PCR

reactions contained: 10 μ L MasterMix, 1 μ M forward and reverse primers, <500 ng of template cDNA and nuclease free water to make the final volume to 20 μ L. The reactions were run in an Eppendorf Mastercycler Gradient thermocycler under the following conditions: initial denaturation 98°C 30 s; and then 30 cycles of 98°C 10 s, 60°C 30 s, 72°C 15 s; followed by a final elongation step of 72°C for 10 min. The annealing temperature was changed to 57°C instead of 60°C for full length gamma transcript. PCR products were run on a 2.5% agarose gel, stained with ethidium bromide for 10 min followed by 10 min wash with double distilled water. The gel was visualized and imaged under UV in AlphaImager 2200 Gel Documentation System (Alpha Innotech). EF1 α 111, a commonly used regulatory housekeeping gene for zebrafish was used as a positive control (Tang, Dodd, Lai, McNabb, & Love, 2007).

2.5 Dissection

For dissection, an embryo was placed in a recording chamber and anaesthetized in 0.02% tricaine (MS-222; Sigma Chemical St. Louis, MO, USA) extracellular solution. The anaesthesia was confirmed with a tail pinch. Two tungsten pins were used to pin the embryo through its notochord into a sylgard lined dish; The first pin was positioned at the level of the yolk sac and the second at the furthest caudal region possible. A pair of fine forceps was used to remove the uppermost layer of skin overlaying the axial musculature between the two pins. After dissection, the viability of the preparation was determined based on the presence of heartbeats. All experiments were performed in accordance with the University of Alberta's animal care guidelines and the Canadian Council of Animal Care (CCAC).

2.6 Identification and Access to Muscle Fibers

Muscle fibers were visualized under Nomarski Differential Interface Contrast (DIC) optics and I could easily identify and access them based on their position and orientation. Red muscle fibers lie just underneath the skin and could easily be accessed once the skin was removed. To access the white fibers, which are situated underneath the red fiber layer, a few of the upper red fibers were removed with fine forceps or a glass pipette pulled for electrophysiology recording.

2.7 Quantitative Real Time PCR (RT-qPCR) of Individual Muscle Fibers

2.7.1 Individual Muscle Fiber Intracellular Content Collection

Patch-clamp pipettes with tip diameters of 4–8 μm were pulled from thin-walled borosilicate glass capillaries, which were filled with a CsCl based intracellular solution (ICS_{CsCl}) consisted of (mM): 130 CsCl, 8 NaCl, 10 HEPES, 10 EGTA, 2 $\text{CaCl}_2 \cdot 2\text{H}_2\text{O}$, 4 Mg-ATP, 0.4 Li-GTP; pH- 7.4 and osmolarity- $290 \pm 2 \text{ mOsmol l}^{-1}$. The whole cell, patch clamp configuration was performed on identifiable single red or white muscle fiber and most of the cellular contents were collected from the fiber by applying small amount of suction. The contents were spilled into 1.5 ml sterile microtube kept in dry ice by breaking the pipette tip at the bottom and applying a small amount of positive pressure. Each microtube contained cellular contents from 3-6 fibers of the same type (red or white) from a single embryo. The tubes were stored in dry ice or at -80°C freezer until further use.

2.7.2 Quantitative Real Time PCR

To analyze the expression of different nAChR subunit mRNA from identifiable red or white fibers from 1.5 dpf, 2 dpf and 5 dpf embryos, pre-validated TaqMan Gene expression assays (Life Technologies) and Ambion Single Cell-to-CT kit (Life Technologies) were used according to the manufacturer's instructions. Predesigned assays were ordered for *chrna1* (nAChR α 1 subunit), *chrnd* (nAChR δ subunit) and *chrne* (nAChR ϵ subunit), and custom designed assays were used for *chrnb1l* (nAChR β 1a subunit), *chrnb1* (nAChR β 1b subunit) and *chrng* (nAChR γ subunit). Predesigned assays for *actb1* (β actin protein) and *rpl13a* (ribosomal protein L13a) were used as endogenous control.

Briefly, 1 μ l of Single Cell DNase I and 9 μ l of Single Cell Lysis Solutions were added to microfuge tubes containing 3-6 cell contents and incubated for 5 min at room temperature. 1 μ l of Single Cell Stop Solution was added thereafter and the mixture was incubated at room temperature for 2 min followed by placing them in ice. For reverse transcription, 3 μ l of Single Cell VILO RT Mix and 1.5 μ l of Single Cell Superscript RT was added and incubated at 25°C for 10 min, 42°C for 60 min and finally at 85°C for 5 min. The reverse transcribed samples were then preamplified by adding 5 μ l of Single Cell PreAmp Mix and 6 μ L of 0.2x pooled TaqMan Gene Expression Assays, and running 1 cycle of 95°C for 10 min, 14 cycle of 95°C for 15 sec + 60°C for 4 min, and finally 1 cycle of 99°C for 10 min. The preamplified products were diluted to 1:20 in 1X TE buffer for Real Time PCR reaction.

Quantitative real-time PCR was carried out with the 7500 Fast system (Applied Biosystems). For each reaction (10 μ l), 5 μ l of 2x TaqMan Gene Expression Mastermix, 0.5 μ l of 20x TaqMan Gene Expression Assay and 2.5 μ l of Nuclease-free water was added to 2 μ l of

preamplified product diluted to 1:20. The thermal profile included a holding step of 50°C for 2 min followed by another holding step of 95°C for 10 min, and 40 cycles including denature at 95°C for 5 sec and anneal/extend at 60°C for 1 min. All samples were run in triplicate and the threshold cycle (C_t) was determined automatically by SDS software (Applied Biosystems). Outliers possibly originating from inaccurate pipetting were omitted and C_t values were averaged. Comparative C_T Method ($\Delta\Delta C_T$) was used for data representation with box plot showing entire range of fold change (upper and lower level), midline representing the mean value. I used *Chrna1* as calibrator, to compare all expression value relative to nAChR $\alpha 1$ subunit, which is an essential subunit of nAChR in muscle. No template controls (NTC) were included for each assay in every plate as negative control. For validation, the ΔC_T values were plotted against log of dilutions to create semi-log regression lines, and their slopes were determined.

2.8 Morpholino Oligonucleotide Mediated Knock-down of nAChR Subunits

Morpholino oligonucleotides (MO) are used to bind to a target sites where they block access of other cellular components. Thus, a MO is designed to bind to a specific sequence of RNA and in so doing, it prevents proper processing of the RNA. MOs are widely used to knockdown expression of proteins in embryonic zebrafish. There are two categories of MOs: translation blocking and splice blocking morpholinos. Translation blocking MOs bind to the 5' untranslated region of mRNA and sterically blocks the translation initiation complex, resulting in a reduction of the translated protein. The level of protein knockdown can be assessed by semi-quantification through western blot or immunohistochemistry, depending on the availability of specific antibodies. However, as it does not degrade or alter the target mRNA, RT-PCR is

ineffective in detecting the efficacy of translation blocking MOs. In contrast, splice blocking MOs bind to the pre-mRNA level. They are usually designed to bind to a junction between an exon and an intron, and modify the pre-mRNA splicing events that generate mRNA. The alteration of the splicing results in an intron inclusion in the mRNA, or an exon is excluded from the mRNA. In either case the alteration results in altered mRNA that leads to the production of an abnormal protein. The efficacy of splice blocking MOs can be assessed by RT-PCR of the mRNA. However, unlike gene knockout, MOs do not reduce the expression of a protein by 100%. Proper delivery of MOs can also be challenging and in zebrafish, they may lose their efficacy after 4-6 days. MOs can also induce off target effects which are often difficult to determine or control (Eisen & Smith, 2008).

2.8.1 Morpholino Design

Morpholino oligonucleotides were obtained from Gene Tools, LLC (Oregon, USA). Sequences for translation blocking MOs were acquired from Mongeon et al. (2011). 5'TGCCGAATCTCTCG GCCACGGCCAT3' was used to block translation of ϵ subunit (MO- E_M), and 5' CATGGTTGAAATCCTGAGAGAAACA3' was used to block translation of γ subunit (MO- G_M). To block specific splice junctions of γ and ϵ subunit pre-mRNA of nAChRs and thereby knocking down their expressions, I used a set of splice blocking MOs. Target mRNA sequence was provided to GeneTools and sequences for splice blocking MOs were requested. According to their design and suggestions, 5'TTTACTGCCAACTCACTTGTTTTCC 3' MO was used to target exon4-intron4 splice junction of ϵ subunit (MO-E) and 5'GCCCATCCACACTTTACACACATAC3' MO was used to target intron4-exon5 splice

junction γ subunit (MO-G). MOs were diluted in sterile water to make a stock solution of 1mM and stored in 4°C.

2.8.2 Microinjection

MOs were microinjected into 1-4 cell stage of zebrafish embryos (0-1 hpf). MO stocks were diluted in 1x Danieau solution (mM: 58.0 NaCl, 0.7 KCl, 0.4 MgSO₄, 0.6 Ca(NO₃)₂, 5.0 HEPES, pH 7.6) containing 0.05% Phenol Red. Microinjection was done using Picospritzer II (General Valve Corporation, NJ, USA) and Borosilicate glass pipette with filament (1.2 mm outer diameter, 0.94 mm inner diameter; Sutter Instrument) pulled with a Flaming/Brown Micropipette Puller (P97, Sutter Instrument). The tip of the pipette was slightly broken to allow a small volume of solution to come out. Pulse duration (ms) and pressure (psi) was calibrated from the picospritzer to eject a droplet of solution with 0.125 mm diameter in mineral oil resulting in the ejection of 1nl solution(Picospritzer III manual).

For translation blocking MOs (MO-E_M and MO-G_M), 1 nl volume was injected from 1 μ M stock concentration of MO solutions. For splice blocking MOs (MO-E and MO-G), each MO was injected in four different concentrations – 1, 2.5, 5 and 7.5 ng/nl - to determine the highest dosage without MO-induced nonspecific toxicity. MO-G induced nonspecific toxicity at 5ng/nL and higher while MO-E showed nonspecific toxicity at 7.5ng/nl. Therefore MO-G and MO-E were used at concentrations of 2.5 and 5 ng/nl respectively.

2.8.3 Confirmation of Altered Splicing

RT-PCR was performed to confirm that splice blocking MOs alter the splicing of pre-mRNA. Splice blocking MOs disrupt splicing of pre-mRNA, producing mRNA with excised

exon, or inclusion of intron. This is shown by a misplaced PCR amplicon band in agarose gel. I collected mRNA from 5 dpf embryos, synthesized cDNA and ran PCR with them as described previously. Primer pairs were designed (Table 2.2) such that they span the MO binding site. Presence of multiple bands confirmed that the MOs resulted in altered splicing. Also, presence of multiple bands confirmed that effects of the splice blocking MOs were persistent at 5 dpf.

2.9 Electrophysiology

2.9.1 mEPC Recording

Whole-cell patch clamp recordings were taken from muscle cells of embryos at 30 hpf, 1.5 dpf, 2 dpf, 3 dpf, 4 dpf and 5 dpf. Recordings were not obtained from fish older than 5 dpf because the larger fibers are prone to space clamp errors. Patch-clamp electrodes were pulled from borosilicate glass (GC150T; World Precision Instruments, Sarasota, FL, USA) on a P-97 pipette puller (Sutter Instrument Co., Novato, CA, USA) and fire-polished (Micro-Forge MF-830; Narishige, Japan); and filled with the ICS_{CsCl}; pH- 7.4 and osmolarity- 290 ± 2 mOsmol l⁻¹. Once filled with intracellular solution, the pipette tips had series resistances of 1.0-3 M Ω . An extracellular solution (ECS), which consisted of (mM): 134 NaCl, 2.9 KCl, 2.1 CaCl₂.2H₂O, 1.2 MgCl₂.H₂O, 10 D-glucose and 10 HEPES, with an osmolarity of 290 ± 2 mOsmol L⁻¹, adjusted to pH 7.8, was bubbled with air and continuously washed over the preparation, starting ≥ 5 minutes prior to recording. The ECS contained the voltage-gated Na⁺ channel blocker tetrodotoxin (TTX; Tocris, UK) at a concentration of 1 μ M in order to block action potentials during mEPC recordings. Previous examination has shown that both muscle fiber types are extensively coupled early in development (Luna & Brehm, 2006), so the gap junction blocker carbenoxolone (Sigma Chemical St. Louis, MO, USA) was included in all extracellular solutions at a concentration of

100 μ M. Red and white muscle fibers were easily and accurately identified based on their orientation within each segment using Nomarski Differential Interference Contrast (DIC) optics (Buckingham & Ali, 2004), and whole cell voltage-clamp recordings were taken over periods of 1 minute. Whole cell currents were recorded at a holding potential of -60 mV using an Axopatch 200B amplifier (Axon Instruments, Sunnyvale, CA, USA), low-pass filtered at 5 kHz and digitized at 40-50 kHz. Once in the whole cell recording mode, the fibers had series resistances from 2-4 M Ω . Synaptic currents were recorded in 1-minute epochs. After each 1-minute recording the series resistance was checked and if it had changed by more than 20%, the recording was aborted. Recordings were maintained as long as the membrane resistance remained greater than 10x the series resistance. Series resistances were compensated by 60-90% using the amplifier's compensation circuitry.

2.9.2 Analysis of mEPCs

Miniature endplate currents (mEPCs) were monitored using AxoGraph X v1.5.4 software (Axon Instruments). Recordings were examined by the software, and synaptic events were detected using a template function. Overlapping or misshapen events were removed and the remaining events were averaged and the properties (amplitudes, decay time constants, frequencies) of the averaged trace were recorded. Decay time constants were determined by fitting single or double exponential functions over the decay component (peak of the event to the baseline) of each individual mEPC event. Additionally, single exponents were fit over the initial (fast) decay portion and over the distal (slow) portion of the decay. For each n, currents were recorded from a single red or white muscle fiber from a single embryo.

2.9.3 Single Channel Recording

Outside-out patch clamp recordings at voltage levels of -60 mV, -70 mV, -80 mV and -100 mV were taken from muscle cells of embryos at 1.5 dpf, 2 dpf and 5 dpf. Outside-out patches were taken from the middle of fiber, where nAChRs are clustered and neuromuscular innervation occurs (Liu & Westerfield, 1992). Patch clamp micropipettes were pulled from thick-walled borosilicate glass tubing (GC150T; World Precision Instruments, Sarasota, FL, USA) as mentioned above. The pipette was filled with a KCl based ICS (ICS_{KCl}) consisted of (mM): 130 KCl, 2 MgCl₂·2H₂O, 10 HEPES, 10 EGTA, 10 D-Glucose, and 4 Mg.ATP; the pH was adjusted to 7.4 and osmolarity was adjusted to 280±2 mOsmol. Once filled with intracellular solution, the pipette tips had series resistances of 3 - 4 MΩ. Same ECS used for mEPC recordings were used for single channel recordings. The ECS also contained the voltage-gated Na⁺ channel blocker tetrodotoxin (TTX; Tocris, UK) at a concentration of 1 μM, however no carbenoxolone was added to it. To activate the nAChRs, 0.6-0.8 (μM) ACh was added to the ECS. For the negative control, 1 μM of curare (nAChR antagonist) in normal ECS+TTX was used. Single channel currents were recorded using an Axopatch 200B amplifier (Axon Instruments, Sunnyvale, CA, USA), low-pass filtered at 5 kHz and digitized at 50 kHz.

2.9.4 Single Channel Analysis

Clampfit 9 software (Axon Instruments, Sunnyvale, CA, USA) was used for single channel analysis. Traces were digitally filtered offline at 5 kHz, and events higher than 20 pS conductance were accepted. Level contribution of 10% were used with automatic level update, and short level changes (<0.2 ms) were ignored. Overlapping events were not analyzed, and patches with significant event overlaps were rejected. Very brief event amplitudes are

affected by filtering and hence their actual amplitude cannot be determined. Therefore, events briefer than 150 μ s in duration were not considered for analysis.

2.9.5 Ensemble Average of Single Channel Recordings

Ensemble averages of single channel events recorded at -100 mV from the outside out patches were built and analyzed using Axograph X. The traces were filtered offline by 5 kHz and single channel events were detected using appropriate templates that identify all the events. All the misshaped and overlaying events were then discarded by visual inspection, and only fully resolved events were selected. These events were then used to create ensemble averages from which the decay time constants were determined in a similar fashion to the mEPC analysis.

2.10 Fictive Swimming of 2 dpf Embryos

2 dpf embryos were immobilized in 2% low-melting point (26-30°C) agarose (LMPA) dissolved in embryo medium (Sigma-Aldrich 2-Hydroxyethylagarose, type VII low gelling temperature). To observe embryo movements, the LMPA was cut away from the embryo's trunk and tails while leaving the heads embedded in the gel. Embryo media was added to the petri dish to ensure that the larvae remained immersed in solution. Embryos were allowed to acclimate to their environment for 20 minutes prior to stimulus application. Borosilicate glass micropipettes (Sutter Instrument; O.D.: 1.2 mm, I.D.: 0.94 mm, 10 cm length) were pulled using a Flaming/Brown Sutter Instrument pipette puller (model P-97). The pipettes were positioned as close as possible to the embryo's otolith without contacting the embryo. Embryo stimulation was performed using a 15 ms pulse of basic 2% phenol red (Sigma-Aldrich) dissolved in embryo media ejected from a Picospritzer II (General Valve Corporation). Behaviors were recorded for

1.5s following the stimulus. This period of time was long enough to film the escape response and periods of swimming following the C-bend. The video-recordings were transferred and analyzed using a Motion Analysis Software, ProAnalyst® (Xcitex Inc., Cambridge, MA, USA).

2.11 Sound Mediated Free-swimming of 5 dpf Larvae

Larvae were taken in a 35mm x 10mm petri dish (Corning Incorp., NY, USA) filled with embryo media, placed under the microscope, and left for 2 mins for acclimatization. Two sound boxes (AOPEN. MS-608 pro) were placed adjacent to the sides of the petri dish to deliver sound tone (300 HZ frequency, 150 ms duration) generated by Audacity open-source software (Audacity 2.1.2) running from a PC. The video-recordings were transferred and analyzed using a Motion Analysis Software, ProAnalyst® (Xcitex Inc., Cambridge, MA, USA).

2.12 Spontaneous Free-swimming Behavior at 5 dpf Larvae

To track behavioral activities, larvae at 5 dpf were placed in a 96 well plate and then their movements were recorded for analysis. Larvae were placed gently into the center of wells containing 150 µl egg water, pH 7.0 and 48 wells were used each time from a 96 well plate in our study (Costar #3599). Prior to video recording, larvae were acclimated in the well plate for 60 minutes. Plates were placed on top of an infrared backlight source and a Basler GenlCaM (Basler acA 1300-60) scanning camera with a 75 mm f2.8 C-mount lens, provided by Noldus (Wageningen, Netherlands) was used for individual larval movement tracking. EthoVision® XT-11.5 software (Noldus) was used to quantify the swimming parameters. Analyzed parameters included % activity (which is the percentage of the total time the fish remain active, measured as changes in pixel level between successive frames), frequency of movement (how many times the

fish moved beyond a set threshold level within a 1 hour period of time), cumulative duration of movement (total length of time the fish was active in an hour), total distance moved in an hour, mean velocity during swimming, maximum velocity and acceleration attained during swimming, mean angle of turn and mean angular velocity. All of these parameters were analyzed automatically by the software. However, data was manually examined for accuracy. If any value was identified to originate from tracking mistake by the software, the data point was manually omitted.

2.13 Statistical Analysis

All data values are given as means \pm SEM. Correlations were calculated with the use of a least-squares linear regression analysis. Significance was determined using a one-way ANOVA followed by a Tukey post-hoc multiple comparisons test where appropriate ($p < 0.05$). When normality tests failed, a Kruskal-Wallis one-way ANOVA on ranks was performed followed by the Dunn's method of comparison. Statistical analysis was done using SigmaPlot 12.0 (Systat Software, San Jose, CA) or GraphPad Prism v7 (GraphPad Software, San Diego, CA).

Table 2.1: List of primers used for RT-PCR

Gene	Primer Sequence (5'□3')	Product Length (bp)
chrna1	TGCCTTACCTCTACGGACCA	452
	GTTCTGCAGGTCGAAGGGAA	
chrnb1	TGTGCAGGCCTACAGTAACG	819
	CCGTCAGGCTGGTATCTGTG	
chrnb11	ACGGCTCTAGGAAGGCATCT	262
	GGAGGAATGCGCACAACATC	
chrng	AGAACAATGTGGATGGGCGT	847
	TCCGCCTTCGCTATTAACCC	
chrnd	CACTCCCAAAGCCACGTACA	260
	ACGCTGGTGGCTGATTGTAA	
chrne	ATCGTCTTGCGTGGAACACA	220
	GGGATTATAAAATGCAGTTGGTCAC	
eefla111	GGCCACGTCGACTCCGGAAAGTCC	392
	TCAAAACGAGCCTGGCTGTAAGG	

Table 2.2. RT-PCR primer sequences used for validation of splice blocking MOs

Gene	Primer Sequence (5'□3')	Product Length (bp)
chrne	TCACTGGGAATGAAGAGTCACA	220
	TACTCAGATGTGTTCCACGCAA	
chrng	ATGGATCAAAACCTTTCCTCAAAA	1061
	TTCAACAACACCTTCTGATGG	
eef1a111	GGCCACGTCGACTCCGGAAAGTCC	392
	TCAAAACGAGCCTGGCTGTAAGG	

Chapter 3. Results- General Development

The current literature on the development of NMJs in zebrafish muscle has contradictory findings. Nguyen et al. (1999) suggested that zebrafish muscle fibers continuously express multiple types of nAChRs throughout the embryonic and early larval developmental period studied (1-6 dpf). In contrast, Mongeon et al. (2011) suggested that zebrafish red and white muscle fibers differ in their expression of nAChRs at 3 dpf time point. To attempt to clarify the ambiguity and to determine the developmental differences at the NMJ of zebrafish red and white muscle fibers, I set out to determine the properties of nAChRs associated with the developing synapses of zebrafish red and white muscle NMJs. I first obtained whole cell patch clamp recordings of mEPCs from red and white muscle fibers between the ages of 1 dpf and 5 dpf. Analysis of the mEPC kinetics revealed synaptic differences between developing red and white muscle fibers. Next, I recorded single channel currents from the fibers at some crucial time points of synaptic development (36 hpf, 2 dpf and 5 dpf) to determine the kinetic properties of underlying nAChRs expressed at the NMJs. Single channel currents provided important insight into the subtype of nAChRs likely present in the muscle fibers. Finally, to identify which subunits of nAChRs were expressed in the developing red and white muscle fibers, I studied the molecular expression of nAChR subunits through RT-PCR and single cell RT-qPCR. The results identified differences in the molecular expression of different subunits in developing red and white muscle fibers.

3.1 mEPC Recording from Developing Red and White Muscle Fibers

To determine if the kinetic properties of nAChRs at red and white muscle fibers differ during development, I recorded miniature end plate currents (mEPCs) from zebrafish red and

white muscle fibers at different ages. I recorded in the whole cell patch clamp mode from muscle fibers of zebrafish embryos and larvae aged 30 hpf, 1.5 dpf, 2 dpf, 3 dpf, 4 dpf and 5 dpf. I recorded very few events from 30 hpf embryos and was unable to perform a proper statistical analysis of the data. In fact, 4 out of 6 recordings were altogether devoid of mEPCs; therefore, I focused on the mEPCs recorded from older fish, aged 1.5 dpf to 5 dpf. Example traces of recordings taken from red and white muscle fibers of 1.5 dpf, 2 dpf and 5 dpf fish are shown in Figure 3.1 and 3.2 respectively.

Nguyen et al. (1999) reported a developmental increase in the frequency and amplitude of mEPCs recorded from dissociated muscle fibers. I observed similar developmental changes in mEPC recordings obtained from in situ, intact red and white fibers (Fig 3.3, 3.4). At 1.5 dpf, mEPC frequency was 0.030 ± 0.005 Hz in red fibers (n=7) and 0.25 ± 0.11 Hz in white fibers (n=6). There was no significant change in frequency for the first 3 days of development, after which the frequency increased significantly to 0.45 ± 0.11 Hz (n=10; p=0.0002) in red fibers and 1.10 ± 0.18 Hz in white fibers (n=8; p=0.0001) by 5 dpf (Fig 3.3). The mean amplitude of mEPCs recorded from red fibers increased significantly from 0.71 ± 30 nA in 1.5 dpf (n=8) to 1.43 ± 0.18 nA in 2 dpf (n=8), but then showed a trend of steady decrease down to 0.81 ± 0.06 nA in 5 dpf fish (n=10) as development proceeded (Fig 3.4 A). In white fibers, there was a significant increase in the mean mEPC amplitude from 0.12 ± 0.06 pA (n=6) at 1.5 dpf to 1.34 ± 0.13 nA (n=9; p, 0.0001) at 2 dpf (Fig 3.4 B). However, contrary to red fibers, no further developmental change in amplitude was observed in mEPCs from white fibers.

For both fiber types, scatter plots of single exponential decay times vs. event amplitudes showed a cluster of long decay, low amplitude events (<250 pA) in the younger embryos;

whereas mEPCs in the older fish tend to have rapid decays (~1-2 ms) and highly variable amplitudes (100 pA – 2.5 nA) (Fig 3.5), as previously shown (Luna & Brehm, 2006; Nguyen et al., 1999).

Next, I examined the exponential decay component of the mEPCs. The decay time reflects the mean open time of the channels that underlie the synaptic event and may offer information with respect to channel properties and channel identity. I fit a single exponential component to the decay portion (peak to baseline) of the averaged mEPCs to make a direct comparison between the time courses of the channels at different ages (Summarized in Table 3.1). My results indicate that there was a significant reduction in decay times throughout development. The greatest change occurred between 1.5 and 2 dpf in both fiber types (Table 3.1). For instance, mEPCs obtained from red fibers showed a reduction in exponential decays, from 3.22 ± 0.77 (n=8; 1.5 dpf) to 1.17 ± 0.1 (n=8; 2 dpf), and then to 1.04 ± 0.08 (n=10) by 5 dpf (Table 3.1).

The decay component of mEPCs from white fibers changed from 5.74 ± 1.07 (n=6; 1.5 dpf) to 0.52 ± 0.07 (n=9; 2 dpf) to 0.26 ± 0.01 ms (n=8) by 5 dpf (Table 3.1; $p < 0.05$). Thus, mEPCs from red muscle were 4 times slower than white muscle in 5 dpf fish. In many instances the decay times of the averaged events were not properly fit with a single exponential component; therefore, I investigated this further with a more stringent analysis of the mEPC decay time course.

I fit the decay component of averaged events with single exponential curves over either the fast (τ_{fast} , blue lines) or slow (τ_{slow} , dashed red lines) decay time courses (Figs 3.6 and 3.7). The values of the individual fast and slow fits are given in Tables 3.2 and 3.3. If the exponential

decay is truly a single component, then fitting either the fast or slow portion of the decay should result in an exponential fit that closely follows the entire synaptic decay. However, if the synaptic decay is best fit with a double exponential curve then separately fitting either the fast or slow component will result in deviations of the fitted curve from the synaptic decay. The decay component of averaged mEPCs from 1.5 dpf red fibers shows that separate fits of the fast and slow component markedly deviate from each other, as observed by visual observations at all the ages (1.5 to 5 dpf) (Fig 3.6 and Table 3.2). The fast exponential component (τ_{fast}) is reduced from a mean of 4.69 ± 1.59 ms at 1.5 dpf (n=8), to 0.68 ± 0.11 ms (n=10) by 5 dpf ($p < 0.05$), while the slow component (τ_{slow}) falls from an average of 9.41 ± 3.99 ms at 1.5 dpf (n=8) to 1.45 ± 0.07 ms by 5 dpf (n=10) ($p < 0.05$).

Similar analysis of mEPCs from white fibers shows that they were also not perfectly fit with single exponents (Fig 3.7 A), particularly in 2 dpf fish (Fig 3.7 B) where the mEPC decay had a τ_{fast} of 0.38 ± 0.05 ms and τ_{slow} of 0.80 ± 0.14 ms (n=9). As fish aged, the mEPCs from white fibers became better fit with single exponential decays, such that by 5 dpf the τ_{fast} of 0.26 ± 0.01 ms was identical to τ_{slow} of 0.25 ± 0.02 ms (n=8) (Figure 3.7 C-E and Table 3.3). These findings suggest that by 5 dpf, zebrafish white skeletal muscle predominantly express a single receptor type at the NMJ, whereas at 2 dpf, at the time of hatching, the NMJs of white fibers express at least 2 types of receptors.

Next, I examined the decay component of each individual mEPC obtained from red and white fibers at all ages to determine if they followed a single or double exponential time course. A plot of the percentage of mEPCs (recorded from each fiber) that were well fit with a single exponential component is shown in Figure 3.8. The majority of mEPCs from red fibers of 1.5 dpf

fish ($94.7 \pm 2.5\%$, $n=8$) are fit with a single exponential decay. However, the majority of mEPCs recorded from fish aged 2 dpf to 5 dpf are better fit with double exponential decays. These data suggest that the NMJs of red fibers in 1.5 dpf fish may express a single type of receptor. But in fish aged 2 dpf and older, most red fiber endplates expressed multiple types of nAChRs.

The majority of mEPCs recorded from 1.5 dpf white fibers ($93.2 \pm 2.0\%$; $n=9$) are fit with a single exponential decay, but by 2 dpf, only $36.6 \pm 6.1\%$ ($n=8$) of the events are well fit with single exponentials. By 3 dpf that percentage climbed back to $80.0 \pm 5.6\%$ ($n=9$) and then by 5 dpf, to $96.8 \pm 0.9\%$ ($n=6$) of the mEPCs were fit with a single exponential function again. The simplest explanation for this data is that in young embryos (~ 1.5 dpf) the NMJ predominantly expresses a single type of nAChR, and that between 1.5 and 2 dpf, a second type of receptor is expressed at the NMJ. As development proceeds, the properties of the nAChRs switch to that of a fast subtype so that by 5 dpf, virtually all of the early nAChRs are no longer present. Interestingly, even though the overwhelming majority of mEPCs at 1.5 dpf are well fit by a single exponential decay, there still are fast and slow components to the decay time courses of the averaged events. This discrepancy is explained by the wide range of single exponential time courses that I observed in 1.5 dpf fish, ranging from approximately 1 ms to 20 ms. When averaged, the resulting time course is represented by a multiple exponential function.

3.2 ACh-activated Single Channel Currents from Red and White Muscle

Fibers

The mEPC data that I obtained suggested that red and white muscle fibers express nAChRs with differing kinetics, and that the expression of the different receptors might be regulated throughout development. To explore this further, I recorded single channel currents from outside-out patches taken from red and white muscle fibers. I focused on fibers obtained from fish aged 1.5 dpf, 2 dpf and 5 dpf as the majority of mEPCs switched from single to double exponential decays between 1.5 dpf and 2 dpf in both types of fibers. Recordings from 5 dpf fish were used as an endpoint for developmental comparison. Moreover, red fibers exhibited a double exponential component up to 5 days post fertilization, while mEPCs from white muscle decayed with a single component.

Outside-out patches were pulled from skeletal muscle and were held at voltages ranging from -100 mV to -60 mV to determine the current-voltage relationship (I-V curve). Potentials more positive than this resulted in single channel currents that were often difficult to detect above background noise levels. Patches showed no single channel activity when washed with normal ECS (Fig 3.9 A). Activity was only present in the presence of ACh (0.6-0.8 μ M) and was fully blocked by the addition of curare (Fig 3.9 B, C), confirming that the single channel activity I recorded was due to the activation of nicotinic acetylcholine receptors. Examples of single channel data acquired from red fibers and white fibers are shown in Figure 3.10 and 3.11 respectively. These events were acquired from patches held at -100 mV and show different channel amplitudes and open times on a millisecond time scale. I noted 2 main current levels in red fibers that correspond to conductance states of around 46-50 pS and 63-66 pS (Fig 3.10,

dashed lines). Single channel recordings obtained from white fibers also indicated the presence of two main conductance states, but with values closer to 54-60 pS and 72-76 pS (Fig 3.11). In addition to these primary levels, I also noted the occasional presence of smaller and larger currents, but these were too few to be quantified and analyzed appropriately. In many cases the smaller level appeared to be filtered and likely represents openings that were too short to be fully resolved. Because I noted two separate current levels in almost all of our patches, I focused our analysis on these two groups.

To analyze this further, I constructed amplitude distributions of the single channel currents obtained from red and white fibers at each age. Nicotinic channels from red fibers displayed 2 clear distributions at each holding potential and at most ages, ranging from -100 mV to -60 mV (Fig 3.12). Recordings obtained from 1.5 dpf embryos primarily showed a main conductance state around ~64 pS, while recordings from 2 dpf to 5 dpf showed two main conductance states. Current-voltage relationships indicated the presence of two main current levels corresponding to ~4.6 pA and 6.5 pA when voltage clamped at -100 mV, as suggested by the single channel data. My data yielded consistent results with respect to the occurrence of these two main groups, such that virtually all patches held at -100 mV contained currents at the 4.5 pA and 6.5 pA levels. Current-voltage relationships constructed from the single channel data yielded what appear to be 2 separate channels: the first has a main conductance state of ~45 pS, while the other has a conductance state of ~65 pS. Open time distributions (Fig 3.12 Aiii, Biii, Ciii) showed the presence of two mean open times at each age: a fast open time of ~ 0.15-0.21 ms and a slower/longer open time of ~ 1.9-2.5 ms.

Nicotinic channels from white fibers exhibited two main conductance states that appear to be greater than those from red muscle, of ~ 55 pS and ~ 73 pS. Occasionally, a lower conductance channel opening in the 45 pS range was identified, but these were infrequent and very few in number to be properly analyzed; for which they were excluded. The higher conductance channel (73 pS) was more abundant throughout development such that by 5 dpf approximately 70% of all channel activity was due to the 73 pS channel. Furthermore, while two open times were present at 1.5 dpf (Fig 3.11 and 3.13 Aiii), the longer open time was largely absent by 5 dpf (Fig 3.13 Ciii). Taken together, the single channel data suggests that in 5 dpf fish, red fibers express at least 2 types of nAChRs that have short and long open times, while white fibers express two different conductance classes that have mainly short open times. This data supports my earlier findings on synaptic activity (Fig 3.6- 3.8) by providing a mechanism for the bi-exponential mEPC time courses of red fibers and the mono-exponential time courses of white fibers. In red muscle fibers the expression of channels with a short and a long open time likely underlie the double exponential decays of the mEPCs until 5 dpf. However, in white fibers the gradual disappearance of the longer open time channel by 5 dpf results in mEPCs with a single time course.

The receptor kinetics, time course of transmitter release, synaptic morphology and the action of acetylcholinesterase can shape the mEPC. But these factors are not present when analyzing single channel data from outside-out patches. Therefore, to tease apart whether the mEPC kinetics are predominantly shaped by the individual receptors or other factors, I built ensemble averages from all of the single channel events obtained from an individual recording. This was done for a number of red and white fibers from each age. The decay time course of the ensemble average was then analyzed and compared with the decay time courses of the mEPCs. I

reasoned that if the single channel events do indeed underlie the mEPCs then the time courses of the ensemble averaged events might be similar to mEPCs. I found similarities between the ensemble averages (Fig 3.14) and the mEPC kinetics. For instance, the ensemble average of red fibers at each age exhibited two exponential decay time courses much like the mEPC decay characteristics. Red fibers at 1.5 dpf had mean decay time constants of 0.28 ± 0.04 ms for τ_{fast} and 1.41 ± 0.25 for τ_{slow} (n=9). At 5 dpf the mean decay time constants of the ensemble averages were 0.35 ± 0.03 for τ_{fast} and 1.66 ± 0.27 for τ_{slow} (n=7); examples are shown in Figure 3.14. There was no significant developmental change in either τ_{fast} or τ_{slow} ($p > 0.05$). These values are remarkably similar to the fast and slow components obtained from mEPCs of 5 dpf red fibers (Table 3.2). Ensemble averages of events from white fibers gave curious results. For instance, at 1.5 dpf the mean decay time constants were 0.23 ± 0.02 for τ_{fast} and 0.29 ± 0.04 for τ_{slow} (n=8), and became significantly slower as development proceeded; at 5 dpf τ_{fast} was 0.32 ± 0.02 and τ_{slow} was 0.46 ± 0.03 ($p < 0.05$; n=8) (Fig 3.14). This suggests that the long mEPCs I recorded at 1.5 dpf were most likely due to synaptic morphology and transmitter release characteristics, rather than nAChR channel activity, as previously shown (Drapeau, Buss, Ali, Legendre, & Rotundo, 2001).

3.3 Expression of nAChR Subunits

The variations observed in the kinetic properties might be contributed by receptors with different subunit composition. Previous studies reported the presence of six nAChR subunits associated with zebrafish skeletal muscle fibers: $\alpha 1$, $\beta 1$ (aka $\beta 1b$), $\beta 1$ -like (aka $\beta 1a$), γ , δ and ϵ (Mongeon et al., 2011; Papke, Ono, Stokes, Urban, & Boyd, 2012; Park et al., 2014). I refer to $\alpha 1$ as α subunit, $\beta 1$ as $\beta 1b$, and $\beta 1$ -like as $\beta 1a$ throughout the rest of the thesis. I examined the

expression of these subunits at various developmental ages by reverse transcriptase PCR. Single bands were observed for all genes including $\beta 1a$ (Fig 3.15), which was previously shown to have a minimal level of expression via PCR and in situ hybridization and did not show any surface expression in zebrafish muscle fibers (Papke et al., 2012).

In mammalian muscle fibers, the expression of the γ subunit is reduced as expression of the ϵ subunit increases developmentally. My RT-PCR result shows continued expression of the γ subunit until adulthood. However, data from whole embryo RT-PCR did not allow me to determine if both muscle fiber types express all the subunits throughout development. Therefore, I attempted to determine the relative expression of various nicotinic receptor subunits in individual muscle fiber types by using a comparative C_T method ($\Delta\Delta C_T$) with real time quantitative RT-PCR. For this purpose, I developed a method to isolate and collect individual red or white muscle fibers by gentle aspiration into patch pipettes. However, it is possible to lose part of the muscle cytoplasm during the collection of individual fibers. Therefore, a pool of 3-6 fibers were used for each fiber type from each embryo ($n=5$). Two housekeeping genes, *actb1* and *rpl13a*, well suited for zebrafish developmental time course studies were used as endogenous controls (Tang et al., 2007) and the PCR expression efficiency of all the subunits was validated by analyzing the slope value of the semi-log regression line for ΔC_T vs. log dilution amount. The absolute values of the slopes of ΔC_T vs. log dilution were < 0.1 for all the subunits (Fig 3.16).

The $\Delta\Delta C_T$ method of RT-qPCR data analysis requires a calibrator gene against which the relative expression of other genes can be determined. In all samples, $\alpha 1$ showed the highest level of expression compared to other subunits. $\alpha 1$ is an essential subunit of functional nAChRs in skeletal muscles; therefore, this was chosen as the calibrator gene to compare relative expression

of other subunits at different ages and between the two fiber types. Relative expressions of different subunits are shown in Table 3.4. The relative expression of the $\beta 1b$ or δ subunits showed no significant differences between age or fiber types (Fig 3.17 A, B). The expression of $\beta 1a$ was extremely low in white fibers compared with red (Fig 3.17 C). These findings are in agreement with previous work showing that $\beta 1a$ is expressed at much lower levels than $\beta 1b$ (Papke et al., 2012), and since the white fibers make up the bulk of the trunk musculature, it is reasonable to assume that whole organism measurements of $\beta 1a$ mRNA would be relatively low. Expression of the γ subunit appeared to be stable among the different ages of the same fibers, but had a lower trend of expression altogether in white fibers compared to red (Fig 3.17 D). In contrast, white fibers showed a relatively higher level of expression for the ϵ subunit compared to red at all the ages (Fig 3.17 E). Thus, the relative expression of nAChR subunits in red and white muscle fibers showed marked trend of differences. Red fibers retained a high level of expression of nAChRs containing the γ subunit, whereas expression in zebrafish white fibers were similar to the mammalian muscle fibers with reducing γ subunit and high ϵ subunit expression. While the trends were observed, statistical significance was often not seen perhaps due to low number of samples.

Table 3.1:

Summary of mEPC decay kinetics after force-fitting all events with a single exponential decay, τ

Age, dpf	White fibers τ , ms	Red fibers τ , ms
1.5	5.74 ± 1.07 (n=9, 382 events)	3.22 ± 0.77 (n=8, 53 events)
2	0.52 ± 0.07^a (n=9, 281 events)	$1.17 \pm 0.10^{a*}$ (n=8, 96 events)
3	0.40 ± 0.05^a (n=9, 543 events)	$1.18 \pm 0.06^{a*}$ (n=9, 357 events)
4	0.33 ± 0.01^a (n=6, 400 events)	$1.19 \pm 0.09^{a*}$ (n=9, 575 events)
5	$0.26 \pm 0.01^{a,b}$ (n=8, 779 events)	$1.04 \pm 0.08^{a*}$ (n=10, 442 events)

^ap<0.05 when compared to 1.5 dpf fish of the same fiber type.

^bp<0.05 when compared to 2 dpf fish of the same fiber type.

*p<0.05 when compared to τ , white fibers at the same age.

Table 3.2:

Decay time course of the fast and slow exponential components from red fibers

Age, dpf	<i>n</i>	τ_{fast} , ms	τ_{slow} , ms
1.5	8	4.69 ± 1.59	$9.41 \pm 3.99^*$
2	8	0.99 ± 0.11^a	$1.16 \pm 0.11^{a,*}$
3	9	0.85 ± 0.06^a	$1.62 \pm 0.06^{a,*}$
4	9	0.92 ± 0.14^a	$1.70 \pm 0.05^{a,*}$
5	10	0.68 ± 0.11^a	$1.45 \pm 0.07^{a,d,*}$

^a $p < 0.05$ when compared to 1.5 dpf fish of the same fiber type.

^d $p < 0.05$ when compared to 4 dpf fish of the same fiber type.

* $p < 0.05$ when compared to τ_{fast} at the same age.

Table 3.3:

Decay time course of the fast and slow exponential components from white fibers

Age, dpf	<i>n</i>	τ_{fast} , ms	τ_{slow} , ms
1.5	9	6.99 ± 0.44	$10.43 \pm 0.89^*$
2	9	0.38 ± 0.05^a	$0.80 \pm 0.14^{a,*}$
3	9	0.35 ± 0.04^a	$0.48 \pm 0.08^{a,b,*}$
4	6	0.32 ± 0.02^a	$0.39 \pm 0.03^{a,b}$
5	8	$0.26 \pm 0.01^{a,b}$	$0.25 \pm 0.02^{a,b,c}$

^a $p < 0.05$ when compared to 1.5 dpf fish of the same fiber type.

^b $p < 0.05$ when compared to 2 dpf fish of the same fiber type.

^c $p < 0.05$ when compared to 3 dpf fish of the same fiber type.

* $p < 0.05$ when compared to τ_{fast} at the same age.

Table 3.4:

Relative mRNA expression ($2^{-\Delta\Delta C_t}$) of nAChR subunits in different fibers

Gene \ Fiber	1.5 dpf Red	1.5 dpf White	2 dpf Red	2 dpf White	5 dpf Red	5 dpf White
$\beta 1a$	0.53±0.16 (n=7)	0.99±0.95 (n=4)	1.11±0.15 (n=7)	0.08±0.04* (n=5; *p=0.0002)	0.94±0.21 (n=4)	0.04±0.02* (n=3; *p=0.0149)
$\beta 1b$	0.12±0.02 (n=7)	0.25±0.1 (n=6)	0.39±0.25 (n=7)	0.28±0.05 (n=6)	0.25±0.04 (n=4)	0.22±0.07 (n=4)
δ	0.83±0.19 (n=7)	2.5±1.1 (n=6)	0.74±0.13 (n=7)	0.57±0.11 (n=6)	0.51±0.2 (n=4)	0.39±0.15 (n=4)
γ	0.13±0.05 (n=5)	0.04±0.01 (n=4)	0.06±0.02 (n=5)	0.01±.003 (n=3)	0.12±0.05 (n=4)	0.01±0.003 (n=3)
ϵ	0.09±0.02 (n=6)	0.2±0.07 (n=6)	0.08±0.02 (n=7)	0.2±0.06 (n=6)	0.06±0.02 (n=4)	0.12±0.0004 (n=4)

*p<0.05 when compared to expression at the same age.

Figure 3.1

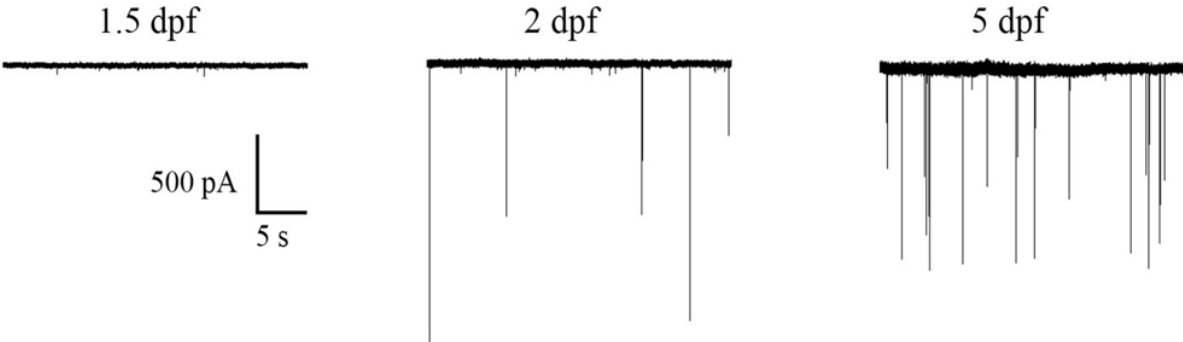


Figure 3.1

Sample miniature end plate current (mEPC) traces from Red muscle fibers.

Electrophysiological recordings of mEPCs were obtained from red muscle fibers under whole cell patch clamp configuration at -60 mV holding potential. The horizontal black trace shows the baseline and downward black lines indicate the events. mEPC events were hardly seen at 1.5 dpf.

Figure 3.2

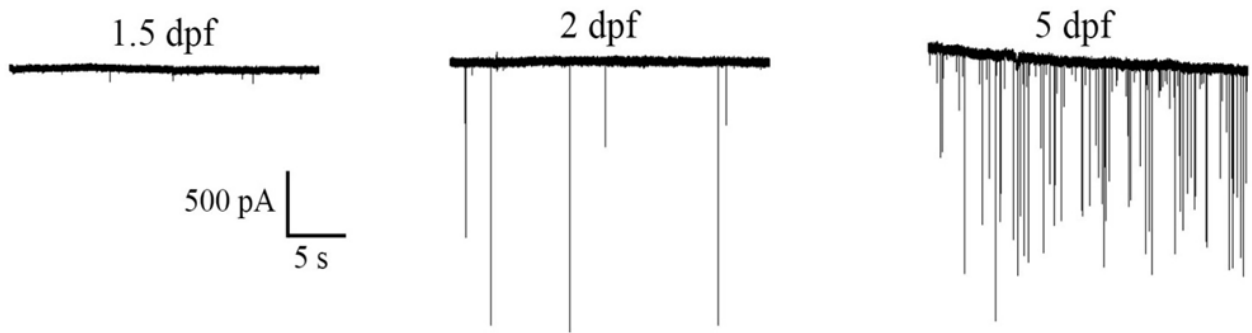


Figure 3.2

Sample mEPC traces from white muscle fibers. Electrophysiological recordings of mEPCs were obtained from white muscle fibers under whole cell patch clamp configuration at -60 mV holding potential. The horizontal black trace shows the baseline and downward black lines indicate the events. mEPC events were hardly seen at 1.5 dpf.

Figure 3.3

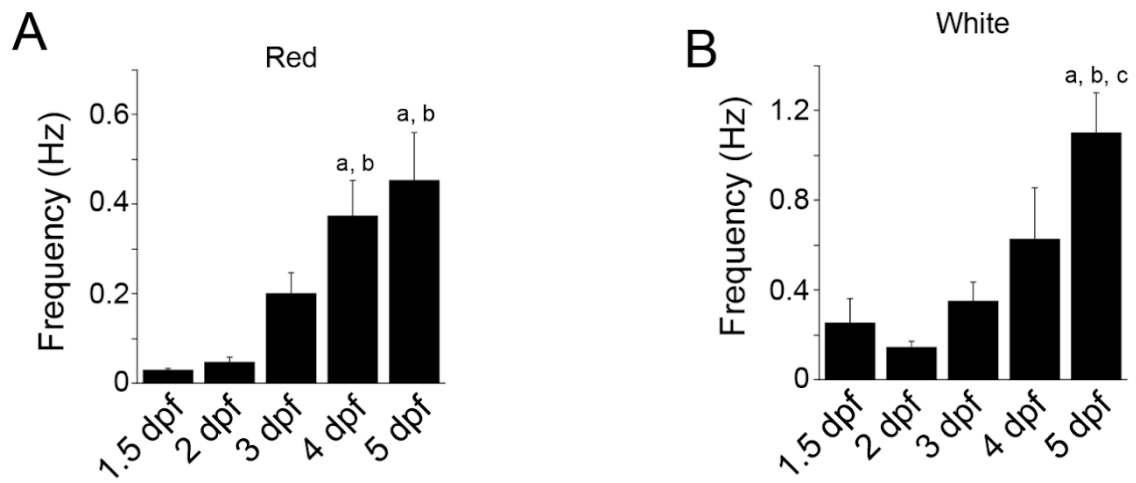


Figure 3.3

Frequency of mEPC events during development. (A) Bar graph shows mEPC event frequency (Hz) obtained from red muscle fibers at 1.5, 2, 3, 4 and 5 dpf. (B) Bar graph shows mEPC event frequency (Hz) obtained from white muscle fibers at 1.5, 2, 3, 4 and 5 dpf.

^a Significantly different from 1.5 dpf fish ($p < 0.05$); ^b Significantly different from 2 dpf fish ($p < 0.05$); ^c Significantly different from 3 dpf fish ($p < 0.05$).

Figure 3.4

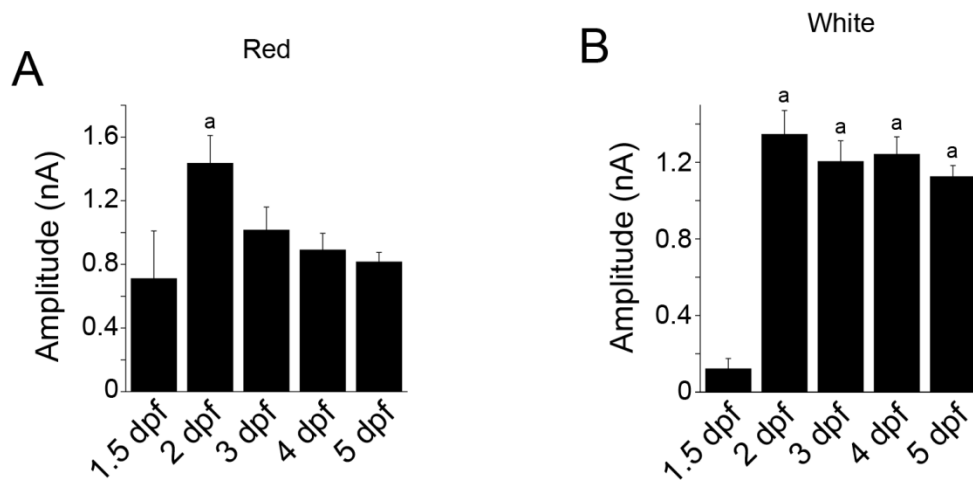


Figure 3.4

Amplitude of mEPC events during development. (A) Bar graph shows average amplitude of mEPC events (nA) obtained from red muscle fibers at 1.5, 2, 3, 4 and 5 dpf. (B) Bar graph shows average amplitude of mEPC events (nA) obtained from white muscle fibers at 1.5, 2, 3, 4 and 5 dpf. ^a Significantly different from 1.5 dpf ($p < 0.05$).

Figure 3.5

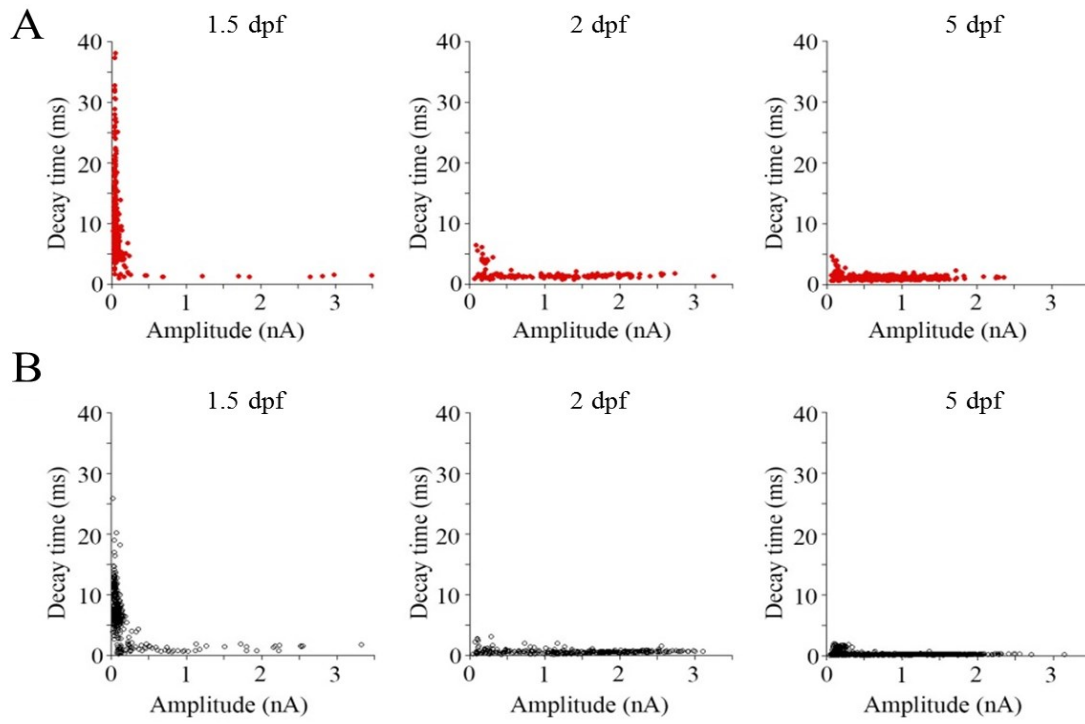


Figure 3.5

Single exponential decay time vs. amplitude distributions of mEPC events recorded from red and white fibers during development. (A) Shows distribution of mEPC events obtained from 1.5 dpf, 2 dpf and 5 dpf red fibers. (B) Shows distribution of mEPC events obtained from 1.5 dpf, 2 dpf and 5 dpf white fibers. In both fibers, mEPCs obtained from 1.5 dpf fish exhibit long rise times and low amplitudes compared with older fish in which the mEPCs have short rise times and higher amplitudes.

Figure 3.6

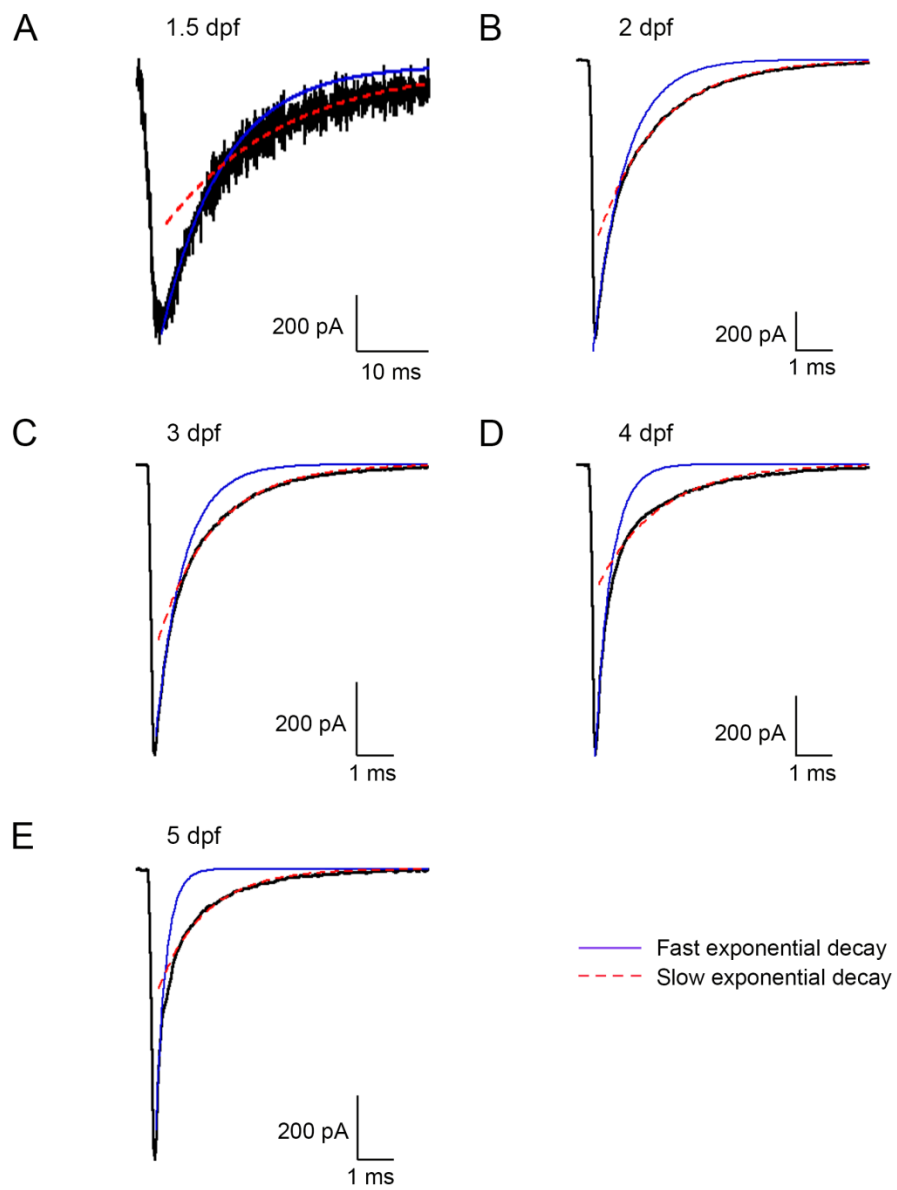


Figure 3.6

Averaged mEPCs obtained from red muscle fit with a single exponential decay over the fast component (τ_{fast} , blue line) or slow component (τ_{slow} , red dashed line). Averaged mEPCs acquired from fish aged 1.5 dpf (**A**; 16 events), 2 dpf (**B**; 35 events), 3 dpf (**C**; 85 events), 4 dpf (**D**; 52 events) and 5 dpf fish (**E**; 35 events) were not well fit by τ_{fast} or τ_{slow} .

Figure 3.7

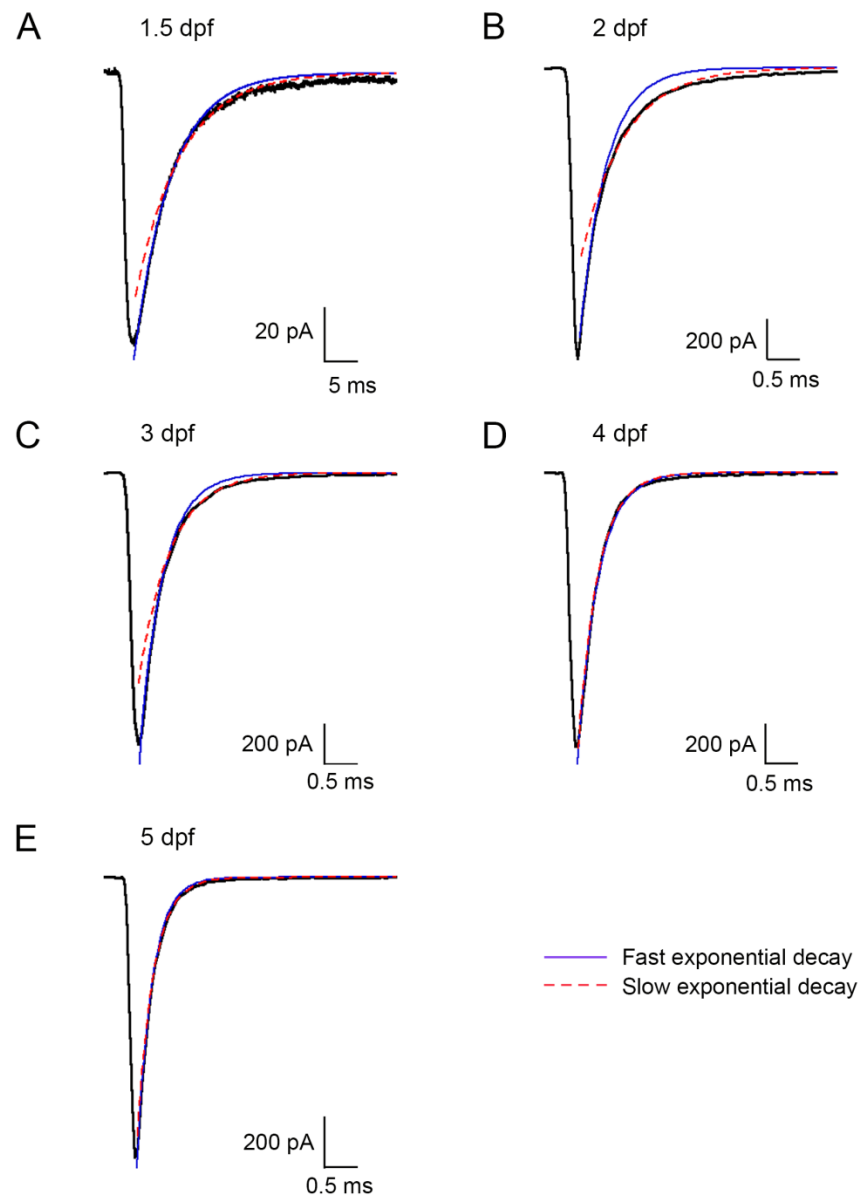


Figure 3.7

Averaged mEPCs obtained from white muscle fit with a single exponential decay over the fast component (τ_{fast} , blue line) or slow component (τ_{slow} , red dashed line).

Averaged mEPCs acquired from fish aged 1.5 dpf (**A**; 216 events), 2 dpf (**B**; 37 events) and 3 dpf (**C**; 38 events) were not perfectly fit by τ_{fast} or τ_{slow} . Averaged mEPCs acquired from 4 dpf (**D**; 56 events) and 5 dpf fish (**E**; 192 events) appear to be well-fit by τ_{fast} and τ_{slow} single exponents.

Figure 3.8

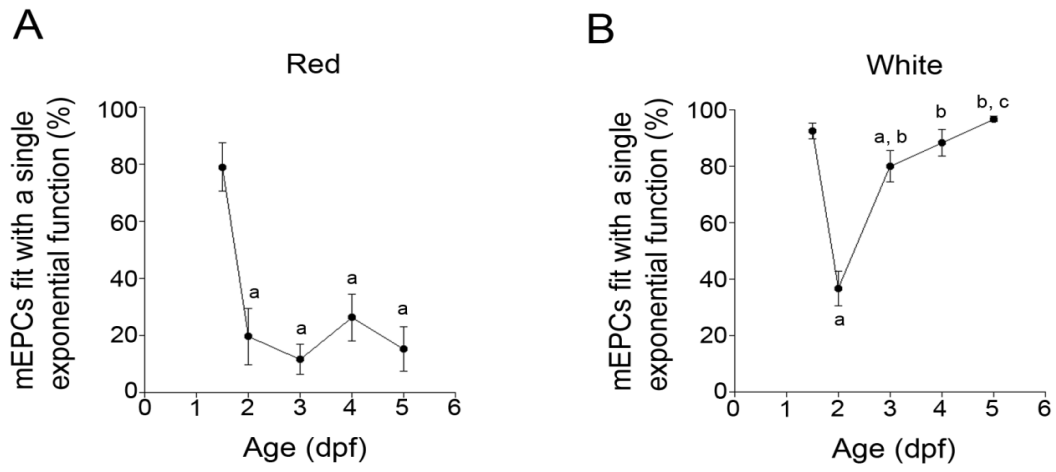


Figure 3.8

Graphs showing the percentage of mEPCs better fit with a single exponential decay component in red and white fibers. Each mEPC from each recording was fit with a single or double exponential component and assigned to a bin (single or double fit) depending on which function properly fit the decay component, as determined by eye. (A) In red fibers the decay portion of most mEPCs obtained from 1.5 dpf fish were well-fit with a single exponent, but the majority of mEPCs from fish aged 2-5 dpf were better fit with two exponents. (B) The majority of mEPCs obtained from white fibers from 1.5, 3, 4 and 5 dpf fish well-fit with a single exponent whereas the majority of events from 2 dpf fish were better fit with two exponents.

^a Significantly different from 1.5 dpf fish ($p < 0.05$). ^b Significantly different from 2 dpf fish ($p < 0.05$). ^c Significantly different from 3 dpf fish ($p < 0.05$).

Figure 3.9

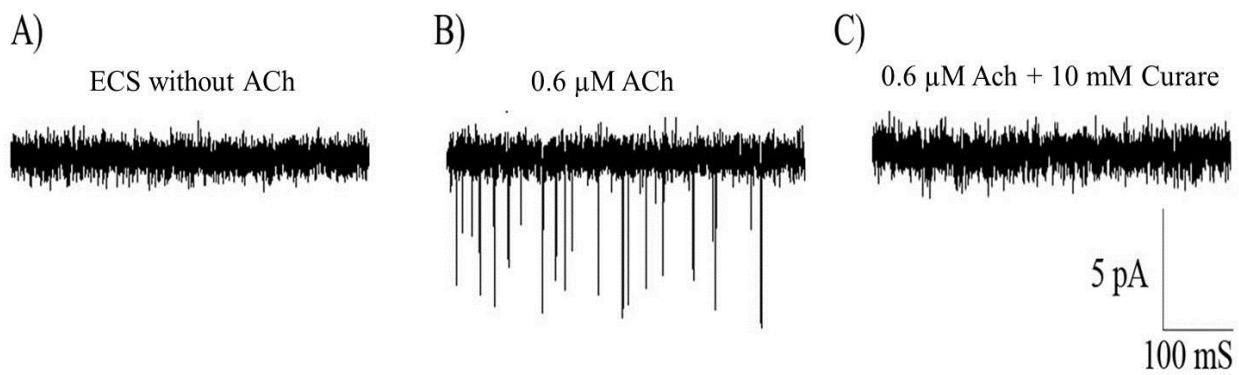


Figure 3.9

Single channel recording of nAChRs from outside-out patch configuration. (A)

Shows baseline current recording with no single channel event when the extracellular solution

(ECS) containing no acetylcholine (ACh). (B) Same recording shows single channel events

(downward lines) when 0.6 μM ACh is washed on with ECS. (C) ACh induced single channels

events are blocked in the same trace when 10 mM curare is washed on along with 0.6 μM ACh.

Appearance of events by ACh and blockage of them by curare confirms that the observed single

channel events are from nAChRs.

Figure 3.10

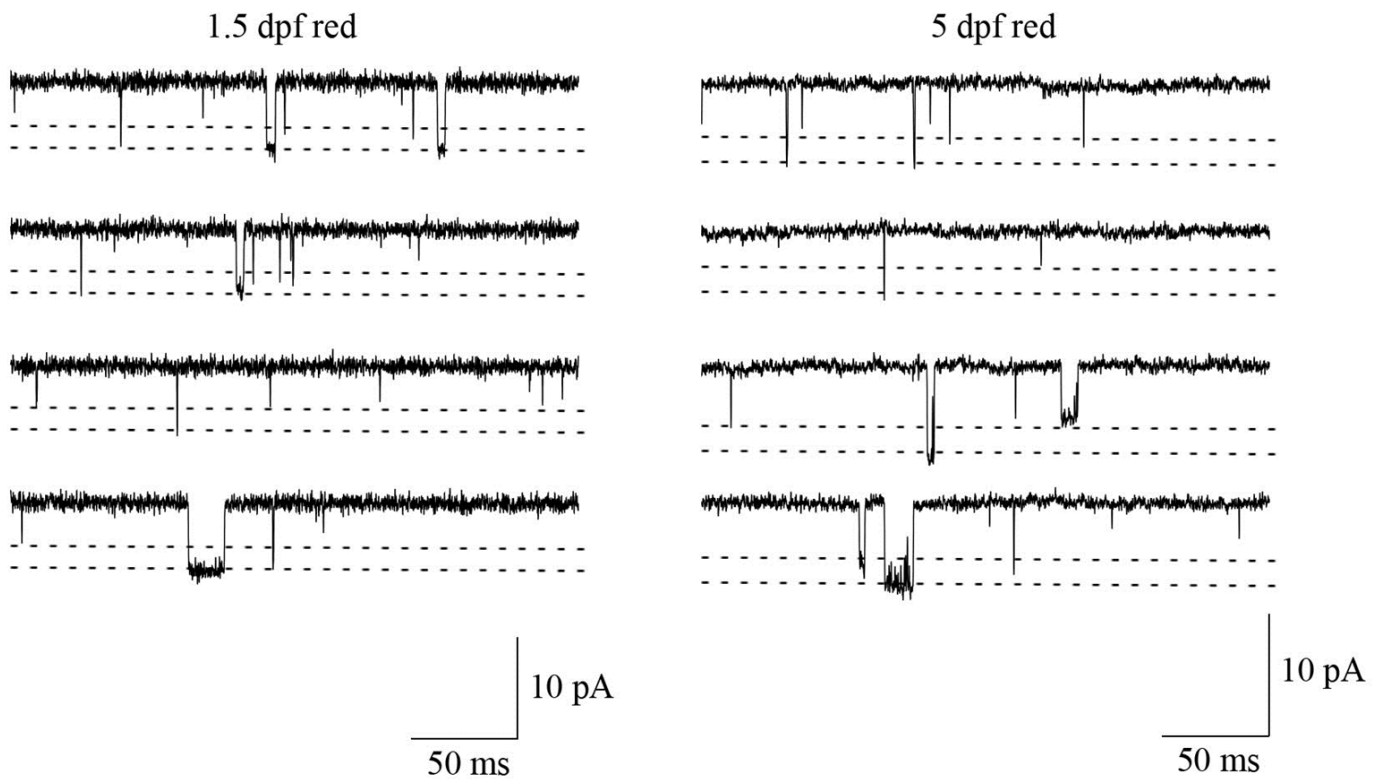


Figure 3.10

Sample traces of single channel events recorded from outside-out patches taken from red fibers at 1.5 and 5 dpf. Sample traces were obtained from recordings from a variety of fibers and were filtered to 2 kHz for the purpose of demonstration. Dashed lines indicate the two principal amplitude levels exhibited by the single channel events. Recordings from red fibers exhibit long and short open channels at both 1.5 and 5 dpf.

Figure 3.11

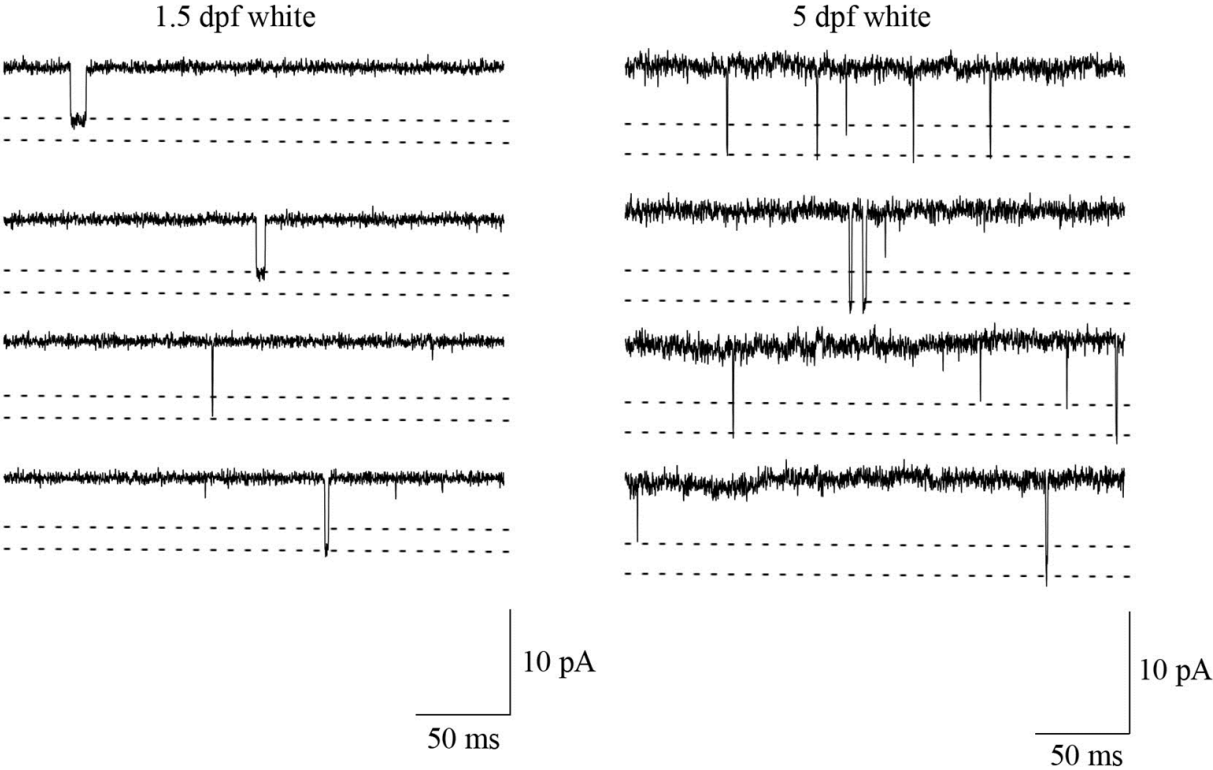


Figure 3.11

Sample traces of single channel events recorded from outside-out patches taken from white fibers at 1.5 and 5 dpf. Sample traces were obtained from recordings from a variety of fibers and were filtered to 2 kHz for the purpose of demonstration. Dashed lines indicate the two principal amplitude levels exhibited by the single channel events. Recordings from white fibers exhibit long and short open channels at 1.5 dpf, whereas only short open channels are present at 5 dpf.

Figure 3.12

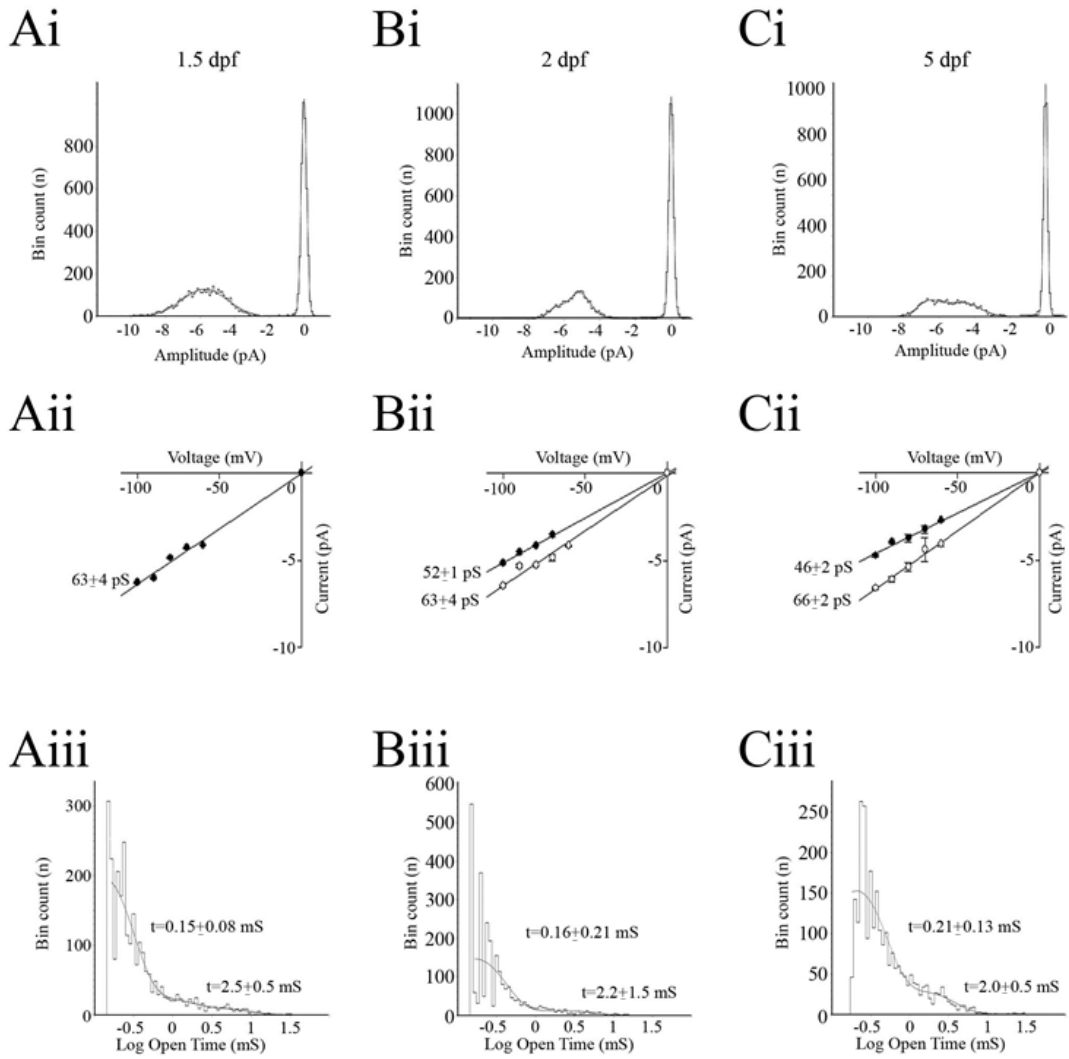


Figure 3.12

Properties of single channel events obtained from red fibers. Ai, Bi, Ci, Amplitude histograms of single openings of pooled events obtained from red fibers held at -100 mV, at 1.5 dpf, 2 dpf and 5 dpf. **Aii, Bii, Cii**, Current-voltage relationship for single channel events obtained from fish aged 1.5 dpf, 2 dpf and 5 dpf. Closed circles represent the lower conductance events, whereas open circles represent the higher conductance events, except for Aii, where closed circles represent the only conductance group present. **Aiii, Biii, Ciii** Open time histograms of nAChR currents indicating the presence of multiple single channel open times.

Figure 3.13

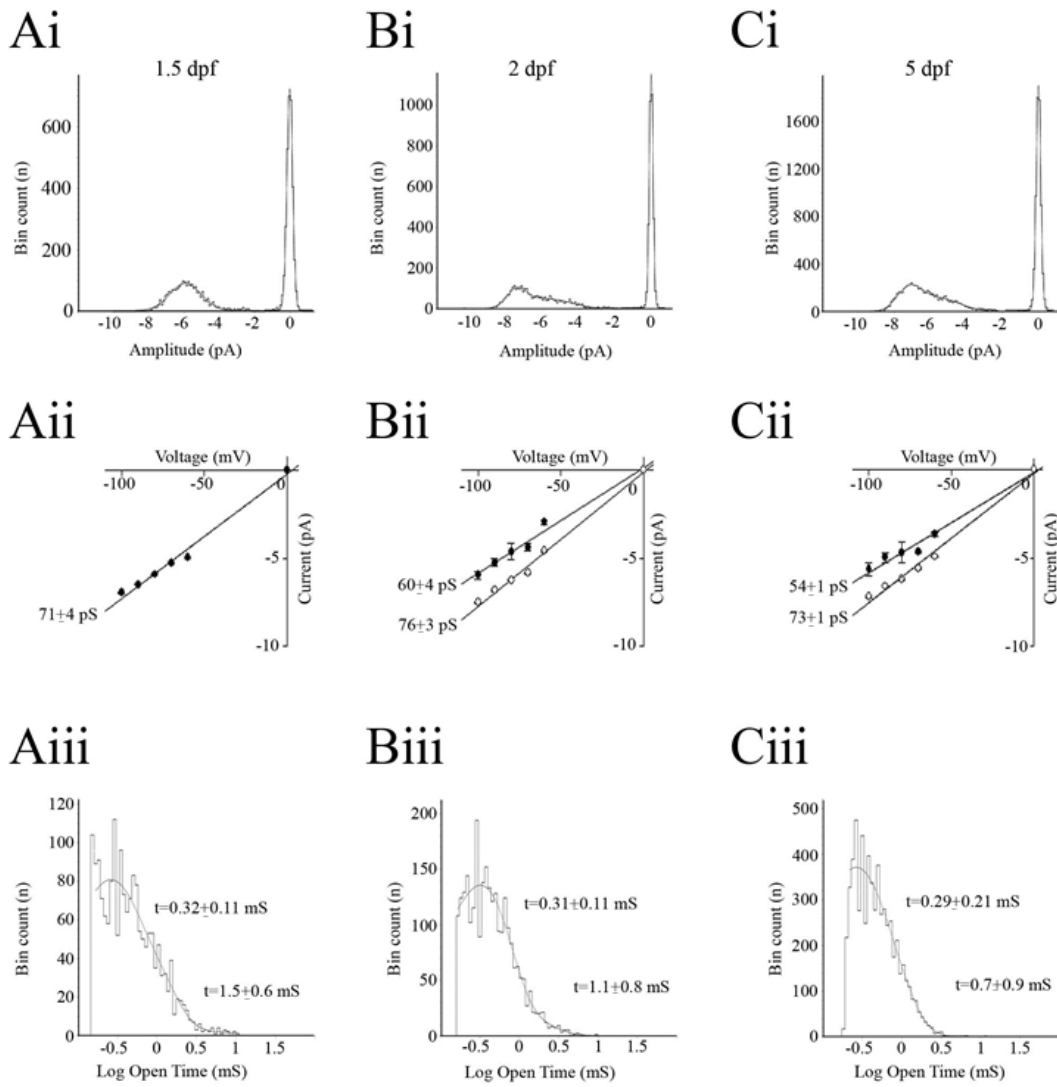


Figure 3.13

Properties of single channel events obtained from white fibers. Ai, Bi, Ci, Amplitude histograms of single openings of pooled events obtained from white fibers held at -100 mV, at 1.5 dpf, 2 dpf and 5 dpf. **Aii, Bii, Cii**, Current-voltage relationship for single channel events obtained from fish aged 1.5 dpf, 2 dpf and 5 dpf. Closed circles represent the lower conductance events, whereas open circles represent the higher conductance events, except for Aii, where closed circles represent the only conductance group present. **Aiii, Biii, Ciii** Open time histograms of nAChR currents indicating the presence of multiple single channel open times.

Figure 3.14

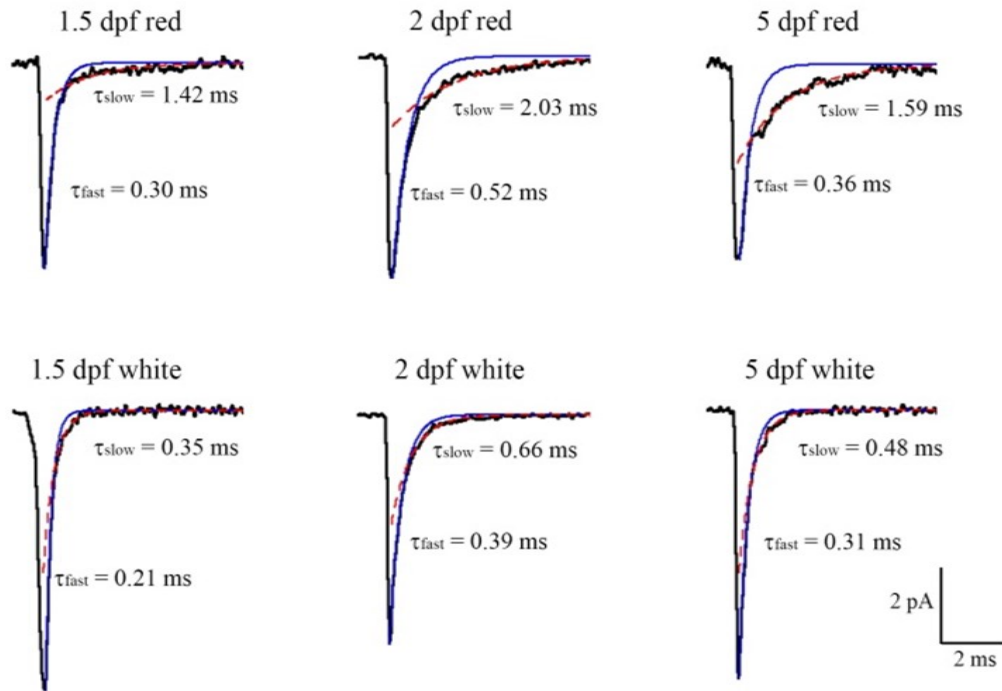


Figure 3.14

Ensemble average of single channel events from patches held at -100 mV for red and white fibers from 1.5 dpf, 2 dpf and 5 dpf fish. Ensemble averages were fit with a single exponential decay over the fast component (τ_{fast} , blue line) and the slow component (τ_{slow} , red dashed line). For each fiber type, average obtained from a single fish is shown as a sample, and decay time constants (τ) of the sample averages are noted.

Figure 3.15

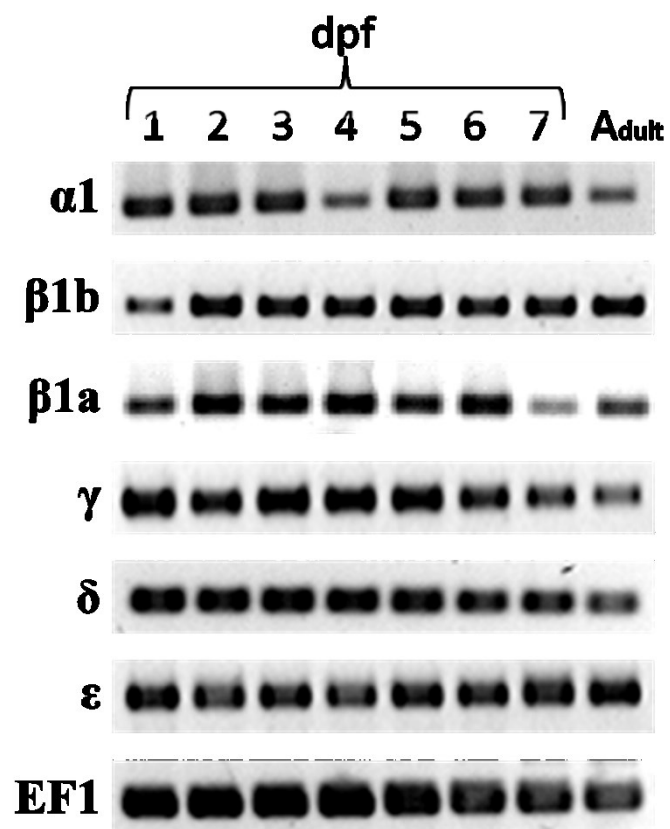


Figure 3.15

RT-PCR bands seen in agarose gels for $\alpha 1$, $\beta 1$, γ , δ and ϵ subunits during various stages of zebrafish life cycle. Expression of nAChR genes were assayed using RT-PCR on RNA harvested from zebrafish embryo (1-3), Larvae (4, 5, 7) and adult (>2years) (N=3 batches in each groups). Efl was used as a control. 30-50 fish were taken for 1-7 dpf age, and muscle of 3 fish were dissected for adults.

Figure 3.16

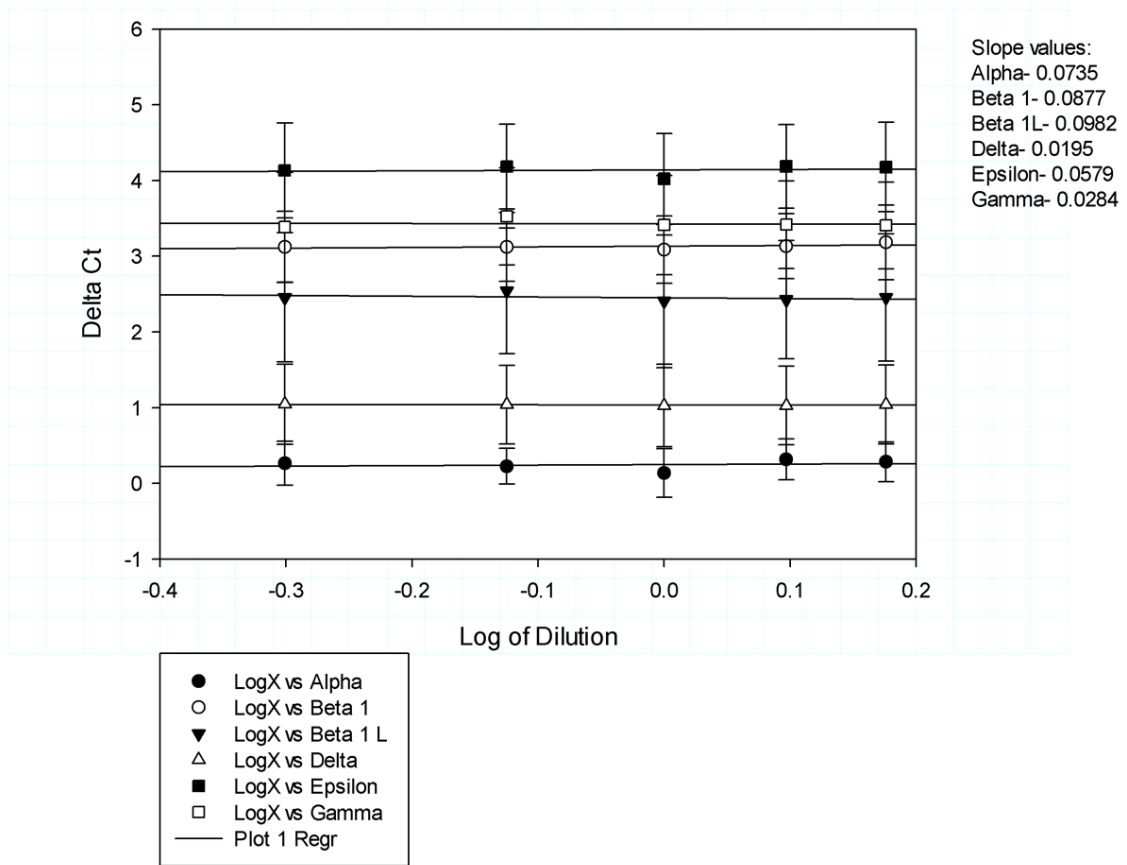


Figure 3.16

Validation of RT-qPCR experiment for nAChR subunit primers by semi-log regression analysis. Semi-log regression plot was generated for delta C_t vs log of sample dilution for each primer. The slopes of the regression lines for all the primers were less than 0.1, which validate the primers and mRNA concentrations, and suggest that the amplification efficiency for target and control primers is equal. N=3 replications were done at each point.

Figure 3.17

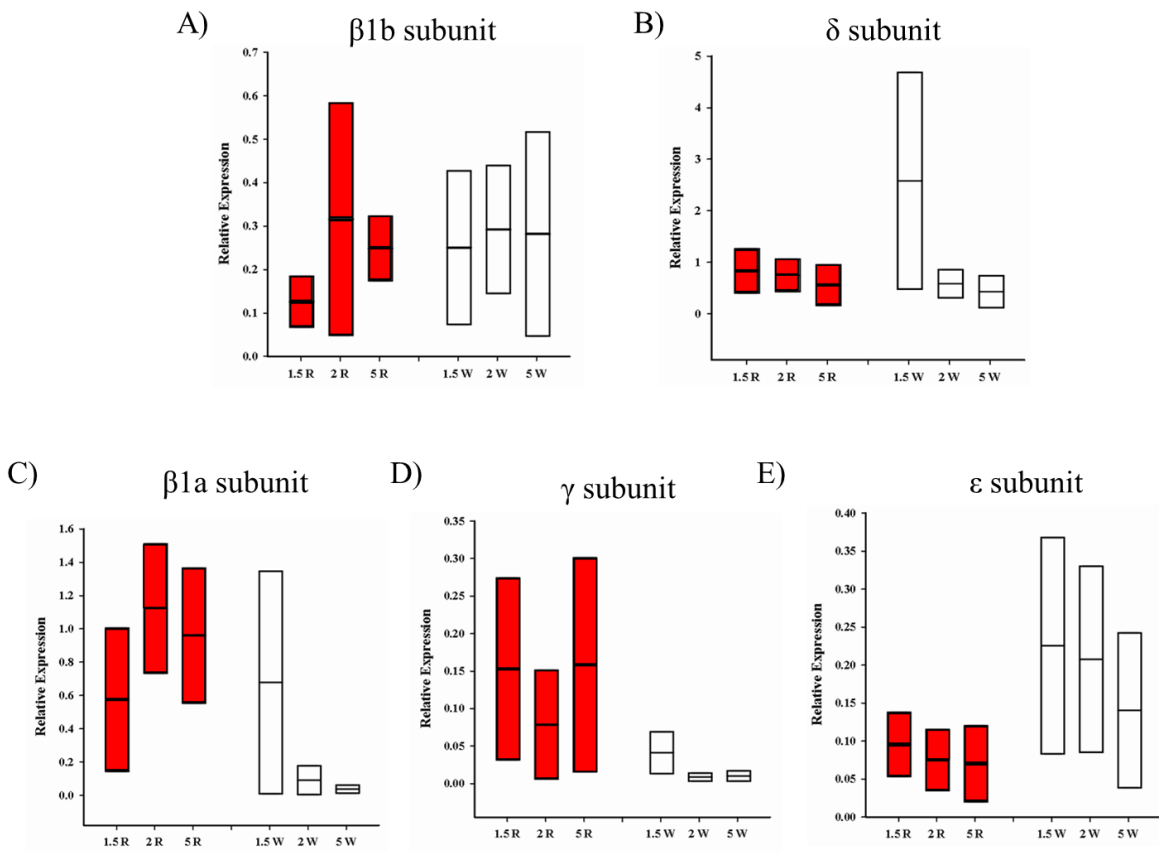


Figure 3.17

Relative expression of various subunits in red vs. white fibers examined by RT-qPCR. Box plots representing the upper to lower limit of relative fold change in mRNA expression in comparison to the α subunit. The midline in the box plot represents mean fold change. mRNA were obtained from single muscle fibers (red or white) from 1.5 dpf, 2 dpf and 5 dpf fish. mRNA from 3-10 fibers obtained from the same fish were pooled together, pre-amplified, reverse transcribed and qPCR was done. $\Delta\Delta C_T$ method was used using *actb1* and *rpl13a* as housekeeping gene and α subunit as calibrator. $\beta 1b$ and δ subunits (A and B) showed stable expressions throughout ages and fiber type. $\beta 1a$ shows higher trend of expression in reds compared to white (C). γ subunit expression remains unchanged during development of the fibers, however there is a higher trend of expression in red compared to white (D). Both the muscle fibers seemed to express ϵ subunits constantly, but white fibers had a higher trend of expression than reds (F). While the data suggests that white muscle fibers express more ϵ subunit than reds, no statistical significance could be resolved with a low power of comparison. We used 5 sets of samples and three technical replicates.

Chapter 4- Results- Effect of γ and ϵ Subunits in Embryonic Development (Translation Blocking MO)

In zebrafish muscle fibers, expression of nAChR γ and ϵ subunits shows developmental changes. Moreover, the expression patterns of these subunits in developing red and white muscle fibers are different. Why do these fibers require different level of these subunits? Is the expression of these subunits necessary for proper development of the embryos? What aspects of embryonic development might be altered if the differential expression of these subunits is absent? Answers to these questions have not been fully addressed. Mongeon et al. (2011) injected Morpholino oligonucleotides (MOs) into zebrafish embryos at the 1-2 cell stage to reduce the expression of γ and ϵ subunits to determine what contribution these receptor subtypes may have to synaptic transmission. The authors suggested that zebrafish white fibers express ϵ subunit containing nAChRs at 72-86 hpf. In contrast, nAChRs in red fibers are comprised of only $\alpha\beta\delta$ subunits. While this was a novel finding, the authors did not report any morphological or physiological effects induced by the MOs. Additionally, they did not report if the morpholinos had any effect on the normal development of the NMJ.

To determine the role of γ and ϵ subunits on embryonic development, I used a set of translation blocking MOs previously used by Mongeon et al. (2011), to reduce the expression of γ subunit (MO- G_M) and ϵ subunit (MO- E_M). Effectiveness of translation blocking MOs can be assessed by quantification of proteins by western-blot or immunohistochemistry. Unfortunately, no functional antibody is available to quantify γ and ϵ subunit in zebrafish, for which I could not assess the efficacy of the selected MOs. Moreover, the authors reported that the MOs were functionally blocking the target sequences, by observing predicted alteration in synaptic

properties. Therefore, I did not test them further, but kept the concentration of the MOs similar to what they reported. I injected 1 nL of the MO solution with a concentration of 0.5 μ M at 1-4 cell stage of the embryos and allowed them to grow up until 5 dpf. Morphological and physiological observations were made at 2 dpf and 5 dpf time points. In their work, Mongeon et al. (2011) compared the effect of these morpholinos with wild type embryos. To remain consistent, I also compared my results of morpholino injected fish with uninjected control ones (wild type AB) only. I particularly set out to determine-

1. If the MO injections induced any morphological, physiological or behavioral effects on zebrafish embryos.

2. If the MOs altered the development of NMJ properties.

4.1 General Morphology

To determine if the MO injections induced any effect on gross morphology of the zebrafish embryo and larvae, I examined the morphant fish for any visible morphological defects. I particularly examined aspects of morphology such as axial malformation, pericardial edema or abnormal tail structure at the 2 dpf and 5 dpf time points. All of the morphant fish appeared to be similar to uninjected animals (Fig 4.1). Injection of the morpholinos did not induce any morphological changes in the embryos or larvae.

4.2 Expression of nAChR

The molecular expression of nAChR subunits in wild type embryos suggests that receptors containing the ϵ subunit should be highly expressed in white muscle, whereas nAChRs

containing the γ subunit should predominate in red muscle. Therefore, knockdown of γ and ε subunits should theoretically cause a reduction in the expression of nAChRs in red and white fibers respectively. However, Mongeon et al. (2011) did not find any changes in the mean amplitude of mEPCs recorded from morphant embryos, suggesting that nAChR expression at NMJs might remain unaltered. To determine if the MO injections caused any alteration in nAChR expression, I labelled the receptors with fluorescently tagged α -bungarotoxin (ATTO-488 conjugated, Alomone Labs). α -bungarotoxin binds permanently to the α subunit of nAChRs and thus labels all the expressed receptors (that contain the α subunit). During visual inspection of the labelling pattern of nAChRs with α -bungarotoxin, no apparent difference could be observed in receptor expression in the morphants at either 2 dpf or 5 dpf (Fig 4.2) compared to uninjected controls.

The staining of nAChRs with α -bungarotoxin shows a thread like pattern along the edge of the muscle cells (myoseptal synapse) and circular puncta at the central region of muscle cells (distributed synapse) (Lefebvre, Jing, Becaficco, Franzini-Armstrong, & Granato, 2007). Myoseptal synapses are expressed in red muscle fibers whereas distributed synapses are principally found in white fibers (Park et al., 2014). In α -bungarotoxin staining, distributed puncta showed various sizes and shapes. Very small dot like puncta were likely the result of residual non-specific binding, immature synapses or extrasynaptic receptors (Ahmed, Amin, Shah, & Ali, 2018). Most of the small, dot-like puncta were observed to be $\sim 1-5 \mu\text{m}^2$ in diameter. Therefore, I excluded any puncta that were smaller than $5 \mu\text{m}^2$. Quantification of the distributed puncta in the morphant fish showed no difference compared to untreated control fish at either age (Fig 4.3). Untreated embryos at 2 dpf had an average of 35 ± 3 puncta/ $1000 \mu\text{m}^2$ ($n=10$). The number of puncta in 2 dpf embryos injected with MO- E_M and MO- G_M was 34 ± 5

(n=6) and 32 ± 4 (n=7) puncta/ $1000 \mu\text{m}^2$ respectively (Fig 4.3 A). At 5 dpf, the number of puncta / $1000 \mu\text{m}^2$ was 35 ± 4 (n=7), 34 ± 4 (n=7) and 40 ± 2 (n=6) for untreated, MO-E_M and MO-G_M fish respectively (Fig 4.3 B). Myoseptal synapses are immuno-stained as a long line along the myoseptal region. In the puncta counts, they are often counted as a single, large puncta, or sometimes small intermittent breaks in staining make them appear as multiple puncta. Thus, counting of puncta in the myoseptal region may provide misleading numbers. Therefore I excluded myoseptal regions from counting.

4.3 Effect on Motor Neuron Axonal Branching

Next, I sought to determine if axonal branching emanating from primary and secondary motor neurons was altered by MO-E_M and MO-G_M. Primary motor neurons innervate white muscle fibers whereas secondary motor neurons innervate both red and white muscle fibers. During embryonic and larval development, dynamic interaction between presynaptic axon and postsynaptic nAChR cluster occurs which helps in precise apposition of pre and post synaptic component as well as modeling and stabilizing the synaptic clusters of NMJ (Flanagan-Steet, Fox, Meyer, & Sanes, 2005). Therefore, alteration in nAChR properties might induce a change in motor neuron innervation pattern.

Zebrafish primary motor neurons are located in the ventral region of the spinal cord. There are four types of primary motor neurons- Rostral (RoP), Middle (MiP), Caudal (CaP) and Variable (VaP) primary motor neurons, each neuron projects an axon towards a specific region of the trunk musculature (Westerfield et al., 1986). Axonal branches of zebrafish primary motor neurons can be immunolabelled by motor neuron specific synaptotagmin-2 marker, anti-znpl1 antibody (Fox & Sanes, 2007; Trevarrow, Marks, & Kimmel, 1990). A primary axonal branch

descends from the cell body of the MN and it then arborizes further to create secondary and tertiary branches which innervate various muscle layers (Bradley, Tossell, Lockley, & McDermid, 2010) . After immunolabelling with the znp1 antibody, I visually inspected the images to see if any gross abnormality in the axonal branching pattern could be discerned in morpholino injected vs control fish. Branching patterns in MO injected fish appeared similar to the untreated control fish at both 2 dpf and 5 dpf (Fig 4.4). These observations suggested that the MOs had no visible effect on primary motor neuron branching.

Next, I examined the pattern of secondary motor neuron branching in morpholino-injected fish at 2 dpf and 5 dpf time points (Fig 4.5). Secondary motor neuron cell bodies are located in the spinal cord and extend their branches to the dorsal, ventral and lateral regions of the trunk (Menelaou & Svoboda, 2009). At 2 dpf, only ventral branching can be observed whereas all of the branches are clearly observed in 5 dpf fish. During visual inspection, I did not see any difference in the branching pattern of secondary motor neurons in the morphant fish compared to control ones in either 2 dpf embryos (n=6 embryos for each comparison group) or 5 dpf larvae (n=5, 6 and 7 for control, MO-E_M and MO-G_M respectively). In all cases, I could clearly identify the ventral branches at 2 dpf and all of the branches at 5 dpf (Fig 4.5). Such observations suggested that the MOs had no visible effect on the secondary motor neuron branching either.

4.4 Effect on Muscle Fiber Morphology

To determine if injection of the MOs had any effect on the growth and morphology of red and white muscle fibers, I immunolabelled red muscle fibers with an anti-myosin heavy chain (fast isoform) antibody (anti-F59 antibody), and white muscle fibers with an anti-myosin light

chain 1 and 3f antibody (anti-F310 antibody). The muscle fibers appeared unaffected following morpholino injections under bright field microscope. But unfortunately, the antibody staining was unclear and inconsistent in many fish. Previously, these antibodies have been successfully used in various studies conducted by myself and others in our lab for many years (Sylvain, Brewster, & Ali, 2010). The fact that multiple batches were no longer providing consistent results suggested a significant problem with the production and efficacy of these antibodies. Fig 4.6 shows sample white muscle fibers from 2 dpf embryos when one set of antibody could properly stain them.

4.5 Effect on Larval Locomotive Behavior at 5 dpf

Next, I determined if the MOs had any effect on larval locomotor activity. To do this, I analyzed spontaneous free-swimming behavior of 5 dpf larvae. Individual larvae were placed in 96-well plates and their spontaneous swimming activity was monitored and tracked for an hour. The spontaneous swimming activity was then analyzed with EthoVision software (Noldus). I examined several parameters including activity (% of total time the fish remain active), frequency of movement (how many times the fish moved in an hour), cumulative duration of movement (total length of time the fish was active), total distance moved in an hour, mean velocity during swimming, maximum velocity and acceleration attained during swimming, mean angle of turn and mean angular velocity. Mean activity of untreated embryos, MO-E_M and MO-G_M injected larvae were $0.04 \pm 0.006\%$ (n=55), $0.05 \pm 0.009\%$ (n=32) and $0.06 \pm 0.007\%$ (n=20) respectively which were not different (Fig 4.7 A). The frequency of movement was also similar between the larvae, exhibiting 0.19 ± 0.02 Hz, 0.21 ± 0.04 Hz and 0.18 ± 0.02 Hz by untreated (n=55), MO-E_M (n=32) and MO-G_M (n=19) larvae (Fig 4.7 B). Cumulative duration of

movement in an hour by untreated, MO-E_M and MO-G_M larvae were also similar, with values of 472 ± 60 s (n=54), 520 ± 95 s (n=31) and 485 ± 59 s (n=19) respectively (Fig 4.7 C). Next, I measured and compared the total distance travelled by the uninjected, MO-E_M and MO-G_M larvae. These values were also similar, measuring 258 ± 30 cm (n=56), 242 ± 42 cm (n=31) and 255 ± 32 cm (n=20) respectively (Fig 4.7 D). Mean velocity of untreated, MO-E_M and MO-G_M larvae was 0.25 ± 0.03 mm/s (n=53), 0.23 ± 0.04 mm/s (n=31) and 0.23 ± 0.03 mm/s (n=20) (Fig 4.7 E). Maximum velocity attained during swimming was 19 ± 1 mm/s (n=51), $19. \pm 2$ mm/s (n=30) and 21 ± 2 mm/s (n=20) by uninjected, MO-E_M and MO-G_M respectively (Fig 4.7 F). The maximum acceleration attained during swimming by untreated, MO-E_M and MO-G_M larvae were 42 ± 3 (n=52), 35 ± 3 (n=26) and 48 ± 5 (n=20) cm/s² respectively (Fig 4.7 G). Mean velocity, maximum velocity and maximum acceleration remained unaffected following either of the morpholino injections.

While most of the swimming parameters remained unaltered, both MO-E_M and MO-G_M larvae showed higher bend angle and higher angular velocity compared to control. Mean bend angle for untreated, MO-E_M and MO-G_M larvae were 2.23 ± 0.06 (n=45), 3.04 ± 0.25 (n=24; p=0.0095) and 2.83 ± 0.2 (n=19; p=0.0238) degrees respectively (Fig 4.7 H). Angular velocity of the larvae were 55.64 ± 1.5 (n=45), 76.08 ± 6.3 (n=24, p= 0.0095) and 70.64 ± 5 (n=19, p=0.0238) degrees/s respectively (Fig 4.7 I). Altogether, these results suggest that the MO injections have very little effect on the swimming ability of the fish.

4.6 Effect on mEPC Recorded from Red and White Muscle Fibers

Mongeon et al. (2011) studied mEPCs recorded from 3 dpf red and white fibers in the control and MO injected embryos. She found that several forms of γ subunit MO did not have

any effect on mEPC properties. In contrast, knockdown of ϵ subunit affected the mEPC kinetics in white fiber, and mEPC amplitude in red muscle fibers. I have previously shown that key developmental alterations at the NMJ start at 2 dpf and continue until 5 dpf. Therefore, I sought to determine if alterations in mEPC properties were also evident at these critical time points following knockdown of the ϵ subunit. I recorded mEPCs from control and ϵ subunit morphant fish in 2 and 5 dpf animals. mEPCs were recorded from both red and white muscle fibers.

Sample traces of the mEPC recordings are shown in Fig 4.8. First, I analyzed the frequency at which the mEPC events occur in red and white muscle fibers in 2 dpf and 5 dpf animals. Frequency of mEPCs in red fibers remained unaltered at both 2 dpf and 5 dpf time points (Fig 4.9 A, C). Mean frequency of mEPCs recorded from 2 dpf red fibers was 0.09 ± 0.03 Hz (control, n= 6) and 0.05 ± 0.02 Hz (MO- E_M , n=7; p=0.1696). In 5 dpf red fibers, mEPCs occurred at a frequency of 0.1 ± 0.02 HZ in controls (n= 8) and 0.09 ± 0.02 Hz in the morphants (n=7; p=0.5358). In contrast, the frequency of mEPCs obtained from white muscle was significantly reduced following MO- E_M injection in both 2 dpf and 5 dpf aged animals (Fig 4.9 B, D). The mean frequency of mEPCs in 2 dpf white fibers was 0.11 ± 0.05 Hz (control, n= 6) and 0.02 ± 0.003 Hz (MO- E_M , n=9; p=0.0108), and in 5 dpf white fibers was 0.25 ± 0.03 HZ (control, n= 8) and 0.1 ± 0.03 Hz (MO- E_M , n=8; p=0.0207).

I determined the mean amplitude of the mEPCs obtained from red and white muscle fibers (Fig 4.10). The mean amplitude of mEPCs in 2 dpf red fibers was 709 ± 127 pA (control, n= 6) and 1015 ± 130 pA (MO- E_M , n=7; p= 0.2343), and in 5 dpf red fibers was 455 ± 41 pA (control, n= 8) and 568 ± 94 pA (MO- E_M , n=7; p= 0.3969). The mean amplitude of mEPCs in 2 dpf white fibers were 646 ± 138 pA (control, n= 6) and 1059 ± 194 pA (MO- E_M , n=9; p=

0.1447), and in 5 dpf white fibers were 416 ± 63 Hz (control, $n=8$) and 707 ± 113 Hz (MO- E_M , $n=8$; $p=0.1049$). Although the mean amplitudes were slightly higher in MO-E injected fish in both fibers at all ages, they were not statistically significant.

Next, I examined the exponential decay of the average mEPCs. Sample average events with their exponential decay fits are shown in Fig 4.11. In control fish, synaptic currents from red muscle fibers show double exponential decay components in both 2 and 5 dpf animals. 2 dpf white muscle fibers also show double exponential decay whereas white muscle mEPCs at 5 dpf decay with a single exponential component. Synaptic currents from MO- E_M injected fish also showed double exponential decay at 2 dpf red, 2 dpf white and 5 dpf red fibers, which are similar to control fish. The decay component of mean mEPCs in most of the 5 dpf white fibers from MO- E_M were also best fit with single exponential decays (five out of eight fish), however three out of eight fish exhibited mean mEPCs that were best fit with double exponential decay.

The (fast and slow) exponential decay time constants of mean mEPCs from 2 dpf red fibers were 0.77 ± 0.09 ms (fast) and 1.94 ± 0.2 ms (slow) in control fish, and 0.95 ± 0.18 ms (fast) and 2.27 ± 0.25 ms (slow) in MO- E_M injected fish, which were not significantly different (Fig 4.12 A). The fast exponential decay time constant in 2 dpf white fibers (0.59 ± 0.03 ms in control, $n=6$ and 0.74 ± 0.15 ms in MO- E_M , $n=9$) were also not different. But the slow decay component in 2 dpf white fibers from MO- E_M (1.25 ± 0.99 ms; $n=9$) was significantly slower compared to control (0.87 ± 0.08 ms; $n=6$; $p=0.018$) (Fig 4.12 B). Both fast (0.78 ± 0.1 ms) and slow (1.43 ± 0.14 ms) decay components of 5 dpf red fibers ($n=7$) were significantly slower in MO- E_M injected fish compared to control ($n=8$; fast- $0.51 \pm .05$ ms, $p=0.03$; slow- 0.99 ± 0.11 ms, $p=0.01$) (Fig 4.12 C). The single decay kinetics of 5 dpf white fibers were similar in control

(0.28 ± 0.01 , $n=8$) and MO- E_M injected fish (0.32 ± 0.02 ms, $n=8$) however 3 out of 8 fibers showed a second decay component with time course of 0.71 ± 0.03 ms (Fig 4.12 D). Thus, mEPC frequency and decay kinetics are affected by MO- E_M injection, with the most prominent effect occurring on the decay of white muscle fibers and only 5 dpf red fibers. However, injections of the MO of either subunit did not seem to have any effect on overall morphology, motor neuron development or locomotive repertoire. Altogether, these results demonstrate that injections of the selected MOs for nAChR γ or ϵ subunit do not affect embryonic development and locomotion of zebrafish, but ϵ subunit affect synaptic properties in the fibers.

Figure 4.1

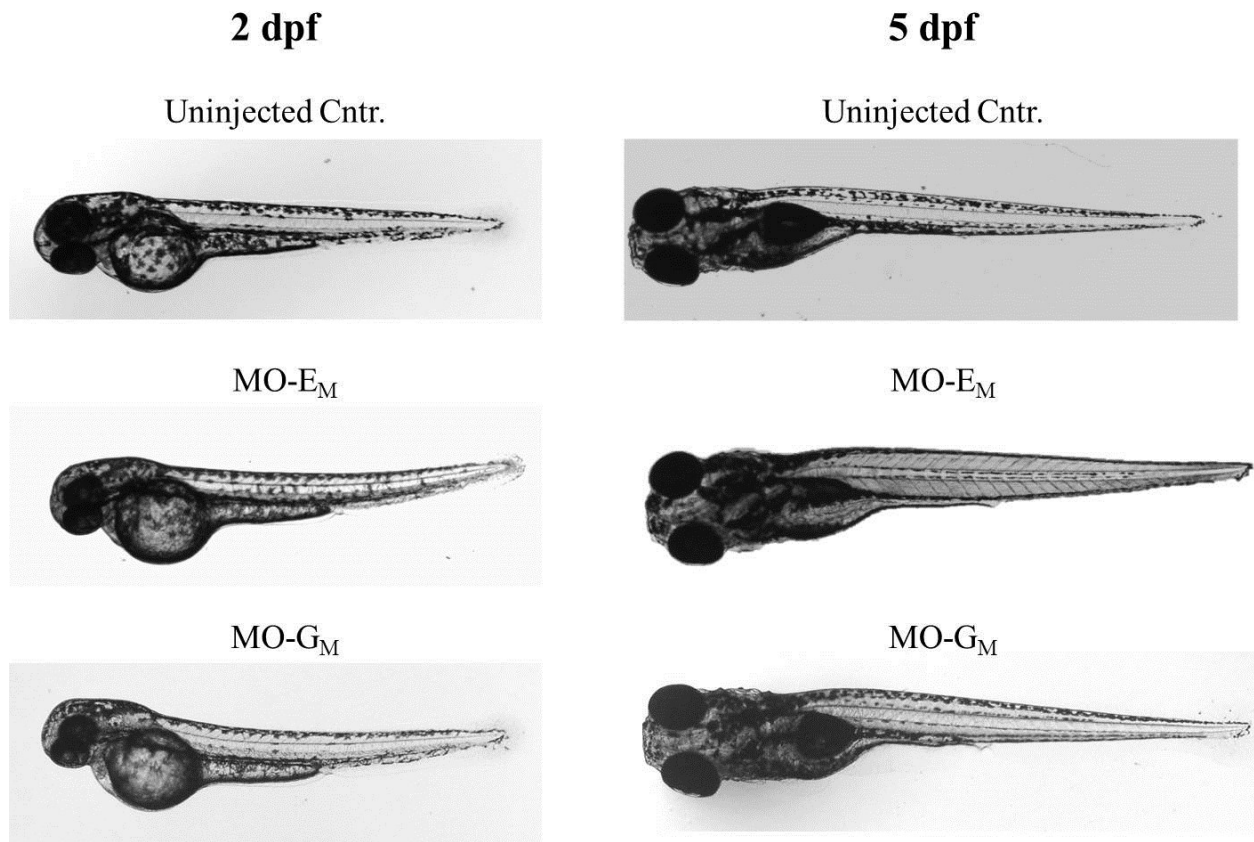


Figure 4.1

Morphology of 2 dpf embryos and 5 dpf larvae following injection of translation blocking MOs. Zebrafish eggs were injected with 1nL of 0.5 nM translation blocking morpholino of *chnE* (MO- E_M), *chnG* (MO- E_G) or remained uninjected. At 2 dpf and 5 dpf time points, images of the fish were taken under bright field microscope. All the fish appeared normal and no visual difference was identified between same age embryos.

Figure 4.2

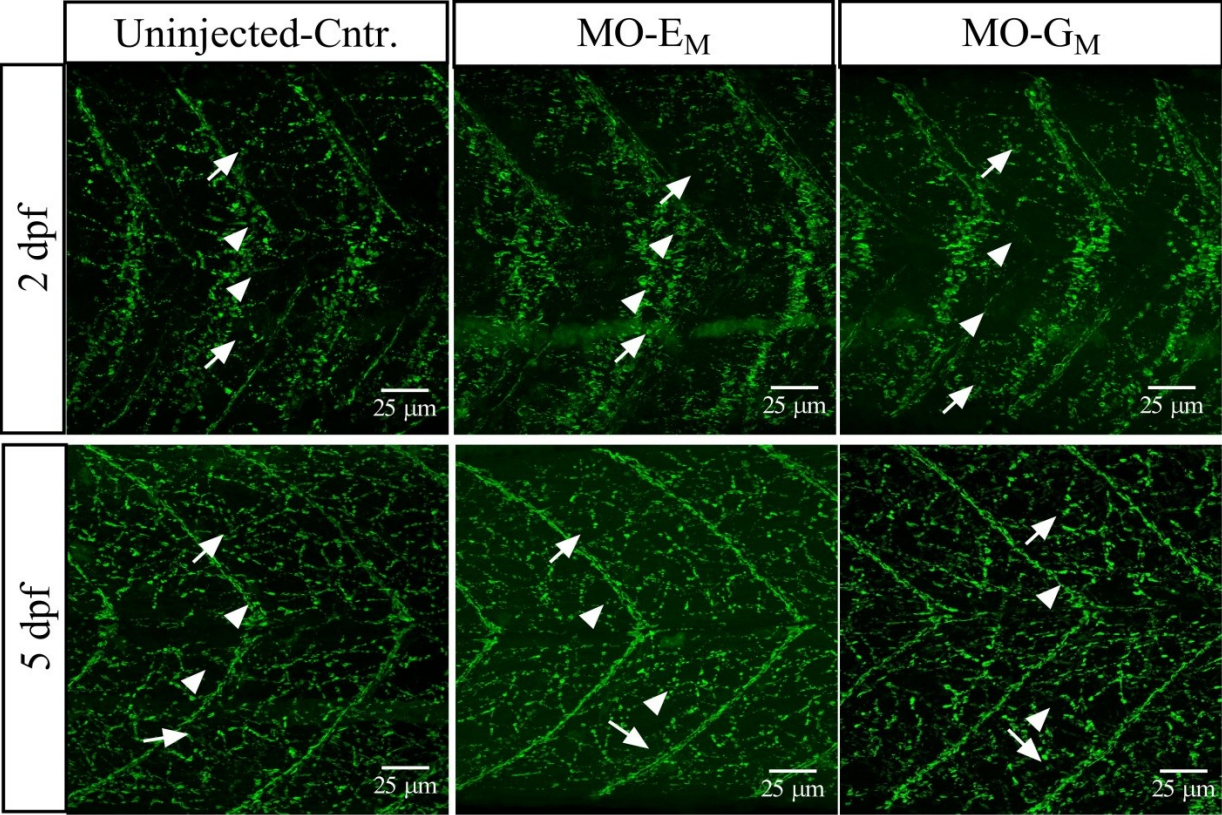


Figure 4.2

α -bungarotoxin staining of nAChRs in 2 dpf and 5 dpf embryos of uninjected control, MO-E_M and MO-G_M. White arrows indicate myoseptal region and white arrowheads indicate distributed synaptic regions. 2 dpf and 5 dpf zebrafish were stained with α -bungarotoxin and Z-stack images were taken under confocal microscopy. Maximum intensity projections made from the z-stack images are shown. No visual difference could be observed in the expression pattern of the clusters between different treatments.

Figure 4.3

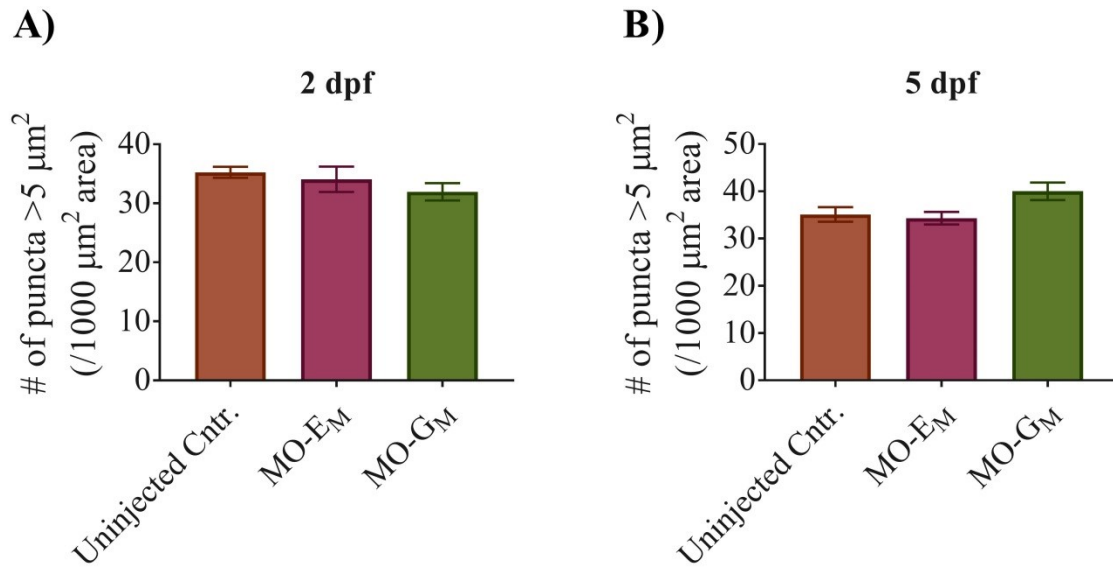


Figure 4.3

Quantification of nAChR clusters in 2 dpf embryos and 5 dpf larvae. nAChR puncta was stained with α -bungarotoxin. nAChR puncta that are $>5 \mu\text{m}^2$ were counted using ImageJ software and compared between uninjected control, MO- E_M and MO- G_M . Number of puncta did not vary between different treatment groups.

Figure 4.4

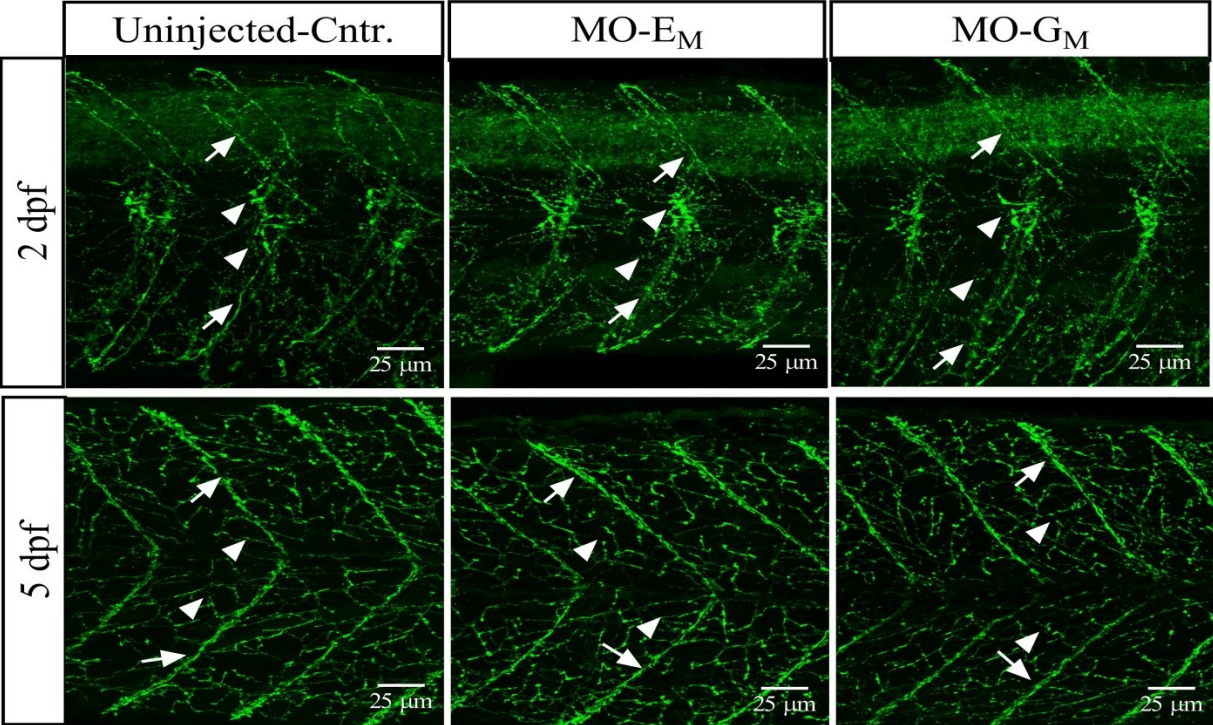


Figure 4.4

Primary motor neuron axonal branching in 2 dpf and 5 dpf fish of uninjected control, MO-E_M and MO-G_M. Axonal branches of primary MNs were immunolabelled with the anti-znp1 antibody and z-stack images were taken under confocal microscopy. Maximum intensity projection is shown, made from the z-stack images. White arrows indicate the primary axonal branches and white arrowheads represent the secondary/tertiary branches ramified from the primary branch. No visual difference in the branching patterns could be specified in between different treatment groups at the same age.

Figure 4.5

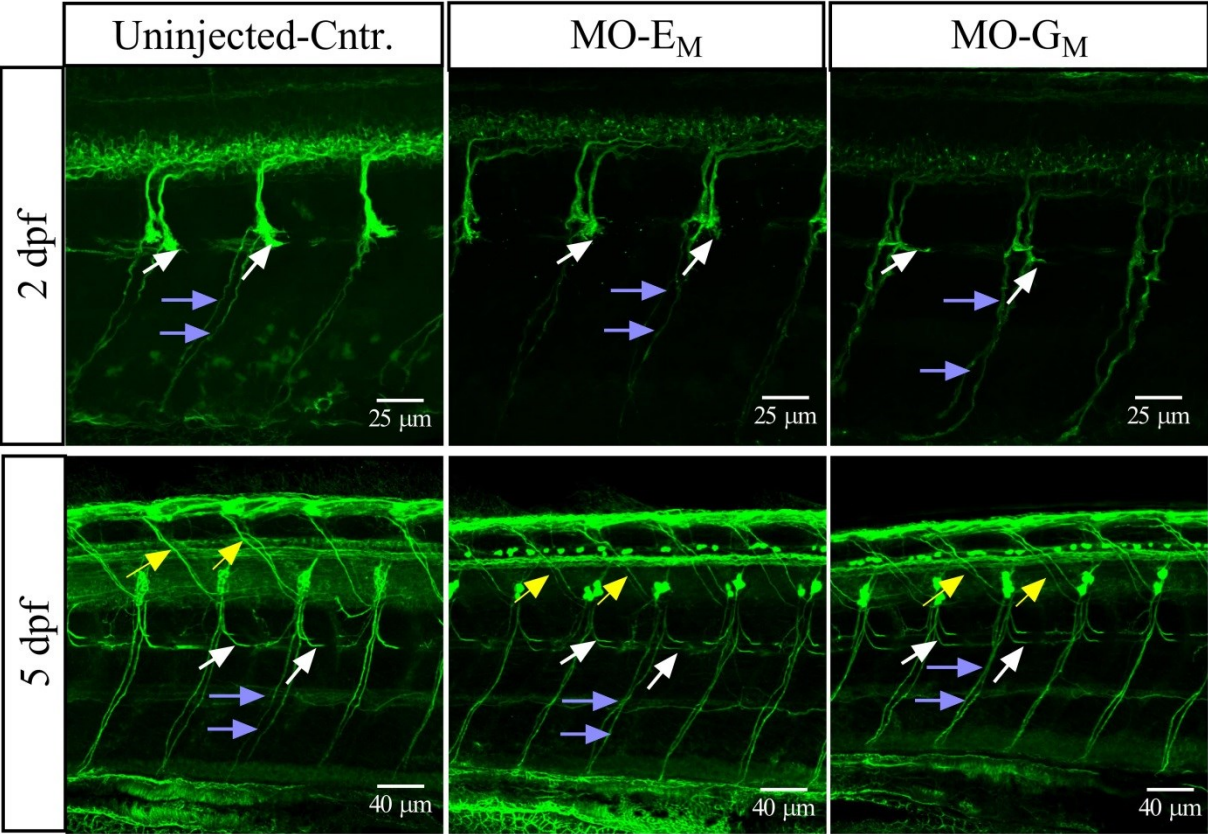


Figure 4.5

Secondary motor neuron axonal branching in 2 dpf embryos and 5 dpf larvae of uninjected control, MO-E_M and MO-G_M. Yellow arrows indicate dorsal branches, white arrows indicate lateral branches and blue arrows indicate ventral branches. Axonal branches of secondary MN were immunolabelled with zn8 antibody and z-stack images were taken under confocal microscopy. Maximum intensity projection is shown, made from the z-stack images. No visual difference in the branching patterns could be specified in between different treatment groups at the same age.

Figure 4.6

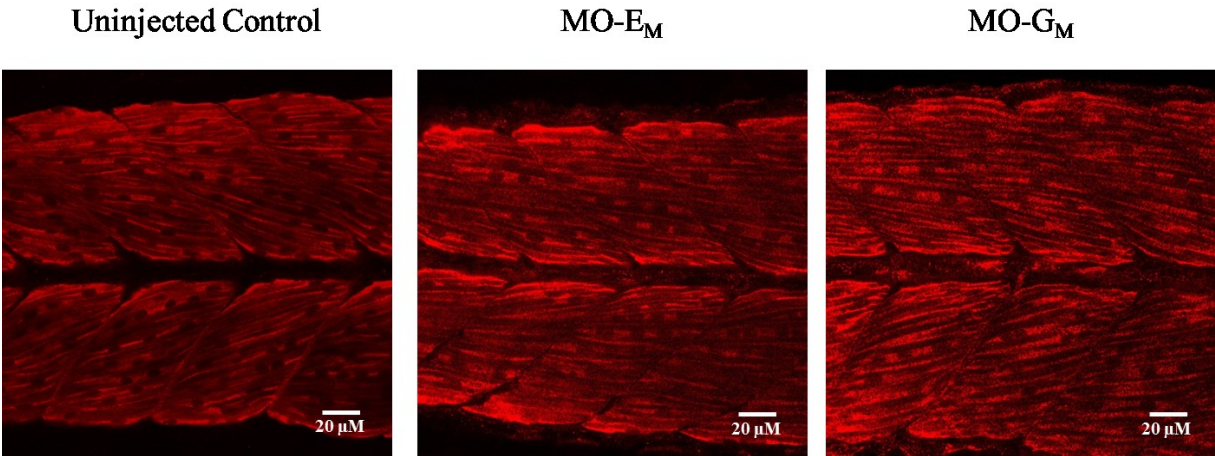


Figure 4.6

White muscle fiber in 2 dpf embryos of uninjected control, MO-EM and MO-GM.

White muscle fibers were immunolabelled with F310 antibody. Z-stack images were taken under confocal microscopy. Maximum intensity projection images are made by selecting a few layers of the z-stack images for clear visualization. The muscle fibers appeared normal in all treatment groups.

Figure 4.7

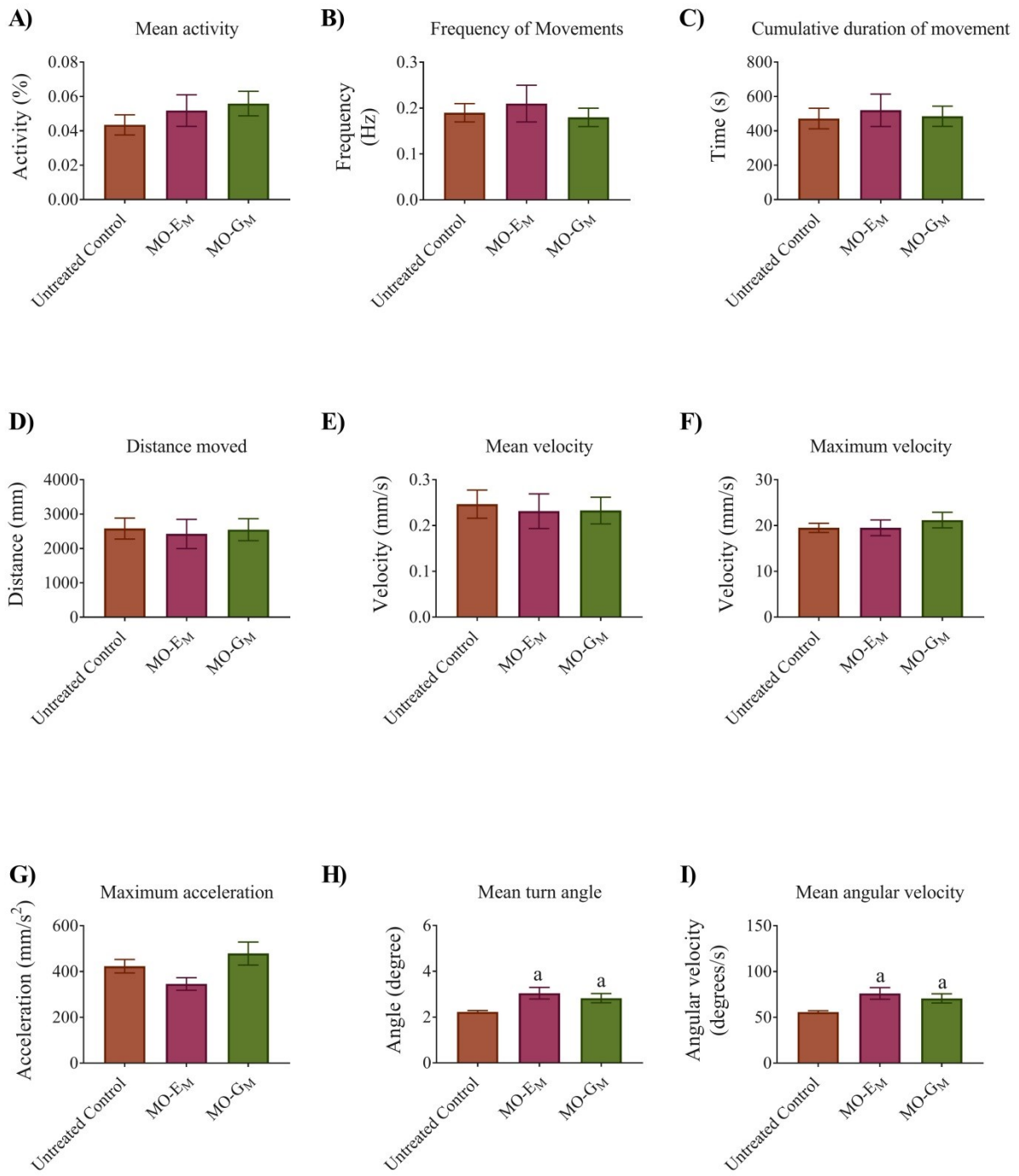


Figure 4.7

Quantification of free-swimming activity in 5 dpf larvae of uninjected control, MO-E_M and MO-G_M. Individual larvae were placed in wells of a 96-well-plate and their spontaneous movements were tracked and analyzed by EthoVision ® XT-11.5 software. Various parameters of the movements were analyzed and compared between uninjected control, MO-E_M and MO-G_M larvae. (A) Shows mean activity of the larvae in an hour. (B) Shows frequency of movements. (C) Shows cumulative duration of movement in an hour. (D) Shows total distance moved by the larvae within an hour. (E) Shows mean velocity during the movement. (F) Shows maximum instantaneous velocity attained during movements. (G) Shows maximum instantaneous acceleration attained during movements. (H) Shows mean turn angle during movements. Note, MO-E_M and MO-G_M shows higher turn angle compared to the control. (I) Shows mean angular velocity during movements Note, MO-E_M and MO-G_M shows higher angular velocity compared to the control. ^a Significantly different from uninjected control (p<0.05).

Figure 4.8

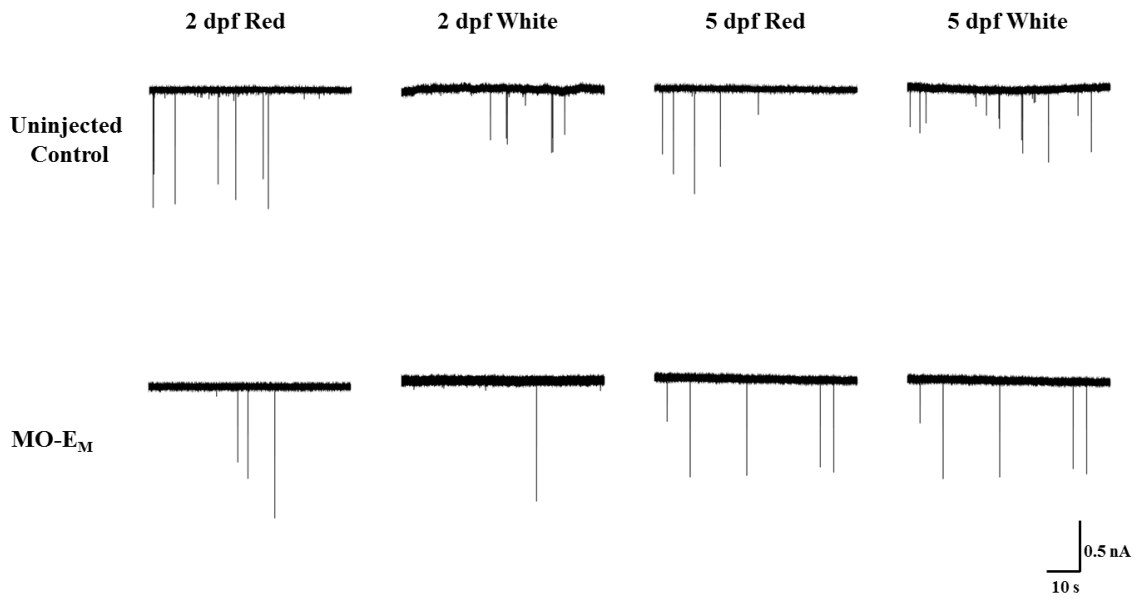
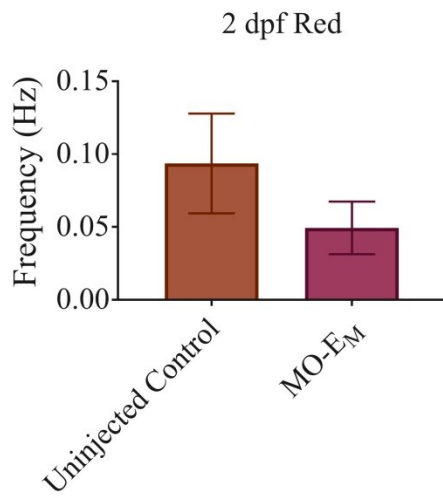


Figure 4.8

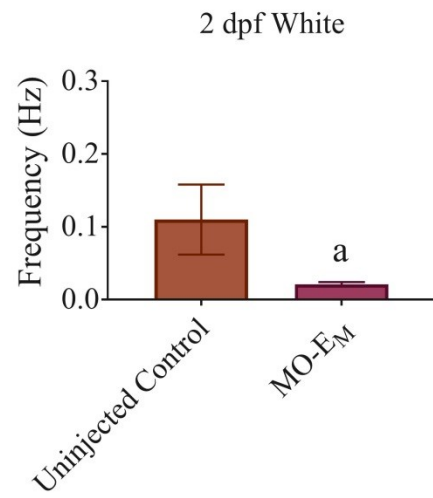
Raw traces of miniature endplate currents (mEPCs) recorded from red and white muscle fibers of embryonic and larval zebrafish. mEPC recordings were obtained from red and white muscle fibers from 2 dpf embryos and 5 dpf larvae of uninjected control and MO- E_M fish. Sample traces show spontaneous events occurring in 60s time period.

Figure 4.9

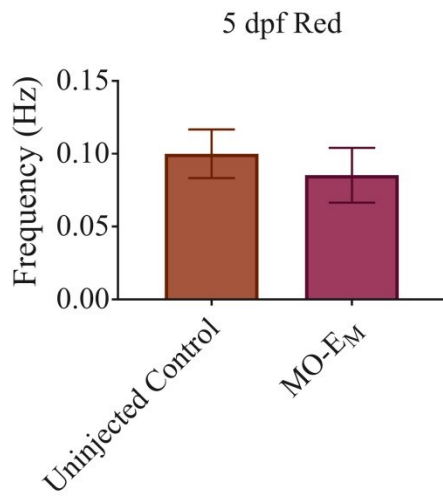
A)



B)



C)



D)

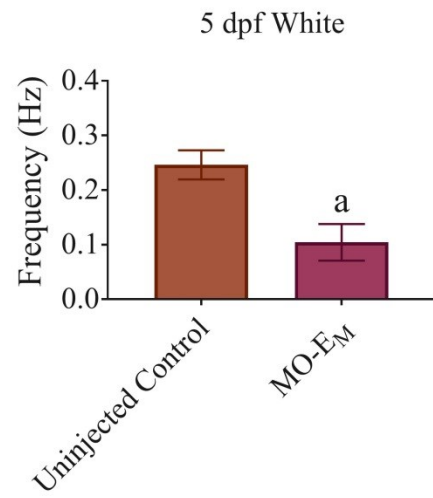


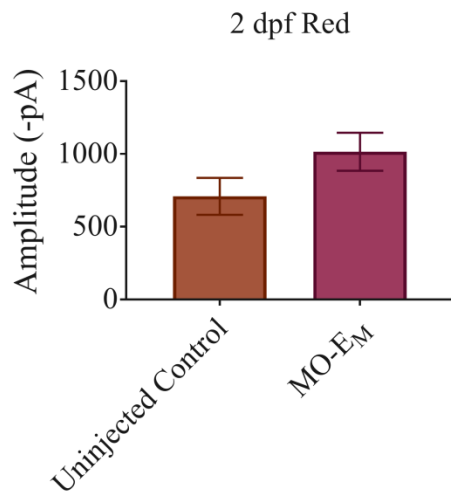
Figure 4.9

Comparison of mEPC frequency recorded from uninjected control and MO-E_M fish.

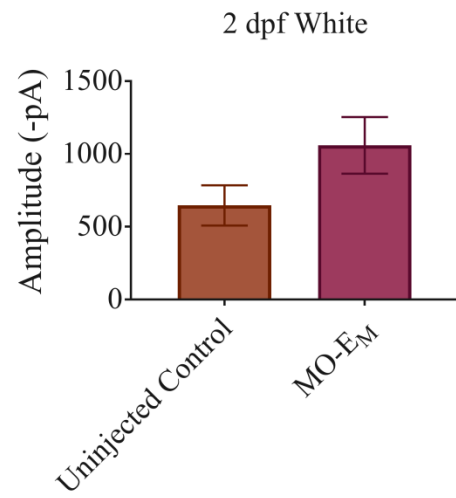
(A) Shows mEPC frequency recorded from 2 dpf red fibers. (B) Shows mEPC frequency recorded from 2 dpf white fibers. Frequency is reduced in MO-E_M compared to uninjected control fish. (C) Shows mEPC frequency recorded from 5 dpf red fibers. (D) Shows mEPC frequency recorded from 5 dpf white fibers. Frequency is reduced in MO-E_M compared to uninjected control fish. ^a Significantly different from uninjected control ($p < 0.05$).

Figure 4.10

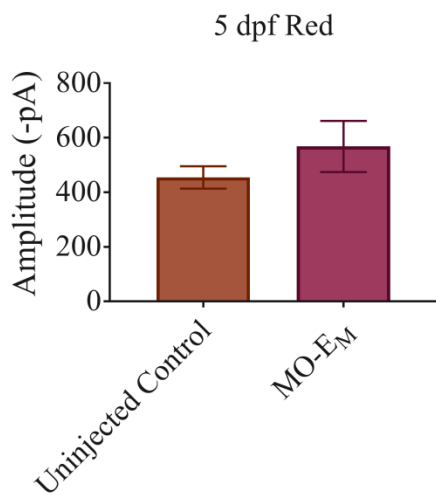
A)



B)



C)



D)

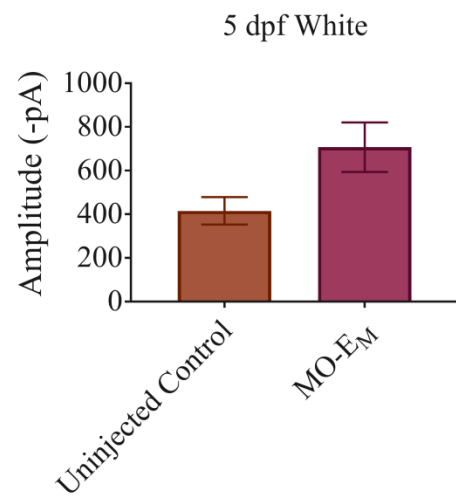


Figure 4.10

Comparison of mEPC amplitude recorded from uninjected control and MO- E_M fish. (A) Shows mEPC amplitude recorded from 2 dpf red fibers. (B) Shows mEPC amplitude recorded from 2 dpf white fibers. (C) Shows mEPC amplitude recorded from 5 dpf red fibers. (D) Shows mEPC amplitude recorded from 5 dpf white fibers. No change in amplitude was observed in between the treatment groups.

Figure 4.11

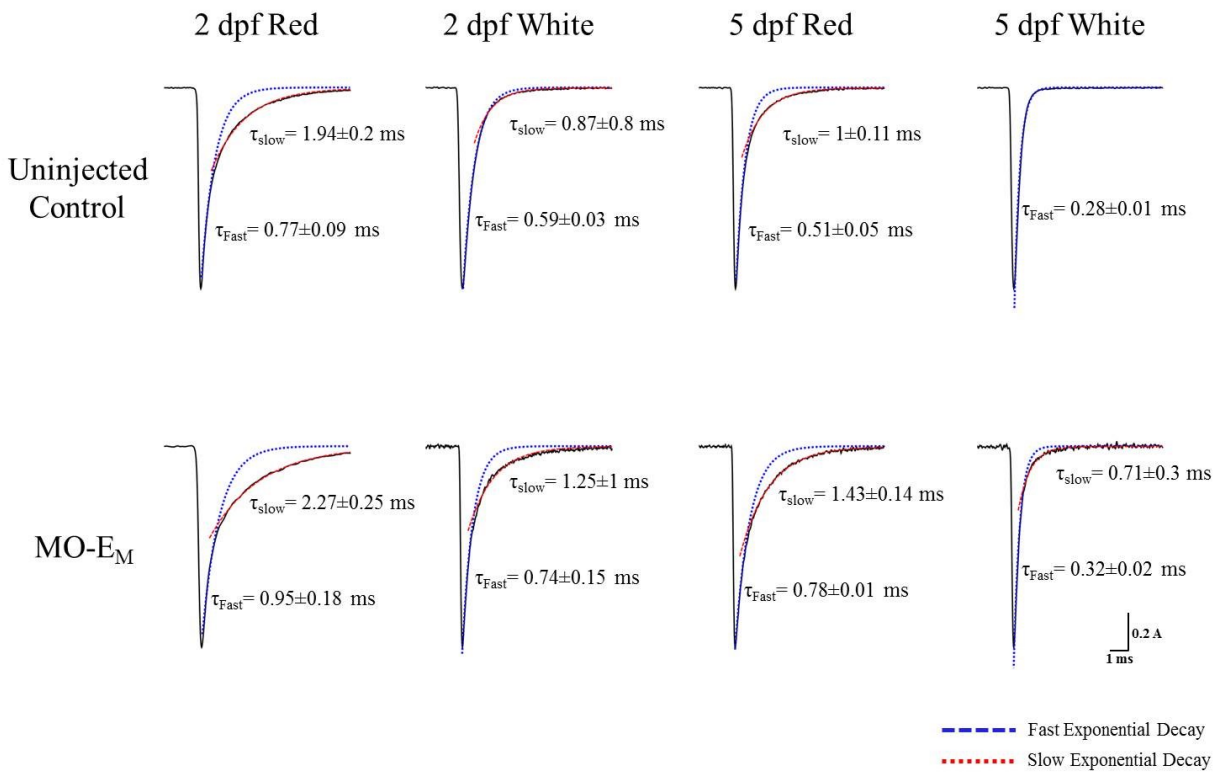


Figure 4.11

Averaged mEPCs fit with a single exponential decay over the fast component (τ_{fast} , blue dashed line) or slow component (τ_{slow} , red dotted line). mEPC events recorded from 2 dpf or 5 dpf red and white fibers were averaged and fit with a single exponential decay over the early phase (fast exponential decay) and late phase (slow exponential decay). Fast time constants (τ_{Fast}) and slow time constants (τ_{Slow}) of average mEPCs are noted aside.

Figure 4.12

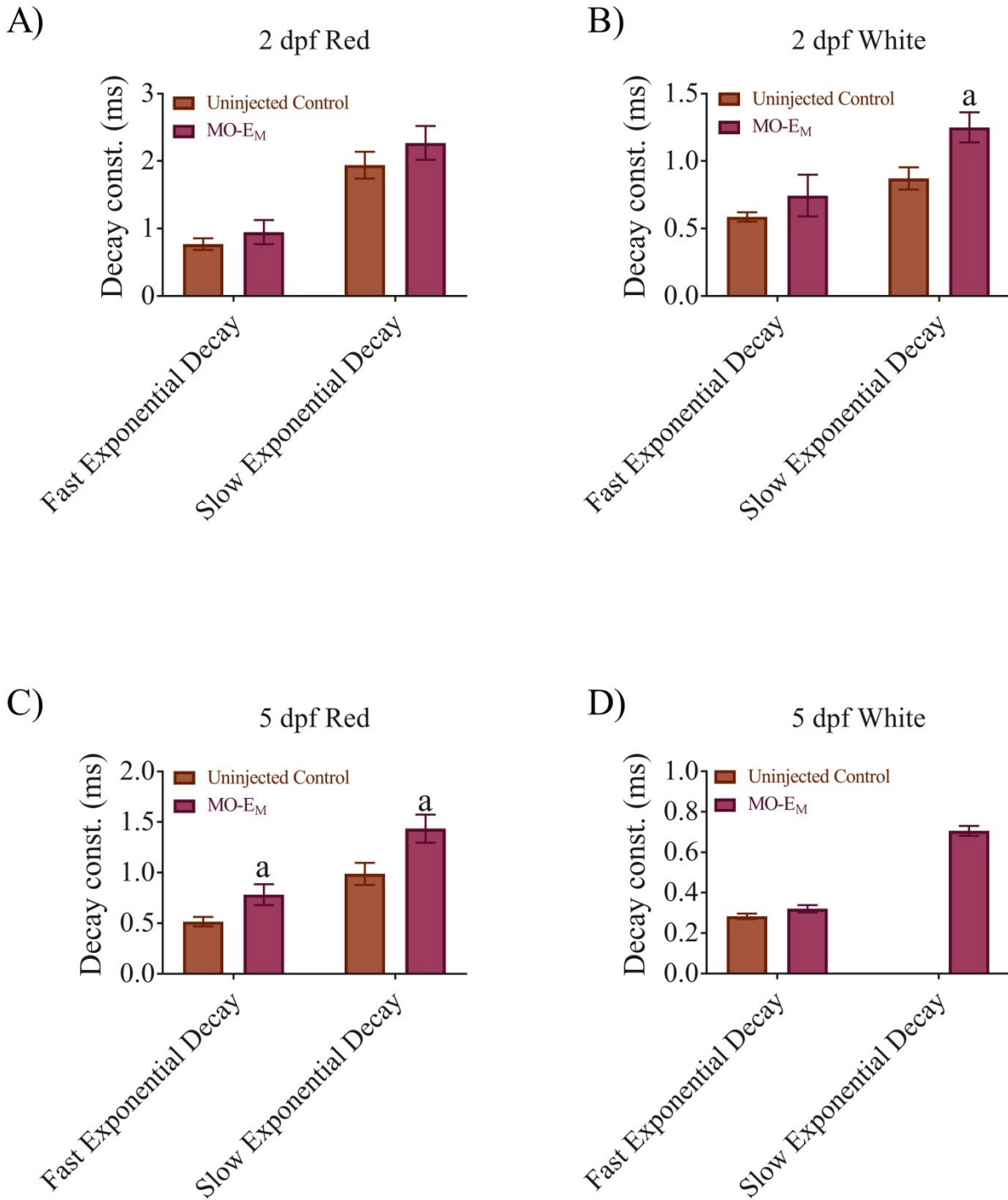


Figure 4.12

Comparison of mEPC decay time constant recorded from uninjected control and MO-E_M fish. Fast and slow exponential decay was fit on mEPC event averages and compared. (A) Shows mEPC decay time constants recorded from 2 dpf red fibers. (B) Shows mEPC decay time constants recorded from 2 dpf white fibers. Slow exponential decay constant in MO-E_M fish was significantly higher than uninjected control fish. (C) Shows mEPC decay time constants recorded from 5 dpf red fibers. Both fast and slow exponential decay constant in MO-E_M fish were significantly higher than uninjected control fish. (D) Shows mEPC decay time constants recorded from 5 dpf white fibers. Note that mEPCs of 5 dpf white fibers from uninjected control larvae fit with a fast single exponential decay only. 5 dpf uninjected fish did not show any slow exponential decay, whereas it was observed in some of the 5 dpf MO-E_M fish. ^a Significantly different from uninjected control of the same group of exponential decay ($p < 0.05$).

Chapter 5- Results- Role of γ and ϵ Subunits in Embryonic Development (Splice Blocking MOs)

An additional control for morpholino knockdown experiments is to rescue the morpholino induced effects by injecting mRNA that is specific for the gene of interest. However, for genes that are expressed in a precise spatiotemporally manner, a rescue is often difficult or impossible. Alternatively, many researchers use different sets of morpholinos such as one set of translation blocking morpholinos and a second set of splice blocking morpholinos, with the assumption that, results obtained using completely different sets of morpholino oligonucleotides targeting different sites in the mRNA should yield similar results if the same gene is targeted (Eisen & Smith, 2008). Since, in the previous experiment, I used translation blocking morpholinos used by Mongeon et al. (2011), I next designed a set of splice blocking MOs against ϵ and γ subunits and tested them at a range of concentrations. Splice blocking MOs alter the splicing of pre mRNA into mature mRNA and the efficacy of the MOs can be tested by RT-PCR.

5.1 Efficacy of Splice-blocking MOs

I used splice blocking morpholino oligonucleotides (MO) designed to knockdown expression of the γ (MO-G) or ϵ (MO-E) subunits of nAChRs. First, I set out to determine the morpholino concentrations required to successfully knockdown each subunit without inducing off-target effects. MO concentrations over 6 ng have been shown to produce extensive off-target effects including neural cell death, severely reduced body axis, abnormal or absent notochord, and distinctive cell deaths (Ekker & Larson, 2001). Therefore, I microinjected 1, 2.5, 5 and 7 ng of each MOs into 1-4 cell stage embryos. MO-G injection resulted in embryos with pericardial

edema and axial malformation at all concentrations. But the embryonic survival rate was not affected by morpholino concentrations up to and including 2.5 ng. Therefore, I decided to deliver 2.5 ng of MO-G for my study. Off-target effects were only seen with the highest concentration of MO-E. Therefore, I chose to inject 5 ng of MO-E for my study. A standard control MO (MO-Cntr.) that does not bind to any zebrafish mRNA was also injected at a concentration of 5 ng, as a control to the experiment.

Splice blocking MOs bind to the Intron-Exon junction of pre-mRNA and modifies their normal splicing event by either including an intron, or by excising an exon from mature mRNA. Appropriate splicing can be confirmed by RT-PCR and gel electrophoresis by showing the presence of altered bands on the agarose gel. I confirmed the successful alteration of splicing of ϵ and γ subunits at 5 dpf larvae following injection of 5 ng of MO-E and 2.5 ng MO-G with RT-PCR (Fig 5.1 A, B). A misplaced or altered band was only present with the injection of MO-E or MO-G, but not in MO-Cntr. or in uninjected embryos.

5.2 Morphological Analysis

Sample images of zebrafish embryo (2 dpf) and larva (5 dpf) with MO-Cntr., MO-E and MO-G injections are shown in Fig 5.2. While most of the fish did not show any sign of axial malformation, pericardial edema or curved tail region with MO-Cntr. injections, slight curvature of tail region was consistently observed in MO-E fish both at 2 and 5 dpf. In contrast, MO-G injected fish exhibited pronounced morphological defects with pericardial edema and axial malformation (Fig 5.2). Next, I quantified the number of fish exhibiting morphological defects. Only $3.3 \pm 5.7\%$ and $6.1 \pm 5.4\%$ zebrafish injected with MO-Cntr. showed some sort of morphological abnormalities at 2 dpf and 5 dpf respectively (N=3 batches) (Fig 5.3). Among

MO-E fish, $77.8 \pm 12.7\%$ embryos (2 dpf, N=3 batches; $p=0.0003$) and $80.5 \pm 19.2\%$ larvae (5 dpf, N=3 batches; $p=0.0008$) exhibited morphological defects, while $89.8 \pm 11.7\%$ embryos (2 dpf, N=3 batches; $p=0.0002$) and $95.2 \pm 8.3\%$ larvae (5 dpf, N=3 batches; $p=0.0003$) injected with MO-G were defective (Fig 5.3).

5.3 Expression of nAChR

If zebrafish muscle fibers express γ and ϵ subunit containing receptors differentially during development, knockdown of the subunits should result in reduction of nAChR expression in an age specific manner. However, expression of nAChRs was unaltered with the translation blocking MOs. The lack of alteration in receptor expression can be caused by ineffective MOs. Alternatively; it is possible that when one subunit is knocked down, there is upregulation of another subunit to compensate for its absence. To confirm that lack of alteration in receptor expression was not caused by ineffectiveness of the translation blocking MOs, I repeated the experiment with splice blocking MOs.

Figure 5.4 shows the α -bungarotoxin labelling of nAChRs at 2 dpf embryos and 5 dpf larvae following injection of MO-Cntr, MO-E and MO-G. AT 2 dpf, nAChRs are labelled as a thin continuous line along myoseptal boundary, whereas they appear as distributed puncta along the medial region of a muscle block. By 5 dpf, the myoseptal region grows thicker, whereas the medial nAChR puncta are distributed along the entire length of the muscle block in MO-Cntr fish. MO-E injected embryos at 2 dpf did not appear to be different from MO-Cntr. embryos. But distributed synapses in MO-E were markedly reduced compared to controls at 5 dpf. In contrast, both myoseptal and distributed nAChRs were disorganized in MO-G injected fish at both 2 dpf

and 5 dpf. Myoseptal nAChRs were often absent or difficult to distinguish from distributed receptors in the MO-G fish (Fig 5.4).

Quantification of the nAChR puncta matched visual observations (Fig 5.5). In 2 dpf animals, the number of puncta in MO-Cntr. embryos was 137 ± 2 (/1000 μm^2 , n=5). The number of puncta in MO-E injected embryos was not significantly different than controls (126 ± 2 puncta /1000 μm^2 , n=8, p= 0.09), but the number in MO-G injected embryos was significantly reduced (119 ± 6 puncta /1000 μm^2 , n=12, p=0.02) compared to control (Fig 5.5 A). In 5 dpf fish, there was a significant reduction in the number of puncta in MO-E injected fish but not in MO-G injected fish, compared to MO-Cntr. injected animals. In particular, MO-Cntr. injected fish expressed 144 ± 8 puncta (/1000 μm^2 , n=5), MO-E injected fish expressed 41 ± 6 puncta (/1000 μm^2 , n=7; p=0.007) and MO-G injected fish had 143 ± 8 puncta (/1000 μm^2 , n=5; p>0.9999) (Fig 5.5 B). These findings suggest that nAChRs containing the γ subunit are predominant at 2 dpf whereas nAChRs containing the ϵ subunit are predominant at 5 dpf. Additionally, the results also suggest that the γ subunit plays a role in the maintenance and the orderly distribution of nAChRs, because knockdown of this subunit results in a disordered distribution of nAChRs.

5.4 Colocalization of Synaptic Vesicles

In muscle fibers, nAChRs are expressed post-synaptically, directly apposed to the nerve terminals of motor neurons. Since the expression pattern of nAChRs was affected in ϵ and γ subunit knockdowns, I wondered whether the distribution of presynaptic terminals was also altered. To examine that, I labelled presynaptic sites with a synaptic vesicle marker, anti-SV₂ antibody, while postsynaptic nAChRs were simultaneously labelled with α -bungarotoxin. The co-labelled images were visually inspected to determine if distinct regions devoid of

superimposed labelling by either α -bungarotoxin or SV₂ could be identified. No quantitative analysis was done on the images.

At 2 dpf, anti-SV2 and α -bungarotoxin staining aligned appropriately in MO-Cntr. embryos (n=4) and in MO-E embryos, suggesting that the distribution of synaptic vesicles remained unaltered and that the lack of the ϵ subunit has very little effect in young animals (Fig 5.6). However, in MO-G injected embryos, while α -bungarotoxin labelling was distributed in an unorganized manner, the corresponding anti-SV2 immunostaining was mostly absent (n=4) (Fig 5.6), indicating that the γ subunit is critical for development of the synaptic region at this age.

In 5 day old animals, knockdown of the ϵ subunit caused a reduction in nAChR expression. But the absence of the receptor did not induce any change in the the presynaptic terminal expression pattern, as the overall anti-SV2 immunostaining pattern remained similar between MO-E (n=7) and MO-Cntr. fish (n=5) (Fig 5.7). Thus, despite the presence of synaptic vesicles, the corresponding nAChR clusters were absent. In contrast, knockdown of the γ subunit did not affect the colocalization of SV2 and α -bungarotoxin (n=5). Synaptic vesicles remained directly apposed to the nAChR clusters. But, similar to the unorganized distribution pattern of nAChR cluster, the distribution pattern of anti-SV2 labelling was also unorganized (Fig 5.7).

5.5 Motor Neuron Branching

Synaptic vesicles are located at the axon terminals of motor neurons. Distribution of synaptic vesicles is affected particularly in γ subunit knockdown zebrafish. However, it is not known whether the disruption in this distribution is limited to changes at only the NMJ or if knockdown of the subunit affects motor neuron branching as well. To examine that, I labelled

the axon branches of primary and secondary motor neurons with anti-znp1 and anti-zn8 antibodies respectively in 2 and 5 dpf fish injected with MO-Cntr., MO-E and MO-G.

At 2 dpf, primary MN branching was greatly reduced in MO-E embryos compared to MO-Cntr. (Fig 5.8). In particular, primary branches emanating from the primary MN were present, but secondary and tertiary branches that ramify from the primary branches were markedly absent in these embryos. The entire organization of the primary MN arborization was disrupted in MO-G embryos (Fig 5.8). In 4 out of 5 MO-G embryos, the spinal cord was found at the midline of the body along the horizontal myoseptum instead of in the dorsal region of the fish. The branching of primary MNs in 5 dpf animals appeared to develop normally in MO-E fish (n=6) but exhibited disrupted organization in MO-G fish (n=6) when compared to MO-Cntr. (n=5) (Fig 5.8). Myoseptal regions in MO-Cntr. and MO-E fish showed chevron shaped branch along with reticular branching pattern along the entire muscle block. Similar chevron shaped myoseptal staining was absent in the MO-G fish as well as the reticular branching pattern was highly disrupted. Thus the γ subunit seems to play a critical role in proper development of primary motor neuron branching.

I also examined the secondary MN branching in these fish (Fig 5.9). At 2 dpf, the ventral branches of secondary MNs were visible in MO-Cntr. fish (n=7), but lateral or dorsal branches were not yet developed. MO-E fish (n=6) showed a similar pattern with prominent ventral branching but no lateral branching, suggesting ϵ subunit knockdown does not affect the development of secondary MN branching at this age (Fig 5.9). Anti-ZN8 immunolabelling could not be identified in 8 out of 11 MO-G embryos, and aberrant ventral branching was observed in 2 out of 11 embryos (Fig 5.9). At 5 dpf, both dorsal, ventral and lateral branches could be easily

identified in MO-Cntr. (n=5) and MO-E fish (n=5) confirming the lack of effect of MO-E in secondary MN development (Fig 5.9). However, the position and branching of secondary MNs were severely affected in MO-G fish (n=4). Neither dorsal nor lateral branches could be identified in these fish (Fig 5.9). Altogether, the results of MN staining suggest that lack of ϵ subunit does not affect the development of MN arborization, but γ subunit containing nAChRs play a critical role in regulating the proper development of MN branching in zebrafish.

5.6 mEPC Recording from Red and White Muscle Fibers

Knockdown of ϵ and γ subunits alter the distribution and quantity of nAChR puncta. They also affect the developing and branching of motor neurons. As both the pre and post-synaptic elements are affected by the knockdown of these subunits, I asked what effect this might have on the properties of synaptic currents. Therefore, I recorded and analyzed mEPC currents from red and white muscle fibers at both 2 dpf and 5 dpf. Sample traces of the recordings are shown in Fig 5.10.

First, I analyzed the frequency of mEPC events (Fig 5.11). Despite the reduction of nAChR puncta, the mEPC frequency remained unaltered in all the ages examined between MO-Cntr. and the subunit knockdowns. In 2 dpf red fibers, mEPC frequencies were 0.04 ± 0.007 , 0.05 ± 0.008 and 0.04 ± 0.02 Hz for MO-Cntr. (n=7), MO-E (n=7) and MO-G (n=6) (Fig 5.11 A). In 2 dpf white fibers, the values were 0.08 ± 0.01 (MO-Cntr., n=6), 0.09 ± 0.005 (MO-E, n=6) and 0.09 ± 0.03 Hz (MO-G, n=8) (Fig 5.11 B). In 5 dpf red fibers, mEPC frequencies increased compared to 2 dpf, but were not different between the groups. MO-Cntr. fish had a frequency of 0.07 ± 0.01 HZ (n=7) whereas MO-E and MO-G injected fish had frequency of 0.12 ± 0.03 (n=6) and 0.08 ± 0.02 HZ (n=7) respectively (Fig 5.11 C). The frequency of mEPCs

recorded from 5 dpf white fibers was also higher compared to 2 dpf, with values of 0.41 ± 0.11 , 0.36 ± 0.07 and 0.26 ± 0.06 HZ for MO-Cntr. (n=8), MO-E (n=9) and MO-G (n=6) respectively (Fig 5.11 D).

Next, I analyzed the mean mEPC amplitude as shown in Fig 5.12. In 2 dpf red fibers, average amplitudes for MO-Cntr. (n=6), MO-E (n=8) and MO-G (n=6) were 679 ± 92 , 598 ± 81 and 401 ± 75 pA respectively, which were not significantly different (Fig 5.12 A). In the 2 dpf white fibers, the mean amplitude was relatively low in MO-E injected embryos (448 ± 119 pA, n=6) and high in MO-G injected embryos (1223 ± 160 pA, n=8), but neither of them was statistically different from MO-Cntr. injected embryos (847 ± 197 pA, n=6) (Fig 5.12 B). In 5 dpf red fibers there was no significant difference in the mean mEPC amplitude recorded from control and morphants. Mean amplitudes were 532 ± 37 , 429 ± 125 and 551 ± 56 for control MO (n=7), MO-E (n=6) and MO-G (n=7) respectively (Fig 5.12 C). A significant reduction of mEPC amplitude is observed in 5 dpf white fibers with MO-E injection (278 ± 44 pA, n=9) compared to MO-Cntr. fish (681 ± 67 pA, n=8) ($p=0.00192$). MO-G fish showed no difference (649 ± 146 pA, n=6) (Fig 5.12 D).

Finally, I analyzed the decay kinetics of the mean mEPCs recorded from red and white muscle fibers at 2 dpf and 5 dpf time points. Sample average mEPCs are superimposed and shown in Fig 5.13. MO-E resulted in no change in 2 dpf red fiber, but the slow exponential decay in 2 dpf white fiber was significantly larger (Fig 5.14 A, B). 5 dpf red fibers also continued with double exponential decay kinetics that were unchanged by MO-G or MO-E (Fig 5.14 C). However, the difference in kinetics was observed at 5 dpf white fibers. While mEPCs from MO-

Cntr. and MO-G fish decayed with single exponential kinetics, MO-E fish had double exponential decay (Fig 5.14 D). The decay kinetics is listed in Table 5.1.

5.7 Single Channel Recording

In mammals, γ subunit containing nicotinic receptors show small amplitude- long open channels, whereas ϵ subunit containing receptors exhibit large amplitude but short open channels (Mishina et al., 1986). In contrast, Mongeon et al. (2011) suggested that long open channel activity in zebrafish results from nAChRs that contain $\alpha\beta\delta$ subunits only, whereas the γ subunit does not participate in the formation of functional receptors. Thus, zebrafish NMJs have a unique receptor combination that has not been documented in other mammals. I wanted to reexamine this observation using the splice blocking MO injected fish. I recorded single channel currents from outside out patches pulled from red and white muscle fibers of MO-E and MO-G injected embryos at 2 dpf (n=7 for MO-G, n=9 for MO-E) and 5 dpf (n=7 for MO-G, n=10 for MO-E) time points. Single channel currents were recorded at -100 mV holding potential in the presence of acetylcholine (0.6 μ M), and they were confirmed to be nAChR currents by washing on curare which blocks all nAChRs. Sample traces of single channel recordings are shown in Fig 5.15. While I was recording single channel events from MO-G and MO-E, my MO-Cntr. solution was used in its entirety, and the re-ordered MO-Cntr. was not readily available. Therefore I compared the results of morpholino injections with my previously recorded single channel currents from uninjected control fish. Unfortunately, the single channel recording rig was disassembled due to labs moving location and I was unable to record additional single channel events from MO-Cntr. fish.

In red muscle fibers, MO injected fish exhibited 2 conductance levels of single channels at both 2 and 5 dpf age. From amplitude distribution plots, I found that the lower conductance level were 39 pS in both 2 and 5 dpf fish injected with MO-E (Fig 5.16 A, B), 42 pS in 2 dpf MO-G injected embryos (Fig 5.16 C) and 43 pS in 5 dpf MO-G injected larvae (Fig 5.16 D). The higher conductance levels were 71 pS, 73 pS, 68 pS and 69 pS for 2 dpf MO-E, 5 dpf MO-E, 2 dpf MO-G and 5 dpf MO-G fish respectively (Fig 5.16). Compared to untreated control embryos which showed single channel conductance values around ~45 pS and ~65 pS, the lower conductance level was a little lower and higher conductance values were slightly higher.

Similar to uninjected control fish, red fibers of both MO-E and MO-G injected fish exhibited 2 groups of channels- short open channels and long open channels, based on open/dwell time. In MO-E injected embryos, dwell time constant of short and long open channels were 0.33 ± 0.29 ms and 1.66 ± 0.13 ms at 2 dpf. The open time of these channels was shorter in 5 dpf larvae, resulting in dwell time constant of 0.27 ± 0.21 ms and 1.51 ± 0.18 ms respectively (Fig 5.17 A, B). In MO-G injected embryos (2 dpf), the dwell time constants were 0.49 ± 0.17 ms and 2.09 ± 0.34 ms respectively which were slower than 2 dpf MO-E injected embryos. These channels also showed age dependent shortening of open time, as the 5 dpf red fibers with MO-G had dwell time constants of 0.36 ± 0.20 ms and 1.61 ± 0.31 ms respectively (Fig 5.17 C, D). However, the time constants were not significantly different from same age uninjected control fish (Fig 5.18).

Single channel conductance and open times were unaltered in red muscle fibers following MO-E and MO-G injections suggesting the kinetics of the nAChRs are not altered by these morpholinos. However, if the subunits contribute to either long or short open channels, there

should be a reduction of specific channel type compared to the others following knockdown of a subunit. Therefore, I compiled all the single channel recordings from specific group (Uninjected, MO-E and MO-G) and compared the relative ratio of short vs long open channels (Fig 5.19). At 2 dpf, 67% of recorded events from red fibers of uninjected control embryos were short open times and 33% comprised the long opening ones. In MO-E injected embryos, the short open channel ratio is greatly reduced to 35% while long open channels were increased to 65%. No alterations in the ratio of events were observed with MO-G injections in comparison to uninjected embryos as short and long open channel contribution were 69% and 31% respectively (Fig 5.19 A). In 5 dpf red fibers, uninjected control embryos exhibited 76% short open channels and 24% long open channels. The contributions were less affected with MO-G injections with 63% short vs 37% long open channels. In contrast, in MO-E injected larvae short and long open channels were almost equal (52% and 48% respectively) (Fig 5.19 B). Thus, it suggests that ϵ subunit perhaps contribute to the short open channels in red fibers, but γ subunits did not exhibit any effect.

Similar to red muscle fibers, white muscle fibers in uninjected control fish also exhibit short and long open channel activity with two conductance levels of ~ 55 pS and ~ 73 pS, however the short open channels are predominant at 2 dpf and almost exclusive by 5 dpf (Ahmed & Ali, 2016). When the ϵ subunit was knocked down, very few single channel events were recorded from 2 dpf white muscle fibers. In 6 out of 9 recordings I found no single channel events at all, while only 3 recordings exhibited very small number of events. In 5 dpf animals, no events were recorded in 10 patches (Fig 5.15). This suggests that the vast majority of nAChRs associated with white muscle fibers contain the ϵ subunit. In contrast, when MO-G was injected,

both the long and short open channels with two conductance levels were recorded, however long open channel events were much less frequent at 2 dpf and almost absent at 5 dpf.

Amplitude distribution plots revealed that 2 dpf MO-E embryos also exhibited single channel events comprised of 2 conductance levels of 40 pS and 76 pS (Fig 5.20 A). With MO-G, the 2 conductance levels at 2 dpf were 38.5 pS and 79 pS (Fig 5.20 C). These values did not change much in 5 dpf larvae, which showed conductance levels of 35 pS and 73 pS (Fig 5.20 D). Interestingly, the smaller conductance levels with both the morpholinos were markedly smaller than uninjected control fish, while the high conductance level was unaffected.

Next, I analyzed open channel distribution properties of the events. The number of events in 2 dpf MO-E embryos was very small, and they were fit with a single open time constant of 0.91 ± 0.20 ms (Fig 5.21 A). With MO-G injections, 96% of events at 2 dpf white fibers were short open channels with dwell time constant of 0.48 ± 0.11 ms, while 4% events had longer dwell time constant of 2.33 ± 2.62 ms (Fig 5.21 C). In 5 dpf larvae, all the events were fit with a single dwell time constant of 0.43 ± 0.06 ms (Fig 5.21 D). When compared to uninjected fish, the fast dwell time constant was significantly higher in 2 dpf MO-E injected embryos (Fig 5.22 A) while MO-G had no effect at either 2 dpf or 5 dpf age (Fig 5.22 A, B).

Altogether, my results suggest that knockdown of the ϵ subunit affected short open channels in both red and white muscle fibers. Knockdown of γ subunit only partially affected the long open channels in white fibers but had no effect on red muscle fibers. These results were consistent with the observations of Mongeon et al. (2011).

5.8 Escape Response and Swimming Behavior

Locomotor activity of zebrafish embryos starts around 17 hpf while the embryos are still in the chorion. At this stage the embryos show spontaneous coiling of their body. These movements coincide with the formation of early NMJs around 17 hpf. By 24 hpf, the embryos respond to visual or tactile stimuli by contracting trunk muscles on the contralateral side of the stimuli. The rapid contraction on one side of the body makes the embryo appear like the letter 'C', which is why this form of escape response is termed as the 'C-bend' escape response. The rapid C-bend movement is followed by a brief period of swimming. At such an early stage, the embryos depend on their yolk for energy; therefore, they don't need to swim continuously. However, by 5 dpf, when the yolk is almost entirely depleted, the larvae start to swim to look for food. The swimming frequency increases more as the larvae continues to develop. This slow and sustained swimming mainly involves the activity of red muscle fibers. White muscle fibers are recruited when faster turns and swim events are required.

In my previous experiments I had shown that ϵ and γ subunits of nAChRs are critical for proper development of NMJs, motor neurons and muscle fibers in zebrafish. I then wanted to determine how these alterations affect locomotor activity. To do that, I examined the escape response of 2 dpf control and morphant embryos following tactile stimulation to the head. I also examined the unstimulated swimming behavior of 5 dpf larvae, and escape responses of larvae following a sound stimulus.

5.8.1 Escape Response at 2 dpf

To determine how knockdown of ϵ and γ subunits contribute to the C-bend escape response, I immobilized 2 dpf embryos in low melting point agarose and cut away the agarose from the trunk. Thus, the embryos were able to move their trunk while their head was still fixed in agar. I cut away a small portion of the agar near the otoliths and applied tactile stimulation to this region by ejecting a small water bolus through a glass pipette connected with picospritzer. Following tactile stimulation, the embryos move their tail eliciting C-bend. I tracked the tail movement during the C-bend and analyzed parameters such as the angle of C-bend, the time to maximum bend, maximum speed and acceleration attained during C-bend, and direction of C-bend.

The angle of the C-bend elicited by the tactile stimulus was not significantly different between MO-Cntr. (216 ± 20 degrees; $n=13$), MO-E embryos (201 ± 25 degrees; $n=12$) and MO-G embryos (165 ± 31 degrees, $n=9$) (Fig 5.23 A). Control embryos took 30 ± 2 ms ($n=13$) to complete a C-bend. MO-E embryos took 38 ± 4 ms ($n=13$) to complete the C-bend which was not significantly different from MO-Cntr., but MO-G embryos took 44 ± 5 ms, which was significantly longer than control (Fig 5.23 B). Upon stimulation, an embryo should bend its tail away from the direction of the stimulus, allowing it to escape. In controls, I saw 1 out of 13 embryos moving towards the stimulus (8%) while 12 of them moved away (92%). In MO-E injected embryos, 2 out of 15 embryos moved towards stimulus (13%) while 13 moved away (87%). In contrast, in MO-G injected embryos, 4 out of 9 animals moved towards the stimulus (44%) while 5 moved away (56%) (Fig 5.23 C).

Next, I analyzed the maximum speed and acceleration attained during the C-bend (Fig 5.24) to determine if morphant embryos were capable of attaining levels of speed and acceleration that were similar to the control fish. Maximum speed and acceleration of MO-Cntr. embryos were 0.2 ± 0.01 mm/s (n=13) and 0.11 ± 0.02 mm/s² (n=13). Mo-E embryos had maximum speed and acceleration of 0.19 ± 0.01 mm/s (n=12) and 0.1 ± 0.01 mm/s² respectively which were similar to control. In contrast, maximum speed and acceleration of MO-G embryos were 0.14 ± 0.01 mm/s (n=9) and 0.06 ± 0.01 mm/s² respectively. Both of them were significantly slower compared to control (p= 0.007 and .049 for speed and acceleration respectively) (Fig 5.24). Thus, knockdown of the γ subunit significantly affected the C-bend escape parameters in 2 dpf embryos.

5.8.2 Response to Sound Stimulus 5 dpf

Knockdown of the γ subunit altered the escape response in 2 dpf embryos, whereas ϵ subunit knockdown had no effect. To determine if knockdown of the subunits had any adverse effect on escape response at 5 dpf, I examined the response rate of the larvae to a sound stimulus (Fig 5.25). A sound pulse was generated through audacity software and played through computer sound boxes placed adjacent to the embryo dish. Upon exertion of the sound pulse, $74 \pm 7\%$ MO-Cntr. larvae (N=4 batches, n= 33 embryos) exhibited a quick C-bend followed by swimming. MO-E larvae showed slightly reduced response rate of $49 \pm 10\%$ (N=3 batches, n=20 embryos) which was not statistically different from control. However, only $13 \pm 1\%$ of MO-G larvae (N=3 batches, n=54 embryos; p=0.001 in comparison to control) exhibited a response to the sound pulse suggesting that knockdown of γ subunit severely disrupted the escape response of zebrafish.

5.8.3 Spontaneous Swimming at 5 dpf

Finally, I sought to determine if knockdown of ϵ and γ subunit also affect the unstimulated swimming of the fish. At 2 dpf, embryos mostly stay dormant unless stimulated. More regular swimming bouts are observed from 4 dpf onwards, when the yolk is mostly depleted, and the larvae need to swim to look for food. Therefore, I chose to analyze swimming activity of 5 dpf larvae.

Swimming activity over an hour were recorded and analyzed. Overall, MO-E and MO-G embryos showed significantly reduced activity compared to MO-Cntr. larvae (Fig 5.26A). Of the total time recorded, MO-Cntr. larvae were actively moving for $0.024 \pm 0.005\%$ of time (n=42). MO-E (n=48) and MO-G larvae were active for $0.009 \pm 0.001\%$ (n=48) and $0.005 \pm 0.004\%$ (n=12) of time respectively. The ϵ and γ knockdown larvae were also active less frequently. For instance, the frequency of movements for MO-Cntr., MO-E and MO-G injected larvae were 0.11 ± 0.02 Hz, 0.04 ± 0.01 Hz and 0.03 ± 0.01 Hz respectively (Fig 5.26 B). The cumulative duration of movements in an hour for MO-G (89 ± 36 s, n=13) was smaller than MO-Cntr. (219 ± 44 s, n=39; p= 0.049) while MO-E (168 ± 36 s, n=46) was similar to MO-Cntr. fish (Fig 5.26 C). Similarly, total distance moved in an hour by the MO-E larvae (813 ± 160 mm) were not significantly different from MO-Cntr. (1223 ± 228 mm), but MO-G injected larvae traversed significantly lower distance (567 ± 230 mm; p=0.02) (Fig 5.27 D).

Next, I analyzed the mean velocity during swimming and found that knockdown of the γ subunit significantly reduced the swimming velocity while ϵ knockdown had no significant effect (Fig 5.27A). Mean velocity for MO-Cntr. (n=40), MO-E (n=46) and MO-G (n=13) were 0.113 ± 0.02 mm/s, 0.06 ± 0.01 mm/s (p=0.13) and 0.05 ± 0.02 mm/s (p=0.01) respectively. The

maximum velocity and maximum acceleration during swimming were unaffected by the knockdown of either subunit (Fig 5.27 B, C). Maximum velocity for MO-Cntr. (n=40), MO-E (n=46) and MO-G (n=13) were 14.76 ± 0.92 mm/s, 13.3 ± 0.72 mm/s ($p=0.67$) and 12.62 ± 2.07 mm/s ($p=0.3$) respectively. Maximum acceleration for MO-Cntr. (n=40), MO-E (n=46) and MO-G (n=13) were 304.2 ± 15.77 mm/s², 289.7 ± 10.56 mm/s² ($p>0.99$) and 244.5 ± 29.23 mm/s² ($p=0.2$) respectively.

During swimming, the larvae often turn to change directions. I found that MO-Cntr. injected larvae make short turns averaging 3.2 ± 0.2 degrees (n=33), and that of MO-E injected larvae was 2.4 ± 0.3 degrees (n=19), which were not significantly different. In contrast, MO-G injected larvae had significantly greater turn angle (15.8 ± 6 degrees, n=10) (Fig 5.28 A). The angular velocity of turning was also significantly higher in MO-G injected larvae (394.5 ± 149.3 degrees/s, n=10) compared to MO-Cntr. (75.96 ± 4.9 degrees/s) and MO-E (74.44 ± 5.7 degrees/s, n=41) injected larvae (Fig 5.28 B). Thus, it shows that overall swimming of 5 dpf larvae are affected when ϵ or γ subunit is knocked down, where γ subunit knockdown has a greater effect on the overall locomotion of these fish.

Table 5.1:

Decay time course of the fast and slow exponential components from red and white fibers following injection of control MO (MO-Cntr.) and splice blocking MOs (MO-E and MO-G)

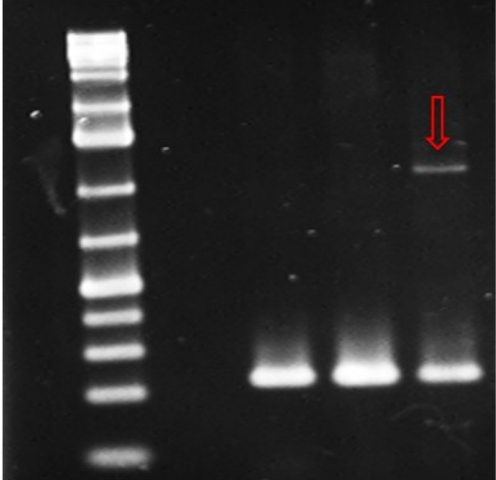
	2 dpf Red		2 dpf White		5 dpf Red		5 dpf White	
	Fast Exponential Time Constant (ms)	Slow Exponential Time Constant (ms)	Fast Exponential Time Constant (ms)	Slow Exponential Time Constant (ms)	Fast Exponential Time Constant (ms)	Slow Exponential Time Constant (ms)	Fast Exponential Time Constant (ms)	Slow Exponential Time Constant (ms)
MO-Cntr.	1.28±0.26 (n=6)	2.32±0.35 (n=6)	0.61±0.06 (n=5)	1.18±0.18 (n=5)	0.67±0.07 (n=7)	1.89±0.14 (n=7)	0.32±0.01 (n=8)	
MO-E	0.84±0.12 (n=8)	2.2±0.19 (n=8)	0.91±0.1 (n=8)	1.89±0.23 ^{a,c} (n=8)	0.7±0.07 (n=6)	1.51±0.2 (n=6)	0.6±0.09 ^a (n=9)	0.9±0.21 ^{a,c} (n=9)
MO-G	1.12±0.1 (n=6)	2.22±0.45 (n=6)	0.65±0.1 (n=8)	1.16±0.19 (n=8)	0.87±0.1 (n=7)	1.73±0.08 (n=7)	0.33±0.03 (n=5)	

^a Significantly different from MO-Cntr. (p<0.05).

^c Significantly different from MO-G (p<0.05).

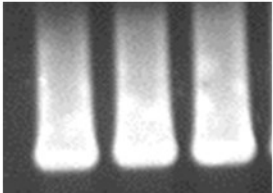
Figure 5.1

A) chrnE mRNA

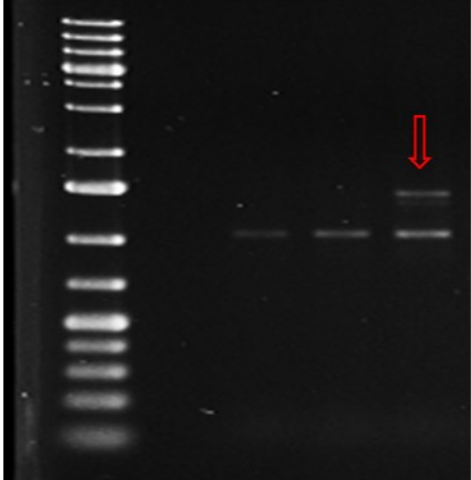


L 1 2 3

ef1a



B) chrnG mRNA



L 1 2 3

ef1a

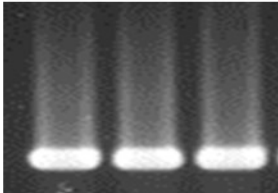


Figure 5.1

RT-PCR exhibiting alternate splicing in 5 dpf larvae following splice blocking morpholino injections. mRNA collected from the larvae were reverse transcribed and amplified in PCR reaction. PCR product was transferred in an agarose gel for electrophoretic separation. After electrophoresis, images of the gels were taken with UV irradiation. Expression of corresponding control mRNA of elongation factor α (*ef1a*) is shown at the bottom. (A) RT-PCR of *chnE* mRNA in uninjected control (1), control MO (MO-Cntr.) (2) and ϵ subunit MO (MO-E) (3) injected larvae. Red arrow indicates alternate spliced band in MO-E injected larvae. L denotes the ladder. (B) RT-PCR of *chnG* mRNA in uninjected control (1), control MO (MO-Cntr.) (2) and γ subunit MO (MO-G) (3) injected larvae. Red arrow indicates alternate spliced band in MO-G injected larvae. L denotes the ladder.

Figure 5.2

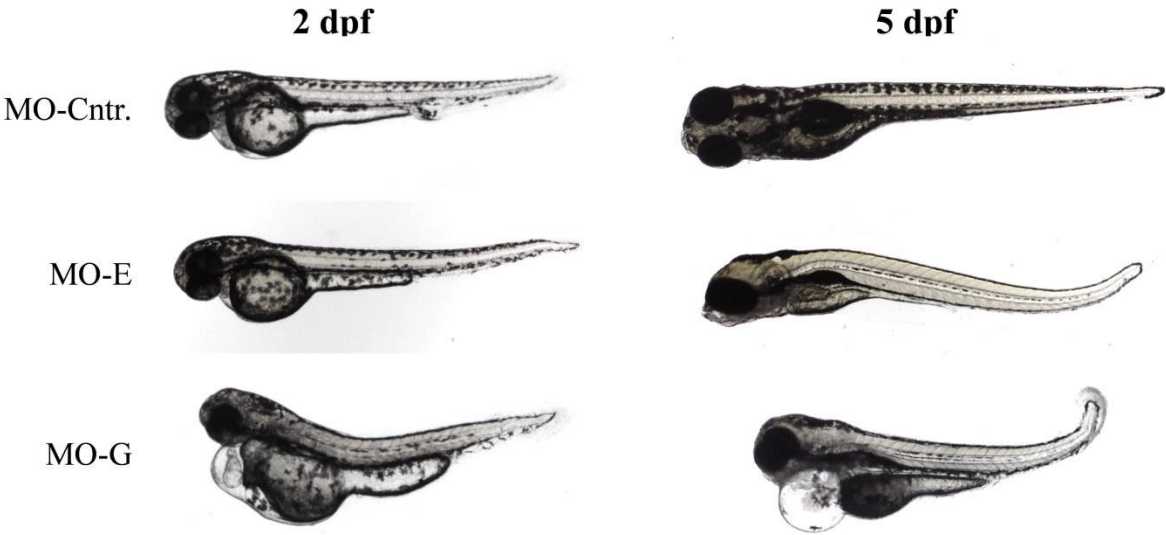


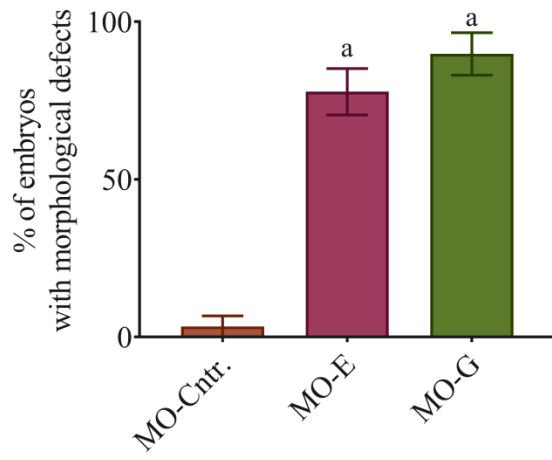
Figure 5.2

Morphology of zebrafish embryos injected with MO-Cntr., MO-E and MO-G.

Morpholino oligonucleotides were injected at 1-4 cell stage of the embryo and were grown in normal embryo media. Images of the fish were taken under bright field microscope. Left panel shows embryos at 2 dpf age and right panel shows the larvae at 5 dpf time point. Note MO-E fish shows slight tail curvature whereas MO-G fish exhibit axial malformation, pericardial edema and tail curvature.

Figure 5.3

A)



B)

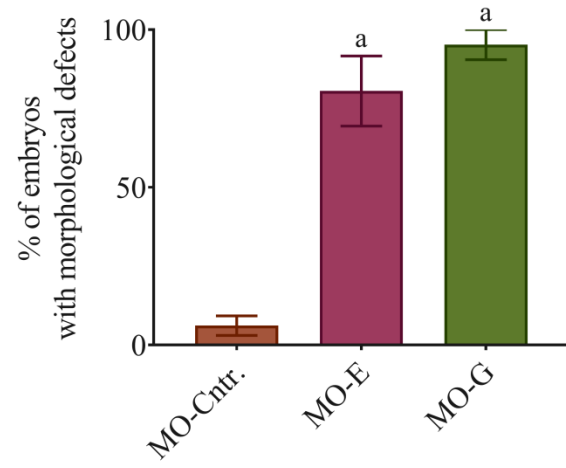


Figure 5.3

Quantification of morphological defects induced by MO-Cntr, MO-E and MO-G.

Morphological defects were observed through a dissecting microscope and ratio against total number of fish surviving at the particular stage was calculated. (A) Bar graph showing % of 2 dpf embryos exhibiting any form of morphological defect (curved tail, bent body axis or pericardial edema). (B) Bar graph showing % of 5 dpf larvae exhibiting any form of morphological defect (curved tail, bent body axis or pericardial edema). ^aSignificantly different from MO-Cntr. (p<0.05).

Figure 5.4

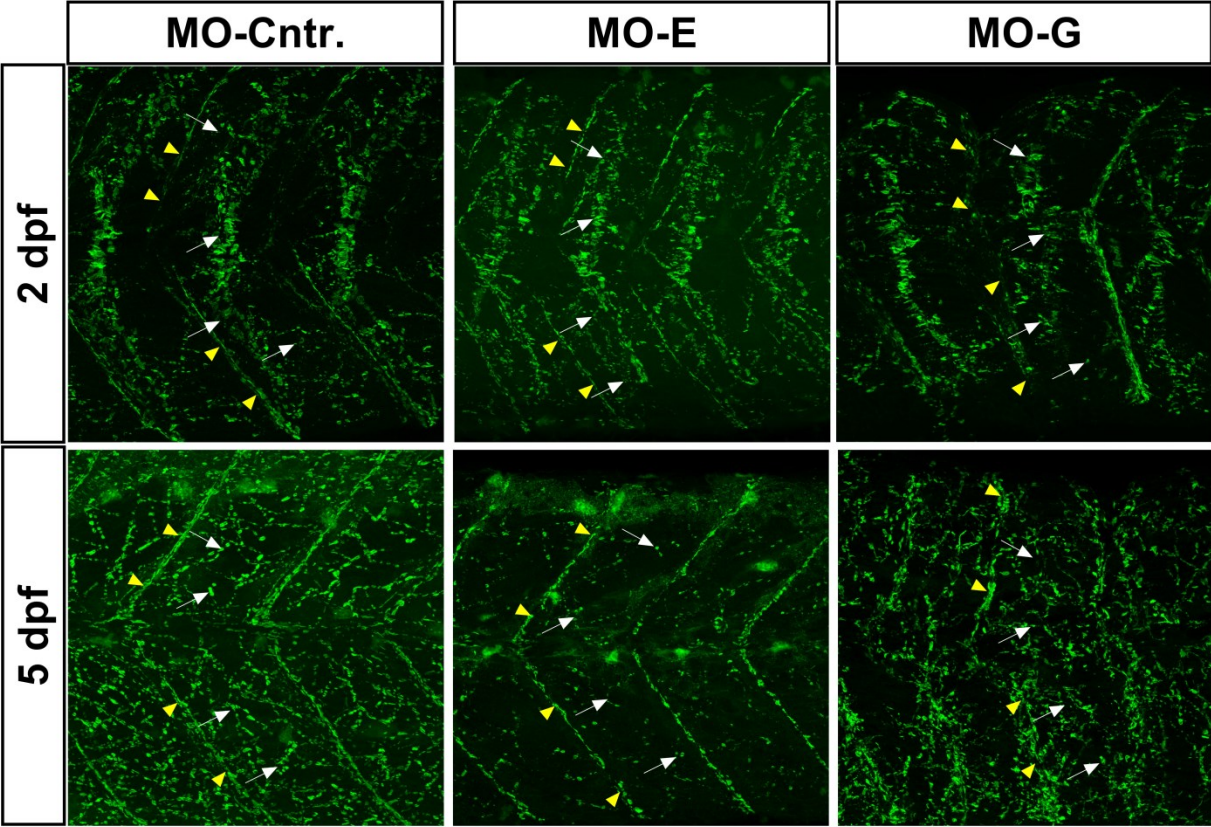


Figure 5.4

α -bungarotoxin staining of nAChRs in 2 dpf embryos and 5 dpf larvae of MO-Cntr., MO-E and MO-G. Yellow arrowheads indicate myoseptal region and white arrows indicate distributed synaptic regions. 2 dpf and 5 dpf zebrafish were stained with α -bungarotoxin and Z-stack images were taken under confocal microscopy. Maximum intensity projections made from the z-stack images are shown.

Figure 5.5

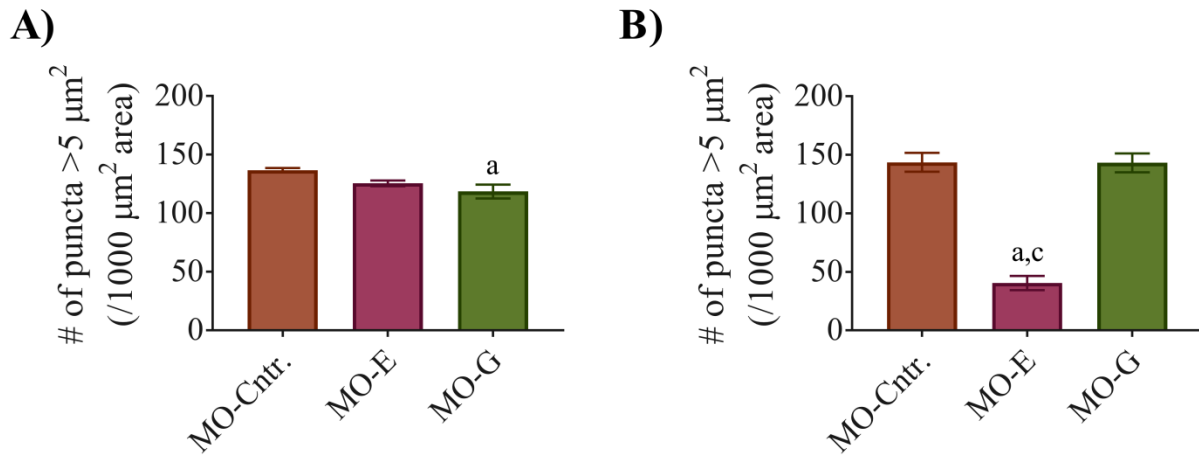


Figure 5.5

Quantification of nAChR puncta in MO-Cntr., MO-E and MO-G. nAChR puncta was stained with α -bungarotoxin. nAChR puncta were counted using ImageJ software and compared between different groups. (A) Shows quantification of nAChR clusters in 2 dpf embryos. nAChR puncta that are $>5\mu\text{m}^2$ were counted and compared between MO-Cntr. (n=5), MO-E (n=8) and MO-G (n=12). (B) Shows quantification of nAChR clusters in 5 dpf larvae. nAChR puncta that are $>5\mu\text{m}^2$ were counted and compared between MO-Cntr. (n=5), MO-E (n=7) and MO-G (n=5). ^a Significantly different from MO-Cntr. ($p<0.05$). ^c Significantly different from MO-G ($p<0.05$).

Figure 5.6

2 dpf

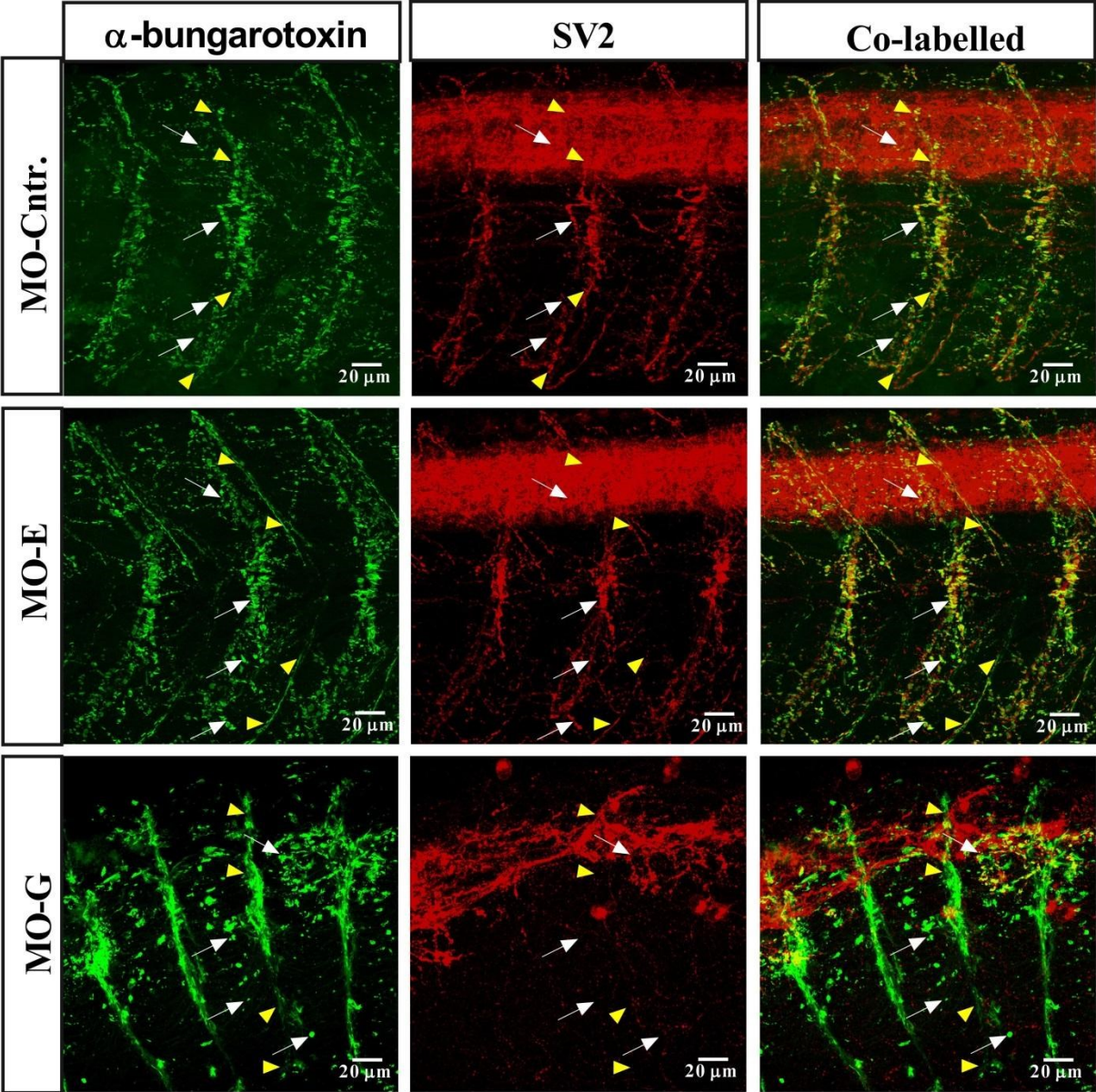


Figure 5.6

Co-localization of nAChRs and synaptic vesicles in 2 dpf embryo of MO-Cntr., MO-E and MO-G. In the same fish, nAChRs were stained with α -bungarotoxin conjugated with Alexa-488 while synaptic vesicles were immunostained with anti SV₂ antibody and Alexa 555 secondary antibody. Z-stack images of both the staining were simultaneously captured under a confocal microscope. Maximum intensity images were obtained from z-stack compilation selecting individual channel for α -bungarotoxin and SV₂ or both the channels together for the colabelled image. Left column shows nAChRs stained with α -bungarotoxin. Middle column shows synaptic vesicles immunolabelled with SV₂ antibody. Rightmost column shows colabelling with α -bungarotoxin and SV₂ staining. Yellow arrowheads indicate myoseptal regions and white arrows indicate distributed synaptic regions.

Figure 5.7

5 dpf

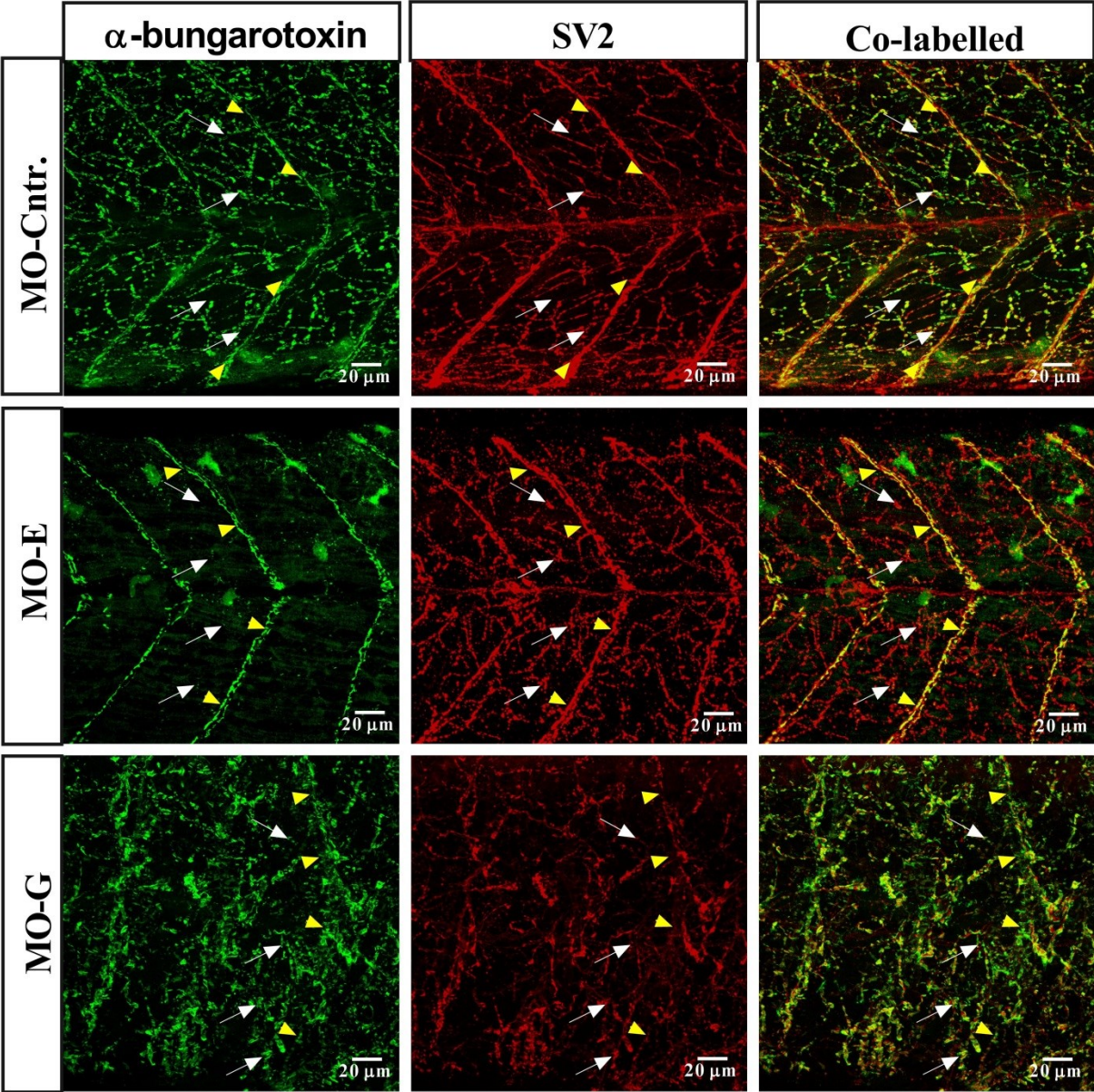


Figure 5.7

Colocalization of nAChRs and synaptic vesicles in 5 dpf larvae of MO-Cntr., MO-E and MO-G. In the same fish, nAChRs were stained with α -bungarotoxin conjugated with Alexa-488 while synaptic vesicles were immunostained with anti SV₂ antibody and Alexa 555 secondary antibody. Z-stack images of both the staining were simultaneously captured under a confocal microscope. Maximum intensity images were obtained from z-stack compilation selecting individual channel for α -bungarotoxin and SV₂ or both the channels together for the colabelled image. Left column shows nAChRs stained with α -bungarotoxin. Middle column shows synaptic vesicles immunolabelled with SV₂ antibody. Rightmost column shows colabelling with α -bungarotoxin and SV₂ staining. Yellow arrowheads indicate myoseptal regions and white arrows indicate distributed synaptic regions.

Figure 5.8

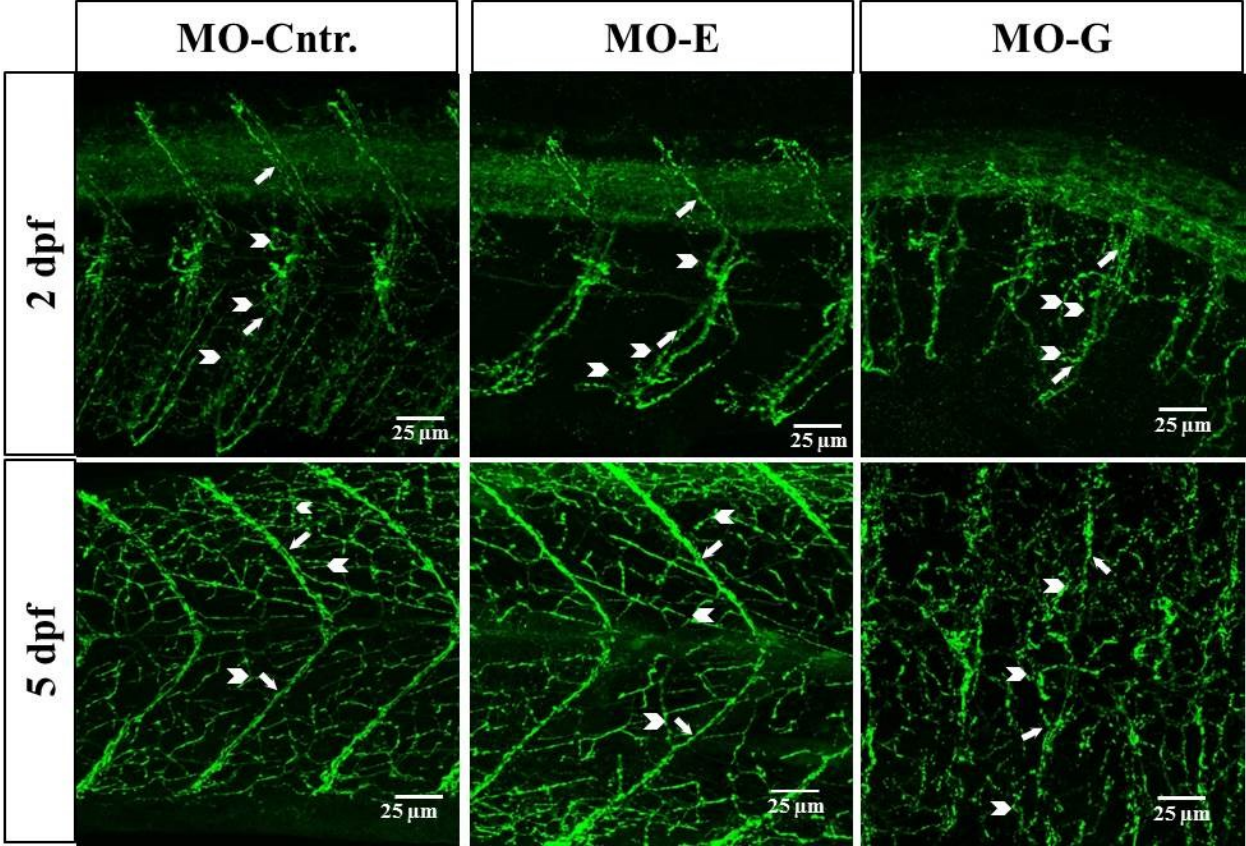


Figure 5.8

Primary MN branching in 2 dpf embryos and 5 dpf larvae of MO-Cntr., MO-E and MO-G. Axonal branches of primary MNs were immunolabelled with znp1 antibody and z-stack images were taken under confocal microscopy. Maximum intensity projection is shown, made from the z-stack images. White arrows indicate primary branches extending along the myoseptal region and white arrowheads indicate secondary branches that extend along the medial region of the muscle fibers.

Figure 5.9

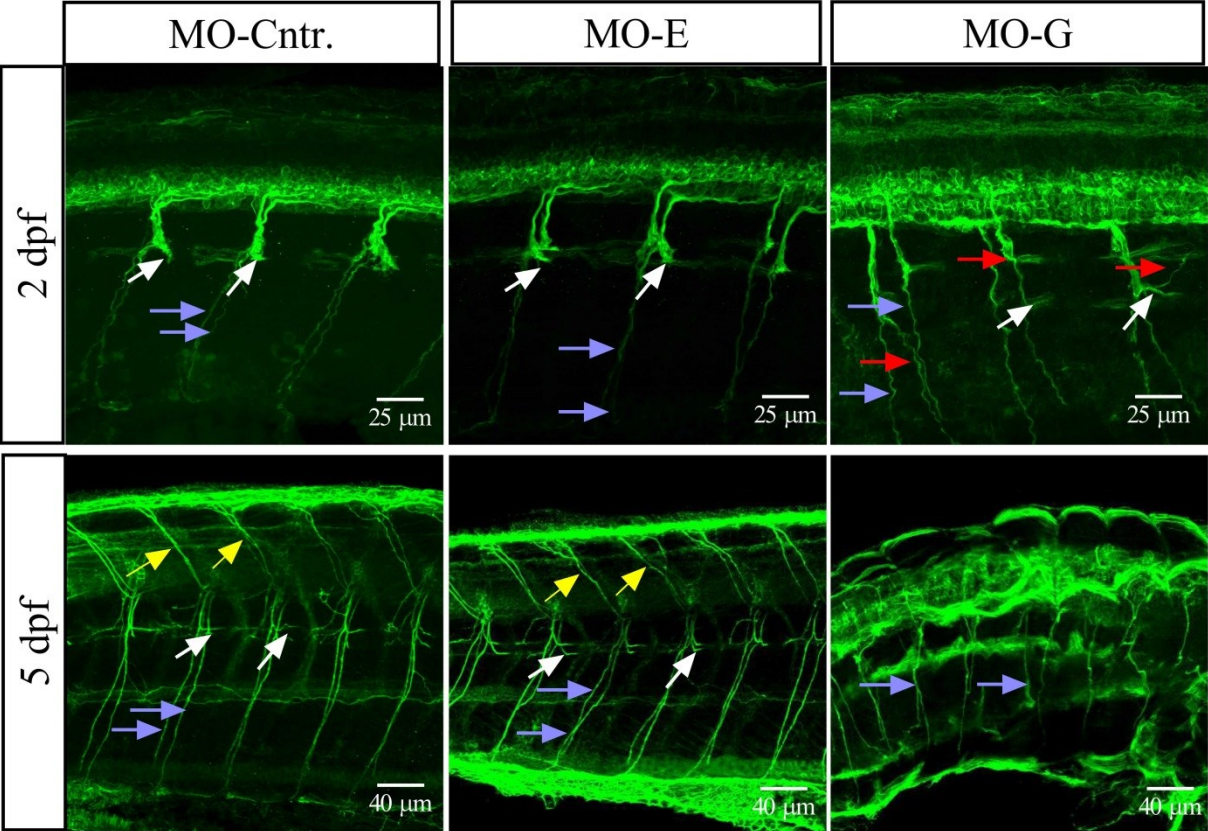


Figure 5.9

Secondary MN branching in 2 dpf embryos and 5 dpf larvae of MO-Cntr. MO-E and MO-G. Axonal branches of secondary MN were immunolabelled with zn8 antibody and z-stack images were taken under confocal microscopy. Maximum intensity projection is shown, made from the z-stack images. Yellow arrows indicate dorsal branches, white arrows indicate lateral branches and blue arrows indicate ventral branches. Red arrows in 2 dpf MO-G fish indicate some aberrant branching. Note, no dorsal or lateral branching could be identified in 5 dpf MO-G fish.

Figure 5.10

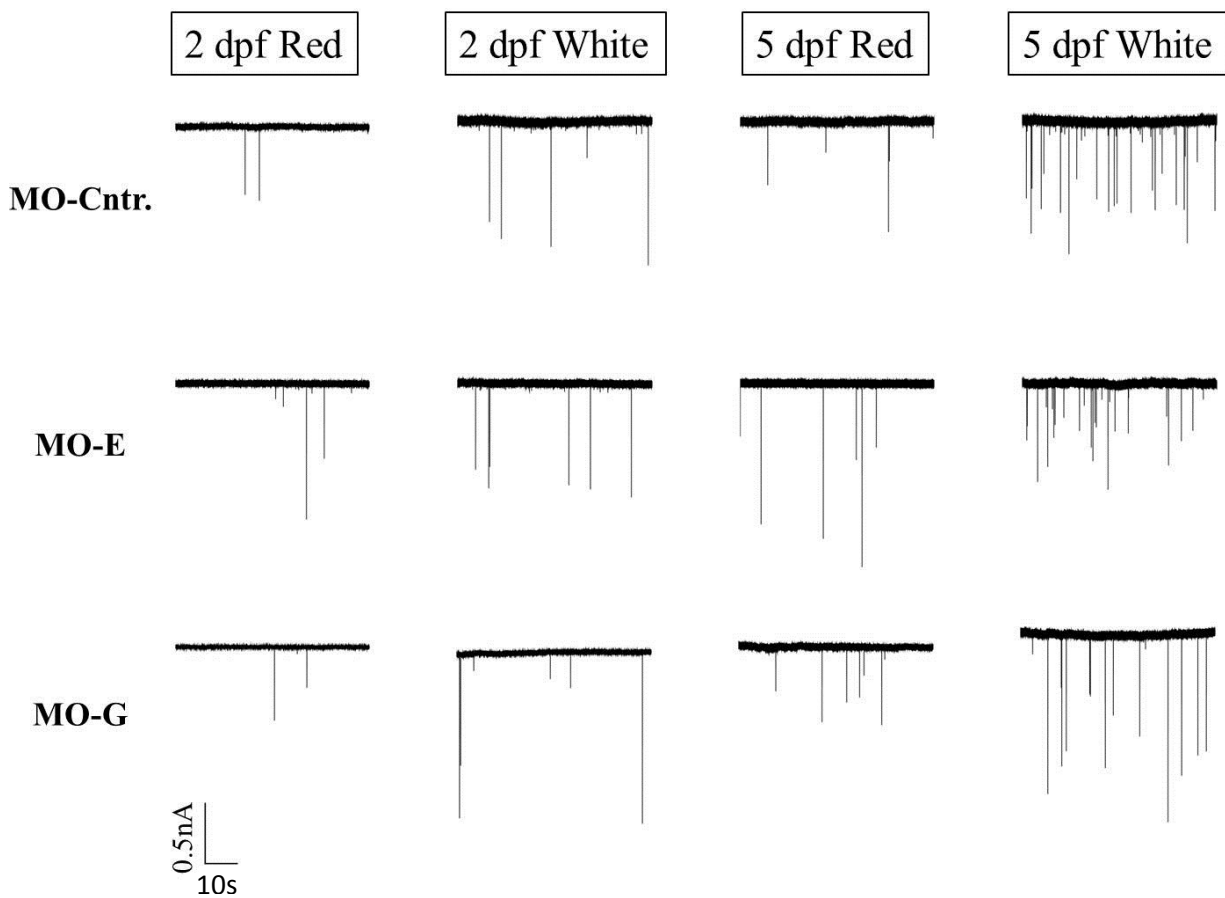


Figure 5.10

Raw traces of miniature endplate currents (mEPCs) recorded from red and white muscle fibers of embryonic and larval zebrafish of MO-Cntr., MO-E and MO-G. mEPC recordings were obtained from red and white muscle fibers from 2 dpf embryos and 5 dpf larvae. Sample traces show spontaneous events occurring in 60s time period.

Figure 5.11

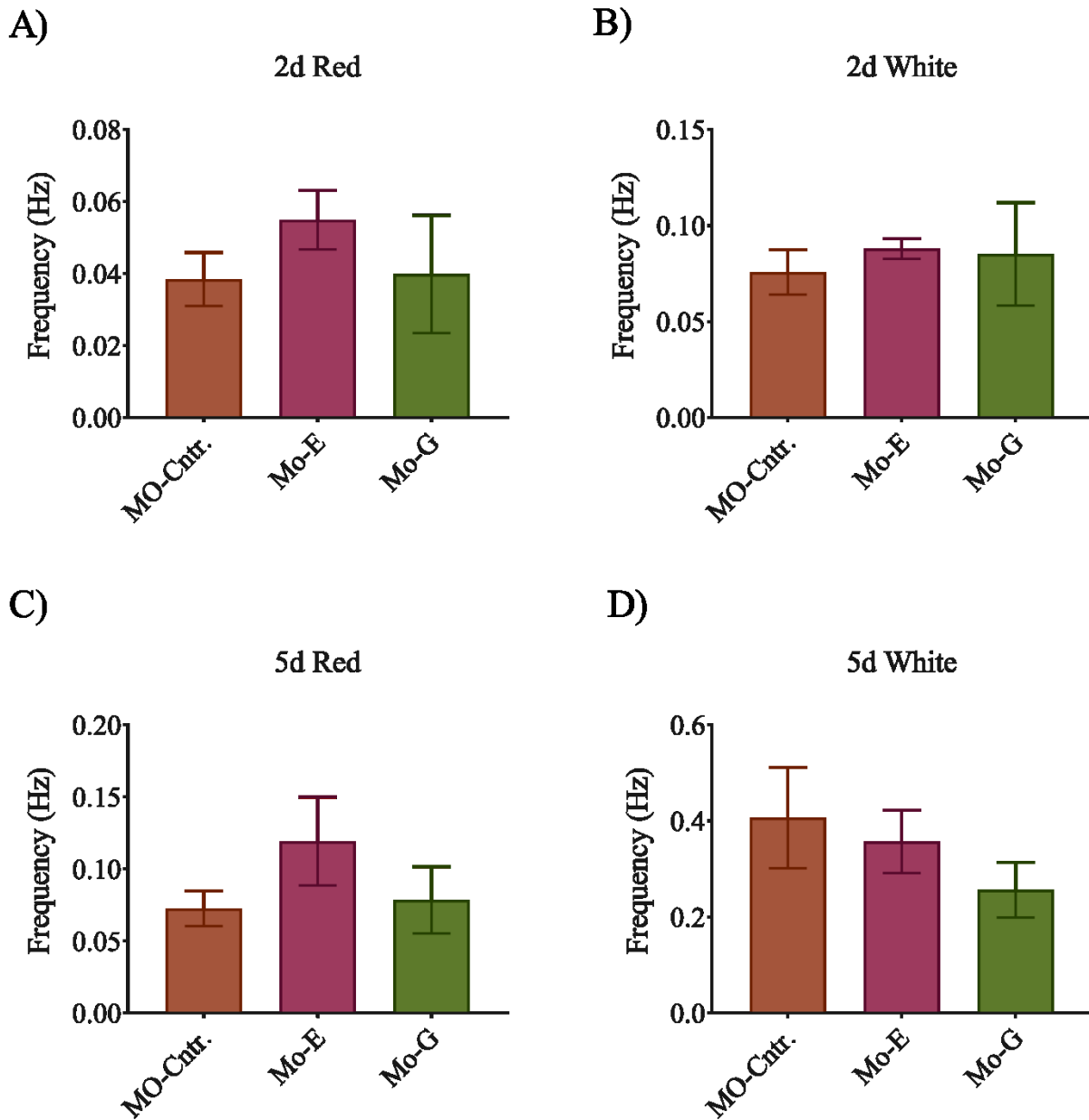


Figure 5.11

Comparison of mEPC frequency recorded from MO-Cntr., MO-E and MO-G fish.

- (A) Shows mEPC frequency recorded from 2 dpf red fibers. (B) Shows mEPC frequency recorded from 2 dpf white fibers. (C) Shows mEPC frequency recorded from 5 dpf red fibers. (D) Shows mEPC frequency recorded from 5 dpf white fibers.

Figure 5.12

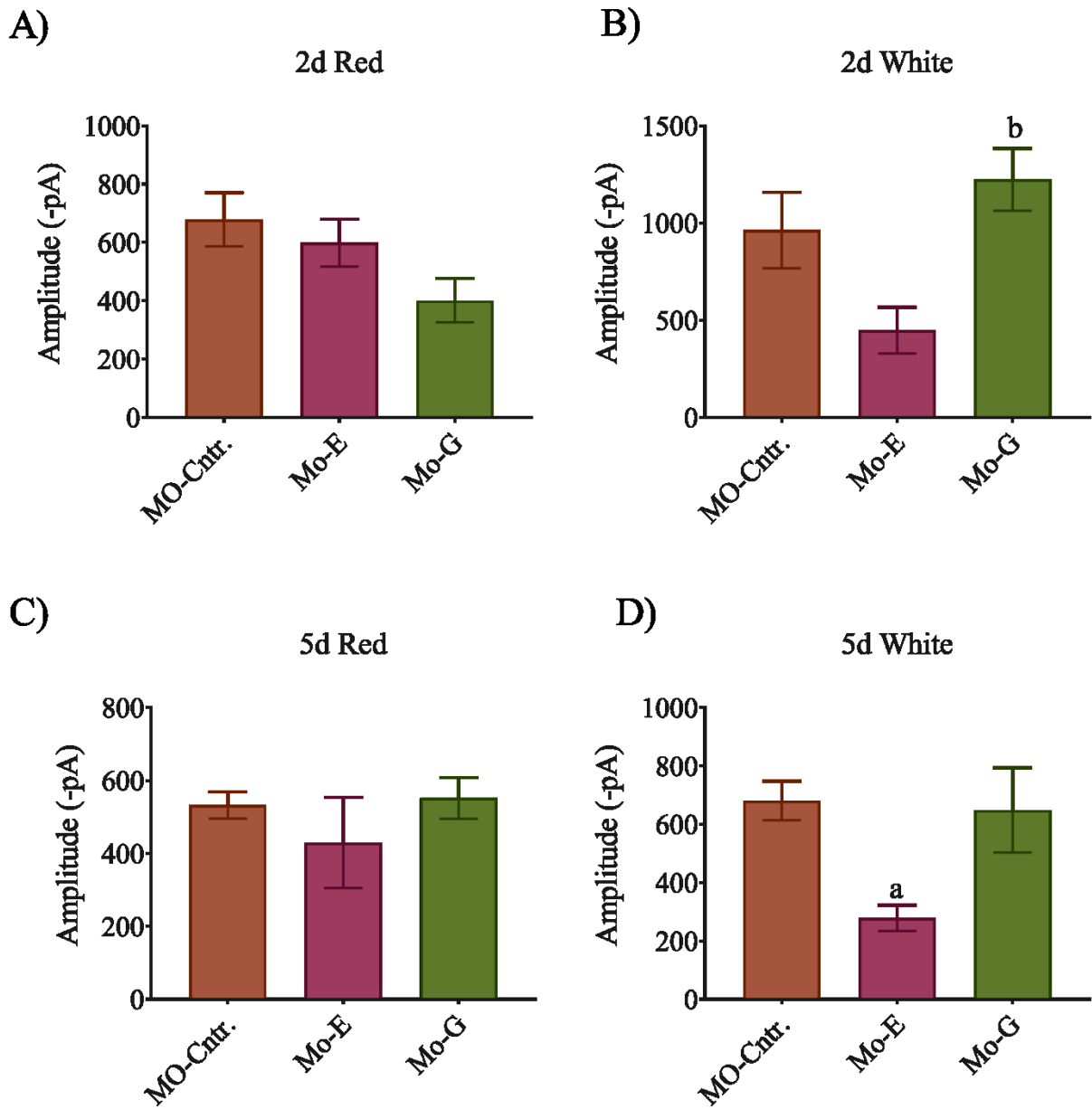


Figure 5.12

Comparison of mEPC amplitude recorded from MO-Cntr., MO-E and MO-G fish.

(A) Shows mEPC amplitude recorded from 2 dpf red fibers. (B) Shows mEPC amplitude recorded from 2 dpf white fibers. (C) Shows mEPC amplitude recorded from 5 dpf red fibers. (D) Shows mEPC amplitude recorded from 5 dpf white fibers. ^a Significantly different from MO-Cntr. ($p < 0.05$). ^b Significantly different from MO-E ($p < 0.05$).

Figure 5.13

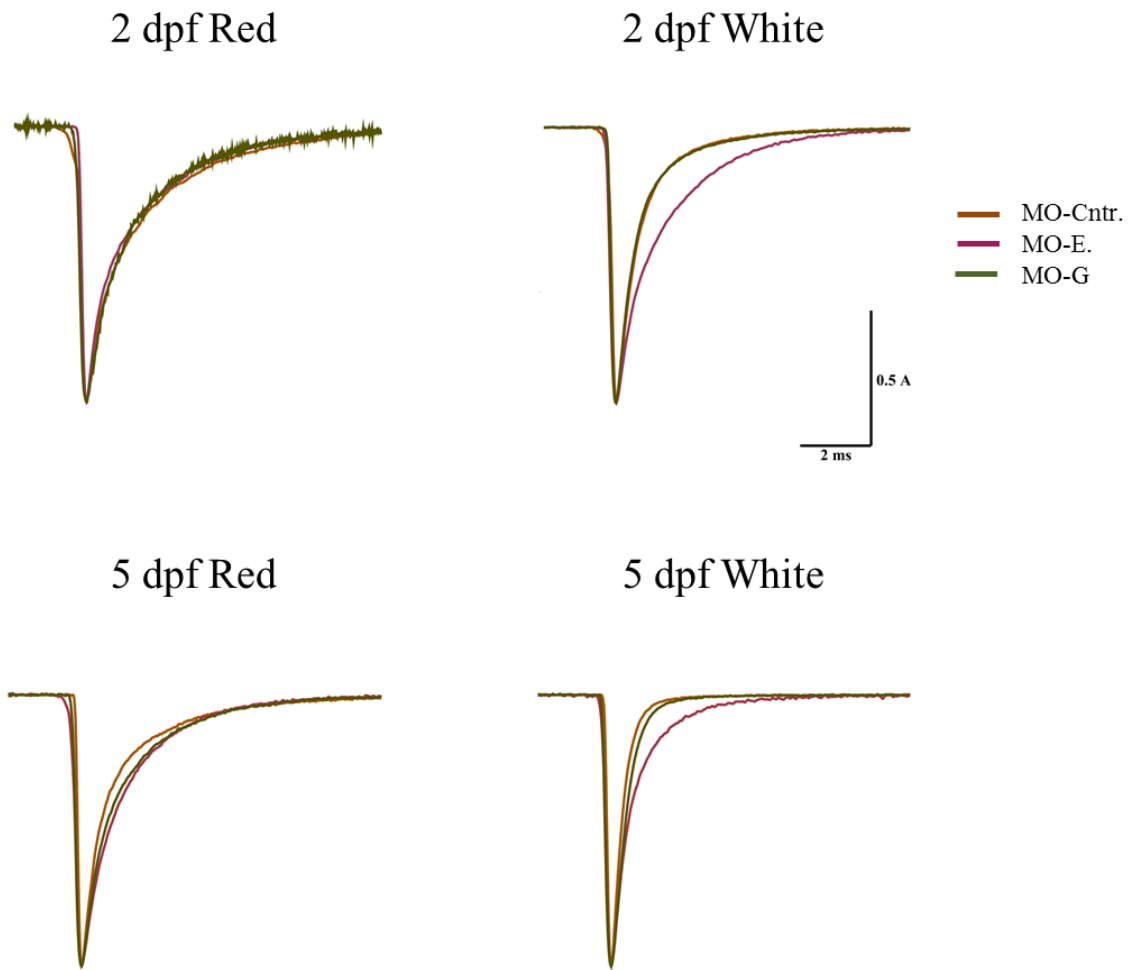


Figure 5.13

Comparison of the average mEPC events recorded from MO-Cntr., MO-E and MO-G fish. mEPC events recorded from a single fiber were averaged and the amplitude was normalized. (A) Shows superimposed average of mEPCs recorded from 2 dpf red fibers. (B) Shows superimposed average of mEPCs recorded from 2 dpf white fibers. MO-E exhibits prolonged decay (C) Shows superimposed average of mEPCs recorded from 5 dpf red fibers. (D) Shows superimposed average of mEPCs recorded from 5 dpf white fibers. MO-E exhibits prolonged decay.

Figure 5.14

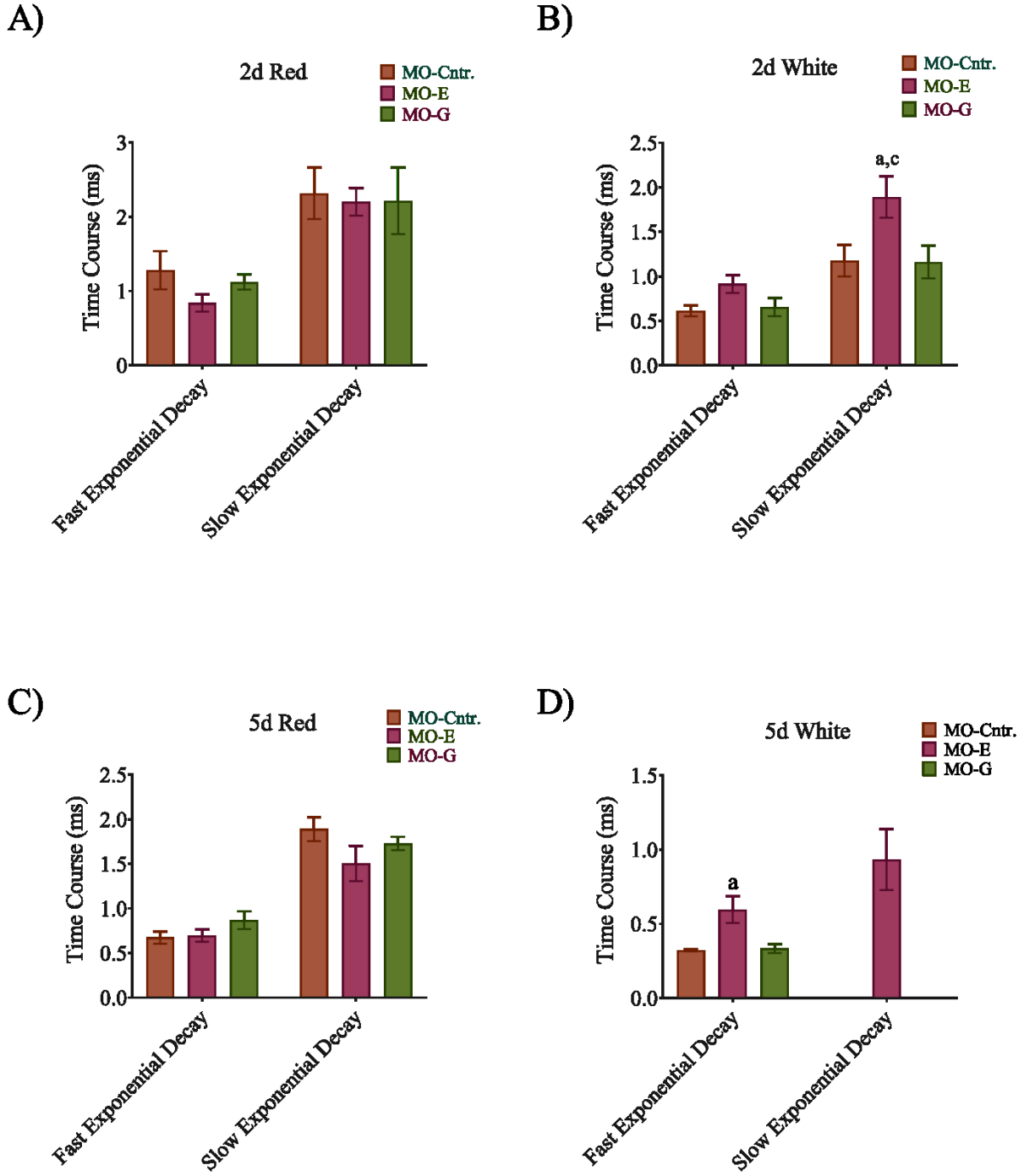


Figure 5.14

Comparison of mEPC decay time constant recorded from MO-Cntr., MO-E and MO-G fish. Fast and slow exponential decay was fit on mEPC event averages and compared. (A) Shows mEPC decay time constants recorded from 2 dpf red fibers. (B) Shows mEPC decay time constants recorded from 2 dpf white fibers. (C) Shows mEPC decay time constants recorded from 5 dpf red fibers. (D) Shows mEPC decay time constants recorded from 5 dpf white fibers. mEPCs recorded from 5 dpf white fibers of MO-Cntr. and MO-G larvae fit with a fast single exponential decay only whereas events from MO-E larvae decay with both fast and slow exponential time course. ^a Significantly different from MO-Cntr. ($p < 0.05$) ^c Significantly different from MO-G ($p < 0.05$).

Figure 5.15

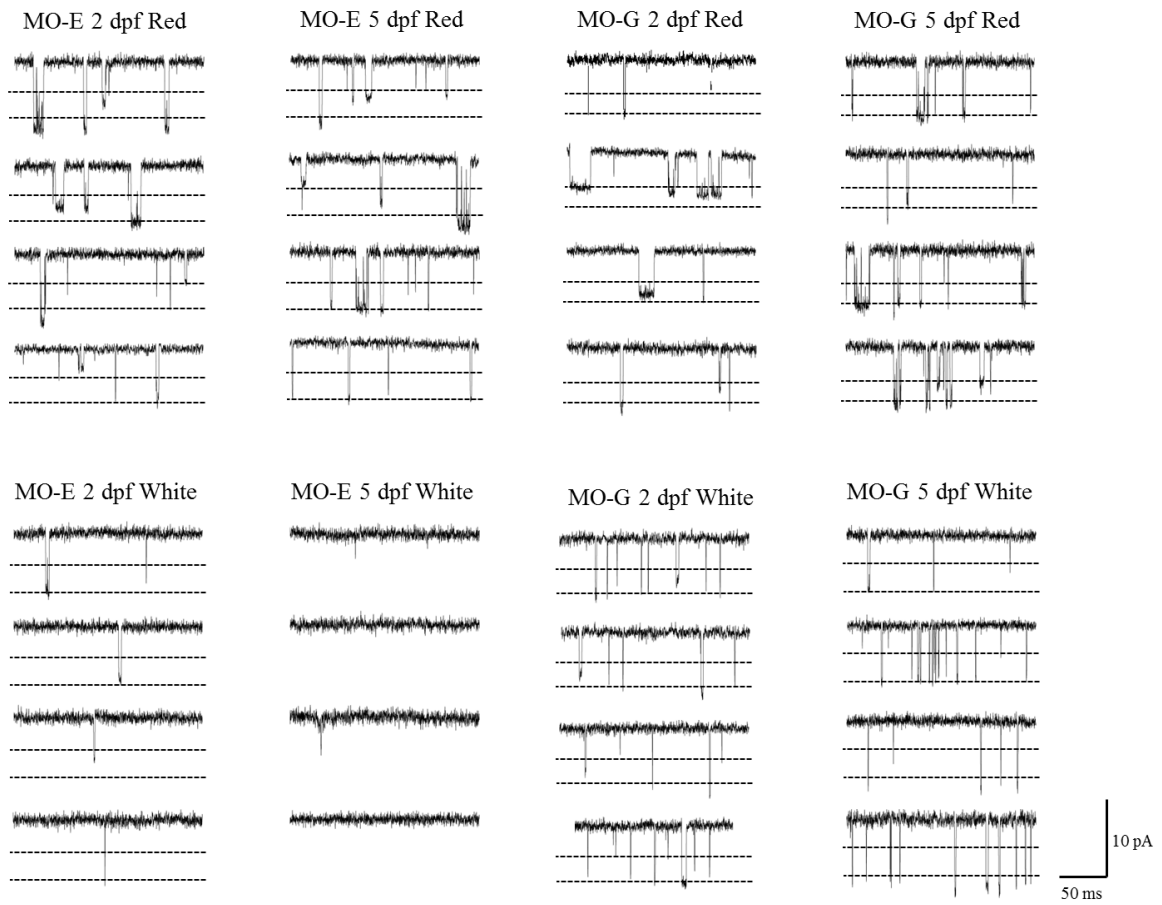


Figure 5.15

Single channel events obtained from outside-out patches of red and white fibers at 2 dpf and 5 dpf time points from MO-E and MO-G fish. Patches were held at -100 mV and events were filtered at 2 kHz. Black dotted lines show the two amplitude levels exhibited by the single channel events. No single channel events could be seen from 5 dpf white fibers of MO-E fish.

Figure 5.16

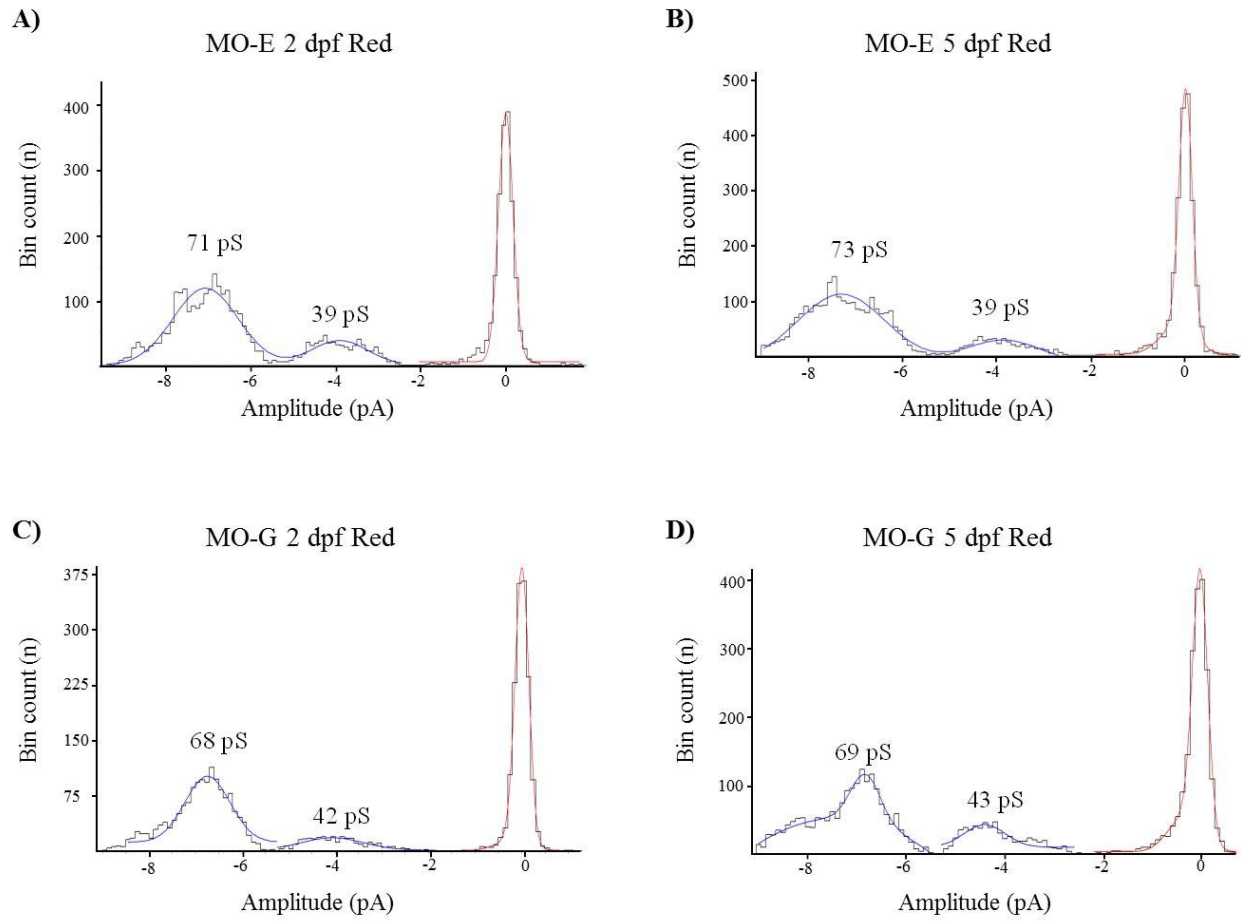


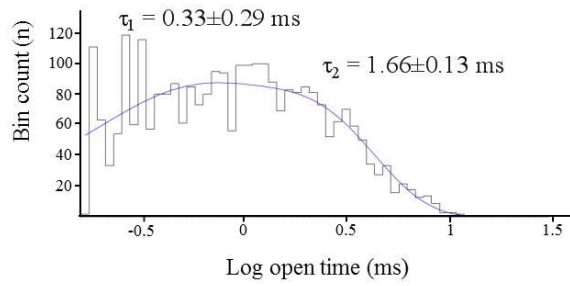
Figure 5.16

Amplitude histograms of single channel events obtained from MO-E and MO-G fish red fibers held at -100 mV. All the single channel events recorded from the same fiber groups were pooled together and the amplitude distribution was fit. Red line fits over the closed state, whereas blue line fits over the open channel state. Corresponding cord conductance (pS) at -100 mV holding potential is calculated as (conductance=event amplitude/holding voltage) and shown above the event groups. (A) Shows amplitude distribution of events recorded from 2 dpf red fibers of MO-E. (B) Shows amplitude distribution of events recorded from 5 dpf red fibers of MO-E. (C) Shows amplitude distribution of events recorded from 2dpf red fibers of MO-G. (D) Shows amplitude distribution of events recorded from 5 dpf red fibers of MO-G.

Figure 5.17

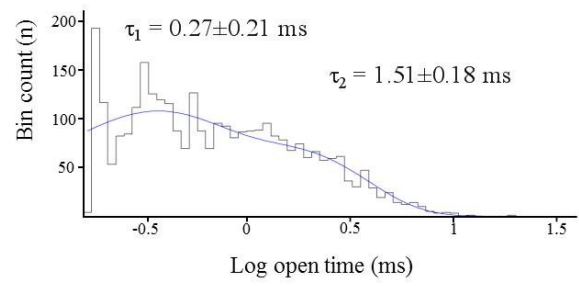
A)

MO-E 2 dpf Red



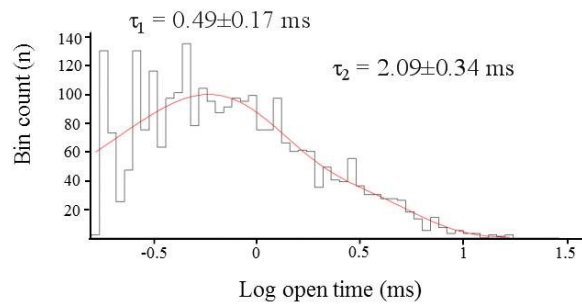
B)

MO-E 5 dpf Red



C)

MO-G 2 dpf Red



D)

MO-G 5 dpf Red

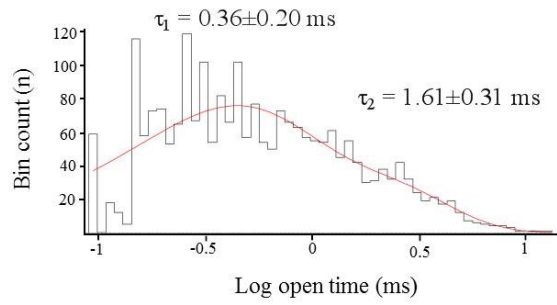


Figure 5.17

Histograms of dwell time constant of single channel events obtained from MO-E and MO-G fish red fibers. All the single channel events recorded at -100 mV from the same fiber groups were pooled together and the distribution of dwell time constant was fit with exponential function. τ_1 represents time constant of the channels that remain open for short time (fast channels), whereas τ_2 represents time constant of the channels that remain open for longer time (slow channels). (A) Shows dwell time distribution of events recorded from 2dpf red fibers of MO-E. (B) Shows dwell time distribution of events recorded from 5 dpf red fibers of MO-E. (C) Shows dwell time distribution of events recorded from 2 dpf red fibers of MO-G. (D) Shows dwell time distribution of events recorded from 5 dpf red fibers of MO-G.

Figure 5.18

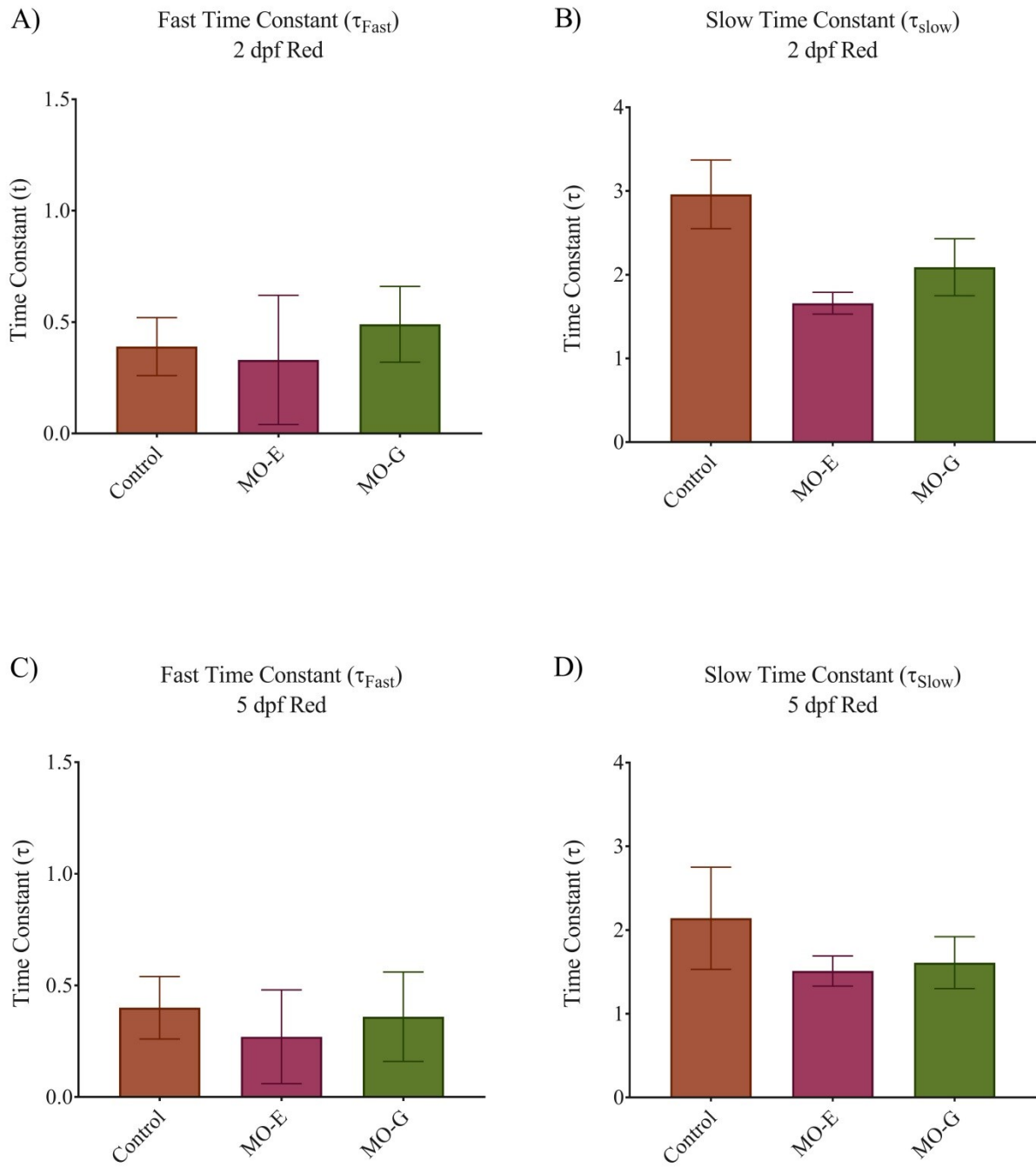
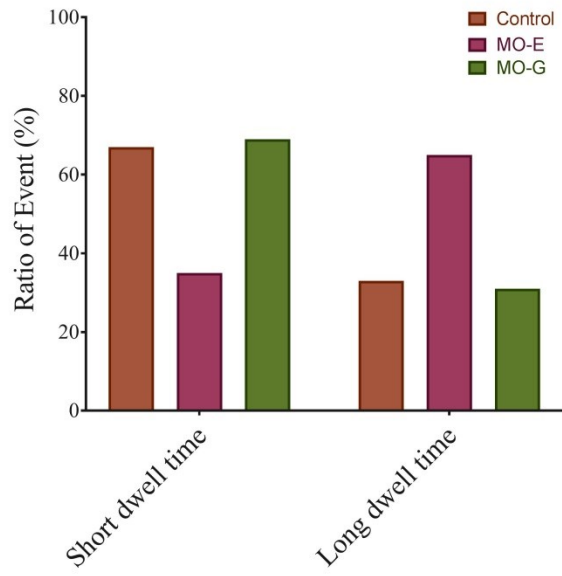


Figure 5.18

Comparison of single channel dwell time constants recorded from red fibers of untreated control, MO-E and MO-G fish. (A) Shows comparison of dwell time constant of fast channels (τ_{Fast}) recorded from 2 dpf red fibers. (B) Shows comparison of dwell time constant of slow channels (τ_{Slow}) recorded from 2 dpf red fibers. (C) Shows comparison of dwell time constant of fast channels (τ_{Fast}) recorded from 5 dpf red fibers. (D) Shows comparison of dwell time constant of slow channels (τ_{Slow}) recorded from 5 dpf red fibers.

Figure 5.19

A) Ratio of Events with Different Dwell Times
2d Red



B) Ratio of Events with Different Dwell Times
5d Red

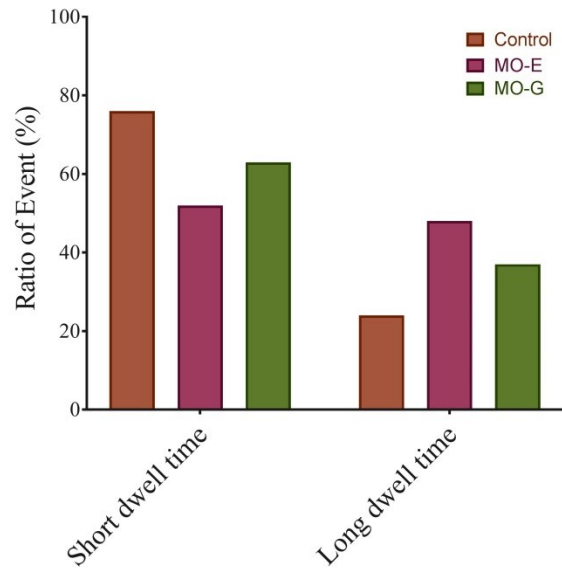


Figure 5.19

Comparison of events (%) with short and long dwell times recorded from red fibers of uninjected control, MO-E and MO-G. Single channel events recorded from the same fiber group were pooled together and fit with dwell time distribution (τ_{Fast} and τ_{Slow}). Ratio of total events that fit with short dwell time (τ_{Fast}) and long dwell time (τ_{Slow}) was recorded. (A) Shows comparison of events recorded from 2 dpf red fibers. (B) Shows comparison of events recorded from 5 dpf red fibers.

Figure 5.20

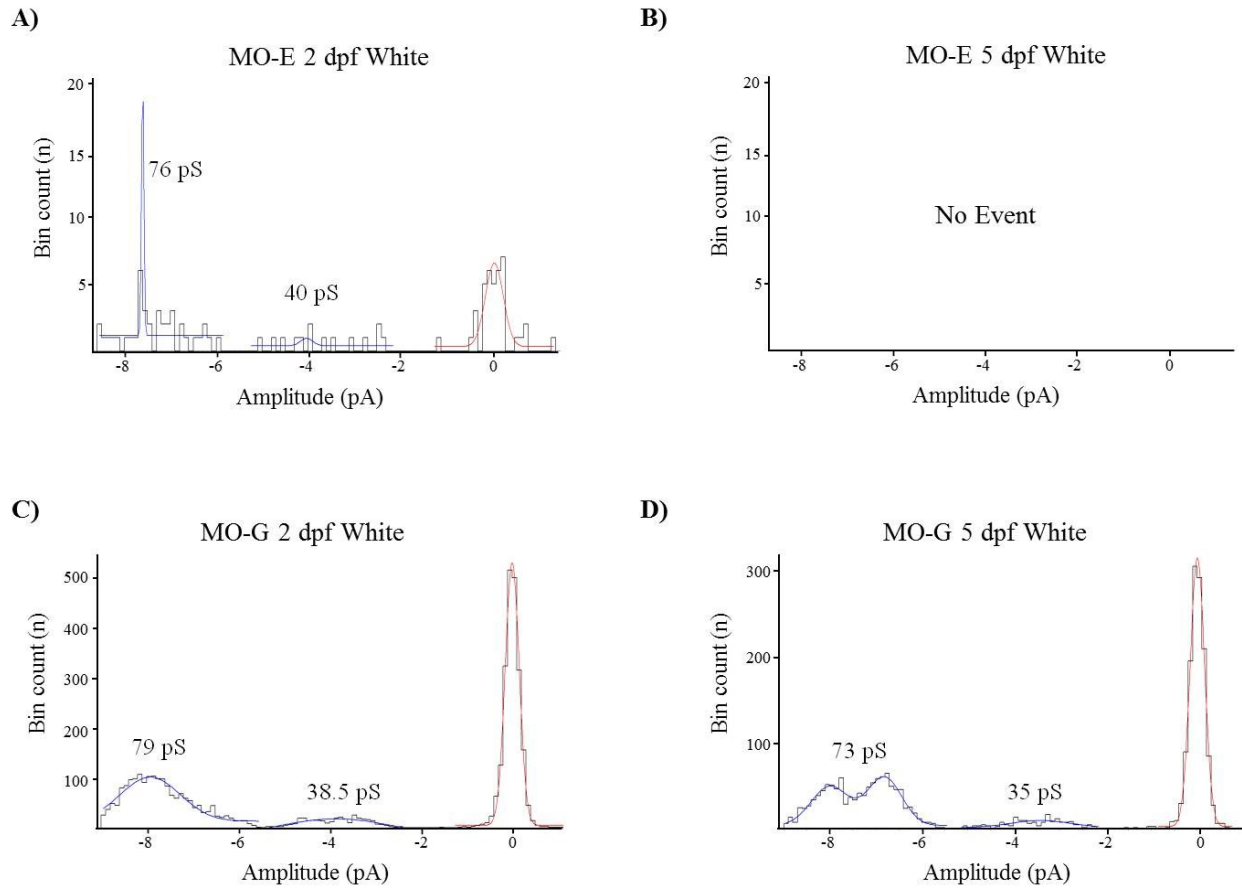


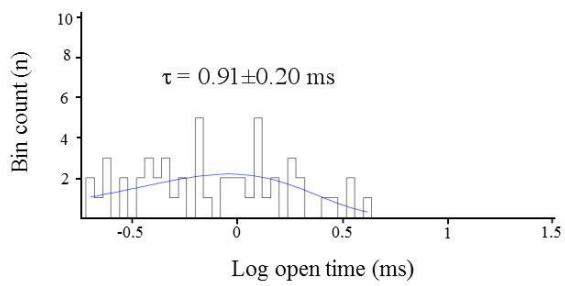
Figure 5.20

Amplitude histograms of single channel events obtained from MO-E and MO-G fish white fibers held at -100 mV. All the single channel events recorded from the same fiber groups were pooled together and the amplitude distribution was fit. Red line fits over the closed state, whereas blue line fits over the open channel state. Corresponding cord conductance (pS) at -100 mV holding potential is calculated as (conductance=event amplitude/holding voltage) and shown above the event groups. (A) Shows amplitude distribution of events recorded from 2 dpf white fibers of MO-E. Very few events could be recorded from these fibers. (B) No single channel events could be recorded from 5 dpf white fibers of MO-E. (C) Shows amplitude distribution of events recorded from 2 dpf white fibers of MO-G. (D) Shows amplitude distribution of events recorded from 5 dpf white fibers of MO-G.

Figure 5.21

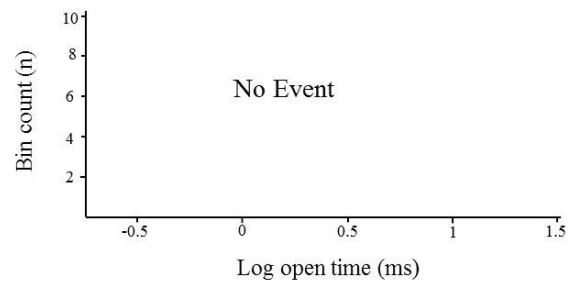
A)

MO-E 2 dpf White



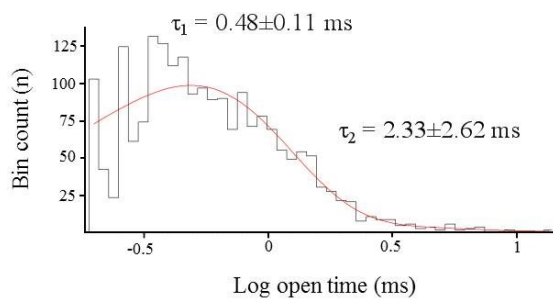
B)

MO-E 5 dpf White



C)

MO-G 2 dpf White



D)

MO-G 5 dpf White

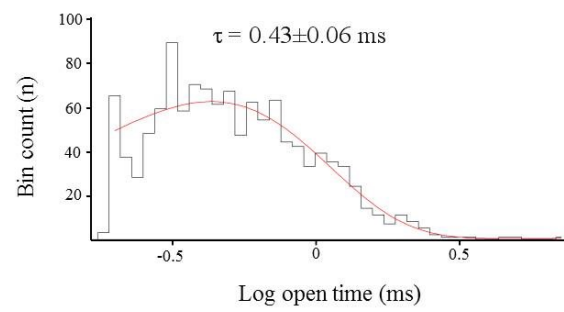


Figure 5.21

Histograms of dwell time constant of single channel events obtained from MO-E and MO-G fish white fibers. All the single channel events recorded at -100 mV from the same fiber groups were pooled together and the distribution of dwell time constant was fit with exponential function. τ_1 represents time constant of the channels that remain open for short time (fast channels), whereas τ_2 represents time constant of the channels that remain open for longer time (slow channels). (A) Shows dwell time distribution of events recorded from 2 dpf white fibers of MO-E. Very few events could be recorded from these fibers, and the events fit with a single dwell time constant (τ). (B) No events could be recorded from 5 dpf white fibers of MO-E. (C) Shows dwell time distribution of events recorded from 2 dpf red fibers of MO-G. (D) Shows dwell time distribution of events recorded from 5 dpf white fibers of MO-G. All the events recorded from these fibers fit with a single dwell time constant (τ).

Figure 5.22

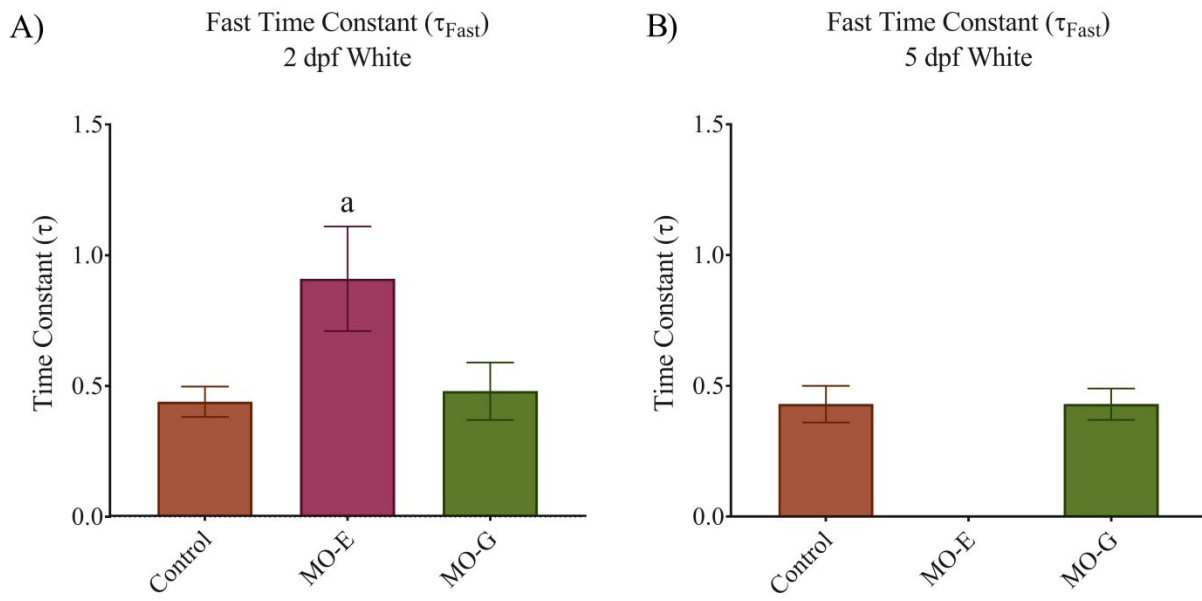


Figure 5.22

Comparison of fast dwell time constants (τ_{Fast}) recorded from white fibers of uninjected control, MO-E and MO-G fish. (A) Shows comparison of dwell time constant of fast channels (τ_{Fast}) recorded from 2 dpf white fibers. (B) Shows comparison of dwell time constant of single channels recorded from 5 dpf white fibers. All single channel events from 5 dpf white fibers of both untreated control and MO-G injected fish shows only short open channels. No channel activity is seen in 5 dpf white fibers of MO-E fish. ^a Significantly different from uninjected control ($p < 0.05$)

Figure 5.23

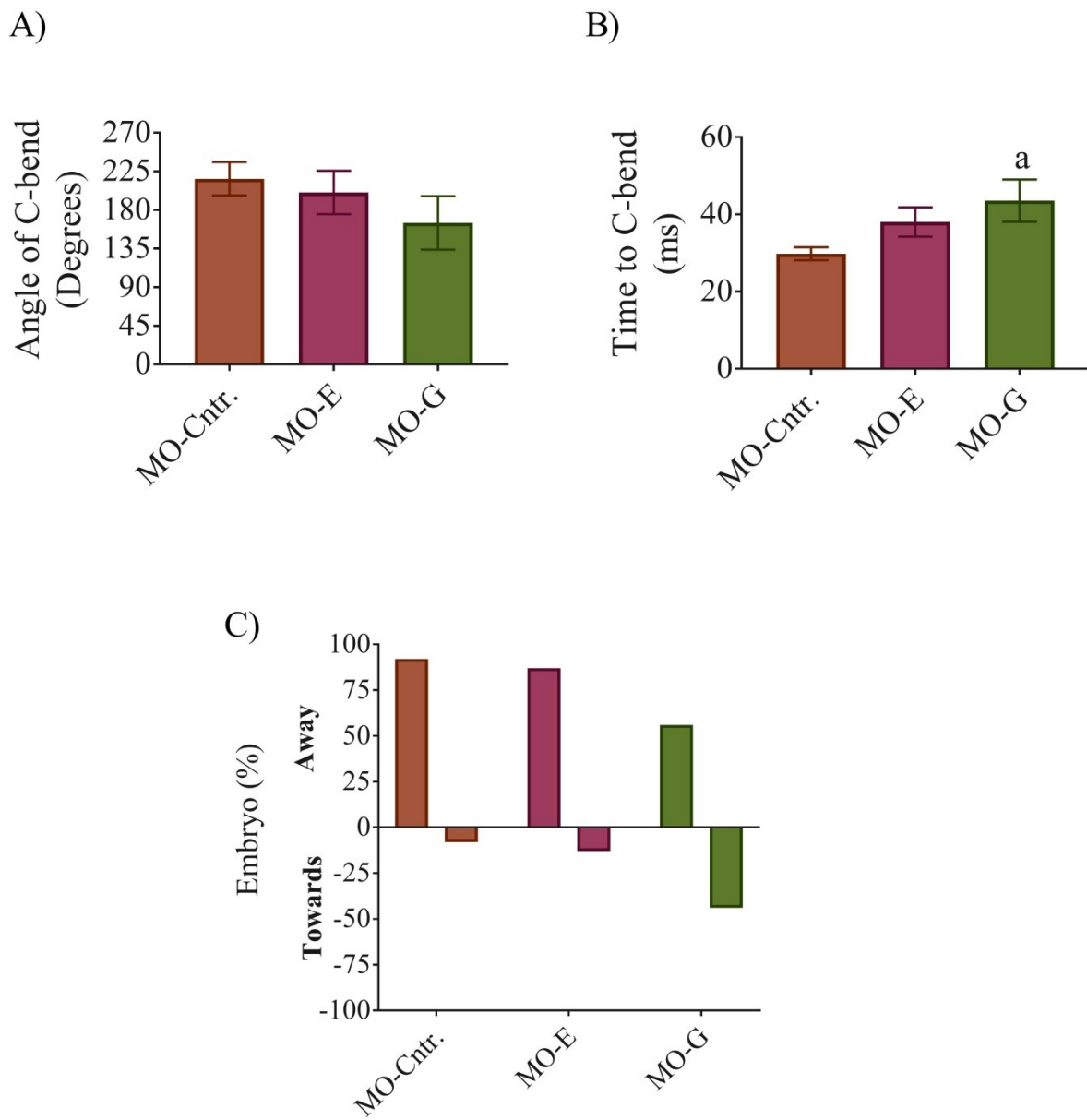


Figure 5.23

Quantification of C-bend escape response in 2 dpf embryos following tactile stimulation at the head. 2 dpf embryos were restrained by head in low-melting-point agarose and a tactile stimulation was provided to head via picospritzer. Embryos respond to the stimulus with a fast bending of the tail which was video recorded at 1250 frames/sec. Movement of the tail during the response was tracked and analyzed. (A) Bar graph shows the maximum angle of bend for MO-Cntr. (n=13), MO-E (n=12) and MO-G (n=9) embryos. (B) Bar graph shows the time for tail to reach the maximum angle. (C) Shows ratio of embryos (%) with the direction of C-bend towards or away from the stimulus. The appropriate response is always away from the stimulus. ^aSignificantly different from MO-Cntr (p<0.05).

Figure 5.24

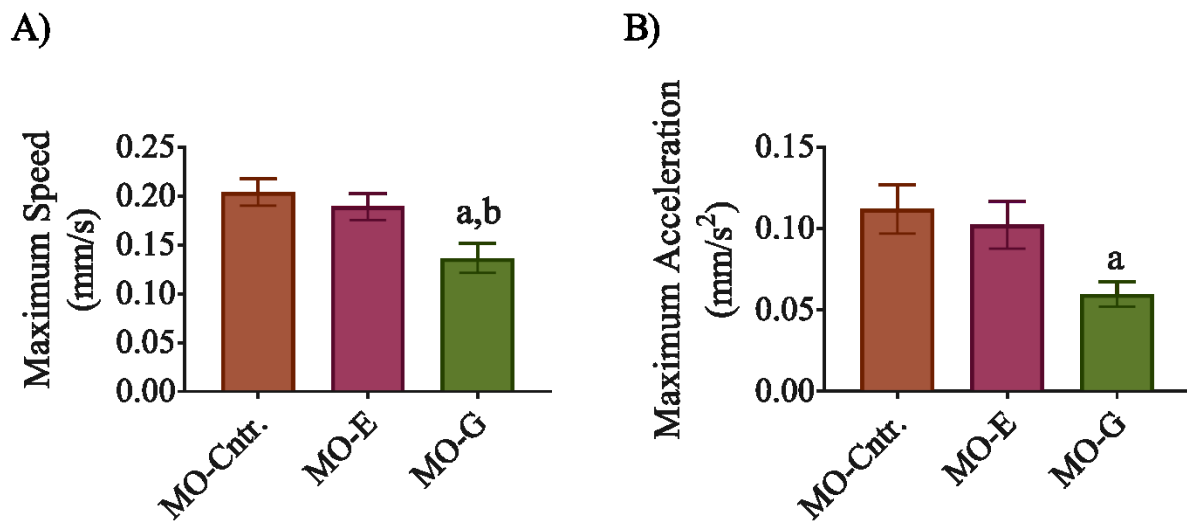


Figure 5.24

Comparison of maximum speed and acceleration attained during eliciting a C-bend escape response by MO-Cntr., MO-E and MO-G embryos at 2 dpf. (A) Bar graph showing the maximum instantaneous speed, (B) Bar graph showing the maximum instantaneous acceleration attained during the C-bend. ^a Significantly different from MO-Cntr ($p < 0.05$). ^b Significantly different from MO-E ($p < 0.05$).

Figure 5.25

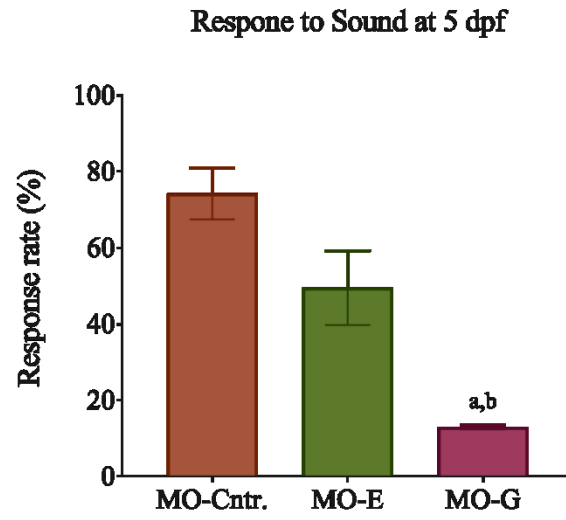


Figure 5.25

Comparison of response rate of 5 dpf MO-Cntr., MO-E and MO-G larvae responding to sound stimulus. 5 dpf larvae were put in a 35 mm petri dish and a sound tone was delivered. Number of embryos responding with an escape response was counted and response rate was calculated in percentile. Response rates were compared between MO-Cntr. (N=4 batches, n= 33 embryos), MO-G (N=3 batches, n=20 embryos) and MO-E (N=3 batches, n=54 embryos) larvae.

Figure 5.26

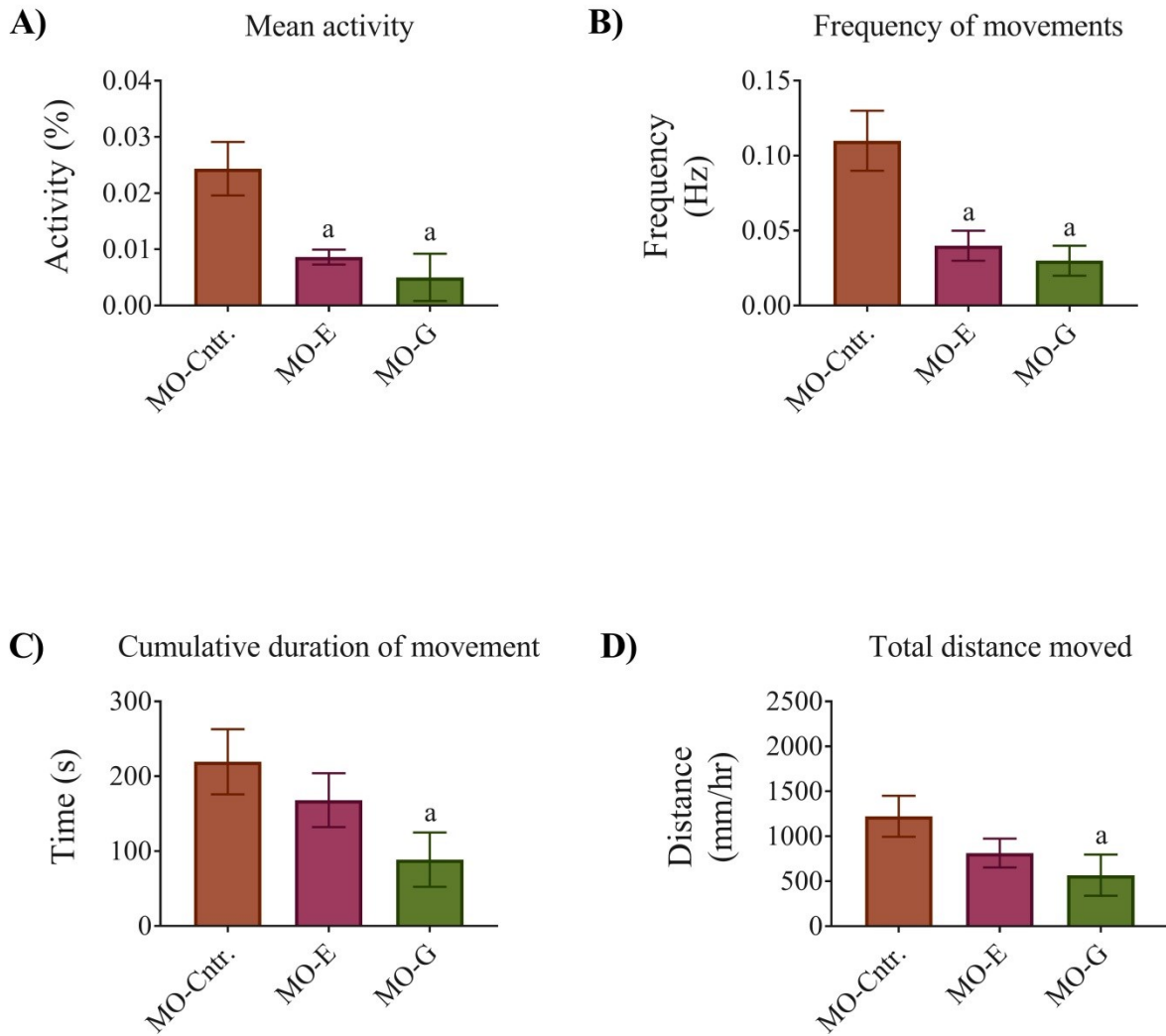


Figure 5.26

Quantification of free-swimming activity in 5 dpf larvae of MO-Cntr., MO-E and MO-G. Individual embryos were placed in wells of a 96-well-plate and their spontaneous movements were tracked and analyzed by EthoVision® XT-11.5 software. (A) Shows mean activity of the larvae in an hour. (B) Shows frequency of movements in an hour. (C) Shows cumulative duration of movement in an hour. (D) Shows total distance moved by the larvae within an hour. ^aSignificantly different from MO-Cntr (p<0.05).

Figure 5.27

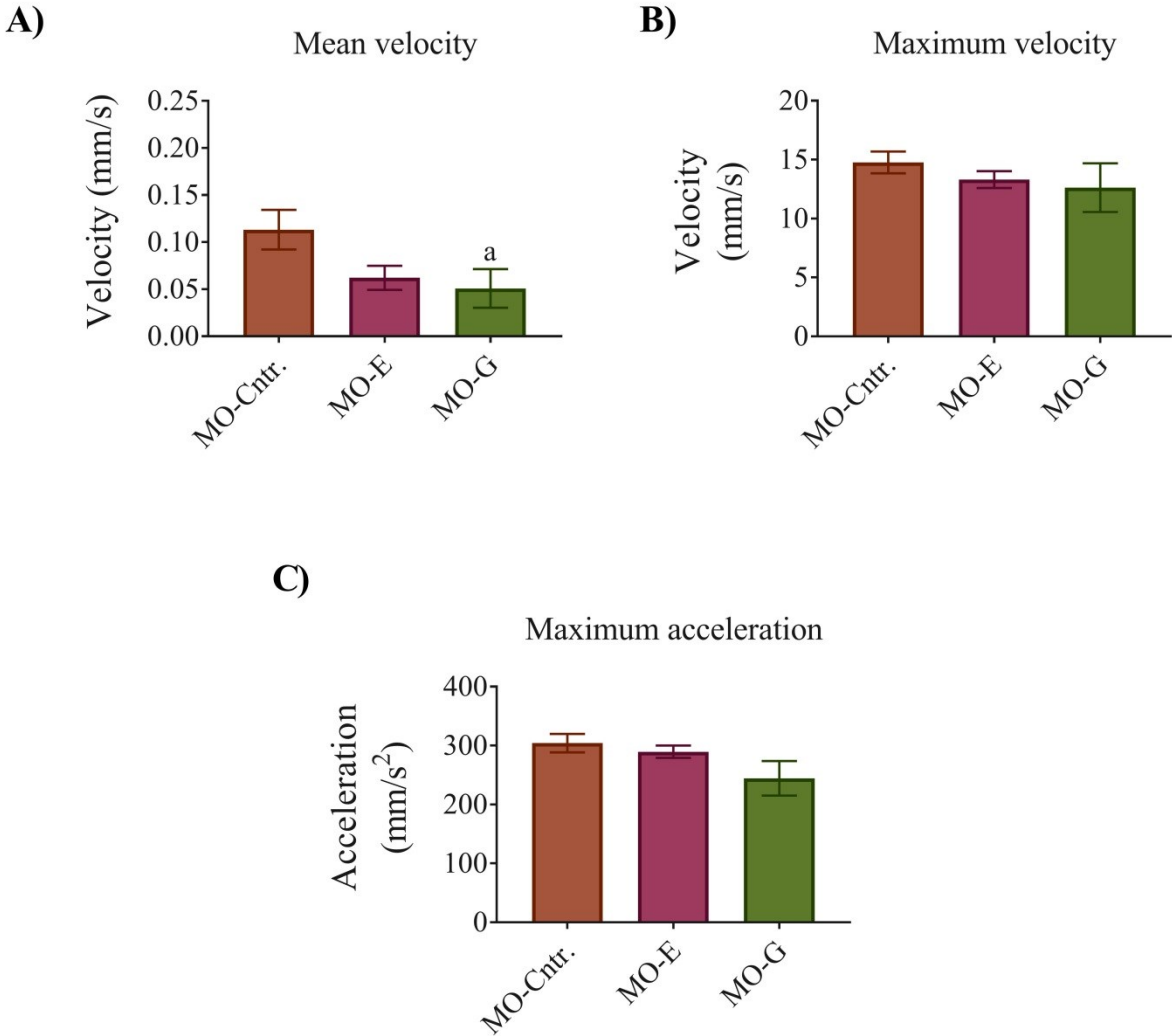


Figure 5.27

Comparison of velocity and acceleration of 5 dpf MO-Cntr., MO-E and MO-G larvae during spontaneous free-swimming activity. Mean velocity (A), Maximum velocity (B) and Maximum acceleration (C) were recorded and compared between MO-Cntr., MO-E and MO-G larvae. ^a Significantly different from MO-Cntr (p<0.05).

Figure 5.28

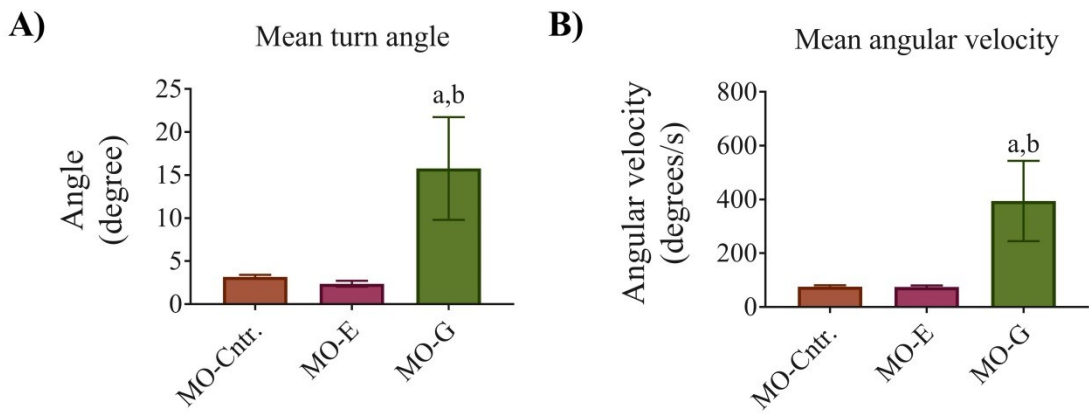


Figure 5.28

Comparison of turn angle and angular velocity of 5 dpf MO-Cntr., MO-E and MO-G fish during spontaneous free-swimming activity. (A) Shows mean turn angle, and (B) Shows mean angular velocity. ^a Significantly different from MO-Cntr. ($p < 0.05$). ^b Significantly different from MO-E ($p < 0.05$).

Chapter 6. Discussion

The focus of this thesis was to characterize the development of nAChR activity in red and white muscle fibers between 1.5 dpf and 5 dpf of zebrafish. I also aimed to elucidate the roles played by the γ and ϵ subunit of nAChRs- the subunits that show developmental switching in vertebrate- in the development of NMJs and muscle fibers. I used whole cell patch clamp recordings to determine the kinetic properties associated with nAChRs in red and white muscle fibers and compared these kinetic properties among developing fish. With outside-out single channel recordings, I tried to characterize the channel properties of individual nAChRs expressed in the developing muscle fibers. With RT-PCR and single cell RT-qPCR, I tried to determine the expression of specific subunits in these fibers. These results helped me to understand the development of kinetic properties in red and white muscle fibers, which were different from each other. Additionally, I used morpholino oligoneucleotides to knockdown two subunits of nAChRs- γ and ϵ subunits, which show different expression patterns in red and white muscle fibers. At first, I used a set of morpholinos previously used by another group and found that they showed minimal effects. Then, I designed a new set of splice blocking morpholinos, validated their efficacy by RT-PCR, and then assessed the effect of the knockdowns in developing fish. I focused on gross morphology of the animals, motor neuron branching patterns, expression and kinetic properties associated with nAChRs and locomotor activity of the fish. With the new sets of morpholinos, I determined the differential role played by the two subunits during early developmental of zebrafish.

6.1 Synaptic Development in White and Red Muscle Fibers

My findings revealed that white fibers of zebrafish skeletal muscle express two main conductance classes of nicotinic acetylcholine receptors (~55 pS and ~73 pS channels) throughout the first 5 days of development. The 55 pS channel was less prevalent in 1.5 dpf muscle. The kinetics of both conductance classes showed fast and slower time courses in embryonic animals but were not slow enough to shape the long synaptic events at 1.5 dpf. By 5 dpf, synaptic events were much faster than in the embryos with a single exponential decay of ~0.26 ms and were primarily shaped by single channel kinetics. Additionally, nAChRs in white fibers no longer exhibited long open times at either conductance level.

In contrast, red fibers expressed two main conductance classes of nAChRs (~45 pS and ~65 pS), with the 65 pS channel predominating at 1.5 dpf. Both conductance classes had short and long mean open times; however, unlike white fibers, the long open time was either retained throughout the first 5 days of development, or the channels became capable of opening for longer periods by entering into a bursting mode not seen at 1.5 dpf. The synaptic events of red fibers maintained a double exponential decay throughout development.

To confirm that the single channel kinetics closely approximates synaptic activity, I constructed ensemble averages from single channel events for each fiber. Ensemble averages from the single channel events obtained from 1.5 dpf embryos, have fast time courses suggesting that the long mEPCs from the 1.5 dpf embryos are largely shaped by immature synaptic morphology rather than nAChR channel properties. These findings are in agreement with a previous study conducted by Drapeau et al. (2001). Drapeau and coworkers found that the appearance of the ACh hydrolytic enzyme, acetylcholinesterase (AChE) is delayed at the NMJs

of developing zebrafish between the ages of 1dpf and 6dpf, which is required to shape the fast synaptic events observed in larval zebrafish (Nguyen et al., 1999). Nerve endings in embryonic muscles are also poorly differentiated compared to larval muscles. These ultrastructural differences appeared to be the major contributors of the kinetic differences observed in synaptic events recorded from embryonic zebrafish muscle fibers (Drapeau et al., 2001). By 5 dpf, channel properties outweigh morphology in shaping synaptic currents. The ensemble averages from my recordings confirmed that they closely approximate mEPC decay properties, for both white and red fibers.

My RT-PCR data showed the expression of α , $\beta 1a$, $\beta 1b$, γ , δ and ϵ subunits up until 5 dpf. Expression of these subunits was consistent in red fibers throughout the development. In white muscle fibers, $\beta 1a$ and γ subunits decreased during development while expression of the ϵ subunit remained consistent. Thus, white and red muscle fibers showed major differences in subunit expression. Altogether, these results suggested that red and white muscle fibers express nAChRs in different patterns, and that the two muscle fibers differ in their development of NMJ. Based on my findings, a probable expression pattern of nAChRs in zebrafish red and white muscle fibers during development is shown in Figure 6.1.

My findings are in general agreement with published literature, but with interesting and potentially important differences. White muscle fibers are fast twitch fibers used during rapid swimming and are capable of high contraction rates (Buss & Drapeau, 2000, 2002). They arise from a different population of precursor cells (the lateral presomitic cells) than red fibers and make up the bulk of the trunk musculature (Devoto, Melançon, Eisen, & Westerfield, 1996). They are innervated by a single primary motor neuron and up to 3-4 secondary motor neurons

(De Graaf, van Raamsdonk, van Asselt, & Diegenbach, 1991; Liu & Westerfield, 1988; van Raamsdonk, Bosch, Smit-Onel, & Maslam, 1996; Westerfield et al., 1986). The majority of mEPCs from 1.5 dpf white fibers exhibited time courses that were long and variable in length and were well fit by single exponential decays. By 2 dpf most mEPCs were better fit with a double exponential decay, and by 5 dpf, >95% of the mEPCs were fit with a single exponent again. During this period (2 dpf to 5 dpf) as the mEPCs transitioned from a double fit to a single fit, their kinetics sped up significantly. These findings suggest that the white muscle fibers in zebrafish express nAChR subtypes along a developmental pattern similar to mammals and amphibians, whereby a population of embryonic nAChRs is turned over and eventually replaced with a predominantly homogeneous population of adult nAChRs (P Brehm, Kullberg, & Moody-Corbett, 1984; Paul Brehm, Steinbach, & Kidokoro, 1982; Fischbach & Schuetze, 1980; Kullberg, Lentz, & Cohen, 1977; Mishina et al., 1986; Sakmann & Brenner, 1978; Vicini & Schuetze, 1985). During the transition period in zebrafish (<1.5 dpf to 3 dpf), there is a mixed population of nAChR subtypes which gives rise to decay kinetics with double exponents. My single channel data from 2 dpf fish reveals the presence of events with two conductance classes, each with short and long open times. By 5 dpf the two conductance classes are still present, but for the most part, the channels no longer exhibit the long open time behavior. Interestingly, the long open times were present at both the 55 and 73 pS conductance levels, and in both cases were absent by 5 dpf. Patch clamp studies clearly show that the kinetic behavior of individual nicotinic channels associated with skeletal muscle are best described by multiple time courses, usually a short (fast) and a long (slow) open time (Camacho, Liu, Mandel, & Brehm, 1993; Kullberg, Brehm, & Steinbach, 1981; Owens & Kullberg, 1989; Shepherd & Brehm, 1997),

indicating that the short and long open times, at a single conductance level, could reflect the presence of a single channel rather than two completely different ones.

Developmental studies on vertebrate twitch fibers reveal the presence of 2 or 3 different nAChRs at the NMJ with varying conductance; there are low conductance channels (40-50 pS), a mid-conductance channel (50-60 pS) and a high conductance channel (65-70 pS). The 65-70 pS channel represents the adult form of the receptor ($\alpha 2$, β , δ , ϵ) and has a mean open time of ~ 0.8 -1 ms (Mishina et al., 1986). The 45 pS channels represent the embryonic forms of the receptor ($\alpha 2$, β , δ , γ) and have mean open times of about 3-4 ms and 2 ms (Mishina et al., 1986; Shepherd & Brehm, 1997). It is generally believed that the ratio of these channels differs during development such that embryonic synaptic events are largely composed of the 45 pS channels with relatively few or no 60 pS channels present. As development proceeds, there is a gradual decrease in the expression of the 45 pS channels and an increase in the 60 pS channel. Eventually, twitch fibers simply express the adult form of the receptor, with very little or no embryonic forms present. My results are generally consistent with these findings. In fact, I found that the conductance of nAChRs in 5 dpf zebrafish white muscle are essentially identical to those found previously in zebrafish (Mongeon et al., 2011; Nguyen et al., 1999). An earlier study on the zebrafish NMJ identified two independent channel types (a 60 pS and a 45 pS channel) in single channel recordings obtained from dissociated muscle fibers of 24 hpf and 3 dpf fish (Nguyen et al., 1999). These two types have similar conductance to the adult and embryonic receptors found in rat and *Xenopus* (P Brehm et al., 1984; Owens & Kullberg, 1989, 1990), except that their mean open times (~ 0.26 ms) are substantially smaller than those found in other vertebrates. Mongeon et al. (2011) reported the presence of nicotinic channels from zebrafish trunk musculature with main conductance levels around 50 pS and 70 pS from white muscle, and 66 pS and 70 pS from

red muscle. Furthermore, heterologous expression of α , β , γ and δ subunits in oocytes led to the expression of channels with conductance states and mean open times that are similar to those expressed in zebrafish muscle (Mongeon et al., 2011).

If a switch in nAChR subunits is responsible for the speeding up of the kinetics in white fibers, as has been documented in other preparations, then the switch occurs for both the high and low conductance channels, because both types don't exhibit long open times by 5 dpf. My recordings from red fibers show longer channel openings at both conductance levels in each age we examined, from 36 hpf to 5 dpf. It is almost certain that these kinetic differences underlie the biphasic synaptic events from red fibers and the monophasic ones from white fibers. My data suggest that it would be an oversimplification to postulate that during development there is a straightforward shift from low conductance, long open time channels to high conductance, short open time channels, as has been previously theorized.

6.2 Red vs White Fibers

Red fibers do not express voltage gated Na^+ channels and do not support action potentials (Buckingham & Ali, 2004). In zebrafish they arise from adaxial precursor cells very early in development and are functionally and physiologically distinct from the white fibers. In support of this, I found a number of key differences between nAChR properties associated with red and white fibers. First, neuromuscular junctions of red fibers express multiple types of nAChRs by 5 dpf, unlike those of white fibers. Second, the nicotinic channels express different mean open times compared with those in white fibers ascertained by their mEPC time courses and single channel open times. This includes the continued expression of long open time channels by 5 dpf. Third, PCR data suggests a continued upregulation of the $\beta 1a$ and the γ subunits by 5 dpf, in

contrast to white fibers. These findings are similar to previous studies which show that snake and rat tonic fibers express a different nAChR isoform than their twitch fibers (Dionne, 1981; Dionne & Parsons, 1978, 1981). Data on the development of synaptic events associated with slow or tonic fibers is sparse, but studies on garter snakes show the presence of 2 types of nAChRs (fast T-type and slow S-type) at slow endplates (Dionne, 1989), one of which (T-type) is similar to nAChRs at twitch endplates, while the other (S-type) has a smaller conductance and different kinetic behavior to fast twitch channels. Likewise, the slow pyriformis muscle in *Xenopus* expresses two main nAChRs with conductance (Henderson & Brehm, 1989) that are identical to my observations in 5 dpf zebrafish red muscle. In both cases the main conductance states of nAChRs are 45 and 65 pS. Thus, I report the existence of a conductance level around 46 pS, that is similar to previously documented conductance from the slow fibers of garter snake (49 ± 6 pS) (Dionne, 1981, 1989) and *Xenopus* pyriformis muscle (43 ± 1 pS) (Henderson & Brehm, 1989).

An evaluation of the properties of nAChRs associated with zebrafish fast and slow muscle in 3-4 day old fish determined that nAChRs of slow muscle are likely composed of only 3 subunits, $\alpha_2\beta\delta_2$ based upon kinetic and conductance properties (Mongeon et al., 2011). Moreover, expression of $\alpha_2\beta\delta_2$ subunits in *Xenopus* oocytes recapitulated the slow phenotype, while knockdown of the ϵ subunit in fast fibers resulted in a slow fiber phenotype. These data provide strong evidence for the existence of nAChRs composed of $\alpha_2\beta\delta_2$ subunits in slow muscle. In an attempt to determine if there is differential subunit expression during development, I found that red fibers express mRNA coding for all of the subunits at all ages examined. Thus, my RT-qPCR data does not reveal clear-cut developmental changes in the expression of nAChR subunits. A recent study identified a single point mutation in the δ subunit of zebrafish nAChRs that alters its kinetics (Park et al., 2014). Expression of $\alpha\beta\delta$ subunits in oocytes results in a single

channel conductance of ~ 70 pS (Mongeon et al., 2011), and red muscles that express the $\alpha_2\beta\delta_2$ channels exhibit synaptic events with long decay times, while white fibers that express the δ subunit with the point mutation are largely non-functional (Park et al., 2014). Interestingly, antibodies specific for the ϵ/γ subunits do not label red fibers, suggesting that the red fibers may not express the ϵ/γ subunits. In contrast to this earlier study, my results using RT-qPCR suggest the presence of mRNA coding for the ϵ and γ subunits in red fibers. Thus, my findings differ from those of Park and colleagues in this regard. I offer two possible reasons why these differences might arise; first, mRNA presence does not necessarily imply functional expression of the subunits, and secondly, the immunohistochemical assays used by Park et al. (2014) may not be sensitive enough to detect low levels of subunit expression. In fact, immunohistochemistry by Park et al. (2014) showed that nAChR clusters at red muscle fibers are restricted to the myoseptal region. In contrast, motor neuron innervation in all teleost red fibers, including zebrafish, have distributed polyneuronal innervation (Bone & Ono, 1982). It is counterintuitive to have distributed motor axons throughout the muscle but nAChRs being limited at the myoseptal boundary, particularly when these fibers cannot propagate action potentials therefore require distributed receptors to propagate the electric signal for sustained contraction (Buckingham & Ali, 2004).

One of the more interesting aspects of my RT-qPCR data deals with the expression of the $\beta 1a$ subunit. I find that this subunit is expressed at relatively high levels in red fibers and is developmentally regulated in white fibers (Fig 3.17). This pattern of expression suggests that one of the key differences between red and white muscle may actually be the presence of the $\beta 1a$ subunit. However, the $\beta 1a$ subunit is not trafficked or inserted into the membrane, as determined by heterologous expression studies, in situ hybridization and expression of cloned subunits fused

with CFP (Papke et al., 2012). Thus, I do not believe that the $\beta 1a$ subunits plays a functional role at zebrafish NMJs. Based on the present data I propose that nAChR development at the endplates of white fibers in zebrafish follow a developmental paradigm that is similar to that in mammals and amphibians whereby the embryonic form of the receptor $\alpha_2\beta\delta\gamma$ (50 pS), is largely present in young embryos and that there is a gradual transition to the adult form of the receptor $\alpha_2\beta\delta\varepsilon$ (70 pS), by 3-4 dpf. As development proceeds, the γ subunit is slowly lost as channels containing the ε subunit are upregulated; however, the $\alpha_2\beta\delta\gamma$ channel is still expressed by 5 dpf. In contrast, red fibers express at least two nAChR channels at all stages of development, one of which is the $\alpha_2\beta\delta_2$ (~65-70 pS) form, with possible contributions from $\alpha_2\beta\delta\gamma$ and $\alpha_2\beta\delta\varepsilon$ subtypes.

Why are red muscle fibers different from white, and what does this mean for the physiology of the organism? Slow muscles in teleost occupy the outermost muscle layer of the trunk in embryos and larvae. The muscle extends the entire length and breadth of the trunk, whereas in adults it is confined to a region close to the midline but runs from the most rostral to caudal points. The term “slow muscle”, initially coined by Kuffler and Vaughan Williams (Kuffler & Williams, 1953), refers to special muscle fibers that do not propagate action potentials and do not show a reversal of the membrane potential (i.e. do not overshoot). They are multiply innervated (innervated via more than one motor neuron), and often have longer membrane time constants and length constants than twitch fibers by virtue of having a larger membrane resistance (R_m). Slow fibers, often referred to as tonic fibers to distinguish them from slow-twitch muscle, receive *en grappe* synapses as opposed to the usual *en plaque* type found on twitch muscle (Hess, 1970; D. L. Morgan & Proske, 1984). *En grappe* synapses do not appear to have deep junctional folds where voltage-gated Na^+ channels are found (Hess, 1970). Indeed, the lack of propagating action potentials suggests that voltage gated Na^+ channels are either absent

or non-functional, as is the case in zebrafish red muscle (Buckingham & Ali, 2004). In mammals slow fibers are rare, but occur in about 20% of the extraocular muscles (EOM) of the eye and in the superior vocalis muscles of vocal chords (Han, Wang, Fischman, Biller, & Sanders, 1999; Spencer & Porter, 1988). Slow tonic fibers are common in birds (Bormioli, Sartore, Vitadello, & Schiaffino, 1980; Kennedy, Zak, & Gao, 1991; D. L. Morgan & Proske, 1984; Zhang, Rushbrook, & Shafiq, 1985) and amphibians (Bormioli et al., 1980; Franzini-Armstrong, 1984; D. L. Morgan & Proske, 1984; Pliszka, Strzelecka-Gołaszewska, Pantaloni, & d'Albis, 1981). They express a myosin heavy chain isoform that is unique to their allotype, a term used to denote distinct muscle classes (Porter & Baker, 1996), and they can be identified immunohistochemically by an antibody (anti-ALD) that distinguishes them from slow twitch muscle (Bormioli et al., 1980). Gene expression profiling of mice EOM, of both twitch and slow tonic fibers, show a significantly different profile compared with masticatory and limb allotypes based on myosin expression (Porter et al., 2001). Overall, slow tonic fibers are significantly different from any other muscle fiber type. These differences, along with their unique contractile properties make these fibers well suited to sustained contractions that require relatively little energy (compared with twitch fibers), and that can be altered in fine gradations. Fine tuning of sustained contraction can occur through the recruitment of different subsets of motor neurons synapsing onto the same muscle fiber. Expressing nAChRs with high bursting properties, or with relatively long open time constants allows for sufficient charge transfer to the muscle for a long enough period of time to allow for sustained contractions. Once synaptic activity has occurred, the long time-constant and space-constant coupled with a small cell size ensures that adequate depolarization spreads a significant distance away from the synaptic site. Thus, slow muscles are

well-positioned to play important roles in maintaining tonic contractile events suited to mobility, locomotion and posture.

6.3 Different Effects of γ and ϵ Subunit Knockdown on Development

Interestingly, γ and ϵ subunits had different expression patterns in zebrafish red and white muscle fibers. While white fibers showed a reduction of γ subunits during development, which is the common pattern observed in vertebrates, red muscle fibers continued to express γ subunits up until 5 dpf, the end point of my study. Why red and white fibers express different nAChRs during development is unknown. To investigate their role, I used MOs against γ and ϵ subunits to knock down their expression, examined the synaptic properties of the NMJs and the development of NMJ in these morphants, and finally looked into their locomotion.

To start, I used the translation blocking morpholinos designed by Mongeon et al. (2011) that targeted the knockdown of the γ and ϵ subunits. The kinetics of the miniature synaptic events in my experiments varied only slightly from Mongeon et al. (2011). In white muscle fibers, I found that injection of ϵ subunit MO further prolonged the slow exponential decay of mEPCs both at 2 dpf and 5 dpf, which is consistent with their findings for 3 dpf embryos. In red fibers, ϵ subunit MO did not alter the kinetics at 2 dpf in my recordings, which is also similar to their work. However, both the slow and fast exponential decays were significantly prolonged at 5 dpf, suggesting that MO injection affected red fibers later in development. While the synaptic events were slightly altered, morphology, neuronal development and locomotor activity were unaltered following ϵ subunit MO injection. Injection of γ subunit MO had almost no effect on zebrafish development either.

ϵ subunit MO altered the kinetic properties of synaptic currents at the NMJ but did not affect general development and locomotion of the fish (Mongeon et al., 2011). In my experiments, I also observed a similar result when I injected the translation blocking MOs used by Mongeon et al. (2011) at same concentrations. These results are surprising, given the fact that nAChRs have been found to be critical for normal development of NMJ and muscle in mammals, and alteration of the receptors induce pathophysiological conditions (Hoffmann et al., 2006; Missias et al., 1997; N. V Morgan et al., 2006; V Witzemann et al., 1996). Therefore, the results raised the question- whether the morpholinos were effective in properly knocking down the subunits. Unfortunately, no commercial antibody is available that is specific for zebrafish γ and ϵ subunit. Therefore, the efficacy of knockdown by these MOs could not be tested. I also noticed that the quantity of the MOs injected by Mongeon et al. (2011) was ~ 1000 fold less than normal concentration of MOs generally used in zebrafish (Kamachi, Okuda, & Kondoh, 2008; Sumanas & Larson, 2002; Westerfield, 2007). It is possible that such low quantity of MOs did not sufficiently knocked down the subunits.

To validate the findings, I designed and injected a second set of morpholinos to knockdown ϵ and γ subunits. The injected morpholinos were $\sim 1000x$ greater in concentration, which followed recommended morpholino concentrations used by many other studies (Kamachi et al., 2008; Sumanas & Larson, 2002; Westerfield, 2007). These new morpholinos were splice blocking, which caused an intron inclusion in the mRNA, as seen by the RT-PCR. Injection of these new morpholinos exhibited results that differed from the previous set of morpholinos. With the new splice blocking MOs, I found that knockdown of the ϵ subunit induced slight morphological defects such as a slight curvature in the tail. nAChRs were absent in distributed synapses of white muscle fiber at 5 dpf while they were unaffected at 2 dpf. The mean amplitude

of mEPCs was reduced in white muscle fibers, but not in red. The slow exponential decay of mEPCs was also prolonged in white fibers. But the knockdown did not have considerable effects on motor neuron branching or locomotor activity.

Knockdown of the γ subunit by the splice blocking MOs had quite different results compared to the ϵ subunit knockdown. The morphology of the fish was greatly affected as the fish exhibited severe axial malformation and pericardial edema. Expression of nAChRs puncta was not reduced, but the organization of the synapses, particularly myoseptal synapses was unorganized. Axonal branches of both primary and secondary MNs were aberrant. The locomotion of these fish was also severely affected. However, synaptic properties remained unaltered in red and white fibers at either 2 dpf or 5 dpf. While the effects of the ϵ subunit knockdown were largely restricted to synaptic properties associated with white muscle fibers, the effects of the γ subunit knockdown were actually not synaptic and were generally more global in nature. Thus I suggest different roles played by the nAChRs during development, as shown in Fig 6.2.

I observed that distributed synapses were largely absent in zebrafish when the ϵ subunit was knocked down, but nAChRs at the myoseptal region were present. In contrast, distributed nAChRs were unaffected, while myoseptal nAChRs were unorganized in γ knockdown fish. It suggests that myoseptal nAChRs do not contain ϵ subunit but may contain γ subunit. Myoseptal synapses are localized in red fibers, whereas distributed synapses are present in white muscle fibers (Park et al., 2014; Saint-Amant et al., 2008). Previous studies postulated that nAChRs in zebrafish red muscle fibers contain only α , β and δ subunits whereas γ and ϵ subunit containing receptors are exclusive to white muscle fibers (Mongeon et al., 2011; Park et al., 2014). My

results show that white muscle fibers at 5 dpf exclusively express ϵ subunit containing receptors, which confirms the previously published postulations, but I was unable to reliably determine the expression pattern of γ subunit containing receptors. It would be possible to determine the expression pattern of these receptors if antibodies that specifically target ϵ subunit containing and γ subunit containing receptors are available for zebrafish. Alternatively, genetic tagging of the receptors would also allow me to identify the expression patterns of these proteins. To date, no commercial antibody is available that can tag zebrafish γ and ϵ subunits separately, and fluorescent tagging of the subunits have not been established either.

The miniature synaptic events recorded from red and white muscle fibers show different kinetic properties whereby events obtained from red muscle fibers show much slower decay profiles compared with those obtained from white fibers. The synaptic decay kinetics speed up in each type of muscle fiber as the embryos age. However, even at 5 dpf, red muscle fibers show double exponential decay kinetics, whereas mEPCs from white fibers decay rapidly. I postulated that this alteration is caused by the differential expression of γ and ϵ subunit containing nAChRs- red fibers continue to express the γ subunit until 5 dpf, whereas white fibers express both of the subunits at 2 dpf, but not the γ subunit by 5 dpf. When I injected morpholinos to knockdown the ϵ subunit, the results obtained were in alignment with my postulation about the expression pattern in white fibers. The white fibers of 2 dpf embryos exhibited many α -bungarotoxin labeled nAChR puncta, which were not present at 5 dpf suggesting that zebrafish white fibers do not express γ subunit containing receptors in older animals. Furthermore, the mean amplitude of mEPCs recorded from 5 dpf white fibers was small compared with controls, and the synaptic decay was much slower. Surprisingly, when morpholino for the γ subunit was injected, mEPC kinetics remained unaffected. Park et al. (2014) suggested that nAChRs in zebrafish red fibers do

not express either the γ or the ϵ subunit. How the $\alpha\beta\delta$ receptors account for the bi-exponential decay property of mEPCs recorded from red fibers requires further explanation. Interestingly, simulations of mEPCs using rate constants of γ and ϵ containing nAChRs showed that the γ subunit contributes to slow decay kinetics whereas the ϵ subunit contributes to fast kinetics (Nayak & Auerbach, 2013). The researchers also found that the γ subunit has a higher affinity for ACh at lower concentrations, resulting in higher peak currents compared with ϵ -containing nAChRs. When high concentrations of ACh are present, such as during synaptic transmission at mature NMJ, the peak response from ϵ -containing nAChRs is larger because of the larger single channel conductance of these receptors. Nevertheless, deactivation of γ -AChR is slower at all concentrations because of the slower channel closing rate constant of γ -nAChRs (Nayak & Auerbach, 2013). In developing NMJs, wider synaptic gaps limit the ACh concentration available to developing synapse (Aidoo & Ward, 2006). In such situations, nAChRs containing γ subunits would be critical for maintaining synaptic transmission. In addition, it makes sense that red muscle fiber would retain γ subunit for activation of nAChRs. The slow diffusion and dissociation of ACh molecules would also allow the γ -AChRs in red muscle fibers to be active in a sustained manner, which is required for the fish for slow but sustained swimming behavior.

Changes in expression of nAChR genes have been seen in various conditions including muscle fiber type composition (Jin, Wernig, & Witzemann, 2008), denervation (Gattenlöhner et al., 2002), nerve injury (Ma et al., 2007), muscle activity (Rotzler & Brenner, 1990) and pathological conditions including amyotrophic lateral sclerosis (Tsujihata et al., 2001), diabetic neuropathy (Gattenlöhner et al., 2002) and myasthenic diseases. Mice lacking ϵ subunits show fast to slow twitch fiber transition (Jin et al., 2008). They also exhibit delayed onset congenital myasthenic syndrome (Missias et al., 1996). When the ϵ subunit was knocked down in mice, the

γ subunit was subsequently found to be persistently expressed in juvenile and adults. These mice exhibited impaired neuromuscular transmission, progressive muscle weakness, and atrophy, and died prematurely at 2 to 3 months after birth (V Witzemann et al., 1996). Lack of the ϵ subunit also gradually changed the NMJ structure and cytoskeletal assembly (Missias et al., 1997). While my results only focused on early development, longer term studies with ϵ subunit knockdown in zebrafish may find similar results, since I also observed a progressive loss of nAChRs and lack of movement at 5 dpf but not at 2 dpf.

In an earlier study on mice, it was found that the decay kinetics of mEPCs recorded from ϵ knockdown mice were prolonged (Missias et al., 1997). The prolongation of synaptic decay is also seen in many zebrafish mutants and has been associated with slow channel congenital myasthenic syndrome (SCCMS), an inherited human myasthenic condition (Engel, Ohno, & Sine, 2003). Prolonged activation episodes of the nAChR channel result in overloading of Ca^{2+} at the postsynaptic region causing massive destruction of the junctional folds, nuclear apoptosis, and vacuolar degeneration near the endplates (Engel et al., 2003). Progressive spinal deformities and respiratory problems are common complications associated with SCCMS. In patients with other forms of congenital myasthenic syndrome where various mutations in the nAChR subunits lead to nAChR deficiency, loss of the ϵ subunits are often compensated by the γ subunit. In such cases, mEPP amplitudes were found to be reduced, whereas mEPP frequency was increased. These patients generally exhibit mild symptoms of CMS (congenital myasthenic syndrome) (Engel et al., 2003). Interestingly, in my experiments, knockdown of the ϵ subunit by splice blocking MOs resulted in effects that were similar to the CMS patients. The fish exhibited very little morphological and behavioral changes. But α -bungarotoxin staining revealed lack of

distributed nAChRs whereas myoseptal synapses were intact. mEPC amplitudes were also markedly reduced while frequency was unaffected.

Electrophysiological studies have shown that the switch in the composition of nAChRs from γ to ϵ is a key process in the maturation of the NMJ. Channel mean open times decrease and the mean channel conductance increases. nAChRs containing the ϵ subunit have higher Ca^{2+} influxes than γ subunit-containing receptors, which is required for development and maintenance of adult NMJ structure (Francis & Papke, 1996). Lack of Ca^{2+} has been associated with zebrafish *relaxed* mutant that exhibits weak contraction of trunk muscle and slow swimming (Hirata et al., 2007). But the fast kinetics of ϵ containing receptors also maintain the proper Ca^{2+} level, since overload of Ca^{2+} is detrimental for the muscle (Castro, Martinello, Grassi, Eusebi, & Engel, 2007). Furthermore, the shorter mean open time of adult nAChRs helps in stabilizing the initial nerve–muscle contacts and synapse maturation in differentiated muscles (Schwarz, Giese, Müller, Koenen, & Witzemann, 2000).

6.4 Role of γ Subunit during Development

In γ knockdown fish, morphological defects were severe and locomotor activity was greatly perturbed. The mean mEPC amplitude was also slightly increased at 2 dpf, but not in 5 day old animals, whereas mEPC frequency and kinetics remain unaltered. α -bungarotoxin staining revealed a slight decrease in nAChR puncta at 2 dpf, but not at 5 dpf.

Immunohistochemistry revealed that MN branching and synaptic contacts appeared disorganized. These results indicate that the γ subunit may not be crucial for channel gating properties but may play an important role in embryonic development. Missias et al. (1997) found that in the ϵ -deficient mutant mice, the absence of a nAChR subunit switch (from γ to ϵ) elicited

no change in the acquisition of mature endplate geometry, the localization of synaptic antigens, or the rate of synapse elimination (Missias et al., 1997). Thus, the γ subunit likely plays a more pivotal role in controlling these developmental phenomena rather than in synaptic kinetics. Indeed, mutation of the γ subunit in humans has been observed in multiple pterygia (MP) patients (Hoffmann et al., 2006; N. V Morgan et al., 2006). The mutation can lead to prenatal death (Lethal Multiple Pterigium Syndrome- LMPS), or in some cases a non-lethal form of MP (Escobar Variant Multiple Pterigium Syndrome-EVMPS). MPs patients exhibit severe morphological deformities including congenital webbing of neck, elbows, knees and joint contractures, subcutaneous edema, curvature of spine, facial anomalies, fetal akinesia, intrauterine growth retardation, cryptorchidism, intestinal malrotation, cardiac hypoplasia, diaphragmatic hernia, obstructive uropathy, microcephaly, or cerebellar and pontine hypoplasia (N. V Morgan et al., 2006). The congenital contractures are related to reduced fetal movement, which is likely caused by the absence of functional γ containing nAChRs (J. G. Hall, 1997). Knockout of γ subunit in mice was also found to be lethal. Most of the mice died before birth, and only a few survived up to 2 days. Mice that survived had curved bodies, low body weight, irregular respiration, and disrupted limb movement. Spontaneous muscle action potentials were not developed in these mice (Takahashi et al., 2002). My findings in zebrafish are consistent with these studies on the absence or knockdown of the γ subunit in development.

In my experiments, I have found that when the γ subunit was reduced, MN branching pattern was altered at all ages examined. Furthermore, a study by Koenen, Peter, Villarroel, Witzemann, & Sakmann (2005) found that genetically replacing the γ -AChRs with ϵ -AChRs in mice preserved normal end-plate formation but the patterning of the motor nerve branching was altered at postnatal stages. These results imply that the γ subunit ensures the orderly innervation

of skeletal muscle fibers. Upregulation of γ subunits is particularly observed during nerve injury, and muscular myopathies. In humans, patients with neurogenic and myogenic disorders often showed upregulation of γ subunit, however it was restricted in type-1 fibers (Gattenlöhner et al., 2002).

How does the reduction of γ subunit affect development? Francis & Papke (1996) reported that the key function of nAChR γ subunit is to regulate Ca^{2+} permeation. When expression of the γ subunit was prevented, a greater amount of Ca^{2+} permeated through the nAChRs. Ca^{2+} is a key regulator of several enzymes and second messenger systems. At the NMJs, Ca^{2+} modulates nAChR synthesis, clustering, phosphorylation of the receptors and alters receptor desensitization (Huganir & Greengardt, 1990; McManaman, Blosser, & Appel, 1981; Parsons, 1978; Peng, 1984). Higher Ca^{2+} entry at NMJs can cause cationic overload and excitotoxicity leading to degeneration of the endplate fine structure, degeneration of the junctional fold and loss of nAChRs at the junction (Grassi & Fucile, 2014). Ca^{2+} overload at the NMJ also induces extensive muscle necrosis with dissolution of Z discs, dilation of mitochondria and breakdown of the sarcoplasmic reticulum (Leonard & Salpeter, 1979).

6.5 nAChRs and MN Development

Activation of nAChRs prevents neurite outgrowth and induces retraction of the neurites in chick ciliary ganglion neurons (Pugh & Berg, 1994) and *Xenopus* spinal neurons (Zheng, Felder, Connor, & Poo, 1994). MN survival is also affected by neuronal nAChRs, as application of nAChR blocker prevented the developmentally occurring MN death in chick spinal cord (Hory-Lee & Frank, 1995). In zebrafish, activation of nAChRs by embryonic exposure of

nicotine induced behavioral changes and delayed development of MNs (Svoboda, Vijayaraghavan, & Tanguay, 2002).

In twister mutant zebrafish, a gain of function mutation of nAChR α subunit, ectopic MN branching and disrupted muscle fiber organization were accompanied by prolonged decay of synaptic currents (Lefebvre et al., 2004). Disruption of nAChR clusters leads to aberrant branching of the MNs. At the same time, excess NMJ activity interferes with muscle fiber differentiation. In zebrafish, abnormal MN development is often but not always observed along with abnormal muscle development as seen in several zebrafish mutants and toxicology studies, suggesting the two phenomena might be closely related, but not be directly associated (Birely et al., 2005; Welsh, Tanguay, & Svoboda, 2009).

In my results, I observed that knockdown of the ϵ subunit delays MN development, but does not cause major disruptions in axonal branching pattern. In contrast, knockdown of the γ subunit had pronounced effects on organization of MN branching. It is possible that, as γ subunits are likely expressed at time points when MN growth cones are being extended, knockdown of these subunits affects MN branching and NMJ activity which is required for proper muscle development. The role of the ϵ subunit might be limited in maintaining synaptic transmission only.

Why do embryonic muscles express nAChRs with γ subunits whereas adult muscles express nAChRs with ϵ subunit? It has been found that activity and nerve induced factors such as agrin mediates upregulation of ϵ subunit and downregulation of γ subunit (Martinou & Merlie, 1991). nAChRs are expressed prior to neuronal innervation. At such stages, lack of neuronal factors allows the γ subunit to be expressed. The γ subunit is also upregulated following

denervation and injury (Ma et al., 2007; Osta et al., 2010). Therefore, the γ subunit might play a critical role in the function of nAChRs where presynaptic inputs are absent. They might provide cues for neuronal growth cones for potential NMJ formation, as NMJ formation generally occurs precisely where nAChR clusters are formed. Whether these channels are active in aneuronal synapses is not known. I did not observe any effects on synaptic activity after knockdown of γ subunits in 2 or 5 dpf. It is possible that γ subunits play a role in the properties of synaptic currents at 36 hpf or earlier, but this has not been studied. Though mEPCs were hardly observed in embryos younger than 30 hpf, studying spontaneous or induced synaptic currents between 18-36 hpf might provide more insight into the functional significance of γ subunits in synaptic transmission of nAChRs. Indeed, γ subunits are expressed in muscles exhibiting spontaneous contraction, and it is possible that it promotes formation of the postsynaptic membrane specializations and muscle development (Koenen et al., 2005). It is worth mentioning that in developing muscle fibers, voltage gated sodium channels (Na_v) are expressed later during development, around the same time that the γ to ϵ switch occurs (Slater, 2003). As such, a lack of Na_v channel activity might be another factor which is compensated for by expressing γ subunit containing receptors. The longer open time of this subunit would allow signal transduction in the muscle that cannot traverse action potentials without Na_v . While these assumptions require further investigations to be proved/disproved, my results suggest that γ subunits play a critical role in early development of MN and muscle, which has not been extensively studied yet.

6.6 Conclusion and Future Directions

Overall, my study clarifies previous ambiguities particularly emanating from Nguyen et al. (1999) and Mongeon et al. (2011) about the development of synaptic properties in zebrafish

red and white muscle fibers. My results clearly show that the NMJ of zebrafish red and white muscle fibers develop differently. One of the key differences is the sustained expression of embryonic type γ subunit of nAChR in red fibers, whereby white fibers replaces the γ subunit with the adult type ϵ subunits by 5 dpf. When I used MOs to knockdown the ϵ subunit, clustering of nAChRs at 5 dpf white fibers were reduced as well as synaptic properties associated with the white muscle NMJs were altered. The results clearly indicate that the ϵ subunit of nAChR is an important subunit for proper synaptic transmission particularly at white muscle NMJs. While synaptic currents were affected, no effect was observed for morphological and motor neuron development during the studied time period. In contrast, when I used MOs to knockdown the γ subunit, I found that synaptic currents were not altered in either red or white muscle fibers. But lack of the γ subunit severely affected the morphological development, motor neuron branching and locomotion. Clearly, physiological function of the γ subunit is more critical in maintaining proper embryonic development rather than ensuring synaptic kinetics.

Thus, my results provide further insight into the physiological role of nAChRs in different types of muscle fibers. In particular, the importance of the expression of the embryonic form of nAChRs has not been extensively studied. My thesis work provides a background to study the role of the γ subunit using zebrafish as a model organism. To further extend our understanding about the role of nAChR subunits at synaptic transmission and development of NMJ, the following areas of research could be addressed:

1. Generation of knockout of γ and ϵ subunit of nAChRs using CRISPR technology. So far, I have used morpholinos to reduce the expression of γ and ϵ subunits. However, morpholinos only partially prevent the expression of a protein. Thus, the partial expression of the receptor

subunits might have complicated my observations. If a total absence of the subunits can be achieved via gene knockout technology e.g. CRISPR-Cas9 method, physiological role of the subunits in embryonic development could be more clearly identified.

2. Role of the subunits in later stages of development and adulthood. My study only focuses on the early development of zebrafish while it is indicated by my RT-PCR and RT-qPCR results that zebrafish likely retain γ subunit even at adulthood. Why does the fish require a continued expression of the γ subunit? What would happen to the juvenile and adult fish if ϵ subunit is not available for proper synaptic transmission? These questions can be addressed if viable knockout of the subunits can be generated.

3. Role of primary and secondary motor neurons in the expression and maintenance of the subunits. Zebrafish white muscle fibers are innervated by both primary and secondary MNs, whereas red fibers are innervated by secondary MNs only (Westerfield et al., 1986). Whether this difference in the innervation has any effect on the expression of the subunits is not known. Specific MNs can be ablated using a laser ablation method, and then a combination of RT-qPCR, in situ hybridization and immunohistochemistry can be performed to study the expression and maintenance of the subunits.

4. Mechanism of γ -subunit dependent development. My results show that the γ subunit of nAChRs is crucial for proper embryonic development. Similar results have been seen in human with multiple pterygia (Hoffmann et al., 2006; N. V Morgan et al., 2006). But the molecular mechanism of how γ subunit regulates development is not known. Total RNA or total proteins can be extracted from γ subunit knockout or knockdown fish, and the subsequent molecular changes can be studied using RNA-seq or proteomic analysis. Changes in the expression in

knockout/knockdown fish vs control fish can be used for bioinformatics analysis to assess which molecular pathways are affected and how they are regulated by the γ subunit.

5. Prevention and recovery of γ -subunit dependent developmental defects. As the lack of γ subunit induces severe developmental defects, the most important future study would be to determine how these defects can be prevented or recovered. Understanding of the molecular mechanism of γ subunit dependent development would be crucial for this. If the molecular pathway is known, different modulators of the pathway can be tested to determine if the defects can be prevented or rescued. Moreover, mutation of the nAChR- γ subunit should be checked during the prenatal genetic testing, which would provide a precautionary note to the parents and caregivers regarding the expected life scenarios of the baby.

Figure 6.1

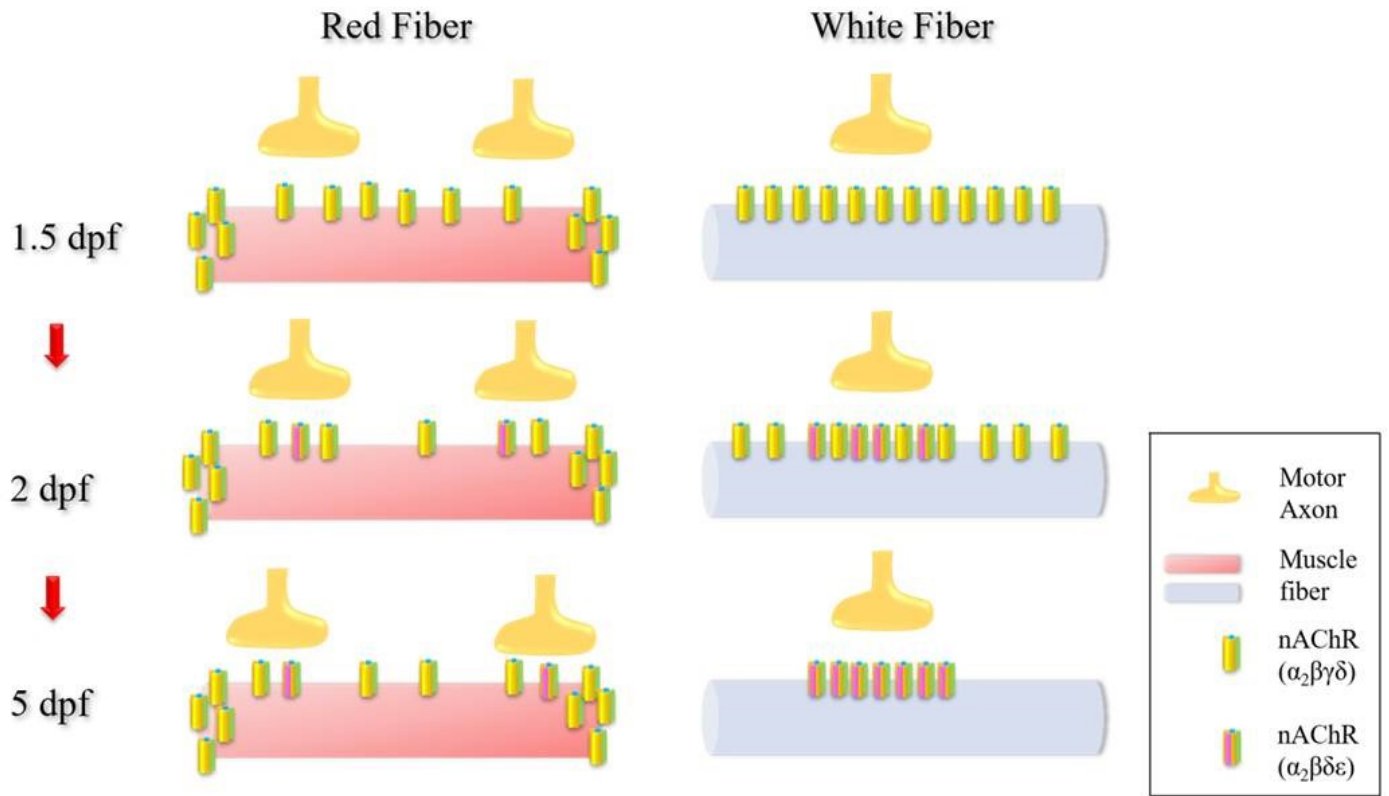


Figure 6.1

Schematic of nAChR expression pattern in zebrafish red and white muscle fibers during development. Expression pattern of nAChRs are shown at 1.5 dpf, 2 dpf and 5 dpf. The expression pattern differs between red fibers (left column) and white fibers (right column). Red fibers have myoseptal cluster of nAChRs at high density whereas distributed clusters of nAChRs are less concentrated. White fibers have distributed nAChR clusters which are highly dense. At 36 hpf, both red and white fibers express γ -nAChRs. Emergence of ϵ -nAChRs happen at around 2 dpf. At 5 dpf, red fibers have both γ and ϵ -nAChRs, whereas white fibers only express ϵ -nAChRs. Position of MN axon is arbitrary.

Figure 6.2

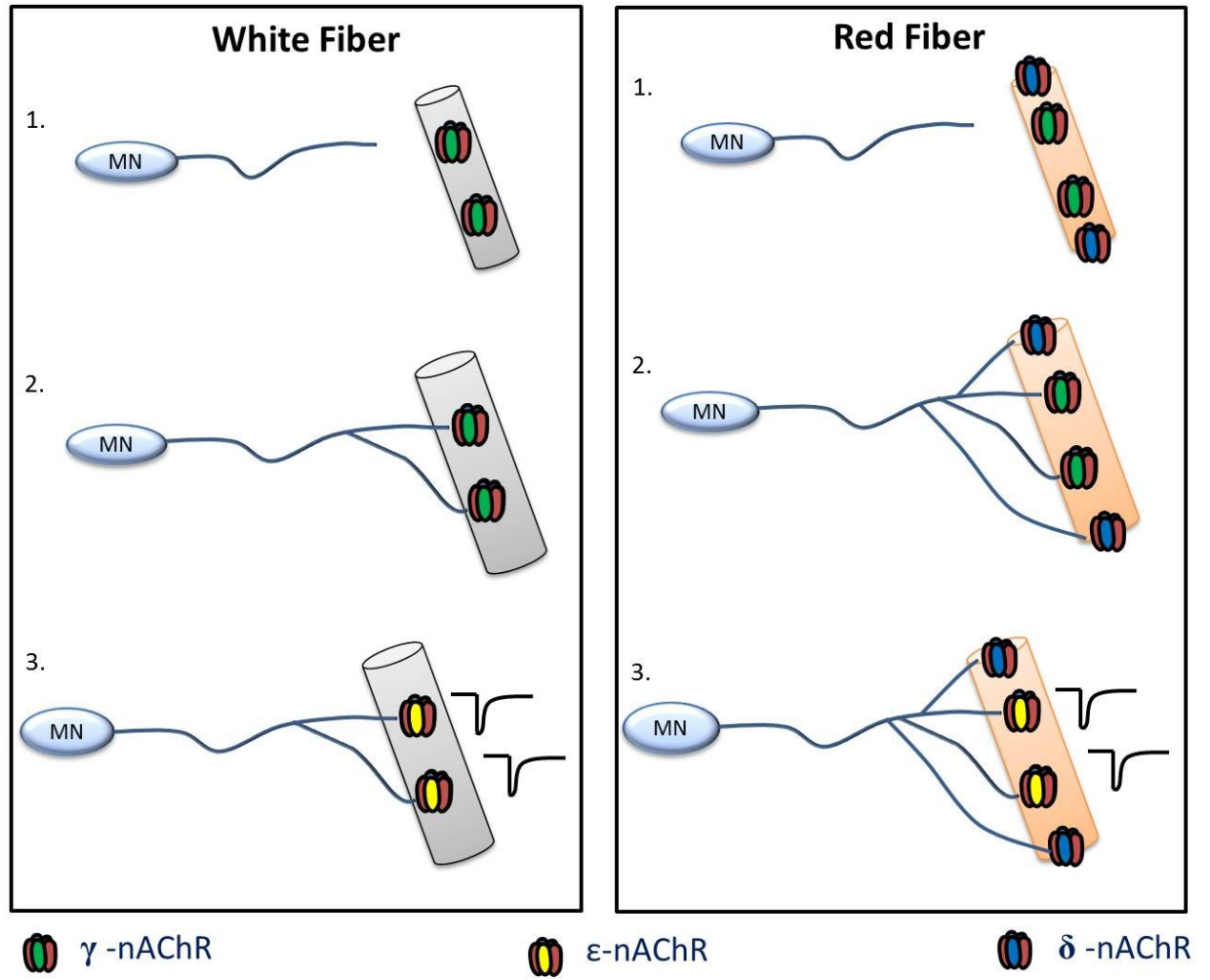


Figure 6.2

Schematic of my proposed role of different nAChR subunits during development of MN. Based on my results on the expression pattern of nAChR subunits and effects of MOs, I propose that at the earlier time points during development, both red and white fibers express γ subunit containing nAChRs, while red fibers may or may not express γ/ϵ less nAChRs (1). In the presence of γ -nAChRs, developing MN axon properly branches to form orderly synapses and allow growth of the muscle fibers (2). γ -nAChRs are eventually replaced by the ϵ -nAChRs to allow synaptic currents to occur properly (3). Note, as I did not test expression and function of γ/ϵ less nAChRs, I adhered to the proposals of Mongeone et al (2011) and Park et al (2014), suggesting that these receptors are exclusively expressed at the myoseptal region of red muscle fibers and likely mediate synaptic currents in these fibers.

References

- Ahmed, K. T., & Ali, D. W. (2016). Nicotinic acetylcholine receptors (nAChRs) at zebrafish red and white muscle show different properties during development. *Developmental Neurobiology*, 76(8), 916–936. <https://doi.org/10.1002/dneu.22366>
- Ahmed, K. T., Amin, M. R., Shah, P., & Ali, D. W. (2018). Motor neuron development in zebrafish is altered by brief (5-hr) exposures to THC (Δ^9 -tetrahydrocannabinol) or CBD (cannabidiol) during gastrulation. *Scientific Reports*, 8(1), 10518. <https://doi.org/10.1038/s41598-018-28689-z>
- Aidoo, A. Y., & Ward, K. (2006). Spatio-temporal concentration of acetylcholine in vertebrate synaptic cleft. *Mathematical and Computer Modelling*, 44(9–10), 952–962. <https://doi.org/10.1016/j.mcm.2006.03.003>
- Akiyama, K., Alberdi, A., Alef, W., Asada, K., Azulay, R., Baczko, A.-K., ... Ziurys, L. (2019). First M87 Event Horizon Telescope Results. I. The Shadow of the Supermassive Black Hole. *The Astrophysical Journal*, 875(1), L1. <https://doi.org/10.3847/2041-8213/ab0ec7>
- Albuquerque, E. X., Pereira, E. F. R., Alkondon, M., & Rogers, S. W. (2009). Mammalian Nicotinic Acetylcholine Receptors: From Structure to Function. *Physiological Reviews*, 89(1), 73–120. <https://doi.org/10.1152/physrev.00015.2008>
- Alder, N. N., & Johnson, A. E. (2004). Cotranslational membrane protein biogenesis at the endoplasmic reticulum. *The Journal of Biological Chemistry*, 279(22), 22787–22790. <https://doi.org/10.1074/jbc.R400002200>
- Bernard, C. (1857). *Leçons sur les effets des substances toxiques et médicamenteuses*. Retrieved

from <https://archive.org/stream/leonssurlesef00bern#page/n7/mode/1up>

Birely, J., Schneider, V. A., Santana, E., Dosch, R., Wagner, D. S., Mullins, M. C., & Granato, M. (2005). Genetic screens for genes controlling motor nerve–muscle development and interactions. *Developmental Biology*, *280*(1), 162–176.

<https://doi.org/10.1016/J.YDBIO.2005.01.012>

Blount, P., Smith, M. M., & Merlie, J. P. (1990). Assembly intermediates of the mouse muscle nicotinic acetylcholine receptor in stably transfected fibroblasts. *The Journal of Cell Biology*, *111*(6 Pt 1), 2601–2611. <https://doi.org/10.1083/JCB.111.6.2601>

Bone, Q., & Ono, R. D. (1982). Systematic implications of innervation patterns in teleost myotomes. *Breviora*, *470*, 1–23. <https://doi.org/10.5962/bhl.part.28053>

Bormioli, S. P., Sartore, S., Vitadello, M., & Schiaffino, S. (1980). “Slow” myosins in vertebrate skeletal muscle. An immunofluorescence study. *The Journal of Cell Biology*, *85*(3), 672–681. <https://doi.org/10.1083/jcb.85.3.672>

Boyd, R. T. (1996). Transcriptional regulation and cell specificity determinants of the rat nicotinic acetylcholine receptor alpha 3 gene. *Neuroscience Letters*, *208*(2), 73–76. [https://doi.org/10.1016/0304-3940\(96\)12561-1](https://doi.org/10.1016/0304-3940(96)12561-1)

Bradley, S., Tossell, K., Lockley, R., & McDermid, J. R. (2010). Nitric oxide synthase regulates morphogenesis of zebrafish spinal cord motoneurons. *Journal of Neuroscience*, *30*(50), 16818–16831. <https://doi.org/10.1523/JNEUROSCI.4456-10.2010>

Brehm, P., Kullberg, R., & Moody-Corbett, F. (1984). Properties of non-junctional acetylcholine receptor channels on innervated muscle of *Xenopus laevis*. *The Journal of Physiology*,

350(1), 631–648. <https://doi.org/10.1113/jphysiol.1984.sp015222>

Brehm, Paul, Steinbach, J. H., & Kidokoro, Y. (1982). Channel open time of acetylcholine receptors on *Xenopus* muscle cells in dissociated cell culture. *Developmental Biology*, 91(1), 93–102. [https://doi.org/10.1016/0012-1606\(82\)90012-4](https://doi.org/10.1016/0012-1606(82)90012-4)

Buckingham, S. D., & Ali, D. W. (2004). Sodium and potassium currents of larval zebrafish muscle fibres. *The Journal of Experimental Biology*, 207(Pt 5), 841–852. <https://doi.org/10.1242/jeb.00839>

Budick, S. A., & O'Malley, D. M. (2000). Locomotor repertoire of the larval zebrafish: swimming, turning and prey capture. *The Journal of Experimental Biology*, 203(Pt 17), 2565–2579. Retrieved from <http://www.ncbi.nlm.nih.gov/pubmed/10934000>

Buss, R. R., & Drapeau, P. (2000). Physiological Properties of Zebrafish Embryonic Red and White Muscle Fibers During Early Development. *Journal of Neurophysiology*, 84(3), 1545–1557. <https://doi.org/10.1152/jn.2000.84.3.1545>

Buss, R. R., & Drapeau, P. (2001). Synaptic Drive to Motoneurons During Fictive Swimming in the Developing Zebrafish. *Journal of Neurophysiology*, 86(1), 197–210. <https://doi.org/10.1152/jn.2001.86.1.197>

Buss, R. R., & Drapeau, P. (2002). Activation of embryonic red and white muscle fibers during fictive swimming in the developing zebrafish. *Journal of Neurophysiology*, 87(3), 1244–1251. <https://doi.org/10.1152/JN.00659.2001>

Camacho, P., Liu, Y., Mandel, G., & Brehm, P. (1993). The epsilon subunit confers fast channel gating on multiple classes of acetylcholine receptors. *The Journal of Neuroscience*, 13(2),

605–613. <https://doi.org/10.1523/JNEUROSCI.13-02-00605.1993>

Castro, A. Di, Martinello, K., Grassi, F., Eusebi, F., & Engel, A. G. (2007). Pathogenic point mutations in a transmembrane domain of the ϵ subunit increase the Ca^{2+} permeability of the human endplate ACh receptor. *The Journal of Physiology*, *579*(3), 671–677.

<https://doi.org/10.1113/jphysiol.2007.127977>

Changeux, J.-P., Kasai, M., & Lee, C.-Y. (1970). Use of a Snake Venom Toxin to Characterize the Cholinergic Receptor Protein. *Proceedings of the National Academy of Sciences*, *67*(3), 1241–1247. <https://doi.org/10.1073/pnas.67.3.1241>

Colbourne, H. (2007). *Inquiry Into Biology*. Toronto, ON: Toronto : McGraw-Hill Ryerson.

Colombo, S. F., Mazzo, F., Pistillo, F., & Gotti, C. (2013). Biogenesis, trafficking and up-regulation of nicotinic ACh receptors. *Biochemical Pharmacology*, *86*(8), 1063–1073.

<https://doi.org/10.1016/j.bcp.2013.06.023>

Dahl, R., Larsen, S., Dohlmann, T. L., Qvortrup, K., Helge, J. W., Dela, F., & Prats, C. (2015). Three-dimensional reconstruction of the human skeletal muscle mitochondrial network as a tool to assess mitochondrial content and structural organization. *Acta Physiologica*, *213*(1), 145–155. <https://doi.org/10.1111/apha.12289>

Dale, H. H., Feldberg, W., & Vogt, M. (1936). Release of acetylcholine at voluntary motor nerve endings. *The Journal of Physiology*, *86*(4), 353–380.

<https://doi.org/10.1113/jphysiol.1936.sp003371>

De Graaf, F., van Raamsdonk, W., van Asselt, E., & Diegenbach, P. C. (1991). Histochemical profiles of motoneurons innervating muscle fibres with different activity patterns in the

zebrafish, *Brachydanio rerio*. *The Histochemical Journal*, 23(6), 273–280.

<https://doi.org/10.1007/bf01045046>

Del Castillo, J., & Katz, B. (1956). Biophysical aspects of neuro-muscular transmission.

Progress in Biophysics and Biophysical Chemistry, 6, 121–170. Retrieved from

<http://www.ncbi.nlm.nih.gov/pubmed/13420190>

Devoto, S. H., Melançon, E., Eisen, J. S., & Westerfield, M. (1996). Identification of separate

slow and fast muscle precursor cells in vivo, prior to somite formation. *Development*,

122(11), 3371–3380. Retrieved from <http://www.ncbi.nlm.nih.gov/pubmed/8951054>

Dionne, V. E. (1981). Acetylcholine receptor kinetics at slow fiber neuromuscular junctions.

Federation Proceedings, 40(11), 2614–2617. Retrieved from

<http://www.ncbi.nlm.nih.gov/pubmed/6268461>

Dionne, V. E. (1989). Two types of nicotinic acetylcholine receptor channels at slow fibre end-plates of the garter snake. *The Journal of Physiology*, 409(1), 313–331.

<https://doi.org/10.1113/jphysiol.1989.sp017499>

Dionne, V. E., & Parsons, R. L. (1978). Synaptic channel gating differences at snake twitch and slow neuromuscular junctions. *Nature*, 274(5674), 902–904.

<https://doi.org/10.1038/274902a0>

Dionne, V. E., & Parsons, R. L. (1981). Characteristics of the acetylcholine-operated channel at twitch and slow fibre neuromuscular junctions of the garter snake. *The Journal of*

Physiology, 310(1), 145–158. <https://doi.org/10.1113/jphysiol.1981.sp013541>

Drapeau, P., Buss, R. R., Ali, D. W., Legendre, P., & Rotundo, R. L. (2001). Limits to the

- Development of Fast Neuromuscular Transmission in Zebrafish. *Journal of Neurophysiology*, 86(6), 2951–2956. <https://doi.org/10.1152/jn.2001.86.6.2951>
- Drapeau, P., Saint-Amant, L., Buss, R. R., Chong, M., McDearmid, J. R., & Brustein, E. (2002). Development of the locomotor network in zebrafish. *Progress in Neurobiology*, 68(2), 85–111. [https://doi.org/10.1016/S0301-0082\(02\)00075-8](https://doi.org/10.1016/S0301-0082(02)00075-8)
- Eaton, R. C., Lee, R. K. K., & Foreman, M. B. (2001). The Mauthner cell and other identified neurons of the brainstem escape network of fish. *Progress in Neurobiology*, 63(4), 467–485. [https://doi.org/10.1016/S0301-0082\(00\)00047-2](https://doi.org/10.1016/S0301-0082(00)00047-2)
- Edstrom, L., & Kugelberg, E. (1968). Histochemical composition, distribution of fibres and fatiguability of single motor units. Anterior tibial muscle of the rat. *Journal of Neurology, Neurosurgery & Psychiatry*, 31(5), 424–433. <https://doi.org/10.1136/jnnp.31.5.424>
- Eisen, J. S. (1991). Motoneuronal development in the embryonic zebrafish. *Development Supplement, Suppl 2*, 141–147. Retrieved from http://dev.biologists.org/content/develop/113/Supplement_2/141.full.pdf
- Eisen, J. S., Myers, P. Z., & Westerfield, M. (1986). Pathway selection by growth cones of identified motoneurons in live zebra fish embryos. *Nature*, 320(6059), 269–271. <https://doi.org/10.1038/320269a0>
- Eisen, J. S., & Smith, J. C. (2008). Controlling morpholino experiments: don't stop making antisense. *Development*, 135(10), 1735–1743. <https://doi.org/10.1242/dev.001115>
- Ekker, S. C., & Larson, J. D. (2001). Morphant technology in model developmental systems. *Genesis (New York, N.Y. : 2000)*, 30(3), 89–93. <https://doi.org/10.1002/gene.1038>

- Engel, A. G., Ohno, K., & Sine, S. M. (2003). Congenital myasthenic syndromes: Progress over the past decade. *Muscle & Nerve*, 27(1), 4–25. <https://doi.org/10.1002/mus.10269>
- Fatt, P., & Katz, B. (1952a). Spontaneous subthreshold activity at motor nerve endings. *The Journal of Physiology*, 117(1), 109–128.
<https://doi.org/10.1113/JPHYSIOL.1952.SP004735>
- Fatt, P., & Katz, B. (1952b). The electric activity of the motor end-plate. *Proceedings of the Royal Society of London. Series B - Biological Sciences*, 140(899), 183–186.
<https://doi.org/10.1098/rspb.1952.0055>
- Fischbach, G. D., & Schuetze, S. M. (1980). A post-natal decrease in acetylcholine channel open time at rat end-plates. *The Journal of Physiology*, 303(1), 125–137.
<https://doi.org/10.1113/jphysiol.1980.sp013275>
- Flanagan-Steet, H., Fox, M. A., Meyer, D., & Sanes, J. R. (2005). Neuromuscular synapses can form in vivo by incorporation of initially aneural postsynaptic specializations. *Development*, 132(20), 4471–4481. <https://doi.org/10.1242/dev.02044>
- Fox, M. A., & Sanes, J. R. (2007). Synaptotagmin I and II are present in distinct subsets of central synapses. *The Journal of Comparative Neurology*, 503(2), 280–296.
<https://doi.org/10.1002/cne.21381>
- Francis, M. M., & Papke, R. L. (1996). Muscle-type nicotinic acetylcholine receptor delta subunit determines sensitivity to noncompetitive inhibitors, while gamma subunit regulates divalent permeability. *Neuropharmacology*, 35(11), 1547–1556.
[https://doi.org/10.1016/s0028-3908\(96\)00103-7](https://doi.org/10.1016/s0028-3908(96)00103-7)

- Franzini-Armstrong, C. (1984). Freeze-fracture of frog slow tonic fibers. Structure of surface and internal membranes. *Tissue & Cell*, *16*(4), 647–664. [https://doi.org/10.1016/0040-8166\(84\)90038-7](https://doi.org/10.1016/0040-8166(84)90038-7)
- Frontera, W. R., & Ochala, J. (2015). Skeletal Muscle: A Brief Review of Structure and Function. *Calcified Tissue International*, *96*(3), 183–195. <https://doi.org/10.1007/s00223-014-9915-y>
- Fuhrer, C., & Huh, K.-H. (2002). Clustering of Nicotinic Acetylcholine Receptors: From the Neuromuscular Junction to Interneuronal Synapses. *Molecular Neurobiology*, *25*(1), 079–112. <https://doi.org/10.1385/MN:25:1:079>
- Fuiman, L. A., & Webb, P. W. (1988). Ontogeny of routine swimming activity and performance in zebra danios (Teleostei: Cyprinidae). *Animal Behaviour*, *36*(1), 250–261. [https://doi.org/10.1016/S0003-3472\(88\)80268-9](https://doi.org/10.1016/S0003-3472(88)80268-9)
- Galzi, J. -l., & Changeux, J. -p. (1995). Neuronal nicotinic receptors: Molecular organization and regulations. *Neuropharmacology*, *34*(6), 563–582. [https://doi.org/10.1016/0028-3908\(95\)00034-4](https://doi.org/10.1016/0028-3908(95)00034-4)
- Gattenlöhner, S., Schneider, C., Thamer, C., Klein, R., Roggendorf, W., Gohlke, F., ... Marx, A. (2002). Expression of foetal type acetylcholine receptor is restricted to type 1 muscle fibres in human neuromuscular disorders. *Brain*, *125*(6), 1309–1319. <https://doi.org/10.1093/brain/awf136>
- Goldman, D., & Staple, J. (1989). Spatial and temporal expression of acetylcholine receptor RNAs in innervated and denervated rat soleus muscle. *Neuron*, *3*(2), 219–228.

[https://doi.org/10.1016/0896-6273\(89\)90035-4](https://doi.org/10.1016/0896-6273(89)90035-4)

Grassi, F., & Fucile, S. (2014). *Nicotinic AChR in Congenital Myasthenic Syndromes BT - Pathologies of Calcium Channels* (N. Weiss & A. Koschak, eds.).

https://doi.org/10.1007/978-3-642-40282-1_33

Green, W. N., & Claudio, T. (1993). Acetylcholine receptor assembly: Subunit folding and oligomerization occur sequentially. *Cell*, *74*(1), 57–69. [https://doi.org/10.1016/0092-8674\(93\)90294-Z](https://doi.org/10.1016/0092-8674(93)90294-Z)

Hall, C. E., Jakus, M. A., & Schmitt, F. O. (1946). An investigation of cross striations and myosin filaments in muscle. *The Biological Bulletin*, *90*(1), 32–50.

<https://doi.org/10.2307/1538060>

Hall, J. G. (1997). Arthrogyrosis multiplex congenita: etiology, genetics, classification, diagnostic approach, and general aspects. *Journal of Pediatric Orthopedics. Part B*, *6*(3), 159–166. Retrieved from <http://www.ncbi.nlm.nih.gov/pubmed/9260643>

Han, Y., Wang, J., Fischman, D. A., Biller, H. F., & Sanders, I. (1999). Slow tonic muscle fibers in the thyroarytenoid muscles of human vocal folds; a possible specialization for speech.

The Anatomical Record, *256*(2), 146–157. [https://doi.org/10.1002/\(SICI\)1097-0185\(19991001\)256:2<146::AID-AR5>3.0.CO;2-8](https://doi.org/10.1002/(SICI)1097-0185(19991001)256:2<146::AID-AR5>3.0.CO;2-8)

Henderson, L. P., & Brehm, P. (1989). The single-channel basis for the slow kinetics of synaptic currents in vertebrate slow muscle fibers. *Neuron*, *2*(4), 1399–1405.

[https://doi.org/10.1016/0896-6273\(89\)90078-0](https://doi.org/10.1016/0896-6273(89)90078-0)

Hess, A. (1970). Vertebrate slow muscle fibers. *Physiological Reviews*, *50*(1), 40–62.

<https://doi.org/10.1152/physrev.1970.50.1.40>

Hesselmans, L. F. G. M., Jennekens, F. G. I., Van Den Oord, C. J. M., Veldman, H., & Vincent, A. (1993). Development of innervation of skeletal muscle fibers in man: Relation to acetylcholine receptors. *The Anatomical Record*, *236*(3), 553–562.

<https://doi.org/10.1002/ar.1092360315>

Hirata, H., Watanabe, T., Hatakeyama, J., Sprague, S. M., Saint-Amant, L., Nagashima, A., ... Kuwada, J. Y. (2007). Zebrafish relatively relaxed mutants have a ryanodine receptor defect, show slow swimming and provide a model of multi-minicore disease. *Development*, *134*(15), 2771–2781. <https://doi.org/10.1242/dev.004531>

Hoffmann, K., Müller, J. S., Stricker, S., Megarbane, A., Rajab, A., Lindner, T. H., ... Mundlos, S. (2006). Escobar Syndrome Is a Prenatal Myasthenia Caused by Disruption of the Acetylcholine Receptor Fetal γ Subunit. *The American Journal of Human Genetics*, *79*(2), 303–312. <https://doi.org/10.1086/506257>

Horton, R. M., Manfredi, A. A., & Conti-Tronconi, B. M. (1993). The “embryonic” gamma subunit of the nicotinic acetylcholine receptor is expressed in adult extraocular muscle. *Neurology*, *43*(5), 983–986. <https://doi.org/10.1212/wnl.43.5.983>

Hory-Lee, F., & Frank, E. (1995). The nicotinic blocking agents d-tubocurare and alpha-bungarotoxin save motoneurons from naturally occurring death in the absence of neuromuscular blockade. *The Journal of Neuroscience*, *15*(10), 6453–6460. Retrieved from <http://www.ncbi.nlm.nih.gov/pubmed/7472408>

Huganir, R. L., & Greengardt, P. (1990). Regulation of neurotransmitter receptor desensitization

by protein phosphorylation. *Neuron*, Vol. 5, pp. 555–567. [https://doi.org/10.1016/0896-6273\(90\)90211-W](https://doi.org/10.1016/0896-6273(90)90211-W)

Huxley, A. F., & Niedergerke, R. (1954). Structural Changes in Muscle During Contraction: Interference Microscopy of Living Muscle Fibres. *Nature*, *173*(4412), 971–973. <https://doi.org/10.1038/173971a0>

Huxley, H., & Hanson, J. (1954). Changes in the Cross-Striations of Muscle during Contraction and Stretch and their Structural Interpretation. *Nature*, *173*(4412), 973–976. <https://doi.org/10.1038/173973a0>

Jayne, B. C., & Lauder, G. V. (1994). How swimming fish use slow and fast muscle fibers: implications for models of vertebrate muscle recruitment. *Journal of Comparative Physiology A*, *175*(1), 123–131. <https://doi.org/10.1007/BF00217443>

Jin, T.-E., Wernig, A., & Witzemann, V. (2008). Changes in acetylcholine receptor function induce shifts in muscle fiber type composition. *FEBS Journal*, *275*(9), 2042–2054. <https://doi.org/10.1111/j.1742-4658.2008.06359.x>

Kalamida, D., Poulas, K., Avramopoulou, V., Fostieri, E., Lagoumintzis, G., Lazaridis, K., ... Tzartos, S. J. (2007). Muscle and neuronal nicotinic acetylcholine receptors. *FEBS Journal*, *274*(15), 3799–3845. <https://doi.org/10.1111/j.1742-4658.2007.05935.x>

Kamachi, Y., Okuda, Y., & Kondoh, H. (2008). Quantitative assessment of the knockdown efficiency of morpholino antisense oligonucleotides in zebrafish embryos using a luciferase assay. *Genesis*, *46*(1), 1–7. <https://doi.org/10.1002/dvg.20361>

Katz, B. (1979). Elementary components of synaptic transmission. *Die Naturwissenschaften*,

66(12), 606–610. <https://doi.org/10.1007/bf00405119>

Katz, B., & Miledi, R. (1967a). A study of synaptic transmission in the absence of nerve impulses. *The Journal of Physiology*, *192*(2), 407–436.

<https://doi.org/10.1113/jphysiol.1967.sp008307>

Katz, B., & Miledi, R. (1967b). The timing of calcium action during neuromuscular transmission. *The Journal of Physiology*, *189*(3), 535–544.

<https://doi.org/10.1113/jphysiol.1967.sp008183>

Kennedy, J. M., Zak, R., & Gao, L. (1991). Myosin expression in hypertrophied fast twitch and slow tonic muscles of normal and dystrophic chickens. *Muscle & Nerve*, *14*(2), 166–177.

<https://doi.org/10.1002/mus.880140212>

Kimmel, C. B., Ballard, W. W., Kimmel, S. R., Ullmann, B., & Schilling, T. F. (1995). Stages of embryonic development of the zebrafish. *Developmental Dynamics*, *203*(3), 253–310.

<https://doi.org/10.1002/aja.1002030302>

Kimmel, C. B., Eaton, R. C., & Powell, S. L. (1980). Decreased fast-start performance of zebrafish larvae lacking mauthner neurons. *Journal of Comparative Physiology*, *140*(4),

343–350. <https://doi.org/10.1007/BF00606274>

Kimmel, C. B., Sessions, S. K., & Kimmel, R. J. (1981). Morphogenesis and synaptogenesis of the zebrafish mauthner neuron. *The Journal of Comparative Neurology*, *198*(1), 101–120.

<https://doi.org/10.1002/cne.901980110>

Koenen, M., Peter, C., Villarroel, A., Witzemann, V., & Sakmann, B. (2005). Acetylcholine

receptor channel subtype directs the innervation pattern of skeletal muscle. *EMBO Reports*,

6(6), 570–576. <https://doi.org/10.1038/sj.embor.7400429>

Kreienkamp, H.-J., Maeda, R. K., Sinet, S. M., & Taylor, P. (1995). Intersubunit contacts governing assembly of the mammalian nicotinic acetylcholine receptor. *Neuron*, *14*(3), 635–644. [https://doi.org/10.1016/0896-6273\(95\)90320-8](https://doi.org/10.1016/0896-6273(95)90320-8)

Kuffler, S. W., & Williams, E. M. V. (1953). Properties of the ‘slow’ skeletal muscle fibres of the frog. *The Journal of Physiology*, *121*(2), 318–340. <https://doi.org/10.1113/jphysiol.1953.sp004949>

Kullberg, R. W., Brehm, P., & Steinbach, J. H. (1981). Nonjunctional acetylcholine receptor channel open time decreases during development of *Xenopus* muscle. *Nature*, *289*(5796), 411–413. <https://doi.org/10.1038/289411a0>

Kullberg, R. W., Lentz, T. L., & Cohen, M. W. (1977). Development of the myotomal neuromuscular junction in *Xenopus laevis*: an electrophysiological and fine-structural study. *Developmental Biology*, *60*(1), 101–129. [https://doi.org/10.1016/0012-1606\(77\)90113-0](https://doi.org/10.1016/0012-1606(77)90113-0)

Kuo, I. Y., & Ehrlich, B. E. (2015). Signaling in muscle contraction. *Cold Spring Harbor Perspectives in Biology*, *7*(2). <https://doi.org/10.1101/cshperspect.a006023>

Lai, K.-O., & Ip, N. Y. (2003). Central synapse and neuromuscular junction: same players, different roles. *Trends in Genetics : TIG*, *19*(7), 395–402. [https://doi.org/10.1016/S0168-9525\(03\)00147-1](https://doi.org/10.1016/S0168-9525(03)00147-1)

Lefebvre, J. L., Jing, L., Becaficco, S., Franzini-Armstrong, C., & Granato, M. (2007). Differential requirement for MuSK and dystroglycan in generating patterns of neuromuscular innervation. *Proceedings of the National Academy of Sciences of the United*

States of America, 104(7), 2483–2488. <https://doi.org/10.1073/pnas.0610822104>

Lefebvre, J. L., Ono, F., Puglielli, C., Seidner, G., Franzini-Armstrong, C., Brehm, P., & Granato, M. (2004). Increased neuromuscular activity causes axonal defects and muscular degeneration. *Development*, 131(11), 2605–2618. <https://doi.org/10.1242/dev.01123>

Leonard, J. P., & Salpeter, M. M. (1979). Agonist-induced myopathy at the neuromuscular junction is mediated by calcium. *The Journal of Cell Biology*, 82(3), 811–819. <https://doi.org/10.1083/jcb.82.3.811>

Liu, D. W., & Westerfield, M. (1988). Function of identified motoneurons and co-ordination of primary and secondary motor systems during zebra fish swimming. *The Journal of Physiology*, 403(1), 73–89. <https://doi.org/10.1113/jphysiol.1988.sp017239>

Liu, D. W., & Westerfield, M. (1992). Clustering of muscle acetylcholine receptors requires motoneurons in live embryos, but not in cell culture. *The Journal of Neuroscience : The Official Journal of the Society for Neuroscience*, 12(5), 1859–1866. <https://doi.org/10.1523/JNEUROSCI.12-05-01859.1992>

Luna, V. M., & Brehm, P. (2006). An Electrically Coupled Network of Skeletal Muscle in Zebrafish Distributes Synaptic Current. *The Journal of General Physiology*, 128(1), 89–102. <https://doi.org/10.1085/jgp.200609501>

Ma, J., Shen, J., Garrett, J. P., Lee, C. A., Li, Z., Elsaidi, G. A., ... Koman, L. A. (2007). Gene expression of myogenic regulatory factors, nicotinic acetylcholine receptor subunits, and GAP-43 in skeletal muscle following denervation in a rat model. *Journal of Orthopaedic Research*, 25(11), 1498–1505. <https://doi.org/10.1002/jor.20414>

- Martinou, J. C., & Merlie, J. P. (1991). Nerve-dependent modulation of acetylcholine receptor epsilon-subunit gene expression. *The Journal of Neuroscience*, *11*(5), 1291–1299.
<https://doi.org/10.1523/JNEUROSCI.11-05-01291.1991>
- Marx, A., Kirchner, T., Hoppe, F., O'Connor, R., Schalke, B., Tzartos, S., & Müller-Hermelink, H. K. (1989). Proteins with epitopes of the acetylcholine receptor in epithelial cell cultures of thymomas in myasthenia gravis. *The American Journal of Pathology*, *134*(4), 865–877.
Retrieved from <http://www.ncbi.nlm.nih.gov/pubmed/2468286>
- McManaman, J., Blosser, J., & Appel, S. (1981). The effect of calcium on acetylcholine receptor synthesis. *The Journal of Neuroscience*, *1*(7), 771–776.
<https://doi.org/10.1523/JNEUROSCI.01-07-00771.1981>
- Melnikova, I. N., & Gardner, P. D. (2001). The signal transduction pathway underlying ion channel gene regulation by SP1-C-Jun interactions. *The Journal of Biological Chemistry*, *276*(22), 19040–19045. <https://doi.org/10.1074/jbc.M010735200>
- Menelaou, E., & McLean, D. L. (2012). A Gradient in Endogenous Rhythmicity and Oscillatory Drive Matches Recruitment Order in an Axial Motor Pool. *Journal of Neuroscience*, *32*(32), 10925–10939. <https://doi.org/10.1523/JNEUROSCI.1809-12.2012>
- Menelaou, E., & Svoboda, K. R. (2009). Secondary motoneurons in juvenile and adult zebrafish: Axonal pathfinding errors caused by embryonic nicotine exposure. *Journal of Comparative Neurology*, *512*(3), 305–322. <https://doi.org/10.1002/cne.21903>
- Merlie, J. P., & Lindstrom, J. (1983). Assembly in vivo of mouse muscle acetylcholine receptor: Identification of an α subunit species that may be an assembly intermediate. *Cell*, *34*(3),

747–757. [https://doi.org/10.1016/0092-8674\(83\)90531-7](https://doi.org/10.1016/0092-8674(83)90531-7)

Millar, N. S., & Harkness, P. C. (2008). Assembly and trafficking of nicotinic acetylcholine receptors (Review). *Molecular Membrane Biology*, 25(4), 279–292.

<https://doi.org/10.1080/09687680802035675>

Mishina, M., Takai, T., Imoto, K., Noda, M., Takahashi, T., Numa, S., ... Sakmann, B. (1986).

Molecular distinction between fetal and adult forms of muscle acetylcholine receptor.

Nature, 321(6068), 406–411. <https://doi.org/10.1038/321406a0>

Missias, A. C., Chu, G. C., Klocke, B. J., Sanes, J. R., & Merlie, J. P. (1996). Maturation of the Acetylcholine Receptor in Skeletal Muscle: Regulation of the AChR γ -to- ϵ Switch.

Developmental Biology, 179(1), 223–238. <https://doi.org/10.1006/dbio.1996.0253>

Missias, A. C., Mudd, J., Cunningham, J. M., Steinbach, J. H., Merlie, J. P., & Sanes, J. R.

(1997). Deficient development and maintenance of postsynaptic specializations in mutant mice lacking an “adult” acetylcholine receptor subunit. *Development*, 124(24), 5075–5086.

Retrieved from <http://www.ncbi.nlm.nih.gov/pubmed/9362465>

Mongeon, R., Walogorsky, M., Urban, J., Mandel, G., Ono, F., & Brehm, P. (2011). An acetylcholine receptor lacking both γ and ϵ subunits mediates transmission in zebrafish slow muscle synapses. *The Journal of General Physiology*, 138(3), 353–366.

<https://doi.org/10.1085/jgp.2011110649>

Morgan, D. L., & Proske, U. (1984). Vertebrate slow muscle: its structure, pattern of innervation, and mechanical properties. *Physiological Reviews*, 64(1), 103–169.

<https://doi.org/10.1152/physrev.1984.64.1.103>

- Morgan, N. V., Brueton, L. A., Cox, P., Grealley, M. T., Tolmie, J., Pasha, S., ... Maher, E. R. (2006). Mutations in the embryonal subunit of the acetylcholine receptor (CHRNA3) cause lethal and Escobar variants of multiple pterygium syndrome. *American Journal of Human Genetics*, 79(2), 390–395. <https://doi.org/10.1086/506256>
- Myers, P. Z., Eisen, J. S., & Westerfield, M. (1986). Development and axonal outgrowth of identified motoneurons in the zebrafish. *The Journal of Neuroscience*, 6(8), 2278–2289. <https://doi.org/10.1523/JNEUROSCI.06-08-02278.1986>
- Navaneetham, D., Penn, A. S., Howard, J. F., & Conti-Fine, B. M. (2001). Human thymuses express incomplete sets of muscle acetylcholine receptor subunit transcripts that seldom include the δ subunit. *Muscle & Nerve*, 24(2), 203–210. [https://doi.org/10.1002/1097-4598\(200102\)24:2<203::AID-MUS50>3.0.CO;2-F](https://doi.org/10.1002/1097-4598(200102)24:2<203::AID-MUS50>3.0.CO;2-F)
- Nayak, T. K., & Auerbach, A. (2013). Asymmetric transmitter binding sites of fetal muscle acetylcholine receptors shape their synaptic response. *Proceedings of the National Academy of Sciences of the United States of America*, 110(33), 13654–13659. <https://doi.org/10.1073/pnas.1308247110>
- Nguyen, P. V., Aniksztejn, L., Catarsi, S., & Drapeau, P. (1999). Maturation of Neuromuscular Transmission During Early Development in Zebrafish. *Journal of Neurophysiology*, 81(6), 2852–2861. <https://doi.org/10.1152/jn.1999.81.6.2852>
- Nicholls, J. G., Martin, A. R., Fuchs, P. A., Brown, D. A., Diamond, M. E., & Weisblat, D. A. (2012). From neuron to brain, 5th ed. In *From neuron to brain, 5th ed.* Sunderland, MA, US: Sinauer Associates.

- Osta, W. A., El-Osta, M. A., Pezhman, E. A., Raad, R. A., Ferguson, K., Mckelvey, G. M., ... Perov, S. (2010). Nicotinic Acetylcholine Receptor Gene Expression Is Altered in Burn Patients. *Anesthesia & Analgesia*, *110*(5), 1355–1359.
<https://doi.org/10.1213/ANE.0b013e3181d41512>
- Owens, J. L., & Kullberg, R. (1989). Three conductance classes of nicotinic acetylcholine receptors are expressed in developing amphibian skeletal muscle. *The Journal of Neuroscience*, *9*(7), 2575–2580. Retrieved from <http://www.ncbi.nlm.nih.gov/pubmed/2746339>
- Owens, J. L., & Kullberg, R. (1990). Junctional acetylcholine receptor channel open time is not presynaptically regulated in developing muscle. *Developmental Biology*, *142*(1), 250–254. Retrieved from <http://www.ncbi.nlm.nih.gov/pubmed/2227099>
- Papke, R. L., Ono, F., Stokes, C., Urban, J. M., & Boyd, R. T. (2012). The nicotinic acetylcholine receptors of zebrafish and an evaluation of pharmacological tools used for their study. *Biochemical Pharmacology*, *84*(3), 352–365.
<https://doi.org/10.1016/j.bcp.2012.04.022>
- Parichy, D. M., Elizondo, M. R., Mills, M. G., Gordon, T. N., & Engeszer, R. E. (2009). Normal table of postembryonic zebrafish development: Staging by externally visible anatomy of the living fish. *Developmental Dynamics*, *238*(12), 2975–3015.
<https://doi.org/10.1002/dvdy.22113>
- Park, J.-Y., Mott, M., Williams, T., Ikeda, H., Wen, H., Linhoff, M., & Ono, F. (2014). A single mutation in the acetylcholine receptor δ -subunit causes distinct effects in two types of neuromuscular synapses. *The Journal of Neuroscience*, *34*(31), 10211–10218.

<https://doi.org/10.1523/JNEUROSCI.0426-14.2014>

Parsons, R. L. (1978). *Role of Calcium in Desensitization at the Motor End-Plate of Skeletal Muscle BT - Calcium in Drug Action* (G. B. Weiss, Ed.). https://doi.org/10.1007/978-1-4684-3354-8_12

Pedersen, S. E., & Cohen, J. B. (1990). d-Tubocurarine binding sites are located at alpha-gamma and alpha-delta subunit interfaces of the nicotinic acetylcholine receptor. *Proceedings of the National Academy of Sciences of the United States of America*, *87*(7), 2785–2789. <https://doi.org/10.1073/pnas.87.7.2785>

Peng, H. B. (1984). Participation of calcium and calmodulin in the formation of acetylcholine receptor clusters. *The Journal of Cell Biology*, *98*(2), 550–557. <https://doi.org/10.1083/jcb.98.2.550>

Pike, S. H., Melancon, E. F., & Eisen, J. S. (1992). Pathfinding by zebrafish motoneurons in the absence of normal pioneer axons. *Development*, *114*(4), 825–831. Retrieved from <http://dev.biologists.org/content/develop/114/4/825.full.pdf>

Pliszka, B., Strzelecka-Gołaszewska, H., Pantaloni, C., & d'Albis, A. (1981). Comparison of myosin isoenzymes from slow-tonic and fast-twitch fibers of frog muscle. *European Journal of Cell Biology*, *25*(1), 144–149. Retrieved from <http://www.ncbi.nlm.nih.gov/pubmed/6456909>

Porter, J. D., & Baker, R. S. (1996). Muscles of a different “color”: the unusual properties of the extraocular muscles may predispose or protect them in neurogenic and myogenic disease. *Neurology*, *46*(1), 30–37. <https://doi.org/10.1212/wnl.46.1.30>

Porter, J. D., Khanna, S., Kaminski, H. J., Rao, J. S., Merriam, A. P., Richmonds, C. R., ...

Andrade, F. H. (2001). Extraocular muscle is defined by a fundamentally distinct gene expression profile. *Proceedings of the National Academy of Sciences*, 98(21), 12062–12067. <https://doi.org/10.1073/pnas.211257298>

Pugh, P. C., & Berg, D. K. (1994). Neuronal acetylcholine receptors that bind alpha-

bungarotoxin mediate neurite retraction in a calcium-dependent manner. *The Journal of Neuroscience*, 14(2), 889–896. Retrieved from <http://www.ncbi.nlm.nih.gov/pubmed/8301367>

Rotzler, S., & Brenner, H. R. (1990). Metabolic stabilization of acetylcholine receptors in

vertebrate neuromuscular junction by muscle activity. *The Journal of Cell Biology*, 111(2), 655–661. <https://doi.org/10.1083/JCB.111.2.655>

Saint-Amant, L., & Drapeau, P. (1998). Time course of the development of motor behaviors in the zebrafish embryo. *Journal of Neurobiology*, 37(4), 622–632.

[https://doi.org/10.1002/\(SICI\)1097-4695\(199812\)37:4<622::AID-NEU10>3.0.CO;2-S](https://doi.org/10.1002/(SICI)1097-4695(199812)37:4<622::AID-NEU10>3.0.CO;2-S)

Saint-Amant, L., & Drapeau, P. (2001). Synchronization of an Embryonic Network of Identified

Spinal Interneurons Solely by Electrical Coupling. *Neuron*, 31(6), 1035–1046.

[https://doi.org/10.1016/S0896-6273\(01\)00416-0](https://doi.org/10.1016/S0896-6273(01)00416-0)

Saint-Amant, L., Sprague, S. M., Hirata, H., Li, Q., Cui, W. W., Zhou, W., ... Kuwada, J. Y.

(2008). The zebrafish *nui* behavioral mutation disrupts acetylcholine receptor localization and motor axon stability. *Developmental Neurobiology*, 68(1), 45–61.

<https://doi.org/10.1002/dneu.20569>

- Sakmann, B., & Brenner, H. R. (1978). Change in synaptic channel gating during neuromuscular development. *Nature*, *276*(5686), 401–402. <https://doi.org/10.1038/276401a0>
- Schiaffino, S., & Reggiani, C. (2011). Fiber Types in Mammalian Skeletal Muscles. *Physiological Reviews*, *91*(4), 1447–1531. <https://doi.org/10.1152/physrev.00031.2010>
- Schwarz, H., Giese, G., Müller, H., Koenen, M., & Witzemann, V. (2000). Different functions of fetal and adult AChR subtypes for the formation and maintenance of neuromuscular synapses revealed in ϵ -subunit-deficient mice. *European Journal of Neuroscience*, *12*(9), 3107–3116. <https://doi.org/10.1046/j.1460-9568.2000.00195.x>
- Sharma, G., & Vijayaraghavan, S. (2002). Nicotinic receptor signaling in nonexcitable cells. *Journal of Neurobiology*, *53*(4), 524–534. <https://doi.org/10.1002/neu.10114>
- Shepherd, D., & Brehm, P. (1997). Two types of ACh receptors contribute to fast channel gating on mouse skeletal muscle. *Journal of Neurophysiology*, *78*(6), 2966–2974. <https://doi.org/10.1152/jn.1997.78.6.2966>
- Slater, C. R. (2003). Structural determinants of the reliability of synaptic transmission at the vertebrate neuromuscular junction. *Journal of Neurocytology*, *32*(5–8), 505–522. <https://doi.org/10.1023/B:NEUR.0000020607.17881.9b>
- Spencer, R. F., & Porter, J. D. (1988). Structural organization of the extraocular muscles. *Reviews of Oculomotor Research*, *2*, 33–79. Retrieved from <http://www.ncbi.nlm.nih.gov/pubmed/3153651>
- St John, P. A. (2009). Cellular trafficking of nicotinic acetylcholine receptors. *Acta Pharmacologica Sinica*, *30*(6), 656–662. <https://doi.org/10.1038/aps.2009.76>

- Stifani, N. (2014). Motor neurons and the generation of spinal motor neuron diversity. *Frontiers in Cellular Neuroscience*, 8, 293. <https://doi.org/10.3389/fncel.2014.00293>
- Sumanas, S., & Larson, J. D. (2002). Morpholino phosphorodiamidate oligonucleotides in zebrafish: A recipe for functional genomics? *Briefings in Functional Genomics and Proteomics*, 1(3), 239–256. <https://doi.org/10.1093/bfgp/1.3.239>
- Svoboda, K. R., Vijayaraghavan, S., & Tanguay, R. L. (2002). Nicotinic receptors mediate changes in spinal motoneuron development and axonal pathfinding in embryonic zebrafish exposed to nicotine. *The Journal of Neuroscience*, 22(24), 10731–10741. <https://doi.org/10.1523/JNEUROSCI.22-24-10731.2002>
- Sylvain, N. J., Brewster, D. L., & Ali, D. W. (2010). Zebrafish embryos exposed to alcohol undergo abnormal development of motor neurons and muscle fibers. *Neurotoxicology and Teratology*, 32(4), 472–480. <https://doi.org/10.1016/j.ntt.2010.03.001>
- Takahashi, M., Kubo, T., Mizoguchi, A., Carlson, C. G., Endo, K., & Ohnishi, K. (2002). Spontaneous muscle action potentials fail to develop without fetal-type acetylcholine receptors. *EMBO Reports*, 3(7), 674. <https://doi.org/10.1093/EMBO-REPORTS/KVF128>
- Tang, R., Dodd, A., Lai, D., McNabb, W. C., & Love, D. R. (2007). Validation of zebrafish (*Danio rerio*) reference genes for quantitative real-time RT-PCR normalization. *Acta Biochimica et Biophysica Sinica*, 39(5), 384–390. <https://doi.org/10.1111/j.1745-7270.2007.00283.x>
- Thompson, A. J., Lester, H. A., & Lummis, S. C. R. (2010). The structural basis of function in Cys-loop receptors. In *Quarterly Reviews of Biophysics* (Vol. 43).

<https://doi.org/10.1017/S0033583510000168>

Trevarrow, B., Marks, D. L., & Kimmel, C. B. (1990). Organization of hindbrain segments in the zebrafish embryo. *Neuron*, 4(5), 669–679. [https://doi.org/10.1016/0896-6273\(90\)90194-K](https://doi.org/10.1016/0896-6273(90)90194-K)

Tsujihata, M., Ito, H., Satoh, A., Yoshimura, T., Motomura, M., & Nakamura, T. (2001). Semiquantitative measurement of acetylcholine receptor at the motor end-plate in myasthenia gravis. *Internal Medicine (Tokyo, Japan)*, 40(5), 376–381. <https://doi.org/10.2169/internalmedicine.40.376>

Tsunoyama, K., & Gojobori, T. (1998). Evolution of Nicotinic Acetylcholine Receptor Subunits. *Mol. Biol. Evol.*, 15(5), 518–527. Retrieved from <https://academic.oup.com/mbe/article-abstract/15/5/518/987852>

van Raamsdonk, W., Bosch, T. J., Smit-Onel, M. J., & Maslam, S. (1996). Organisation of the zebrafish spinal cord: distribution of motoneuron dendrites and 5-HT containing cells. *European Journal of Morphology*, 34(2), 65–77. <https://doi.org/10.1076/ejom.34.2.65.13021>

van Raamsdonk, W., Pool, C. W., & Te Kronnie, G. (1978). Differentiation of Muscle Fiber Types in the Teleost Brachydanio rerio. *Anatomy and Embryology*, (153), 137–155. <https://doi.org/https://doi.org/10.1007/BF00343370>

van Raamsdonk, W., van't Veer, L., Veeken, K., Heyting, C., & Pool, C. W. (1982). Differentiation of muscle fiber types in the teleost Brachydanio rerio, the zebrafish. Posthatching development. *Anatomy and Embryology*, 164(1), 51–62. <https://doi.org/10.1007/bf00301878>

- Vicini, S., & Schuetze, S. M. (1985). Gating properties of acetylcholine receptors at developing rat endplates. *The Journal of Neuroscience*, 5(8), 2212–2224.
<https://doi.org/10.1523/JNEUROSCI.05-08-02212.1985>
- Wanamaker, C. P., Christianson, J. C., & Green, W. N. (2003). Regulation of Nicotinic Acetylcholine Receptor Assembly. *Annals of the New York Academy of Sciences*, 998(1), 66–80. <https://doi.org/10.1196/annals.1254.009>
- Waterman, R. E. (1969). Development of the lateral musculature in the teleost, *Brachydanio rerio*: A fine structural study. *American Journal of Anatomy*, 125(4), 457–493.
<https://doi.org/10.1002/aja.1001250406>
- Welsh, L., Tanguay, R. L., & Svoboda, K. R. (2009). Uncoupling nicotine mediated motoneuron axonal pathfinding errors and muscle degeneration in zebrafish. *Toxicology and Applied Pharmacology*, 237(1), 29–40. <https://doi.org/10.1016/J.TAAP.2008.06.025>
- Westerfield, M. (2000). *The Zebrafish Book. A Guide for the Laboratory Use of Zebrafish (Danio rerio)* (4th ed.). Eugene: University of Oregon Press, Eugene.
- Westerfield, M. (2007). *The zebrafish book. A guide for the laboratory use of zebrafish (Danio rerio)* (5th Editio). Eugene: Univ. of Oregon Press.
- Westerfield, M., McMurray, J. V., & Eisen, J. S. (1986). Identified motoneurons and their innervation of axial muscles in the zebrafish. *The Journal of Neuroscience*, 6(8), 2267–2277. <https://doi.org/10.1523/JNEUROSCI.06-08-02267.1986>
- Witzemann, V, Schwarz, H., Koenen, M., Berberich, C., Villarroel, A., Wernig, A., ... Sakmann, B. (1996). Acetylcholine receptor epsilon-subunit deletion causes muscle weakness and

- atrophy in juvenile and adult mice. *Proceedings of the National Academy of Sciences of the United States of America*, 93(23), 13286–13291. <https://doi.org/10.1073/pnas.93.23.13286>
- Witzemann, Veit, Barg, B., Criado, M., Stein, E., & Sakmann, B. (1989). Developmental regulation of five subunit specific mRNAs encoding acetylcholine receptor subtypes in rat muscle. *FEBS Letters*, 242(2), 419–424. [https://doi.org/10.1016/0014-5793\(89\)80514-9](https://doi.org/10.1016/0014-5793(89)80514-9)
- Witzemann, Veit, Barg, B., Nishikawa, Y., Sakmann, B., & Numa, S. (1987). Differential regulation of muscle acetylcholine receptor γ - and ϵ -subunit mRNAs. *FEBS Letters*, 223(1), 104–112. [https://doi.org/10.1016/0014-5793\(87\)80518-5](https://doi.org/10.1016/0014-5793(87)80518-5)
- Xu, X., Scott, M. M., & Deneris, E. S. (2006). Shared long-range regulatory elements coordinate expression of a gene cluster encoding nicotinic receptor heteromeric subtypes. *Molecular and Cellular Biology*, 26(15), 5636–5649. <https://doi.org/10.1128/MCB.00456-06>
- Yamane, A., Saito, T., Nakagawa, Y., Ohnuki, Y., & Saeki, Y. (2002). Changes in mRNA Expression of Nicotinic Acetylcholine Receptor Subunits during Embryonic Development of Mouse Masseter Muscle. *Zoological Science*, 19(2), 207–213. <https://doi.org/10.2108/zsj.19.207>
- Yan, Z., Lira, V. A., & Greene, N. P. (2012). Exercise training-induced regulation of mitochondrial quality. *Exercise and Sport Sciences Reviews*, 40(3), 159–164. <https://doi.org/10.1097/JES.0b013e3182575599>
- Zhang, Y., Rushbrook, J. I., & Shafiq, S. A. (1985). Avian adductor profundus muscle: characterization of a pure slow tonic region by histochemical, monoclonal antibody and peptide mapping studies. *Journal of Muscle Research and Cell Motility*, 6(3), 333–345.

Retrieved from <http://www.ncbi.nlm.nih.gov/pubmed/2933426>

Zheng, J. Q., Felder, M., Connor, J. A., & Poo, M. M. (1994). Turning of nerve growth cones induced by neurotransmitters. *Nature*, *368*(6467), 140–144.

<https://doi.org/10.1038/368140a0>